Margrete Hånes Wesenberg

Gas Heated Steam Reformer Modelling

Doctoral thesis
for the degree of doktor ingeniør

Trondheim, April 2006

Norwegian University of Science and Technology
Faculty of Natural Sciences and Technology
Department of Chemical Engineering

NTNU
Innovation and Creativity

NTNU
Norwegian University of Science and Technology

Doctoral thesis
for the degree of doktor ingeniør

Faculty of Natural Sciences and Technology
Department of Chemical Engineering

© Margrete Hånes Wesenberg

ISBN 82-471-7905-9 (printed version)
ISBN 82-471-7904-0 (electronic version)
ISSN 1503-8181

Doctoral theses at NTNU, 2006:77

Printed by NTNU-trykk

Gas Heated Steam Reformer Modelling

Margrete Hånes Wesenberg

SUMMARY

Conversion of natural gas is becoming increasingly relevant in the future as the world energy market will demand cleaner fuels, cleaner production of fuels and better utilization of the large, remote, and still undiscovered gas reserves in the world. The refining of the natural gas to synthetic gasoline, diesel and future energy fuels such as methanol and hydrogen is a solution for making the most of these gas reserves.

The intermediate process step in gas refining, the synthesis gas production from natural gas, represents 60–80 % of the total investment cost of a methanol or synthetic fuels plant. This drives the technological development within this process field towards improvements for increasing the efficiency and reducing the costs. The synthetic gas production by steam reforming is a widely used, expensive and energy demanding technology. Steam reformers demand large base areas and are heated by natural gas combustion. Technological developments over the past two decades have lead to an alternative steam reformer, the gas heated reformer, which is a compact unit heated by flue gas or by further converted and heated synthesis gas.

This doctoral thesis is treating the gas heated steam reformer (GHR). The motivation was to develop a complete mathematical model combining of the reactor side and the hot gas side of the reformer and furthermore to investigate the best mathematical descriptions of the heat transport mechanisms involved. The complete model should be as simple as possible but nevertheless be on a level where the important heat transport mechanisms are adequately modelled.

The resulting model is a two-dimensional, finite difference model of a packed bed catalytic tube enclosed by an annular section for counter current flow of the heating gas. The separate partial models, the reactor model and the annulus model, are connected by iterative solution with direct substitution of the temperature and heat flux profiles of the outer reactor tube wall.

The reactor model comes in two versions: a heterogeneous model and a pseudo-homogeneous model. The species transport is described by radial dispersion, axial convection and chemical reaction. The heat transport is modelled with terms for radial conduction, axial convection and the heat sink related to the net endothermic reactions.

The annulus model is a simplified plug flow model disregarding the turbulence present. The effect of the turbulent flow on the radial heat transport is still included, by using an effective radial thermal conductivity in the temperature equation. The values for the effective radial thermal conductivities are provided by external simulations in computational fluid dynamics (CFD), where turbulence is modelled by the k-ε turbulence model. The radial heat transport by gas radiation is included by solving the radiative intensity equations by the discrete ordinates method.

The method of importing data for the effective radial thermal conductivity calculated with CFD was evaluated by running test simulations comparable to the CFD simulations. The results showed almost identical axial and radial temperature profiles in the two models when all dissimilarities in the models were allowed for. This simplifying method was thus approved adequate for the purpose.

It was also found that the inclusion of the radial profile of the effective radial thermal conductivity was significant for the overall GHR simulations. Using a mean value for the effective radial thermal conductivity did not result in temperature profiles similar to the profiles of the CFD simulations where turbulence was modelled.

The restrictions related to the mass and heat transport between the gas bulk and the porous pellets were investigated. These resistances are usually neglected in heterogeneous steam reformer modelling based on assumptions that they do not affect the overall reactor simulation results. The heterogeneous reactor model of this thesis includes all pellet transport resistances. Estimations showed that the reaction effectiveness factors, which are defined relative to the pellet surface conditions, were greater than the alternative effectiveness factors defined relative to the bulk conditions. This implies that there exist transport limitations between the two phases. These transport restrictions were found to be of importance when evaluating local effects, as reaction kinetics in general and approach to equilibrium for the coke reactions responsible for catalyst deactivation. On the other hand, the overall reactor simulations were hardly influenced by the interphase transport limitations. This was seen from comparative simulations of the pseudo-homogeneous model using the effectiveness factors and the alternative effectiveness factors. These simulation results were almost equal, while the latter was identical to the results of the heterogeneous model accounting for the resistances.

LIST OF PAPERS AND PRESENTATIONS

Paper 1:

Wesenberg, M.H. and Svendsen, H.F., "Mass and heat transfer limitations in a heterogeneous model of a gas heated steam reformer", submitted to *Ind. Eng. Chem. Res.* (2006)

My contribution: Build the mathematical model, based on an existing reactor model, evaluate the results and write the article.

Paper 2:

Wesenberg, M.H., Ströhle, J. and Svendsen, H.F., "A study of the heating section of a gas heated reformer", submitted to *Int. J. Chem. Reactor Eng.* (2006)

My contribution: Build the mathematical model, based on an existing reactor model, evaluate the results and write the article.

Presentation 1:

Wesenberg, M.H., Grislingås, A. and Grevskott, S., "Modelling of steam reformer tubes", paper no. 961, *6th World Congress of Chemical Engineering*, Melbourne (2001)

My contribution: Define the scope for the test simulations, run the simulations, evaluate the results and write the article.

Presentation 2:

Wesenberg, M.H., Ströhle, J. and Svendsen, H.F., "Gas heated steam reformer; two-dimensional finite difference model with heater side discrete ordinates radiation scheme", paper no. P16-007, *7th World Congress of Chemical Engineering*, Glasgow, (2005)

My contribution: Build the mathematical model, based on an existing reactor model, evaluate the results and write the article and the poster presentation.

ACKNOWLEDGEMENTS

This thesis is the result of three years of work done at the Department of Chemical Engineering, Norwegian University of Science and Technology (NTNU). It was done according to the wish of Statoil Research Centre during my employment there. I am very grateful for the financial support from Statoil and for the possibility to work on this doctoral thesis.

First of all I wish to thank my supervisor, Professor Hallvard F. Svendsen, for accepting me as one of his doctoral students, even if my subject was not part of his recent projects. Thank you for all the good ideas and advices, for all I have learned from you during this work, for your deep interest in this subject and for your high spirits.

I am very grateful for the help I got from Jochen Ströhle when he worked at SINTEF, Trondheim. Thank you for the basic understanding of the discrete ordinates method and for the development of its solution procedure. What I learned from you was impossible to find in any textbook.

Rune Engeskaug at SINTEF, Trondheim, helped me with my work with FLUENT and GAMBIT. Thanks for all the good advices and the help whenever I was stuck in new problems.

I also wish to thank John Morud at SINTEF, Trondheim, for the help I got with the MATLAB-codes to speed up the computer calculations. The result was 30 % less calculation time, and that is noticeable for calculations that might take 10 hours.

I appreciate the discussions with my colleagues Ola Olsvik (who was also my co-supervisor on this thesis), Roger Hansen and Carl Birger Jenssen at Statoil Research Centre. It was very useful to get your inputs on the focus areas in this project.

And of course, I owe my deepest gratitude to my two most important deliveries during these three project years (that consequently took five years); my daughters Andrea and Louise. Thank you for making me forget all about modelling problems and differential equations every afternoon and for giving me good laughs. And most of all; Harald, I am deeply grateful for all your support, encouragements, positive attitude and patience. My thanks also go to your project managers who released you this last year so that we could manage this together.

TABLE OF CONTENTS

NOMENCLATURE

Symbol	Definition	Unit
a_q	Weight factor for the *q*-th fictive grey gas in the WSGG model	
a_v	Specific outer pellet surface area	m_c^2/m_r^3
A_{ad}	Pre-exponential factor for adsorption	
A_c	Cross sectional area	m^2
A_j	Arrhenius constant	
$Bi_{w,p}$	Biot number, defined in Equation (2-2)	
C_i	Concentration of component *i*	kmole/m^3
c_P	Specific heat capacity	J/kg K
d	Diameter	m
d_0	Pore diameter	m
d_k	Equivalent particle diameter	m
d_p	Equivalent particle diameter	m
D	Diffusion coefficient	m^2/ s
D_{er}	Effective radial dispersion coefficient	m^2/ s
DEN	Denominator in the expressions for the reaction rates	
E	Dispersion coefficient	m^2/ s
E	Activation energy	kJ/ kmole
f	Friction factor	
F_C	Correction factor for heat transfer coefficients in annular ducts	
F^0_P	Correction factor for polarity effects in the gas viscosity model	
F^0_Q	Correction factor for quantum effects in the gas viscosity model	
GZ	Graetz number	
h	Normalized axial coordinate	
h	Heat transfer coefficient	W/m^2 K
I	Radiation intensity	W/m^2 sr
k	Mass transfer coefficient	m/ s
k_q	Absorption coefficient of the *q*-th fictive grey gas in the WSGG model	
k_j	Rate coefficient for reaction *j*	
K_i	Adsorption coefficient of component *i*	
K_1	Equilibrium constant for reaction *1*	bar^2
K_2	Equilibrium constant for reaction *2*	
K_3	Equilibrium constant for reaction *3*	bar^2
$K_{1,h}$	Slope parameter	

Symbol	Definition	Unit
$K_{2,h}$	Damping parameter	
K_∞	Constant	
L	Tube length	m
M	Mole weight	kg/ kmole
n	Molar rate	kmole/ s
n	Scaling exponent for pressure scaling in the WSGG model	
N	Molar flux	kmole/ s m^3
N	Number of numerical discrete points	
NU_{dt}	Nusselt number based on tube diameter and radial mean gas temperature, defined in Equation (2-45)	
$\overline{NU}_{d_t}$	Integrated axial average of NU_{dt}, defined in Equation (2-46)	
Nu_w	Wall Nusselt number, defined in Equation (2-1)	
p	Partial pressure	Pa
Pe_E	Peclet number based on dispersion, defined in Equation (2-8)	
Pe_h	Peclet number for radial heat transfer	
Pe_m	Peclet number for mass transfer	
Pe_p	Thermal Peclet number, defined in Equation (2-7)	
Pr	Prandtl's number, defined in Equation (2-4)	
q	Heat flux	kW/ m^2
q'	Volumetric heat source	kW/ m^3
Q	Heat	kW
R	Gas constant	Pa m^3/kmole K
R	Radius	m
R_{ext}	External radius of catalyst pellet of cylindrical shape	m
R_{hole}	Radius of the holes in the catalyst pellet of cylindrical shape	m
R_p	Equivalent particle radius	m
Re_h	Reynolds number for annular ducts	
Re_p	Reynolds number for fixed beds, defined in Equation (2-3)	
Sc	Schmidt number, defined in Equation (2-5)	
Sh	Sherwood's number, defined in Equation (2-6)	
T	Temperature	K
u	Normalized superficial velocity	
v	Velocity	m/ s
V	Volume	m^3
w	Quadrature weight factor for radiative directions	
x	Mole fraction	
X	Fraction of pellet radius defining the active layer of the pellet	
y	Depth coordinate for catalyst pellets	m
z	Axial co-ordinate	m
Z	Compressibility factor	
$\sum_i V$	Diffusion volumes for binary diffusion model	

Greek letters

α	Parameter for cylindrical co-ordinates in the discrete ordinates method

Symbol	Definition	Unit
β	Parameter defined in Equation (2-36)	
β	Normalized pressure	
β_i	Normalized partial pressure of component *i*	
ΔC	Concentration difference	kmole/m^3
ΔH	Enthalpy	kJ/ kg
ΔH_{ad}	Adsorption enthalpy	kJ/ kmole
ΔH_j	Heat of reaction	kJ/ kmole
ΔH°	Standard enthalpy of formation	kJ/ kmole
ΔT	Temperature difference	K
ΔQ	Change in internal energy	kJ/ s
ε	Emissivity	
ε	Void fraction of packed bed	m^3 void/m_r^3
ε_p	Catalyst porosity	m^3 void/m_c^3
ϕ	Factor for estimating thermal conductivity and viscosity of gas mixtures	
η	Directional cosines for angular directions	
η	Reaction effectiveness factor relative to surface conditions	
η'	Reaction effectiveness factor relative to bulk conditions	
κ	Absorption coefficient for gas	m^{-1}
λ	Thermal conductivity	W/ m K
μ	Dipole moment	
μ	Directional cosines	
μ	Viscosity	Pa s
ν	Stoichiometric coefficient of chemical reaction	
θ	Normalized temperature	
ρ	Density	kg/m^3
ρ_c	Density of catalyst bulk	kg cat./m_r^3
ρ_w	Wall reflectivity	
σ	Stefan Boltzmann's constant	W/ m^2 K^4
τ	Tortuosity factor	
ω	Normalized radial co-ordinate	
ω_p	Normalized co-ordinate for pellet depth	
ξ	Reduced, inverse viscosity	
ψ	Azimuthal angle	rad
ζ	Evaluation parameter defined in Equation (2-19)	

Subscripts

1	Position at inner wall of reactor tube
2	Position at outer wall of reactor tube
3	Position at outer wall of annular section
a	Annulus
b	Reactor bed
B	Blackbody
c	Catalyst bulk

Symbol	Definition	Unit
c	Critical	
e	Effective	
film	Gas film surrounding the catalyst pellets	
g	Gas	
h	Hydraulic	
i	Component number	
j	Reaction number	
k	Component number	
K	Knudsen	
m	Mean value with respect to radius	
m	Gas mixture	
p	Pellet	
r	Radial	
r	Reduced	
rad	Radiation	
s	Superficial	
t	Tube	
tot	Total	
w	Wall	
z	Axial	

Superscripts

0	Stagnant
0	Inlet condition
bulk	At bulk conditions
e	Effective
m	Angular direction in the discrete ordinates method
s	Surface of pellets
$\bar{}$	Average value by axial integration

Abbreviations

ATR	Autothermal reforming
F-T	Fischer-Tropsch
GHR	Gas Heated Reformer
GTL	Gas To Liquids
LNG	Liquefied Natural Gas
POX	Partial Oxidation
S/C	Steam-to-carbon ratio
SN	Stoichiometric number

1 INTRODUCTION

1.1 Motivation

The background for this thesis was the request to develop a complete mathematical model of a gas heated steam reformer and also investigate the heat transport mechanisms involved in steam reforming processes. Steam reformers are of great interest to Statoil, the financier of this project, due to their interests in both gas refining and hydrogen production for hydrogenation in oil refineries. The relevant gas refining interests are the methanol plant in Tjeldbergodden, Norway, and research projects within methanol and Fischer-Tropsch synthesis and within hydrogen as an energy carrier. New technologies within reforming processes should therefore be continuously supervised with an eye on the possible cost savings and emission reductions. Mathematical models of the new technologies under development can serve as an aid for understanding the technological concepts and being able to raise the relevant questions. The gas heated steam reformer is a reactor concept still too immature for the combination with methanol and Fischer-Tropsch synthesis, but that is developing towards feasible operation. Gas heated reformers are already operating in hydrogen and ammonia plants.

The large gas reserves of the world are still largely undiscovered. As the world oil production decreases natural gas as an energy carrier will become more important, and this increases the relevance of gas refining. The utilization of the associated natural gas separated from unstabilized crude oil will also be relevant as this is often flared or reinjected to increase the recovery rate of oil from the wells. Even stronger restrictions on emissions enforce efficient utilizations of these gas reserves, and technological improvements are a natural consequence of this. Many of the large gas reserves in the world are located in remote areas far from the world energy markets, and the natural gas can therefore not be economically transported in pipelines. The natural gas may instead be liquefied (to LNG) or refined to liquid products (as methanol or synthetic gasoline or diesel) and shipped on tankers to the market. The gas refining products are more easily saleable than the LNG as the LNG requires installations for gasification and a grid for gas transport at the receiving points. These installations are developed only a few places in the world and are generally not wanted in built-up areas by security considerations.

Steam reforming of natural gas is the part of the gas refining process where the natural gas is converted to synthesis gas (syngas), which further is used in the synthesis to methanol or Fischer-Tropsch products. Hydrogen rich syngas can also be used directly for hydrogen enrichment. The technology for steam reforming is of great interest because this part of the process represents a substantial portion of the investment costs. The reforming section costs about 60–80 % of the total cost of the entire gas refining plant. Improvements and cost savings in the reforming section will therefore become very noticeable in the total plant cost. The steam reforming concept looked into in this thesis, the gas heated reformer (GHR), is a future alternative reactor unit with potential cost savings and efficiency improvements. Steam reforming and the GHR are described in detail in Section 1.4.

Mathematical models of chemical reactors in general are useful tools for operating, developing and improving reactors and when process conditions are changed. The models developed for this thesis are able to calculate gas temperatures, gas composition and pressure at the reactor outlet when inlet conditions and reactor size is specified. They can also give profiles of gas temperatures, wall temperatures, catalyst surface temperatures, pressures and species concentrations as function of the position in the reactor, which in turn can indicate if the reactor is operating under safe conditions concerning catalyst poisoning and tube material lifetime. Finally, the models may be a useful tool for evaluating optimum geometry and configuration for a given requirement of a reactor.

1.2 Scope of work

The main focus in this project has been the development of a mathematical model of the gas heated reformer (GHR) in steady state. The idea behind this modelling task was to achieve a model that was as simple as possible while it on the other hand was able to include the mechanisms that affect the heat and mass transports in the reactor. The model should also be available for as many users as possible and was therefore programmed in MATLAB, which is a mathematical tool available for many in both Statoil and NTNU. The two variations of two-dimensional finite-difference models for the reactor tube developed by Svendsen et al. (1996) were modified and extended to interact with a heating section of the GHR. This model was presented at the 7th World Congress of Chemical Engineering in 2005 (Wesenberg et al., 2005). The main part of the modelling work done has been the developing of this heating section model and the implementation of the discrete ordinates method radiation model which describes the radiative heat transport in the high temperature heating section. The heating section model was made on the same mathematical platform as the reactor models; two dimensions, finite difference numerical method and cylindrical coordinates. A GHR model with such a complete heating section model has not been published previously. Only two publications are found, and these both simplify the radiative heat flux in the heating section to a radiative contribution to the convective heat flux. The GHR model with emphasis on the heating section has been submitted for publication in the International Journal of Chemical Reactor Engineering in 2006 (Wesenberg et al., 2006).

The second major part of the thesis has been to study the different heat transfer mechanisms existing in the catalytic bed of steam reformers and to obtain an overview of research previously published within the field. This involves a critical literature study of the empirically derived correlations used in packed bed models in general, and the evaluation to find the suitable correlations for reactor models of steam reformers in special. The investigation of wall heat transfer coefficients suitable for steam reformer reactor models was presented at the 6th World Congress of Chemical Engineering in 2001 (Wesenberg et al., 2001).

Finally, the reactor models were examined to evaluate the reaction effectiveness factors and the mass and heat transport limitations present in the fixed bed reactors of steam reformers. This was done to achieve an improved framework for recommendations for which simplifications can be made regarding transport limitations in steam reformer reactor models. Many publications exist on modelling of the catalytic bed of steam reformers and they all claim that restrictions in mass and heat transport between the gas bulk and the porous pellets are negligible. But, until now, none have proven this statement. This research within the heterogeneous reactor model of the GHR model was submitted for publication in Industrial & Engineering Chemistry Research in 2006 (Wesenberg and Svendsen, 2006).

1.3 Outline

This thesis summarizes the four publications and goes more thoroughly into parts omitted in these articles.

Section 2 gives a literature review within empirical correlations for fixed bed radial heat transport and also evaluations of models suitable in steam reformer modelling.

Section 3 summarizes the background information used when deciding which gas radiation model is suitable for the annular section model.

Section 4 holds the complete GHR model; the heterogeneous and the pseudo-homogeneous reactor models and the annulus model, with all submodels.

Section 5 shows the justification of the choices of all empirical correlations used in the GHR model. The choices are based on background test simulations presented in this section.

Section 6 contains the results regarding the decision of the numerical resolution in the GHR and in the pellet calculations.

Section 7 presents the simulation results of the chosen simulation cases. The local and overall effects of implementing the gas-pellet mass and heat transport restrictions in the heterogeneous reactor model are analyzed. Finally, a reproduction with analysis of a publication of a GHR model is given as a case study.

Section 8 summarizes the conclusions drawn in the thesis and gives some suggestions for future extensions of the annulus model.

1.4 Syngas production by steam reforming of natural gas

Synthesis gas – or syngas – is produced from natural gas or coal and is the building block in the synthesis of ammonia, methanol, Fischer-Tropsch (F-T) fuels, hydrogen for hydro cracking at oil refineries, oxo-alcohols and other fine chemicals. Syngas is a mixture of H_2, CO, CO_2 and H_2O, with perhaps some N_2 from air and some unreacted CH_4. The gas composition varies with the intended use of the syngas; ammonia production requires a molar H_2/N_2 ratio of 3, and for hydrogen production the H_2 contents should be as high as possible. Because of the active shift reaction (Equation (1-3) below) both CO and CO_2 are reactants in the methanol synthesis and in high temperature F-T synthesis, and the syngas composition is therefore specified by a stoichiometric number ($SN = [H_2–CO_2] / [CO+CO_2]$) which should be close to 2. On the other hand only CO is a reactant for the low temperature F-T synthesis, and the syngas should have a H_2/CO ratio close to 2. These different syngas compositions are achieved by using different types of reactor technology and by varying the amount of added steam and possibly oxygen or air, which is discussed below. The syngas composition is also dependent on the feed gas composition and on the outlet temperature and pressure of the reforming reactor.

Catalytic steam reforming of natural gas is the most widely used technology concept for syngas production. The reactions taking place here are the two endothermic steam reforming reactions of methane and the parallel exothermic water gas shift, respectively:

$$CH_4 + H_2O \rightleftharpoons CO + 3\,H_2 \tag{1-1}$$

$$CH_4 + 2\,H_2O \rightleftharpoons CO_2 + 4\,H_2 \tag{1-2}$$

$$CO + H_2O \rightleftharpoons CO_2 + H_2 \tag{1-3}$$

As can be seen, reaction (1-2) is a combination of reactions (1-1) and (1-3).

The natural gas also contains higher hydrocarbons which are converted to methane in an adiabatic prereformer upfront the steam reformer. The prereforming takes place at temperatures of about 350–550 ºC and makes it possible to preheat the steam reformer feed to higher temperatures without getting problems with olefin formation from the higher hydrocarbons. Olefins are unwanted in the steam reformer feed as they generally cause coking of the catalyst pellets at high temperatures. Preheating of the steam reformer feed is of great advantage because the reformer unit can be scaled down to a minimum size (Aasberg-Petersen et al., 2001).

The reactions are catalysed by pellets coated with nickel and are highly endothermic overall. Effective heat transport to the reactor tubes and further into the centre of the catalytic fixed bed is therefore a very important aspect during design and operation of steam reformers. The reactions take place in several tubular fixed bed reactors of low diameter-to-height ratio to ensure efficient heat transport in radial direction. The process conditions are typically 20–40 bar with inlet temperature of 300–650 ºC and outlet temperature of 700–950 ºC. There is often an approach to equilibrium

of about 5–20 ºC, which means that the outlet temperature is slightly higher than the equilibrium temperature calculated from the actual outlet composition (Rostrup-Nielsen et al., 1988).

1.4.1 Fired steam reformers

The most common reactor concept for steam reforming of natural gas is the fired steam reformer. Natural gas and the tail gas from the synthesis loop are burned in a firebox where several reactor tubes are placed in rows with a number of 40 to 400 tubes. The reactor tubes are about 10–12 m long, with diameters of about 10–12 cm. The reactions for conversion of natural gas to syngas take place over the catalytic beds in the reactor tubes. The burners can be located in different places: on the roof, on the floor, on levelled terraces on the walls, or on the walls ("side fired" or "radiant wall"). These configurations are shown in Figure 1-1. The top fired steam reformer must be operated carefully as the tube wall temperature and heat flux show a peak in the upper part of the reformer. The bottom fired reformers achieve a stable heat flux profile along the tube length, which causes high tube skin temperatures at the reactor outlet. The terrace wall fired reformer is a modification of the bottom fired reformer and has some smaller problem with high metal temperatures. The side fired reformer has the most effective design and is also the most flexible reformer, both in design and in operation (Dybkjær, 1995). It has the highest total heat flux possible combined with lowest heat flux where the tube skin temperature is at its highest. In this type of reformer it is possible to combine a low steam-to-carbon ratio with a high outlet temperature. The most critical operation parameter is the maximum temperature difference over the tube wall, not the maximum heat flux (Aasberg-Petersen et al., 2001).

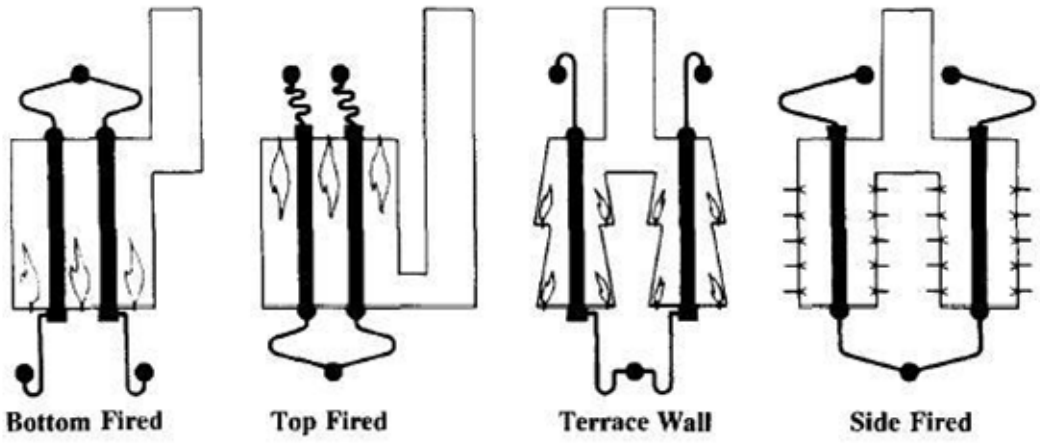

Figure 1-1. Bottom fired, top fired, terrace wall fired and side fired steam reformer furnaces (Dybkjær, 1995).

The flue gas from the fire box is lead to the heat recovery section where it is utilized to preheat the natural gas coming into the syngas plant. Only about 50 % of the fired energy is transferred directly to the reactor tubes but the overall thermal efficiency of the fired duty will approach 90 to 97 %.

The number of tubes in one unit is decided by the maximum feasible tube length. It would be economical to rather have a few long tubes than many short tubes but there is a limit of tube length determined by the risk of tube bending and by the pressure drop in the fixed beds (Dybkjær, 1995). The maximum tube diameter is decided by the ability for efficient radial heat transport in the packed bed and the minimum tube diameter is restricted to the practical possibility for catalyst loading.

1.4.2 Gas heated steam reformers

The gas heated steam reformer is one of many names of this type of compact, convective steam reformer. The names are mainly associated with a specific licensor. Some of the other names used are convective steam reformer, (gas heated) heat exchange reformer, enhanced gas heat transfer reformer, compact reformer, convection reformer and heat exchanger type reformer.

The gas heated reformer (GHR) is a compact alternative to the fired steam reformer. The high manufacturing costs, the high weight and the large base area of the fired steam reformer maintain the interest for a compact and less expensive alternative. The GHR is still at an early development stage but has been commercially proven for large scale ammonia and hydrogen purposes where the steam excess in the reformer unit is large. There is also interest for the GHR in relation to F-T and methanol production but this will only be profitable if the steam-to-carbon ratio of the feed gas can be reduced below 1.5. This causes problems connected to the resulting high partial pressures of methane and carbon monoxide, which may take the operation above the equilibrium limit of the coking reactions. Further development of catalyst materials is thus required in order to achieve rapid gasification of coke and thereby avoid catalyst poisoning.

The heating medium in the GHRs can either be syngas from a secondary reformer or flue gas from the burning of natural gas. For the case of syngas as heat source the GHR must work as a primary reformer operating together with a secondary reformer. A primary reformer converts only parts of the methane feed while the remaining methane is converted in the secondary reformer. The secondary reformer is generally an autothermal reformer (ATR), i.e. an internally fired reformer, where syngas is produced from the endothermic steam reforming reactions of Equations (1-1) and (1-2), the water gas shift of Equation (1-3), and the exothermic reactions with oxygen, which is represented by the following equilibrium (Aasberg-Petersen et al., 2001):

$$CH_4 + 1.5\,O_2 \rightleftharpoons CO + 2\,H_2O \tag{1-4}$$

The secondary reformer may also be a partial oxidation (POX) reformer where syngas is formed from reaction of methane with oxygen. In a POX reactor the natural gas is burned with oxygen to form syngas together with the water gas shift in Equation (1-3) (De Groote and Froment, 1995):

$$CH_4 + 2\,O_2 \rightleftharpoons CO_2 + 2\,H_2O \tag{1-5}$$

Syngas as a heat source in a primary gas heated steam reformer contains sufficient energy as it has been brought to a higher temperature after full conversion of methane and has an increased mass flow due to further addition of oxygen (and possibly steam) in the secondary reformer. If flue gas is used as heat source the GHR is supplied with a combustor at the bottom which leads the flue gas upwards to the shell side of the heat exchanger section of the unit. There are great challenges for the tube material associated with syngas as heating medium. The material is exposed to a high-temperature gas with high partial pressure of CO which causes great risk of metal dusting. Metal dusting is a serious corrosion problem which is described in Section 1.4.3.2. Research to find suitable materials is therefore in progress with GHR licensors to make operation with low steam-to-carbon ratios feasible. Some licensors claim that a steam to carbon ratio (S/C) below 1.5 will be feasible in the future.

The GHR heated by product gas from a secondary reformer (ATR) is energy efficient as it utilizes the excess heat from the internally fired ATR to the highly endothermic steam reforming reactions. It can be beneficial in revamp projects in combination with an existing ATR as it increases both the carbon efficiency and the plant capacity (Loock et al., 2005). Increased carbon efficiency means lower CO_2-emissions. Other advantages with the GHR technology compared with the fired steam reformer are 1) the small size and the low footprint, which can be essential when increasing capacity of existing plants, 2) the lower investment costs, particularly seen in plant expansions, 3) the reduced steam utility size and cost, 4) its chance of de-bottlenecking maximum train size in existing ATR plants, and 5) that the complete unit is transported to the processing plant for installation, which is cost saving when the plant is located far from infrastructure or in a high-wage country.

A syngas plant based on GHR technology integrated with an ATR can have varying configurations. The GHR and ATR can be placed in series or in parallel, as seen in Figure 1-2, or in combinations of these. In all of these concepts the methane feed is only partly converted in the GHR (about one third) while complete conversion is carried out in the ATR. In series reforming all of the methane is fed into the GHR where it is partly converted. The GHR effluent flows further into the ATR for final conversion. The product gas of the ATR is thereafter fed to the shell side of the GHR for cool-down while providing heat to the steam reformer tubes of the GHR. In a parallel concept the feed gas is split and fed into the GHR and the ATR. Both the product gases of the ATR and the GHR are lead into the shell side of the GHR where this syngas mixture supplies the heat needed for the reactions and the heating in the tubes of the GHR.

The parallel configuration has some advantages in flexibility. Firstly the pressure drop in the ATR will not be as high as in the series concept, which makes future capacity increases possible. Secondly the steam-to-carbon ratios and the inlet temperatures may be adjusted individually for the two reformers (Loock et al., 2005). The series configuration is on the other hand advantageous when oxygen consumption should be low. It also gives lower CO_2 concentration in the syngas owing to its higher exit temperature.

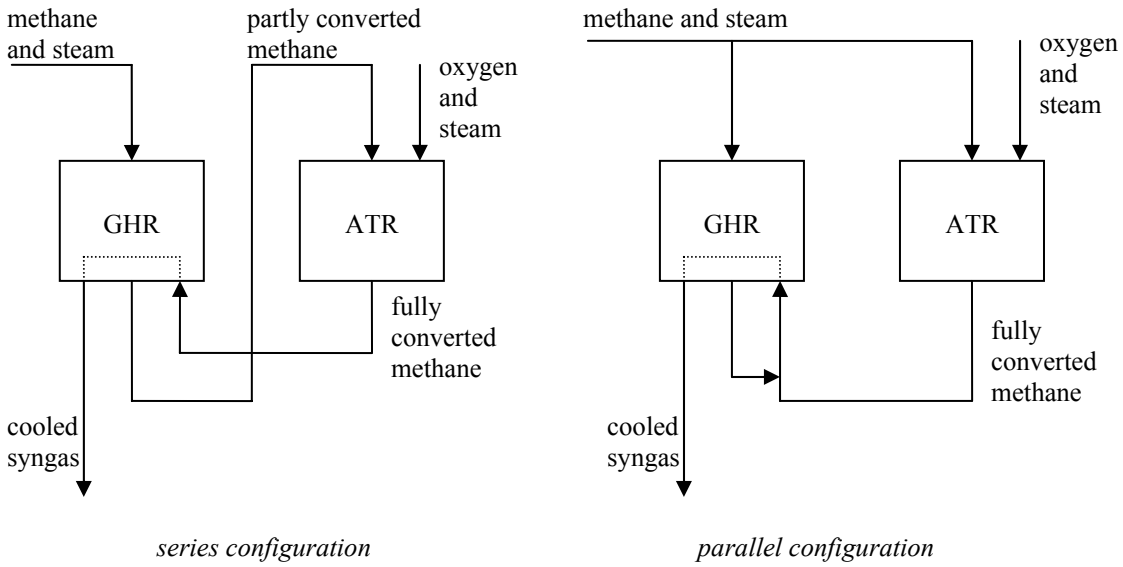

Figure 1-2: Series and parallel configuration of the combination of GHR and ATR.

The geometry of a gas heated reformer comes in various ways. The simplest geometry is a counter current heat exchanger with process gas entering the reactor tubes at the top and heating gas entering the shell side at the bottom. All advanced variations of this come from the need of increasing the heat flux to the tube wall or from mechanical and practical constraints. Examples of equipment that are used to increase the heat flux are longitudinal straight or spiral fins on the reactor tubes, shell side baffles, sheath tubes enclosing the reactor tubes, perforated sheath tubes, and "bayonet tubes" where the product gas leaves the reactor tube through a tube inside the reactor tube and brings heat into the reactor bed from its inside. In many cases these heat transfer enhancement equipments are only employed at the top of the GHR to avoid too high heat flux in the bottom section where the heating medium is at its warmest. This assures that the warmest section avoids too high tube skin temperatures. In that way the heat flux profile can be controlled and optimized without consequently shortening the tube life time.

1.4.2.1 Technological status

In 1984 Haldor Topsøe started the development of their first HER (Heat Exchange Reformer) which was heated with flue gas. This technology was later improved and in 1995 came the first H_2 plant based on the HTCR (Haldor Topsøe Convection Reformer). This reformer utilizes about 80 % of the fired duty. The catalyst beds in the HTCR are located in bayonet tubes (Figure 1-3a) and heated in counter current by flue gas on the outside of the tubes and by its off-gas on the inside (Figure 1-3b) (Haldor Topsøe AS, 2005a).

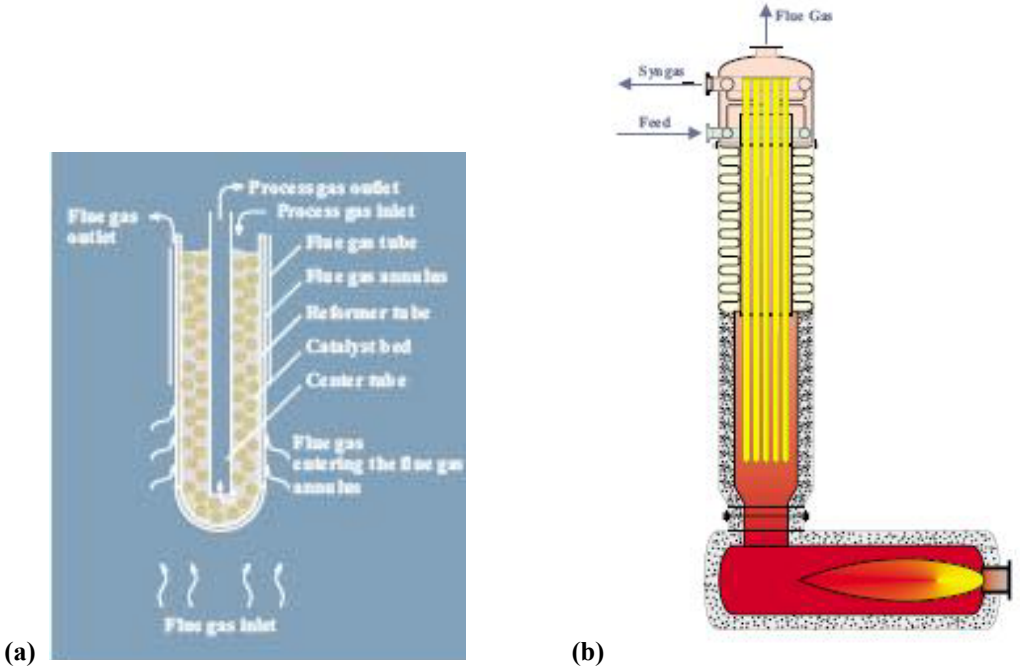

(a) (b)

Figure 1-3. The bayonet tube (a) and the layout (b) of the HTCR of Haldor Topsøe AS (Haldor Topsøe AS, 2005a).

In 1996 Sasol and Haldor Topsøe concluded an agreement to develop a gas heated heat exchange reformer (GHHER) in the Sasol Synfuel Complex in Secunda, South Africa (Loock et al., 2005). The unit was proven at commercial scale in parallel operation with one of the plant's 16 ATRs. The geometry of the GHHER is relatively complex with reactor beds both inside the reactor tubes and in the shell side volume around the tubes (Figure 1-4). The GHHER has been operating with a minimum steam-to-carbon ratio of 1.8. The heating gas (which is the product gas of the ATR) flows in counter current in an annular channel outside the reactor tubes. New materials were tested and showed good resistance to metal dusting. The technology was pronounced commercialized for Sasol in 2005.

Synetix developed their GHR in the 1980s (now taken over by Johnson Matthey) and it is now commercialized for ammonia and methanol production, operating with an ATR in series (Johnson Matthey, 2005). The GHR was in 1998 improved to the advanced gas heated reformer (AGHR), illustrated in Figure 1-5. The lower limit for steam-to-carbon ratio is 2.3 at 40 bars but two materials demonstration units are being tested in cooperation with Methanex for steam-to-carbon ratio 1.5 and 0.9 (and down to 0.6). They have found materials resistant to metal dusting for the ratio of 1.5.

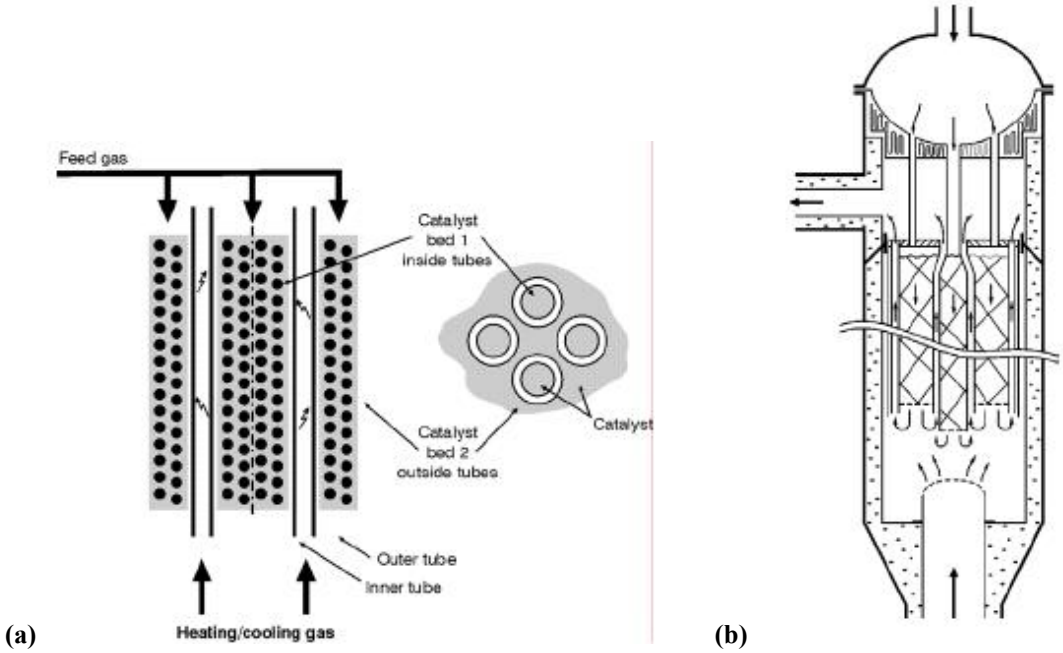

Figure 1-4. The configuration of the Topsøe / Sasol GHHER, illustrating the tubular and shell side catalyst beds and the hot syngas annular channel (a), and the overall layout (b) (Loock et al., 2005).

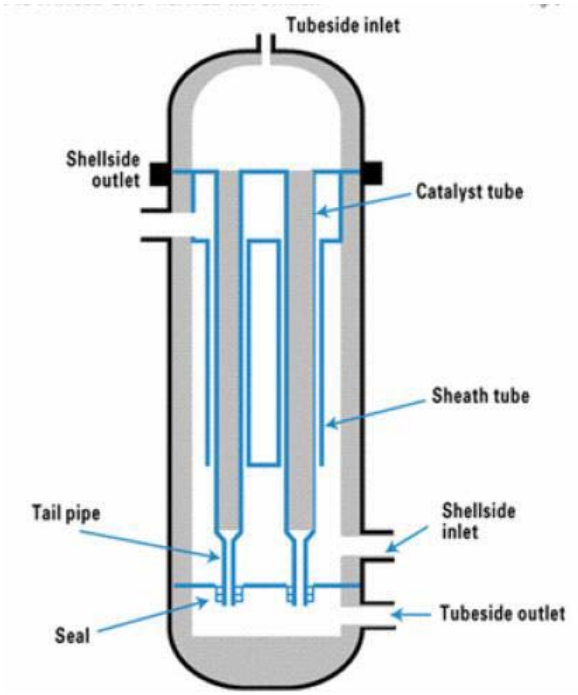

Figure 1-5. The AGHR of Synetix (Abbott and Crewdson, 2002).

APCI (Air Products) has commercialized their EHTR (Enhanced gas Heat Transfer Reforming) for H_2 production under moderate severity metal dusting conditions (APCI, 2002). Further research is in progress to extend the H_2 experience to

$H_2/CO = 2$, as required for GTL. The EHTR is in series or parallel configuration with an ATR or a POX reactor.

1.4.3 Challenges related to unwanted reduction of catalyst and tube material

1.4.3.1 Catalyst deactivation by coke formation

Coking reactions occur in parallel with the reforming reactions and are undesirable as they cause poisoning of the surface of the catalyst pellets. This leads to lower catalyst activity and the need for more frequently catalyst reloading.

The coking reactions are the CO-reduction, methane cracking and Boudouard reaction, given by the respective equilibrium reactions:

$$CO + H_2 \rightleftharpoons C + H_2O \tag{1-6}$$

$$CH_4 \rightleftharpoons C + 2\,H_2 \tag{1-7}$$

$$2\,CO \rightleftharpoons C + CO_2 \tag{1-8}$$

It can be seen from these reaction equations that low steam excess can lead to cirtical conditions causing coke formation, according to the principle of Le Chatelier. Equilibrium calculations of the coking reactions can be a useful tool for predicting the danger for catalyst poisoning but the reaction kinetics may nevertheless be so slow that coking is no concern. A complete analysis should therefore also involve kinetic expressions for these reactions.

Traditionally steam reformers have been run with a steam to carbon ratio of 2–4 to ensure low coking potential. It is desirable to reduce this ratio for methanol and F-T synthesis purposes as this will give great cost savings in form of smaller reformer units with higher methane conversion. New technical developments such as new noble metal catalysts and the use of prereformers, are continually decreasing the feasible S/C.

1.4.3.2 Metal dusting

Metal dusting is the corrosion of metals caused by the combined effect of carburization and oxidation. The carbon is formed by CO-reduction (Equation (1-6)) and the Boudouard reaction (Equation (1-8)) (Loock et al., 2005), and it will therefore not easily gasify when the steam content is low. Metal dusting is a serious damage that considerably shortens the life time of the reactor tubes and can even occur within a few weeks. There is great potential for metal dusting to occur in environments of fully converted syngas of high temperature and high pressure. When the syngas is cooled down sufficiently the kinetics of the carbon formation reactions are so slow that metal dusting is no longer a concern. Metal dusting occurs in the temperature range of 450–800 ºC.

Syngas cooling is normally carried out in a waste heat boiler, where high pressure steam is generated from the heat of the syngas. The steel temperature in the

waste heat boiler holds about the same temperature as the boiling water in the U-tubes, owing to the considerably higher resistance to heat transfer on the gaseous side than on the liquid side. This design is made to minimize metal dusting problems.

When syngas from an ATR is to be cooled down on the shell side of a GHR, metal dusting is of great concern. The GHRs commercialized today must thus be run with high steam-to-carbon ratio to operate safely. For methanol and F-T synthesis purposes the GHRs are not an economical option until the steam-to-carbon ratio can reach below about 1.5. New (and mainly higher priced) materials other than those used for the fired steam reformers must therefore be employed. Research is proceeding with various vendors to find the best suited material for the purpose of GHR.

2 EMPIRICAL CORRELATIONS FOR PACKED BED REACTOR MODELS

2.1 Introduction to packed bed reactor models

Empirical correlations for describing heat and mass transfer in packed beds have been studied theoretically and experimentally for the last 50 years (Dixon and Cresswell, 1979). A great number of researchers have contributed to the knowledge of the heat and mass transfer mechanisms and how these can be transferred to empirical correlations. The estimated parameters from these correlations show great scatters because of the various experimental methods and assumptions regarding the dependencies of the correlations. These dependencies are the geometry of the tube and pellets, the physical properties of the fluid and the fluid velocity. These variations in correlations will be discussed in this section. Also included are descriptions of the different types of models for the fixed bed reactor and forms of modelling of the gas phase radial heat transport and the solid phase mass transport.

Packed bed (or fixed bed) reactor models can be one- or two-dimensional and pseudo-homogeneous or heterogeneous. The pseudo-homogeneous model involves only one phase representing both the gas phase and the solid phase (i.e. the catalyst particles), and in the heterogeneous model both phases are present. The model to choose will depend on the expected particle internal gradients in the reactor system and on the requested precision of the simulation results.

Pseudo-homogeneous reactor models do not distinguish between the gas and solid temperatures in the fixed bed, but rather involve one pseudo-homogeneous phase with averaged properties for both phases. The reaction rates are calculated from bulk concentrations and temperatures and scaled with effectiveness factors to compensate for the concentration differences between the gas and internal in the particles. Heterogeneous models treat the mass and heat transport between the particles and the gas and within the particles, with reaction rates calculated from the particle internal concentrations. The mass and heat transport in the gas phase are modelled similarly as in a pseudo-homogeneous model, using empirically derived *effective* transport parameters representing the pseudo-homogeneous phase.

Heterogeneous models can also be built on a much more detailed level where it employs parameters describing mass and heat transport in and between each phase. This kind of model is generally too complicated for practical reactor simulations as it involves a great number of transport steps, and it is therefore not included in this section.

Most research on gas phase mass and heat transfer correlations in fixed beds is within pseudo-homogeneous models, though the heterogeneous models have some advantages in many cases where chemical reactions are present. Heterogeneous models are able to show the details of pellet internal concentrations and temperatures, which are necessary when evaluating the efficiency and the potential for deactivation of the catalyst. Efficiency factors can only be calculated by the use of heterogeneous models.

One-dimensional models are often sufficient when radial temperature and concentration gradients are negligible. The transport equations are then differentiated along the axial direction (the *z*-direction). The two-dimensional models are widely used as they also include the variations in the radial direction (the *r*-direction). Many fixed bed reactors involve strongly endothermic or exothermic reactions, and there may therefore be a significant temperature difference between the centre of the bed and the wall. In these cases the one-dimensional model will often be insufficient. Recent years three-dimensional modelling by the use of computational fluid dynamics has entered the field. These models include the physical domain of the pellets and are used to study the flow around the pellets.

The empirical based equations are often given on dimensionless form and expressed using the dimensionless parameters listed in Table 2-1. In this section the focus will be on two-dimensional models because this was chosen for the steam reformer model of Section 4. The correlations used to describe mass and heat transport in pseudo-homogeneous phase are discussed in Sections 2.2 and 2.3, respectively. These correlations are also employed in heterogeneous models. The modelling of solid phase transport in heterogeneous models is discussed in Section 2.4.

Table 2-1. Dimensionless groups used in mass and heat transport correlations.

The Nusselt number:	$Nu_w = h_w d_p \big/ \lambda_g$	(2-1)
The Biot number:	$Bi_{w,p} = h_w R_p \big/ \lambda_{er}$	(2-2)
The Reynolds number:	$Re_p = v_{z,s} \rho_g d_p \big/ \mu_g$	(2-3)
The Prandtl number:	$Pr = \mu_g c_{Pg} \big/ \lambda_g$	(2-4)
The Schmidt number:	$Sc = \mu_g \big/ \rho_g D_m$	(2-5)
The Sherwood number:	$Sh = k_g d_p \big/ \rho_g D_m$	(2-6)
The thermal Peclet number:	$Pe_p = v_{z,s} \rho_g c_{p_g} d_p \big/ \lambda_g = Re_p Pr$	(2-7)
The Peclet number for dispersion:	$Pe_E = d_p v_z \big/ E_{er}$	(2-8)
The Peclet number for diffusion:	$Pe_D = d_p v_z \big/ D_i$	(2-9)

2.2 The effective radial dispersion coefficient

Dispersion in a packed bed is the combined effect of molecular diffusion and convection in the gaseous bulk (Delgado, 2006). The volumetric molar flux caused by dispersion is modelled by a Fick's law analogy and the empirical correlation called the effective dispersion coefficient of the packed bed, E_e. For the case of flux in radial direction, this gives:

$$N_i = \frac{1}{r}\frac{\partial}{\partial r}\left(E_{er}\, r\, C_{tot}\frac{\partial x_i}{\partial r}\right) \tag{2-10}$$

According to Delgado (2006) the axial dispersion coefficient is about five times greater than the radial dispersion coefficient when the Reynolds number, Re_p, is greater than 10, and the dispersion coefficients become equal to the molecular diffusion coefficients when the Reynolds number is lower than approximately 1. At Reynolds numbers of 10^3–10^4, as usually seen in steam reformers (Rostrup-Nielsen et al., 1988), the axial dispersion is negligible compared to the axial convection. Therefore, only the radial dispersion coefficients will be treated in this section.

There are many empirical correlations for E_{er} available in literature. E_{er} is usually expressed in the form of the Peclet number for dispersion, denoted Pe_E in this thesis to avoid confusion with the thermal Peclet number defined in Equation (2-7). The definition of Pe_E is given in Equation (2-8).

One commonly used correlation is the one from Fahien and Smith (1955), as also recommended by Froment and Hofmann (1987). This correlation is valid for $10 < Re_p < 1000$:

$$Pe_E = \frac{10}{\varepsilon}\left[1+19.4\left(d_p/d_t\right)^2\right] \tag{2-11}$$

Delgado (2006) gave a thorough review of the empirical correlations for axial and radial dispersion coefficients available from literature and of the experimental methods used to obtain these correlations. New correlations that were developed showed more accurate predictions valid at a wide range. The recommended correlations for estimating the effective radial dispersion coefficient are dependent on a Peclet number based on the molecular diffusion coefficients (denoted Pe_D in this thesis and defined in Equation (2-9)). The effective dispersion coefficient for $Sc \le 550$ and $Pe_D \le 1600$ is:

$$\frac{1}{Pe_E} = \frac{1}{\tau_b}\frac{1}{Pe_D} + \frac{1}{12} - \left(\frac{Sc}{1500}\right)^{4.8}\left(\tau_b\, Pe_D\right)^{3.83-1.3\log_{10}(Sc)} \tag{2-12}$$

For $Sc \le 550$ and $Pe_D > 1600$:

$$Pe_E = 0.058\,Sc + 14 - \left(0.058\,Sc + 2\right)\exp\left(352\,Sc^{0.5}/Pe_D\right) \tag{2-13}$$

For $Sc > 550$ and $Pe_D \leq 1600$:

$$\frac{1}{Pe_E} = \frac{1}{\tau_b}\frac{1}{Pe_D} + \frac{1}{12} - 8.1\cdot 10^{-3}\left(\tau_b\, Pe_D\right)^{0.268} \tag{2-14}$$

For $Sc > 550$ and $Pe_D > 1600$:

$$Pe_E = 45.9 - 33.9\exp\left(-\frac{15\,Sc}{Pe_D}\right)^{4.8} \tag{2-15}$$

τ_b is the tortuosity factor for diffusion of the packed bed. Gunn (1969) suggested τ_b equal to 1.41, 1.93 and 1.8 for spheres, cylinders and hollow cylinders, respectively.

2.3 Radial heat transport parameters

2.3.1 Introduction to empirical correlations

The pseudo-homogeneous model is a simplification of the situation in a packed bed where the heat transport mechanisms involved are too complex to be described separately. These mechanisms are therefore described by a lumped parameter system where the parameters are decided from experiments. Heterogeneous models are usually based on the same simplifications regarding radial transport mechanisms in the reactor and use the same correlations for wall heat transfer and effective radial heat transport. The correlations discussed in the following describe how heat is transferred *radially* in the gas phase in a fixed bed. The mechanisms involved in radial heat transport were listed by Borman et al. (1992):

1. conduction in the solid phase
2. conduction in the gas phase
3. conduction through the film around the contact surface of two adjacent particles
4. conduction between neighbouring particles
5. radiation between particles
6. convective transport between solid phase and gas phase
7. heat dispersion in the gas through mixing of gas streams
8. convective transport between the tube wall and the gas phase
9. conduction through the contact points of solid phase and tube wall
10. radiation between solid phase and tube wall
11. conduction through the tube wall

Most of the heat transfer experiments reviewed here were performed with non-reacting systems where air was the test gas and flow conditions were mild. There is a wide spread in the results found in literature, especially at laminar flow conditions. The correlations developed are typically within 30 % accuracy and limited to the conditions and reactor setup of the experiment. The heat transfer parameters are generally expressed in form of dimensionless groups and constants. There are slightly different opinions on which variables the parameters depend. These are variables describing tube

and pellet geometry, flow and fluid physical data. There are also different views on what kind of correlations and what type of model are best suited. This review goes through many of the empirically developed correlations, together with some of the discussions within the field. It is not possible to draw any final conclusion as to which model and what correlations that best describe a reactor. Nevertheless some research within this area stands out as more reliable or with more physically based theory than others. These articles will be emphasised here.

The temperature difference over the bed radius is mostly smooth but has a relatively large increase or drop in the outer area of the tube radius where the heat is conducted further through the tube wall. A two-dimensional model taking the radial and axial variations into account can describe this phenomenon. Within the two-dimensional model there is the *two-parameter* model and the *one-parameter* model. These two models have different approaches to describe the sudden increase or drop in temperature appearing in the immediate vicinity of the wall. This increase is explained by the naturally looser pellet packing along the wall resulting in a bypass stream of higher velocity than the mean velocity (Achenbach, 1995; Delmas and Froment, 1988; Froment and Bischoff, 1990). The two-parameter model describes the temperature profile throughout the bed by an effective radial thermal conductivity (λ_{er}) and the temperature increase at the wall by a jump condition using a convective heat transfer coefficient (h_w). This heat transfer coefficient represents the heat transfer resistance in an unmixed gas film at the tube wall (*the film theory*) and this gives a discontinuous temperature profile in the transition from gas to tube wall. In the one-parameter model on the other hand, only an effective radial thermal conductivity is used and a continuous, large temperature difference at the wall results because of higher bed porosity at the wall than in the bed centre. The bed porosity in the two-parameter model is usually taken as a constant value.

The two-parameter model is widely used though the correlations from literature scatter widely, especially at low Reynolds numbers. Some authors are of the opinion that the jump condition of the two-parameter model makes no physical sense at low Reynolds numbers where there is a gradual change in temperature at the wall. Under turbulent conditions, however, the flow character changes to form an unmixed sub-layer at the wall where the heat transfer is well described by the heat transfer coefficient. This relation to the flow characteristics is easily seen in the work of Tsotsas and Schlünder (1990) who illustrate in a Nu_w–Re_p diagram a collection of experimental data from different independent publications. These data show a wide spread at low Reynolds numbers and a clear relation between Re_p and Nu_w at increasing Reynolds numbers. They conclude that the two-parameter model therefore is undoubtedly suitable at turbulent flow conditions.

Recent research within one-parameter models has given interesting input to the discussion of the physical meaning of the heat transfer coefficients and the soundness of the film theory when moving from high to low Reynolds numbers (Tsotsas and Schlünder, 1990; Vortmeyer and Haidegger, 1991; Winterberg et al., 2000). Much of this later theory can to a great extent explain the data scatter in the parameters of the two-parameter model. It can therefore be worth considering changing from the well-

known and accepted two-parameter model to a one-parameter model when working with laminar flow in two-dimensional fixed bed models.

The symbols in the equations in this section have been changed from the original symbols in the referred literature to be consistent with symbols used in this thesis. h_w and λ are used for the heat transfer coefficient and the thermal conductivity, respectively, while α_w and k are also commonly used in referred literature. Subscripts w, r, and e refer to the wall, radial direction and effective parameter, respectively.

2.3.2 The two-parameter model

The effective radial thermal conductivity, λ_{er}, accounts for the first seven heat transport mechanisms given in the list of Section 2.3.1 (Borman et al., 1992). The first six mechanisms are modelled through a static contribution and number seven is given by a dynamic contribution. The convective heat transfer coefficient, h_w, is supposed to cover the rest of the mechanisms on the list. λ_{er} and h_w are found in the two-dimensional pseudo-homogeneous energy equation with boundary conditions:

$$\rho_g c_{p_g}\left[v_{z,s}\frac{\partial T}{\partial z}+v_{r,s}\frac{\partial T}{\partial r}\right]=\frac{\partial}{\partial z}\left[\lambda_{ea}\frac{\partial T}{\partial z}\right]+\frac{1}{r}\frac{\partial}{\partial r}\left[r\lambda_{er}\frac{\partial T}{\partial r}\right]+\rho_s(1-\varepsilon)\sum_j\left(-\Delta H_j\right)r_j \quad (2\text{-}16)$$

$$\left.\frac{\partial T}{\partial r}\right|_{r=0}=0 \quad (2\text{-}17)$$

$$-\lambda_{er}\left.\frac{\partial T}{\partial r}\right|_{r=R}=h_w\left(T(R)-T_w\right) \quad (2\text{-}18)$$

The axial term λ_{ea} is often disregarded as it gives little effect compared to the axial convection (as in the case of the GHR reactor model of Section 4.4). This model uses a constant bed void fraction, ε, and an effective thermal conductivity, λ_{er}, to describe the radial conduction in the pseudo-homogeneous phase. This effective conductivity includes conduction in both the solid pellets and the gas phase and also some contribution from turbulence and radiation between pellets.

Most of the empirical correlations for h_w and λ_{er} found in the literature were as mentioned obtained from experiments in packed beds without chemical reaction. The question of the influence of the reaction on h_w and λ_{er} was examined by Wijngaarden and Westerterp (1989). They concluded that there should be no reason why these empirical parameters should be different in a packed bed reactor than in a non-reacting system.

Another important question is if the same parameters h_w and λ_{er} can be used in both pseudo-homogeneous and heterogeneous models. Wijngaarden and Westerterp (1989) compared a pseudo-homogeneous and a heterogeneous two-dimensional model to investigate the consequences of the basic assumption of pseudo-homogeneous modes: the pellet temperature is equal to the gas temperature, i.e. there are no heat transport limitations between gas and solid phase and internally in the pellets. For their study of

wall-cooled fixed beds, the h_w and λ_{er} were assumed obtained by fitting experimental gas temperature profiles with a pseudo-homogeneous model in a *non-reacting* system. In a pseudo-homogeneous model of a fixed bed reactor the reaction rates are predicted from gas temperatures, resulting in over-prediction of the reaction rates for endothermic reactions compared to results from a heterogeneous model. The heterogeneous character of the reactor bed may be lumped into h_w and λ_{er} to compensate for these erroneous reaction rates. Wijngaarden and Westerterp (1989) defined a characteristic parameter ζ which indicates the change in reaction rate, $r_j(T_g)$, when (incorrectly) calculated from the gas temperature (pseudo-homogeneous model), relative to the reaction rate, $r_j(T_p)$, calculated from pellet temperature (heterogeneous model):

$$\zeta_j = \frac{r_j(T_p) - r_j(T_g)}{r_j(T_p)} \tag{2-19}$$

If a pseudo-homogeneous model is used for a reacting system the parameters h_w and λ_{er} should be multiplied with the factor $(1-\zeta)$ to compensate for the assumption of solid temperature equal to gas temperature. This will increase h_w and λ_{er} in the example of endothermic reactions.

The two parameters h_w and λ_{er} are empirically obtained and must be carefully treated as such. Thus one must always observe under what conditions the correlations have been produced.

This means that one must use correlations developed within the relevant geometrical sizes and flow conditions, and that the correlations used for h_w and λ_{er} originate from the same experiments.

2.3.2.1 The wall heat transfer coefficient, h_w

Many researchers have performed experiments to derive empirical correlations for the wall heat transfer coefficient, h_w, together with the effective radial thermal conductivity, λ_{er}. h_w is often expressed in form of the Nusselt number or sometimes the Biot number and usually given as a function of the Reynolds number or the molecular Peclet number and maybe also the tube-to-particle diameter ratio and the Prandtl number. The definitions of the dimensionless groups are given in Table 2-1. A general, dimensionless correlation can be represented by the equation

$$Nu_w = a + b\left(d_t/d_p\right)^c \, Re_p^d \, Pr^e \tag{2-20}$$

where the letters *a* to *e* represent empirical constants or parameters. The correlations included in this review are for simplicity summarised in Table 2-2, and many of them take this form. The conditions for which the correlations are valid are also shown in the table.

Table 2-2: Collection of correlations for h_w from literature.

Reference:	Equation:		Validity:
Borkink and Westerterp (1992)	$Nu_w = 17.94 + 18.4 \cdot 10^{-3} \frac{Pe_p}{\varepsilon}$	(2-21)	Raschig rings $200 < Pe_p/\varepsilon < 900$ $d_p = 6.2$ mm $d_t/d_p = 8–16$
Borman et al. (1992)	$Nu_w = 2.29\, Re_p^{0.41}$	(2-22)	Raschig rings $150 < Re_p < 2000$
De Wasch and Froment (1972)	$Nu_w = h_w^0 + 0.01339\left(d_t/d_p\right) Re_p$	(2-23)	Cylinders $100 < Re_p < 400$
Dixon and Cresswell (1979)	$Bi_{w,p}\left(d_p/R_t\right) = 3.0\, Re_p^{-0.25}$	(2-24)	$Re_p > 40$
Dixon et al. (1984)	$Nu_w = \left[1 - 1.5\left(d_p/d_t\right)^{1.5}\right] Re_p^{0.59} Pr_p^{1/3}$	(2-25)	Spheres $100 < Re_p < 8000$ $3 < d_t/d_p < 12$
Li and Finlayson (1977)	$Nu_w = 0.16\, Re_p^{0.93}$	(2-26)	Cylinders $20 < Re_p < 800$ $0.03 < d_p/d_t < 0.2$
Li and Finlayson (1977)	$Nu_w = 0.17\, Re_p^{0.79}$	(2-27)	Spheres $20 < Re_p < 7600$ $0.05 < d_p/d_t < 0.3$
Martin and Nilles (1993)	$Nu_w = \left(1.3 + 5\frac{d_p}{d_t}\right)\frac{\lambda_{er}}{\lambda_g} + 0.19\, Re_p^{0.75} Pr_p^{0.33}$	(2-28)	Spheres, cylinders and cylinders with hole $1 < Pe_p < 2 \cdot 10^4$ $1.17 < d_t/d_p < 51$
Peters et al. (1988)	$Nu_w = 3.8\left(d_t/d_p\right)^{0.39} Re_p^{0.5} Pr_p^{1/3}$	(2-29)	Cylinders $100 < Re_p < 8000$ $0.1 < d_p/d_t < 0.6$
Peters et al. (1988)	$Nu_w = 4.9\left(d_t/d_p\right)^{0.26} Re_p^{0.45} Pr_p^{1/3}$	(2-30)	Spheres $100 < Re_p < 8000$ $0.1 < d_p/d_t < 0.6$
Wijngaarden and Westerterp (1992)	$Bi_{w,p} = 2.9\, Pe_p^{-0.40}$	(2-31)	Raschig rings $25 < Pe_p < 350$

Li and Finlayson (1977) found a unique Nu_w-Re_p dependency based on data from literature. They eliminated those experimental data influenced by length effects, which is the pre-heating of the inlet gas caused by conduction along the wall from the heated test section to the unheated calming section (Dixon, 1988). They re-examined the remaining data to find correlations for both one- and two-dimensional models and for

spherical and cylindrical packing. In their review article Kulkarni and Doraiswamy (1980) recommend these correlations because of the absence of length effects.

Derkx and Dixon (1997) compared the simulation results from using the correlation of Li and Finlayson (1977) and from Dixon and Cresswell (1979) for a two-dimensional pseudo-homogeneous reactor model at low to moderate Reynolds numbers. The correlation of Dixon and Cresswell (1979) was best suited for these cases. Tsotsas and Schlünder (1990) state that the analysis should be based on physical arguments rather than the more questionable mathematical approach proposed by Li and Finlayson (1977).

Many authors are of the opinion that the correlations of Equations (2-21), (2-22) (2-26) and (2-27) are incomplete as Nu_w also should depend on d_t/d_p and λ_s (Dixon and Cresswell, 1979; Dixon and van Dongeren, 1998; Tsotsas and Schlünder, 1990; Vortmeyer and Haidegger, 1991; Derkx and Dixon, 1996) and on d_t/L when Re_p is low (Tsotsas and Schlünder, 1990). Nevertheless Dixon (1988) states that the wall effects (i.e. the dependence on d_t/d_p) is less important at d_t/d_p larger than about 12 to 15.

Correlations taking the d_t/d_p ratio into account are derived by, among others, De Wasch and Froment (1972), Dixon and Cresswell (1979), Dixon et al. (1984), Martin and Nilles (1993) and Peters et al. (1988). Some of these correlations also include the term $Pr^{1/3}$, but many of the underlying experiments are done without varying the parameters involved in the Prandtl number and give therefore no experimental basis for including this term. A term for stagnant conditions, as the a in Equation (2-20), is in some cases also included (Borkink and Westerterp, 1992; De Wasch and Froment**,** 1972; Martin and Nilles, 1993), and this assures that heat transfer also exists at zero flow.

Dixon and Cresswell (1979) derived their correlation theoretically without any use of empiricism. h_w is expressed by the Biot number and uniquely correlated with the Reynolds number. This should predict h_w for a wide range of conditions (for $Re_p > 40$). The authors claim that this unique correlation stands in contrast to the more common Nu_w versus Re_p correlations because Nu_w should also depend on several other factors, such as d_t/d_p, λ_s, h_{fs}, λ_{rf} and h_{sw}.

Dixon et al. (1984) determined a correlation by analogy with mass transfer experiments. The experiments were performed with water. The heat transfer coefficient expressed in terms of the Nusselt number follows the same correlation as for the mass transfer coefficient given by the Sherwood number. The results showed good agreement with data from heat transfer experiments. For $d_t/d_p = 3.3$ the correlation was in good agreement with heat transfer data for Reynolds numbers up to 8000, but for $d_t/d_p > 7.4$ the authors have only shown good agreement at $Re_p < 500$.

The common way of varying the physical gas properties under heat transfer experiments is to use different gases. Wijngaarden and Westerterp (1992) carried out experiments with altering physical properties by varying the total pressure from 1 to 10 bar. Their resulting empirical correlations for h_w and λ_{er} were in satisfactorily agreement with compared literature data.

2.3.2.2 The effective radial thermal conductivity, λ_{er}

An *effective* thermal conductivity of a pseudo-homogeneous phase is different from a thermal conductivity, which is a material property, as it is also dependent on the geometry (i.e. the shape and size) of the particles and the flow and heat transfer conditions, given by Re_p and Pe (Achenbach, 1995). Most of the correlations developed for effective thermal conductivities involve also a term representing the contribution from stagnant gas (λ^0_e) to ensure non-zero λ_e at stagnant conditions. The dynamic term is usually expressed as function of the Reynolds number or the Peclet number which both describe the flow conditions.

The empirical parameters from the references discussed in Section 2.3.2.1 are listed in Table 2-3 below. From these expressions it is seen that there is a wide variety in how λ_{er} is correlated. This is due to the fact that there is no general understanding of its dependencies, compared to the case of h_w.

Table 2-3. Empirical correlations for the effective radial thermal conductivity for the two-parameter model.

Reference:	Equation:		Validity:
Borkink and Westerterp (1992)	$\frac{\lambda_{er}}{\lambda_g} = 4.5 + \frac{Pe_p}{4.2}$	(2-32)	alumina Raschig rings d_p = 6.2 mm d_t/d_p = 8–16 $100 < Pe_p < 450$
Borman et al. (1992)	$\lambda_{er} = 0.37 + 2.54 \cdot 10^{-3} Re_p$	(2-33)	Raschig rings $50 < Re_p < 1500$
De Wasch and Froment (1972)	$\lambda_{er} = \lambda^0_{er} + \frac{0.0029}{1 + 46\left(d_p/d_t\right)^2} Re_p$	(2-34)	Cylinders $100 < Re_p < 400$
Dixon and Cresswell (1979)	$\lambda_{er} = \lambda_{gr} + \lambda_{sr}\left(1 + \frac{8\,\lambda_{gr}}{h_{wg}\,d_t}\right)\beta$	(2-35)	$Re_p > 40$
	$\beta = \left[\frac{\left(1-\varepsilon\right)\left(d_t/d_p\right)^2}{1 + \lambda_{sr}\,16/3\left(\left[h_{gs}\,d_p\right]^{-1} + 0.1\lambda_p^{-1}\right)}\right]$	(2-36)	
Peters et al. (1988)	$\frac{\lambda_{er}}{\lambda_g} = \frac{\lambda^0_{er}}{\lambda_g} + \frac{Re_p\,Pr}{Pe_m}$	(2-37)	$100 < Re_p < 880$
	$Pe_m = 3.2 + 49.4\,d_p/d_t$	(2-38)	
Wijngaarden and Westerterp (1992)	$\frac{\lambda_{er}}{\lambda_g} = 21 + 0.23\,Pe_p$	(2-39)	$25 < Pe_p < 350$

Lemcoff et al. (1990) conclude that the effective radial thermal conductivity, λ_{er}, decreases with increasing bed length if the axial dispersion term is not included in the

energy equation. However, if the axial effective thermal conductivity, λ_{ea}, is taken into account, no dependency of λ_{er} on L will be observed. Still, for sufficiently long beds, the contribution of λ_{ea} does not influence the results of estimating λ_{er} and h_w.

Dixon and van Dongeren (1998) found that λ_{er} is dependent on d_t/d_p and not on d_t and d_p alone. Winterberg et al. (2000) point out that this dependency often is incorrectly overlooked. According to Borkink and Westerterp (1992) λ_{er} is also strongly influenced by the shape of the packing material.

2.3.3 The one-parameter model

As described in the introduction of Section 2.3.1 the one-parameter model has a different approach than the two-parameter model for describing the difference in wall temperature and the gas temperature close to the wall. Instead of describing this phenomenon by a jump condition as in Equation (2-18), it can rather be described as a continuous temperature profile with a large rise or drop at the wall caused by the looser catalyst packing at the wall than in the bed centre.

If the porosity of the bed is given by a radial distribution function rather than as a constant (the ε in Equation (2-16)), a boundary condition of one of the types

$$T(R) = T_w \tag{2-40}$$

$$\lambda_s \left.\frac{\partial T_s}{\partial r}\right|_R = \lambda_{er} \left.\frac{\partial T_g}{\partial r}\right|_R \tag{2-41}$$

instead of Equation (2-18) will result in a radial temperature profile which is continuous all the way to the wall but still shows the sudden increase or drop close to the wall. The remaining boundary condition is as in the two-parameter model, shown in Equation (2-17).

The one-parameter model can take different forms. Some are based on an overall effective radial thermal conductivity, λ_{er}, as in the work of De Wasch and Froment (1972):

$$\lambda_{er} = \lambda_{er}^0 + \frac{0.0026}{1+120\left(d_p/d_t\right)^2} Re_p \tag{2-42}$$

This model assumes constant bed porosity as in the two-parameter model, and the simulated radial temperature profile will therefore not show the large increase or drop at the wall that is found experimentally. One-parameter models should therefore rather have a radially distributed porosity profile that gives looser packing at the wall than in the bed centre. This will change the velocity profile at the wall and thereby increase the heat transfer resistance giving the large temperature difference as desired.

Delmas and Froment (1988) compared a model accounting for the radial porosity profile with a plug flow model of uniform porosity distribution. They obtained significant differences in the results of the two models.

A correlation for λ_{er} in the one-parameter model was also developed by Winterberg et al. (2000). The correlation is based on experimental data for spherical particles, and its parameters $K_{1,h}$, $K_{2,h}$ and n_h are valid for $5.5 < d_t/d_p < 65.0$ and $24 < Re_p < 2740$:

$$\lambda_{er}(r) = \lambda_{bed}(r) + K_{1,h}\, Pe_0 \frac{v_c}{v_m^0} f(R-r)\, \lambda_f \tag{2-43}$$

$$f(R-r) = \begin{cases} \left(\dfrac{R-r}{K_{2,h}\, d_p} \right)^{n_h} & \text{for } 0 < R-r \le K_{2,h}\, d_p \\ 1 & \text{for } K_{2,h}\, d_p < R-r \le R \end{cases} \tag{2-44}$$

The bed is described by a radial porosity distribution function, $\varepsilon(r)$, which is found in the energy equation (Equation (2-16)).

Simulation results using this model and from the two-parameter model of Martin and Nilles (1993) were compared on the basis of experimental data (Winterberg and Tsotsas, 2000a). The one-parameter model was favoured over the two-parameter model as its predictive performance was somewhat better, its description of all aspects of the wall effect is more realistic, and also as it has better possibilities for considering temperature dependent properties. The model was also developed further to include the parameters that fit data for cylindrical pellets (Winterberg and Tsotsas, 2000b).

2.3.4 Discussions on two- and one-parameter models

Despite the many publications within this field there still is no general agreement about which models describing the heat transport resistances in a fixed bed are physically most correct.

According to Tsotsas and Schlünder (1990) there exists no resistance to heat transport at the wall at low Peclet numbers (which is correlated to the Reynolds number as shown in Equation (2-7)). This means that the heat transfer coefficient at the wall, h_w, has no physical meaning. They interpret the meaning of h_w at low Peclet numbers as a lumped parameter, or a mathematical operator, accounting for axial dispersion of heat and the lateral maldistribution of gas velocity and of thermal conductivity. Alternatively, h_w could simply compensate for experimental errors. The authors show how the heat transfer mechanisms differ at low and at high Peclet numbers: at low Pe_p the main mechanism is molecular conduction while at high Pe_p the main mechanism is the mixing of the fluid in the voids. The critical Peclet number defining the transition from one of these heat transfer mechanisms to the other is about 30-300 for fixed beds with a gaseous fluid phase. In the high range of Pe_p the heat transport in the unmixed sub-layer in the immediate vicinity of the wall takes place by molecular conduction. The authors show that the thickness of this unmixed sub-layer is much smaller than the particle diameter, which justifies modelling h_w by a boundary condition of the type shown in Equation (2-18).

Tsotsas and Schlünder (1990) re-evaluated low Pe_p heat transport data from literature which showed great scatter in a Nu_w–Re_p diagram. They presented them in a $\overline{NU}_{d_t} - GZ_{d_t}$ diagram, which eliminated the dependence on the aspect ratio L/d_t and the diameter ratio d_t/d_p and showed perfect correlation. The new dimensionless group $\overline{NU}_{d_t}$ is defined on basis of tube diameter and radial mean temperature and arises from data integrated along the tube length, as seen in Equations (2-45) and (2-46), respectively:

$$NU_{d_t} = \frac{h\, d_t}{\lambda_{er,m}} = \frac{\dot{q}_{r=R_t}}{T_w - T_m} \frac{d_t}{\lambda_{er,m}} \tag{2-45}$$

$$\overline{NU}_{d_t} = \frac{1}{L} \int_0^L NU_{d_t}\, dz \tag{2-46}$$

The heat transfer coefficient h is defined on basis of radial mean temperature, T_m, in difference from the wall heat transfer coefficient, h_w, which is defined on basis of the fluid temperature close to the wall, $T(R)$. The Graetz number, GZ_{d_t} shown in Equation (2-47), is defined from the aspect ratio, the diameter ratio and the radial mean of the effective Peclet number, $Pe_{p,m}$ (Equation (2-48)):

$$GZ_{d_t} = \frac{Pe_{p,m}}{L/d_t} \frac{d_t}{d_p} \tag{2-47}$$

$$Pe_{p,m} = v_{zs,m}\, \rho_g\, c_{P_g}\, d_p \,/\, \lambda_{er,m} \tag{2-48}$$

Consequently the authors recommend experimental data to be presented in a $\overline{NU}_{d_t} - GZ_{d_t}$ diagram rather than in a Nu_w–Re_p diagram. On the other hand, at high Pe_p they find that experimental results presented in the form of Nu_w correlate well with Re_p or Pe_p, also even if they are originating from mass transfer experiments. If the two-parameter model is to be used at turbulent conditions, the authors recommend the correlation for h_w developed by Dixon et al. (1984).

Vortmeyer and Haidegger (1991) compared the two- and one-parameter model and a modified one-parameter model at the conditions $d_t/d_p = 10$ and $25 < Re_p < 32$. The simulations showed that the one-parameter model was closest to experimental results and that the two-parameter model seemed only applicable at high Reynolds numbers. This is consistent with the discussion by Tsotsas and Schlünder (1990).

Papageorgiou and Froment (1995) studied the one-parameter model by comparing pseudo-homogeneous models with heterogeneous models using porosity and effective thermal bed conductivity as functions of tube radius. They believe that the plug-flow assumption with the use of h_w is inadequate when d_t/d_p is low, due to larger radial variations in voidage. In these cases the fluid flow characteristic is closely linked to the variations in void fraction and is thereby defining the way the heat and mass are transferred throughout the bed.

2.4 Solid phase transport in heterogeneous models

2.4.1 Interphase transport

In fixed bed reactors mass and heat are continuously interchanged between the gas bulk and the catalyst pellet surface. Depending on process conditions there are varying degrees of resistance to mass and heat transport between the gaseous phase and the solid phase. This interphase resistance can be modelled as an unmixed gas film surrounding the pellet, where the extent of concentration and temperature gradients are decided from empirical mass and heat transfer coefficients, respectively. These coefficients are deduced from experiments and are expressed as functions of the physical conditions. Figure 2-1 illustrates this linear concentration or temperature drop across the gas film surrounding a spherical particle.

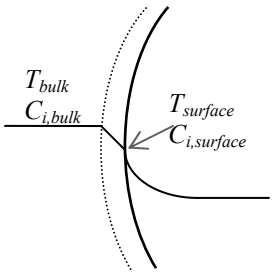

Figure 2-1. Illustration of resistance to mass and heat transport in the fluid film.

The mass and heat transfer coefficients are involved in the component balance equations, in the total mass balance equation and in the heat balance equation in both the bulk model and the solid phase model (also referred to as the pellet model). In the bulk equations the coefficients are found in the source terms for mass and heat, and in the pellet equations they are defining the boundary conditions at the pellet surface. This is seen in Equations (4-25), (4-28) and (4-32), and in Equations (4-41) and (4-44), respectively.

2.4.2 Intraparticle transport

The concentration and temperature gradients in the porous catalyst pellets of a fixed bed reactor may be modelled by the use of effective diffusion coefficients and effective thermal conductivities, respectively.

Temperature gradients may be seen in the particle when the effective thermal conductivity of the solid phase is low and heat is generated or consumed by reaction in the pellets. The effective thermal conductivity is a constant value characteristic for the material and the particle porosity and tortuosity and will therefore not be further discussed here.

When diffusion is the only transport mechanism in the solid phase the mass transfer resistance is modelled by using an effective diffusivity. The concentrations will decrease towards the centre of the particles when the diffusion limitations are significant.

In porous solids both Knudsen diffusion and molecular diffusion (also called bulk or free space diffusion) may be important. The Knudsen diffusivity describes the limitations to transport caused by the molecules colliding with the pore wall, and the molecular diffusivity arises from collisions only between molecules. The Knudsen

diffusivity is therefore dominant in small pores having diameters much smaller than the mean free path length of the molecules. The bulk diffusivity dominates in larger pores and at high pressures.

The correlation for the Knudsen diffusivity is a function of the pore diameter d_0 (Krishna and Wesselingh, 1997):

$$D_{Ki} = \frac{d_0}{3}\sqrt{\frac{8RT}{M_i}} \tag{2-49}$$

The molecular diffusivity may be calculated from empirical correlations. The different correlations found in literature will not be reviewed here, but some of them are evaluated in Section 5.1.3.

Diffusion in porous media has traditionally been modelled by expressing the component flux N_i by Fick's law, although the dusty gas model is now generally considered as a better approach (Krishna and Wesselingh, 1997). Veldsink et al. (1995) compared these models by modelling mass transport combined with chemical reactions in porous media using the Fick model, the extended Fick model and the dusty gas model. The extended Fick model includes an expression for the total pressure gradient in the porous pellet using Darcy's law. They concluded that the Fick model, on simplified form,

$$N_i = -\frac{D_i^e P}{RT}\frac{\partial x_i}{\partial y} = -\frac{D_i^e}{RT}\frac{\partial\left(x_i P\right)}{\partial y} \tag{2-50}$$

was adequate for estimating interfacial fluxes for a pellet with a plane, line or point symmetry. The co-ordinate y represents the pellet depth and D_i^e is the effective diffusivity of species i. Elnashaie and Abashar (1993) compared simulations for a steam reformer when using the dusty gas model and the Fick model. They concluded that the models were in good agreement for low steam-to-methane ratios and that the Fick model was satisfactory for steam reformer models at these conditions. Based on the conclusions of these two studies and on the fact that the dusty gas model requires considerably more computational time (Veldsink et al., 1995), the Fick model was assumed suitable in the heterogeneous reactor model of this thesis.

2.4.2.1 Intraparticle gradients of total pressure

The reactions involved in steam methane reforming increase the number of moles in the gas mixture. This means that the total pressure will build up in the catalyst pellet, although in most cases with negligible effects on the component diffusion fluxes.

Kehoe and Aris (1973) came to the conclusion that pressure gradients have no significant effect on the pore diffusion, meaning that the momentum balance can be ignored from the pellet model. Burghardt and Aerts (1988) evaluated the internal pressure change in a pellet with reaction and mass transfer by Knudsen diffusion, molecular diffusion and viscous convective flow. They drew the conclusion that the pressure changes are probably so small under normal industrial conditions that they can

be neglected in reactor models. Veldsink et al. (1995) came to the same conclusion, which also is referred to in Section 2.4.2. Nan et al. (1995) used the dusty gas model to look into the consequence of including the intraparticle forced convection. They found that the pressure gradients were most significant in the Knudsen diffusion regime where the effectiveness factors of the reactions are enhanced by the intraparticle forced convection.

The conclusions summarized above are brought forward to the heterogeneous reactor model of this thesis to justify the simplifications of the pellet model. Using Fick's law for diffusion the expression for the molar flux is given by:

$$N_i = -\frac{D_i^e P}{RT}\frac{\partial x_i}{\partial y} + x_i \sum_i N_i \tag{2-51}$$

In steam reformers the increase in molar number resulting from the steam reforming reactions, causes a change in density which is synonymous with a net convective transport out of the pellet. This is disregarded in the heterogeneous reactor model of Section 4.4.1.2, based on the discussion above. This eliminates the second term of Equation (2-51) and leads to the simplified Fick equation of Equation (2-50).

The intraparticle component balances in the heterogeneous model of Section 4.4.1 (Equation (4-39)) are expressed with basis on partial pressures, using this simplified Fick diffusion term. Even if total pressure gradients in the particles are disregarded, an increase in total pressure towards the pellet centre is allowed for by solving the component balances for all of the six participating components. When all balance equations are solved independently and the total moles increase due to reaction, the resulting sum of the partial pressures will also increase. This assures the total mass continuity of the overall system, but is an inherent inconsistency of the model.

2.5 Application on steam reformer models

The Reynolds number, Re_p, in steam reformers is normally ranging from 1000 to 10000 (Rostrup-Nielsen et al., 1988), and only empirical correlations valid for this high range are considered for the model developed. This eliminates many of the correlations listed in Section 2.3.

The dominating transport limitations in the steam reforming process result from the intraparticle mass transport and the interphase heat transport (Rostrup-Nielsen et al., 1988). Most numerical models previously made for steam reformer tubes are based on the assumption that all other resistances are negligible compared with the resistance from intraparticle diffusion (De Groote and Froment, 1995; Elnashaie et al., 1992; Ferreira et al., 1992; Pedernera et al., 2003; Piña et al., 2001; Soliman et al., 1988; Xu and Froment, 1989b). Interphase thermal resistance was included in the model of De Deken et al. (1982) and was concluded negligible. The pellet transport limitations have been investigated in this thesis by including models for both interphase and intraparticle mass and heat transport resistances.

The operational pressure in steam reformers is above the limit for where the diffusion coefficient is dependent on the Knudsen diffusion (Rostrup-Nielsen, 1984). Only the molecular diffusion is therefore modelled in the steam reformer model of Section 4.4. In this diffusion regime the elimination of modelling the intraparticle forced convection was concluded sufficient by Nan et al. (1995), as also emphasized in Section 2.4.2.1.

3 CHOICE OF GAS RADIATION MODEL

There exist several different heat radiation models that might be appropriate for the annulus model of this thesis. The advantages and drawbacks connected to these models were therefore evaluated before selecting a model for the annular channel. This evaluation is given here.

The simplest approximation is the use of a radiative heat transfer coefficient, h_{rad}, which acts as a radiative term in addition to the convective heat transfer coefficient, h or h_w (for one- and two-dimensional models, respectively). This approach was chosen for the heating section model of Stehlík (1995) and of Yu and Sosna (2001). It was decided not to use this kind of approximation due to the wish of a more rigorous model which could be flexible to changes in geometry and flow. A second argument was the limited documentation of the exactness of the calculated radiative heat flux.

The method giving solutions closest to exact solutions is the Monte Carlo Ray Tracing method (Viskanta and Mengüç, 1987). This method is recommended because of its flexibility and accuracy, also for irregular geometries (Mahan, 2002). It is on the other hand not easy to combine with convection and conduction differential equations (Siegel and Howell, 2002).

The zonal method (also known as Hottel's zonal method) is attractive because it requires less computational time than most alternative methods (Viskanta and Mengüç, 1987). The drawbacks are that it is usually difficult to couple with the flow and energy equations (Viskanta and Mengüç, 1987; Siegel and Howell, 2002), and that it has limited treatment of the temperature dependent radiative properties of non-grey gases. It is nevertheless a popular method which is widely used in radiative heat transfer calculations.

The multiflux method of Spalding (1980) generally underestimates the radiative fluxes (Viskanta and Mengüç, 1987). A second disadvantage is the arbitrary approximation of the intensity distribution and the absence of coupling between the radiative fluxes in the different directions for non-scattering media (Viskanta and Mengüç, 1987).

The differential, or P_N, approximation is a method where differential equations governing the radiation are approximated to series of polynomials, with the index N representing the order of series. The accuracy and the computational effort increases

with N, though increasing to an even-ordered N, as when replacing the P_1 with the P_2 approximation, has little influence on the accuracy (Mahan, 2002). For media of large temperature and concentration gradients the P_3 approximation is much more reliable than the P_1 approximation, but it requires on the other hand considerable more computational time.

In the discrete ordinates method (DOM or S_N approximation) the integrals in the radiative transport equation are approximated by weighted sums in a volume or area element. The entire solid angle (4π) is discretized using a finite number of ordinate directions and corresponding weight factors. The radiative transfer equation is written for each ordinate and the integral terms are replaced with a quadrature summed over each ordinate. Fiveland (1982) used the discrete ordinates method in two-dimensional cylindrical geometry and obtained good results compared with experimental data for combustion chambers.

The P_3 approximation and the S_4 approximation were considered for the annulus model of the GHR model. The decision fell on the S_4 approximation because this method is implemented in FLUENT, because of the many publications showing the reliability of this method and because of the cumbersome mathematics of the P_3 approximation.

4 THE GAS HEATED REFORMER MODEL

4.1 Review of steam reformer models

Steam reformers for conversion of natural gas are costly units and widely used, as also emphasized in Section 1.4. Mathematical models can increase our knowledge of the operation of steam reformers and of the transport and reaction mechanisms involved, which again may be background for finding optimal operation based on production cost and material lifetime. Steam reformers have thus been modelled several times, and a short review of these publications is given here.

Some of this literature is about evaluating which model is suitable for describing steam reformers (i.e. heterogeneous vs. pseudo-homogeneous models and one-dimensional vs. two-dimensional models) and some are optimization studies with basis in a chosen model type. A few of the articles also focus on the heating section of the unit, i.e. the fire box of a fired reformer or the hot gas side of a gas heated reformer. The previous published models and the discussions of model types will be reviewed here.

According to Rostrup-Nielsen et al. (1988) the pseudo-homogeneous reactor model is sufficient for simulating steam reformers as they are operating in a strongly diffusion controlled regime. This means that intraparticle diffusion is the dominating transport limitation regarding the mass and heat transport between the bulk gas and the catalyst pellets. The pseudo-homogeneous model is based on local reaction rates being calculated from the local bulk gas phase conditions and involving an efficiency factor which should correct for the mass and heat transport limitations in and around the catalyst pellets. Both the pseudo-homogeneous and the heterogeneous models are studied in this thesis and the statement of Rostrup-Nielsen et al. (1988) is investigated.

The radial temperature difference in a reactor tube can be as large as 80 ºC, and the two-dimensional model has therefore been chosen for this study. This gives higher accuracy if the limits of coke formation are to be evaluated. Two-dimensional steam reformer models have been studied several times, both by the use of pseudo-homogeneous models (Kvamsdal et al., 1999; Grevskott et al., 2001; Yu and Sosna, 2001) and by heterogeneous models (De Deken et al., 1982; Pedernera et al., 2003). One-dimensional heterogeneous models are however the most widely used for steam reformers (De Deken et al., 1982; De Groote and Froment, 1995; Elnashaie et al., 1992; Ferreira et al., 1992; Piña et al., 2001; Soliman et al., 1988; Xiu et al., 2003; Xu and

Froment, 1989b). All of the heterogeneous models listed here are simplified by disregarding the intraparticle heat transfer resistance and the interphase mass and heat transport limitations. As apposed to these models, the model presented in this section includes all these transport limitations.

Most of the mentioned studies involve only a model for the reactor tube without the shell side or firebox providing the heat to the reactor. The tube skin temperature is then given as a fixed profile in the boundary conditions of the energy equation. Grevskott et al. (2001) modelled the heat source of a side-fired steam reformer and used the two-flux method of Spalding (1980) for solving the radiative heat transport. De Groote and Froment (1995) modelled the firebox and solved the radiative heat transfer by the zonal method of Hottel and Sarofim (1967). Stehlík et al. (1989) modelled the firebox of a top-fired steam reformer combined with a one-dimensional reactor model and solved the thermal radiation fluxes by the zonal method. Xu and Froment (1989b) used the one-dimensional, heterogeneous model for the steam reformer tube coupled with a zone model for the firebox.

Two papers were found modelling the heating section of a GHR. Yu and Sosna (2001) modelled a GHR with the heating gas flowing in counter current mode through an annulus between the reactor tube and the surrounding sheath tube. The radiative heat transfer from this gas was modelled by the use of a radiative term of the total wall heat transfer coefficient. Stehlík (1995) modelled the shell side of a GHR connected to a reactor model, and described the radiation flux by a radiative term of the total wall heat transfer coefficients. The shell side was modelled as an annular space with cross sectional area equal to the shell side cross sectional area per tube. The "outer wall" of this annulus was modelled as a "gas wall", having all the physical properties of the gas and zero heat loss. Shell side baffles were included. The layout of this GHR is not comparable to the case of this thesis, as the catalytic bed is an annular volume heated on the inner wall by its own product gas and on the outer wall by the syngas from the secondary reformer.

4.2 Introduction to the GHR model

The model presented here is programmed in MATLAB which is a tool for solving numerical mathematics – both linear equations and differential equations. The model also relies on additional calculations from the CFD-tool FLUENT and from the process simulation tool Pro/II. Many of the choices for the GHR model are founded in the desire of having the model as simple as possible.

The GHR model consists of two main models: the fixed bed reactor tube and the shell side heating section. The model is simplified by modelling only one single tube with its corresponding shell side area, here represented by the annular volume between this tube and its enclosing sheath tube, as shown in Figure 4-1. The computation of the reactor model and the annulus model together is done by linking the two models at the outer tube wall surface of the reactor tube and iterating with the use of the calculated temperature and heat flux profiles at this wall. This is described in detail in Section 4.6.

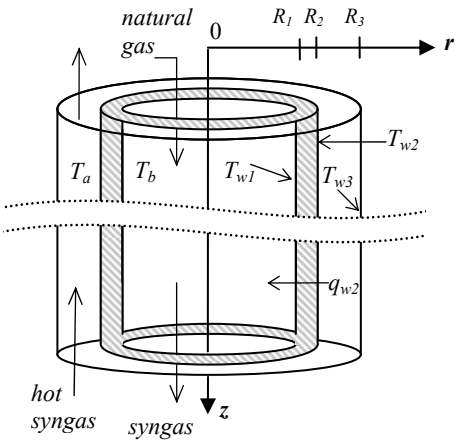

Figure 4-1: Model volumes.

The operating conditions in this study are typical for a primary reformer in series configuration with an ATR as a secondary reformer, where the produced syngas is composed as typically needed for methanol or Fischer-Tropsch synthesis. The properties of the product gas of the ATR are calculated with the process simulation tool Pro/II.

The GHR is built on counter current flow, with natural gas feed entering the reactor tube at axial position $z = 0$ and product gas exiting at $z = L$. The inlet of the hot syngas on the annular side is thus positioned at $z = L$. The radii of the inner and the outer wall of the reactor tube are denoted R_1 and R_2, respectively, and the outer radius inside the annulus is R_3. The tube length is typically about 12 metres and the outer diameter of the reactor tube is about 12 centimetres.

The GHR model is built on two main models: the reactor model and the annulus model. These are described in detail in Sections 4.4 and 4.5, respectively. These models use the same subroutines for the estimation of physical properties, which is done as given in Section 4.3. The models involve only the six components CH_4, H_2O, CO, H_2, CO_2 and N_2. These components are indicated in the model equations by the subscript i, indicating the component number; $i = 1$ for CH_4, $i = 2$ for H_2O, $i = 3$ for CO, $i = 4$ for H_2, $i = 5$ for CO_2 and $i = 6$ for N_2.

4.3 Thermodynamic models for the gas mixtures

All gas streams in the models are assumed ideal and their physical properties are given as function of temperature, pressure and composition.

4.3.1 Density

The ideal gas law is used for estimating the gas density, which is reasonable considering the high temperatures. The mole weight of the mixture is found from the sum of the

component mole weights, M_i, weighted on the component mole fractions, x_i. The density ρ_g of the gas mixture is then expressed by the equation:

$$\rho_g = \frac{P}{RT}\sum_{i=1}^{6} x_i M_i \tag{4-1}$$

4.3.2 Viscosity

The viscosity of a gas mixture, μ_g, is calculated from the pure gas viscosities, μ_i. The pure gas viscosities are estimated by the use of Lucas' method (Poling et al., 2001), repeated here. At first the reduced temperature T_r and the reduced dipole moment μ_r must be calculated from critical constants and the dipole moment μ_i, with values as quoted in Table 4-1:

$$T_{r,i} = T/T_{c,i} \tag{4-2}$$

$$\mu_{r,i} = 52.46\frac{\mu_i P_{c,i}}{T_{c,i}^{\ 2}} \tag{4-3}$$

Then the correction factors that accounts for polarity effects, $F^0_{P,i}$, are chosen depending on $\mu_{r,i}$, $T_{r,i}$ and the critical compressibility factor $Z_{c,i}$:

$$\begin{aligned}
&F^0_{P,i} = 1 && \text{for } 0 \le \mu_{r,i} < 0.022 \\
&F^0_{P,i} = 1 + 30.55\left(0.292 - Z_{c,i}\right)^{1.72} && \text{for } 0.022 \le \mu_{r,i} < 0.075 \\
&F^0_{P,i} = 1 + 30.55\left(0.292 - Z_{c,i}\right)^{1.72}\left|0.96 + 0.1\left(T_{r,i} - 0.7\right)\right| && \text{for } 0.075 \le \mu_{r,i}
\end{aligned} \tag{4-4}$$

The correction factor accounting for quantum effects, $F^0_{Q,i}$, is equal to 1 for all components but H_2:

$$F^0_{Q,H_2} = 1.1708\left(1 + 0.00385\left[\left(T_{r,H_2} - 12\right)^2\right]^{1/M_{H_2}} sign\left(T_{r,H_2} - 12\right)\right) \tag{4-5}$$

where the function *sign*(argument) is equal to +1 or −1 for positive or negative arguments, respectively. The temperature dependency of gas viscosities, μ_i, suggested in Lucas' method is:

$$\mu_i = \frac{F^0_{P,i} F^0_{Q,i}}{\xi_i}\left[0.807\,T_{r,i}^{0.618} - 0.357 e^{\left(-0.449 T_{r,i}\right)} + 0.340\, e^{\left(-4.058 T_{r,i}\right)} + 0.018\right] \tag{4-6}$$

The unit for the viscosity is here μP. ξ is the reduced, inverse viscosity, defined by:

$$\xi_i = 0.176\left(\frac{T_{c,i}}{M_i^3 P_{c,i}^4}\right)^{1/6} \tag{4-7}$$

Table 4-1: Critical temperatures, critical pressures, critical compressibility factors and dipole moments of the components (Poling et al., 2001).

	i = 1 (CH_4)	i = 2 (H_2O)	i = 3 (CO)	i = 4 (H_2)	i = 5 (CO_2)	i = 6 (N_2)
T_c	190.56	647.14	132.85	32.98	304.12	126.20
P_c	45.99	220.64	34.94	12.93	73.74	33.98
Z_c	0.286	0.229	0.292	0.303	0.274	0.289
μ	0	1.8	0.1	0	0	0

The viscosity of gas mixtures, μ_g, was calculated by the method of Wilke, as described by Poling et al. (2001):

$$\mu_g = \sum_{i=1}^{6} \frac{x_i \mu_i}{\sum_{j=1}^{6} x_j \phi_{ij}} \tag{4-8}$$

$$\phi_{ij} = \frac{\left[1 + \left(\mu_i/\mu_j\right)^{1/2} \left(M_j/M_i\right)^{1/4}\right]^2}{8\left(1 + \left(M_i/M_j\right)\right)^{1/2}} \tag{4-9}$$

4.3.3 Thermal conductivity

Thermal conductivities of pure gases, λ_i, are estimated by polynomial expressions given by Reid et al. (1987), with constants as shown in Table 4-2:

$$\lambda_i = A_i + B_i T + C_i T^2 + D_i T^3 \tag{4-10}$$

The thermal conductivity of gas mixtures, λ_g, was calculated by the Wassiljewa equation with the modification of Mason and Saxena (Poling et al., 2001):

$$\lambda_g = \sum_{i=1}^{6} \frac{x_i \lambda_i}{\sum_{j=1}^{6} x_j \phi_{ij}} \tag{4-11}$$

The interaction parameter ϕ_{ij} in Equation (4-9) can be used as an approximation.

Table 4-2: Constants for polynomial in Equation (4-10) (Reid et al., 1987).

	i = 1 (CH_4)	i = 2 (H_2O)	i = 3 (CO)	i = 4 (H_2)	i = 5 (CO_2)	i = 6 (N_2)
A_i	$-1.869 \cdot 10^{-3}$	$7.341 \cdot 10^{-3}$	$0.5067 \cdot 10^{-3}$	$8.099 \cdot 10^{-3}$	$-7.215 \cdot 10^{-3}$	$0.3919 \cdot 10^{-3}$
B_i	$8.727 \cdot 10^{-5}$	$-1.013 \cdot 10^{-5}$	$9.125 \cdot 10^{-5}$	$66.89 \cdot 10^{-5}$	$8.015 \cdot 10^{-5}$	$9.966 \cdot 10^{-5}$
C_i	$1.179 \cdot 10^{-7}$	$1.801 \cdot 10^{-7}$	$-0.3524 \cdot 10^{-7}$	$-4.158 \cdot 10^{-7}$	$0.05477 \cdot 10^{-7}$	$-0.5067 \cdot 10^{-7}$
D_i	$-3.614 \cdot 10^{-11}$	$-9.100 \cdot 10^{-11}$	$0.8199 \cdot 10^{-11}$	$15.62 \cdot 10^{-11}$	$-1.053 \cdot 10^{-11}$	$1.504 \cdot 10^{-11}$

4.3.4 Specific heat capacity

The specific heat capacity of pure gases, $c_{P,i}$, is calculated as given by Poling et al. (2001), with the correlation constants cited in Table 4-3. The equation is defined as function of the gas constant, R, and is here converted from model basis to mass basis:

$$c_{P,i} = \frac{R}{M_i}\left(a_{0,i} + a_{1,i}T + a_{2,i}T^2 + a_{3,i}T^3 + a_{4,i}T^4\right) \tag{4-12}$$

The specific heat capacity of the gas mixture is dependent on the gas composition and is here weighted with the mole fractions:

$$c_{P,g} = \frac{\sum_{i=1}^{6} x_i M_i c_{P,i}}{\sum_{i=1}^{6} x_i M_i} \tag{4-13}$$

Table 4-3: Constants for calculation of $c_{P,i}$ (Poling et al., 2001).

	i = 1 (CH_4)	i = 2 (H_2O)	i = 3 (CO)	i = 4 (H_2)	i = 5 (CO_2)	i = 6 (N_2)
$a_{0,i}$	4.568	4.395	3.912	2.883	3.259	3.539
$a_{1,i}$	$-8.975\cdot10^{-3}$	$-4.186\cdot10^{-3}$	$-3.913\cdot10^{-3}$	$3.681\cdot10^{-3}$	$1.356\cdot10^{-3}$	$-2.610\cdot10^{-4}$
$a_{2,i}$	$3.631\cdot10^{-5}$	$1.405\cdot10^{-5}$	$1.182\cdot10^{-5}$	$-7.720\cdot10^{-6}$	$1.502\cdot10^{-5}$	$7.000\cdot10^{-8}$
$a_{3,i}$	$-3.407\cdot10^{-8}$	$-1.564\cdot10^{-8}$	$-1.302\cdot10^{-8}$	$6.920\cdot10^{-9}$	$-2.374\cdot10^{-8}$	$1.570\cdot10^{-9}$
$a_{4,i}$	$1.091\cdot10^{-11}$	$6.320\cdot10^{-12}$	$5.150\cdot10^{-12}$	$-2.130\cdot10^{-12}$	$1.056\cdot10^{-11}$	$-9.900\cdot10^{-13}$

4.4 The reactor models

The reactor model was made in two versions; a heterogeneous model and a pseudo-homogeneous model. The difference between these two models is that whereas the heterogeneous model involves both the gas phase and the solid catalyst phase, the pseudo-homogeneous model simplifies these phases into one pseudo-homogeneous phase. The reactor models are described by Froment and Bischoff (1990) and were developed by Svendsen et al. (1996). The two principal assumptions in these reactor models are that the local axial mass flux is constant throughout the reactor tube and that the total pressure varies only with axial position. These assumptions imply that the gas density and the linear axial gas velocity are both functions of radial position. The models are also founded on other assumptions and simplifications, and these are discussed for the heterogeneous model in Section 4.4.1. The assumptions regarding the gas bulk model are also valid for the pseudo-homogeneous model.

The input parameters to the reactor models are the inlet conditions, the physical properties and the geometry of the tube and of the catalyst pellets, and the heat flux profile located on the outer wall of the reactor tube. The specifications for the catalyst are given in Appendix F.

A set of empirically derived correlations from literature, partially as discussed in Section 2, are involved in the model equations of the reactor models. These correlations have been selected after evaluation of different correlations, as presented in Section 5. The correlations for the reactor models are summarized in Table 4-4.

Table 4-4. Empirical correlations for mass and heat transfer parameters used in the reactor models.

Correlation:		Reference:
Radial dispersion coefficient:		Froment and Hofmann (1987)
$$E_{er,b} = \frac{d_p v_{z,s}}{10\left(1+19.4\left[d_p/d_t\right]^2\right)}$$	(4-14)	
Effective radial thermal conductivity of the fixed bed:		Peters et al. (1988)
$$\lambda_{er,b} = \lambda^s_{er,b} + \lambda_g \frac{Re_p Pr}{3.2 + 49.4\, d_p/d_t}$$	(4-15)	
Stagnant contribution to Equation (4-15):		Kunii and Smith (1960)
$$\lambda^s_{er,b} = \lambda_g \varepsilon_p + \lambda_g \frac{0.895\left(1-\varepsilon_p\right)\left(\ln\left[\frac{\lambda_p}{\lambda_g} - 0.5439\left(\frac{\lambda_p}{\lambda_g}-1\right)\right] - 0.4561\frac{\lambda_p-\lambda_g}{\lambda_p}\right)}{\frac{1}{2}\cdot 0.7042\left(\frac{\lambda_p-\lambda_g}{\lambda_p}\right)^2}$$	(4-17)	
Wall heat transfer coefficient of fixed bed:		Peters et al. (1988)
$$Nu_w = 4.9\left(d_p/d_t\right)^{0.26} Re_p^{0.45} Pr^{0.33}$$	(4-18)	
Diffusion coefficients in gas mixture:		Wilke (1950)
$$\frac{1}{D_{m,i}} = \sum_{k\neq i} \frac{x_k}{D_{ik}}$$	(4-20)	
Binary diffusion coefficients:		Fuller et al. (1966)
$$D_{ik} = \frac{1.013\cdot 10^{-2} T^{1.75}\left(1/M_i + 1/M_k\right)^{1/2}}{P\left[\left(\sum_i V\right)^{1/3} + \left(\sum_k V\right)^{1/3}\right]^2}$$	(4-21)	
Mass transfer coefficients:		Wakao and Funazkri (1978)
$$Sh_i = 2 + 1.1 Re^{0.6} Sc_i^{1/3}$$	(4-22)	
Interphase heat transfer coefficient:		Handley and Heggs (1968)
$$Nu_p = \frac{0.255}{\varepsilon} Pr^{1/3} Re_p^{2/3}$$	(4-23)	

The model equations presented in this section are normalized before implemented in the MATLAB codes. These normalized equations are listed in Appendix D.

4.4.1 The heterogeneous model

4.4.1.1 The bulk equations

The component balances for the bulk phase involve convective axial flow, radial transport by dispersion and the source term coupled to the reactions in the catalyst pellets. The source term is, for the heterogeneous model, defined with mass transfer coefficients, $k_{g,i}$, and the change in partial pressure from the bulk conditions (p_i) to the pellet surface conditions ($p^s_{p,i}$). The local axial mass flux is assumed constant over the radial positions, which implies zero radial mass flux, being consistent with purely dispersive radial transport. The axial dispersion is omitted as it is negligible compared to the axial convective transport at the operating velocities typical for steam reformers. The transport equation is solved for five of the six components in the bulk phase:

$$\frac{\partial\left(C_i v_{z,s}\right)}{\partial z}-\frac{1}{r}\frac{\partial}{\partial r}\left(r\,E_{er,b}\,C_{tot}\frac{\partial x_i}{\partial r}\right)=-k_{g,i}\,a_v\left(p_i-p^s_{p,i}\right) \tag{4-24}$$

The sixth component results from the total pressure and the sum of the five partial pressures. E_{er} is the effective radial dispersion coefficient and is calculated according to Equation (4-14) in Table 4-4. It involves contributions from molecular and turbulent diffusion and from the dispersion caused by the catalyst particles (Froment and Hofmann, 1987). The mass transfer coefficient, $k_{g,i}$, is calculated from the empirical correlation of Equation (4-22) in Table 4-4. a_v is the specific surface area of the catalyst bulk per reactor volume, i.e. $\mathrm{m}_c{}^2/\mathrm{m}_r{}^3$.

The conservation equations are expressed in terms of partial pressures, p_i, after introducing the ideal gas law and assuming no radial change in total pressure:

$$\begin{aligned}\frac{\partial p_i}{\partial z}=&-\frac{p_i}{v_{z,s}}\frac{\partial v_z}{\partial z}+\frac{p_i}{T}\frac{\partial T}{\partial z}-\frac{k_{g,i}a_v}{v_{z,s}}\left(p_i-p^s_{p,i}\right)\\&+\frac{1}{v_{z,s}}\left(\frac{\partial E_{er,b}}{\partial r}\frac{\partial p_i}{\partial r}+E_{er,b}\frac{\partial^2 p_i}{\partial r^2}-\frac{E_{er,b}}{T}\frac{\partial T}{\partial r}\frac{\partial p_i}{\partial r}+\frac{E_{er,b}}{r}\frac{\partial p_i}{\partial r}\right)\end{aligned} \tag{4-25}$$

The boundary conditions for the partial pressures define symmetry at the centre point of the tube ($r = 0$) and no change at the tube wall ($r = R_I$):

$$\left.\frac{\partial p_i}{\partial r}\right|_{r=0,R_I}=0 \tag{4-26}$$

A flat partial pressure profile is defined from the defined inlet composition and inlet total pressure:

$$p_i\left(z=0\right)=x_i^0\ P^0 \tag{4-27}$$

Summing up the six component balances of Equation (4-25) gives the total mass balance of the bulk, expressed by the axial change in axial superficial gas velocity:

$$\frac{\partial v_{z,s}}{\partial z}=\frac{v_{z,s}}{T}\frac{\partial T}{\partial z}-\frac{v_{z,s}}{P}\frac{\partial P}{\partial z}-\frac{a_v}{P}\sum_i k_{g,i}\left(p_i-p_{p,i}^s\right) \tag{4-28}$$

The initial superficial velocity, $v^0_{z,s}$, is calculated from the molar feed input, n^0:

$$v_{z,s}^0=\frac{R\,n^0\,T^0}{P^0\,A_{c,b}} \tag{4-29}$$

It is assumed that the radial variations in pressure can be neglected, and the radial mean of the velocities, densities and viscosities are therefore used when calculating the change in pressure as a function of the axial position. Radial mean values are calculated as given in Appendix E. Empirical equations for the friction factor in the pressure drop equation is discussed in Section 5.1.8, where it was concluded to apply the equation of Hicks (1970), valid for $Re_p/(1-\varepsilon) > 300$:

$$\frac{dP}{dz}=-6.8\frac{\left(1-\varepsilon\right)^{1.2}}{\varepsilon^3}Re_p^{-0.2}\frac{\rho_m\,v_{sm}^2}{d_p} \tag{4-30}$$

The calculation of the equivalent catalyst pellet diameter, d_p, is given in Equation (F-5), Appendix F. The pressure equation has the initial condition:

$$P\left(z=0\right)=P^0 \tag{4-31}$$

The energy transport in axial direction is dominated by the transport from axial convection, and thus axial conduction is neglected. With no radial convection, the only energy transport mechanism in radial direction is the effective conduction. The energy equation is simplified by assuming constant effective radial thermal conductivity, $\lambda_{er,b}$, as justified in Section 5.1.6. The heat source term caused by reaction is defined by a heat transfer coefficient, h_p, multiplied with the temperature drop over the gas film at the pellet surface:

$$\frac{\partial T}{\partial z}=\frac{1}{\rho_g\,c_{P,g}\,v_{z,s}}\left(\lambda_{er,b}\left(\frac{1}{r}\frac{\partial T}{\partial r}+\frac{\partial^2 T}{\partial r^2}\right)-h_p\,a_v\left(T-T_p^s\right)\right) \tag{4-32}$$

The initial condition is a flat inlet temperature profile:

$$T\left(z=0\right)=T^0 \tag{4-33}$$

The first boundary condition defines symmetry in T at $r = 0$ and the second connects T at $r = R_1$ to the wall temperature T_{w1} by means of the wall heat transfer coefficient h_1. These conditions are represented by the respective equations:

$$\left.\frac{\partial T}{\partial r}\right|_{r=0} = 0 \tag{4-34}$$

$$-\lambda_{er,b}\left.\frac{\partial T}{\partial r}\right|_{r=R_t} = h_t\left(T(R_t) - T_{wt}\right) \tag{4-35}$$

The effective radial thermal conductivity of the fixed bed, $\lambda_{er,b}$, and the wall heat transfer coefficient, h_t, are modelled by the empirical correlations cited in Equations (4-15) and (4-18), respectively, shown in Table 4-4. Different correlations for h_t have been tested in Section 5.1.7.

4.4.1.2 The pellet equations

Two basic assumptions for the pellets are made: negligible change in the internal total pressure and no convective mass transport. The pellet geometry is simplified to a plane surface with depth co-ordinate y. The planar geometry is justified by the reactions taking place only in the outer layer of the catalyst pellets (Xu and Froment, 1989b). Also, the effectiveness factors for the steam reforming reactions are very low, which implies that such a simplification in geometry has almost no effect on the simulation results. The equations for the reaction kinetics are modelled as given by Xu and Froment (1989a), quoted in Appendix A. The component balances for the solid phase include internal diffusion and reaction:

$$D^e_{m,i}\frac{\partial}{\partial y}\left(C_{tot}\frac{\partial x_{p,i}}{\partial y}\right) + \rho_c\sum_{j=1}^{3}\nu_{ij}\,r_j = 0 \tag{4-36}$$

The density of the catalyst, ρ_c, is given in kg catalyst per m^3 of the catalyst pellet. The spatial variations in the effective diffusivities $D^e_{m,i}$ are negligible, and their gradients are therefore not included in this differential equation. $D^e_{m,i}$ is the effective diffusivity for component i within the pores of the catalyst pellet, and it is calculated from the diffusivity $D_{m,i}$, the Knudsen diffusivity D_K, the pellet tortuosity factor τ_p and the pellet porosity ε_p (Rostrup-Nielsen, 1984):

$$D^e_{m,i} = \frac{\varepsilon_p}{\tau_p}\frac{1}{\dfrac{1}{D_{m,i}} + \dfrac{1}{D_K}} \tag{4-37}$$

Rostrup-Nielsen (1984) showed that $D^e_{m,i}$ is independent of the Knudsen diffusivity at pressures typical for steam reformers, which simplifies Equation (4-37) to:

$$D^e_{m,i} = \frac{\varepsilon_p}{\tau_p}D_{m,i} \tag{4-38}$$

The transport equation for component i in the pellet is expressed by partial pressures by introducing the ideal gas law. The internal change in total pressure can be disregarded in the diffusion term (Burghardt and Aerts, 1988; Kehoe and Aris, 1973;

Veldsink et al., 1995). These simplifications are explained in detail in Section 2.4.2.1. The component balances need to be independent to assure the total mass continuity:

$$D_{m,i}^{e}\left(\frac{1}{RT_p}\frac{\partial^2 p_{p,i}}{\partial y^2}-\frac{1}{RT_p^2}\frac{\partial T_p}{\partial y}\frac{\partial p_{p,i}}{\partial y}\right)+\rho_c\sum_{j=1}^{3}\nu_{ij}r_j=0 \tag{4-39}$$

The balance equations are solved for the thickness $X{\cdot}R_p$ which is equal to the active layer of the catalyst pellet. X is a fraction of the equivalent particle radius R_p. The boundary conditions of Equation (4-39) at the depth of the active layer ($y = 0$) and at the pellet surface ($y = X{\cdot}R_p$) define flattening of the partial pressure profile and heat transfer from the bulk, respectively:

$$\left.\frac{\partial p_{p,i}}{\partial y}\right|_{y=0}=0 \tag{4-40}$$

$$D_{m,i}^{e}\left.\frac{\partial p_{p,i}}{\partial y}\right|_{y=X R_p}=k_{g,i}\left(p_i-p_{p,i}^{s}\right) \tag{4-41}$$

The heat balance is composed of conductive heat transfer and reaction heat:

$$\lambda_c\frac{\partial^2 T_p}{\partial y^2}+\sum_{j=1}^{3}\rho_c\, r_j\left(-\Delta H_j\right)=0 \tag{4-42}$$

The thermal conductivity for the catalyst pellets, λ_c, is constant. The boundary conditions for the temperature equation define zero temperature gradient at $y = 0$ and heat transfer from the bulk to the surface at $y = X{\cdot}R_p$, respectively:

$$\left.\frac{\partial T_p}{\partial y}\right|_{y=0}=0 \tag{4-43}$$

$$-\lambda_c\left.\frac{\partial T_p}{\partial y}\right|_{y=X R_p}=h_p\left(T_p^{s}-T\right) \tag{4-44}$$

4.4.1.3 The effectiveness factors of the reactions

The effectiveness factors of the reactions are defined as the real reaction rates relative to the reaction rates for a completely active catalyst with temperature and partial pressures equal to those at the pellet surface (Fogler, 1992). The general expression for the effectiveness factor, valid for any geometry, is:

$$\eta_j=\frac{\int_0^{V_p} r_j\, dv}{V_p\, r_j^{s}} \tag{4-45}$$

The steam reforming catalysts take on a large variety of shapes, but for all only a thin layer close to the external surface is active. Therefore planar geometry can be assumed, as indicated by Equation (4-36). This leads to the volume $a_v \cdot X \cdot R_p$ (m^3/m_r^3) of the active part of the catalysts, with X representing the fraction of the equivalent pellet radius where the pellet is active, and the total catalyst volume $(1-\varepsilon)$ (m_c^3/m_r^3). The following equation can then be deduced for this specific system:

$$\eta_j = \frac{a_v}{(1-\varepsilon)\, r_j^s} \int_0^{X R_p} r_j \, dy \tag{4-46}$$

As long as there is resistance to mass or heat transfer in the pellet, arising from low effective molecular diffusivity or low thermal conductivity, this effectiveness factor will be less than one. Steam reformers operate with very low effectiveness factors; typically below 0.1 (Rostrup-Nielsen et al., 1988).

An analogous effectiveness factor, η_j', which is relative to the reaction rate calculated from bulk conditions instead of from surface conditions, can be defined as:

$$\eta'_j = \frac{a_v}{(1-\varepsilon)\, r_j^{bulk}} \int_0^{X R_p} r_j \, dy \tag{4-47}$$

Consequently, η'_j will be less than η_j if mass or heat transfer limitations in the gas film between the gas bulk and the pellet surface are present.

4.4.2 The pseudo-homogeneous reactor model

The model equations for the pseudo-homogeneous model are basically similar to the bulk equations for the heterogeneous model in Section 4.4.1.1, with equal description of mass and heat transport in axial and radial direction. The difference lies in the source terms connected to reaction which are here replaced by reaction rates calculated from bulk conditions and multiplied with their respective effectiveness factors η_j', defined in Equation (4-47).

The conservation equation of component number i can be expressed as for the heterogeneous model in Equation (4-25):

$$\begin{aligned} \frac{\partial p_i}{\partial z} = & -\frac{p_i}{v_{z,s}}\frac{\partial v_z}{\partial z} + \frac{p_i}{T}\frac{\partial T}{\partial z} + \frac{RT}{v_{z,s}}\sum_j \eta'_j \nu_{ij} r_j \\ & + \frac{1}{v_{z,s}}\left(\frac{\partial E_{er,b}}{\partial r}\frac{\partial p_i}{\partial r} + E_{er,b}\frac{\partial^2 p_i}{\partial r^2} - \frac{E_{er,b}}{T}\frac{\partial T}{\partial r}\frac{\partial p_i}{\partial r} + \frac{E_{er,b}}{r}\frac{\partial p_i}{\partial r} \right) \end{aligned} \tag{4-48}$$

η_j' is strongly dependent on the catalyst geometry and activity and may be simplified to constant values to achieve considerable savings in computation time. The boundary conditions are as for the heterogeneous model (Equation (4-26)).

The total mass balance giving the axial change in axial superficial gas velocity results from the sum of the six component balances:

$$\frac{\partial v_{z,s}}{\partial z} = \frac{v_{z,s}}{T}\frac{\partial T}{\partial z} - \frac{v_{z,s}}{P}\frac{\partial P}{\partial z} + \frac{RT}{P}\sum_j \left(\sum_i \nu_{ij}\right)\eta'_j r_j \tag{4-49}$$

The equation for the bulk temperature is similar to Equation (4-32) except from the reaction source term which is here calculated directly from bulk conditions:

$$\frac{\partial T}{\partial z} = \frac{1}{\rho_g\, c_{P,g}\, v_{z,s}}\left(\lambda_{er,b}\left(\frac{1}{r}\frac{\partial T}{\partial r} + \frac{\partial^2 T}{\partial r^2}\right) + \rho_{cb}\sum_j \left(-\Delta H_j\right)\eta'_j r_j\right) \tag{4-50}$$

The boundary conditions are unchanged from the heterogeneous model (Equations (4-34) and (4-35)).

4.5 The annulus model

The annular section is described by a plug flow model, where the energy conservation equation is the only differential equation. The energy equation involves heat transport caused by axial convection and by radial conduction and radiation. The contribution from conduction to axial heat transport is negligible compared with the convective contribution. Correspondingly, heat transfer by convection is negligible in the radial direction. Turbulent dispersion is the dominant heat transfer mechanism in radial direction, and this effect is included in the parameter $\lambda_{er,a}$, the effective radial thermal conductivity. The radiation from the hot gas is modelled by the discrete ordinates method in the radial direction only.

The energy equation involving heat transport from axial convection, radial conduction and radial radiation describes the temperature profiles in the annulus:

$$\rho_g\, c_{P,g}\, v_z \frac{\partial T}{\partial z} = \frac{1}{r}\frac{\partial}{\partial r}\left(\lambda_{er,a}\, r \frac{\partial T}{\partial r}\right) - \frac{\partial q_{rad}}{\partial r} \tag{4-51}$$

The procurement of the effective radial thermal conductivity, $\lambda_{er,a}$, is described in detail in Section 4.5.1 and the method for calculating the radiative volumetric heat flux, $\partial q_{rad}/\partial r$, is given in Section 4.5.2. The boundary conditions of the energy equation give expressions for the heat balances across the inner and outer walls of the annulus (at $r = R_2$ and at $r = R_3$), respectively:

$$-\lambda_{er,a}\left.\frac{\partial T}{\partial r}\right|_{r=R_2} = h_2\left(T_{w2} - T(R_2)\right) \tag{4-52}$$

$$-\lambda_{er,a}\left.\frac{\partial T}{\partial r}\right|_{r=R_3} = h_3\left(T - T_{w3}(R_3)\right) \tag{4-53}$$

The outer wall of the annulus is adiabatic and this is achieved as given in the text description for Equations (4-72) and (4-73). It is important to note that the radiation heat flux terms of Equations (4-71) and (4-73) should be included on the right-hand side of Equations (4-52) and (4-53) when solving by the finite volume method. These terms vanish when converting to the finite difference form, as shown in Appendix C.

The heat transfer coefficients describing the convective heat transport from the gas in the annulus to the inner and outer wall of the annulus, h_2 and h_3 respectively, are calculated as recommended by Mills (1992). The first step is the calculation of the local Nusselt number for a tube, as correlated by Gnielinski (1976) for $3 \cdot 10^3 < Re_h < 10^6$:

$$Nu_w = F_C \frac{(f/8)(Re_h - 1000)\,Pr}{1 + 12.7\sqrt{f/8}\left(Pr^{2/3} - 1\right)} \tag{4-54}$$

The Nusselt and the Reynolds numbers are based on the hydraulic diameter of the annulus, defined by:

$$d_h = 4\frac{\pi\left(R_3^2 - R_2^2\right)}{2\pi\left(R_2 + R_3\right)} \tag{4-55}$$

The friction factor in Equation (4-54) is calculated from the correlation of Petukhov (1970), valid for $10^4 < Re_h < 5 \cdot 10^6$:

$$f = \left(0.790 \ln Re_h - 1.64\right)^{-2} \tag{4-56}$$

The tube Nusselt numbers are finally multiplied with correction factors F_C given by Petukhov and Roizen (1964) for annular ducts. The respective factors for the Nusselt number at the inner and at the outer wall are:

$$F_{C,2} = 0.86\left(R_2/R_3\right)^{-0.16} \tag{4-57}$$

$$F_{C,3} = 1 - 0.14\left(R_2/R_3\right)^{0.6} \tag{4-58}$$

The algebraic velocity equation is deduced from the ideal gas law, as function of the molar flow rate n and the cross sectional area normal to flow, A_a:

$$v_z = \frac{R\,n\,T}{P\,A_a} \tag{4-59}$$

When iterating from inlet ($z = L$), the pressure drop equation is given by the expression:

$$\Delta P = \frac{f\,\rho_g (L - z)\,v_z^2}{2\,d_{h,a}} \tag{4-60}$$

4.5.1 The FLUENT model for radial thermal conductivity

The flow model for the annulus is simplified by assuming plug flow. The turbulent flow affects the lateral heat transfer by increasing the radial exchange and the heat transfer coefficients at the walls (h_2 and h_3). The radial velocity is zero in the MATLAB model but the *effect* of this enhanced radial heat transfer is included by using an effective radial thermal conductivity of the bulk gas, denoted $\lambda_{er,a}$. This conductivity is defined as the sum of the gas conductivity and the turbulent conductivity, where the latter is the clearly dominating. $\lambda_{er,a}$ can be calculated from complete flow simulations where the turbulent flow is included in the model.

In this case $\lambda_{er,a}$ was calculated in an equivalent annulus model built in the CFD-tool FLUENT, and its values were exported to generate input data to the MATLAB model. The FLUENT model is a two-dimensional model of equal geometry and input data (inlet flow properties, physical properties and boundary conditions) as the MATLAB model. The wall temperature and heat flux profiles were equal in the two simulations. The FLUENT model is more detailed as it involves a model for description of the turbulent flow, the k-ε turbulence model. The resulting calculated $\lambda_{er,a}$ is a function of both radial and axial position.

The sensitivity for the dependency of r and z on $\lambda_{er,a}$ in the MATLAB model was investigated (Section 5.2.2) and it was found that only radial variations in $\lambda_{er,a}$ were of importance for the simulation output. Axial variations were therefore neglected when importing $\lambda_{er,a}$ from the FLUENT model. A function for λ_{er} dependent on radial position only was therefore read from the results of the CFD simulations at a position midway in the axial direction.

4.5.2 The radiation model

The discrete ordinates method (S_N-method or DOM) was applied for calculating the radiation source term in the energy equation and the radiation heat fluxes at the walls. The radiative intensity field can be sufficiently represented by the S_4 approximation (Fiveland, 1982) using 12 different directions in two dimensions (axial and radial), which gives six directions due to symmetry in axial direction. Therefore, six differential equations must be solved for the six intensities I^m. The directions m = 1–6 are illustrated in Figure 4-2.

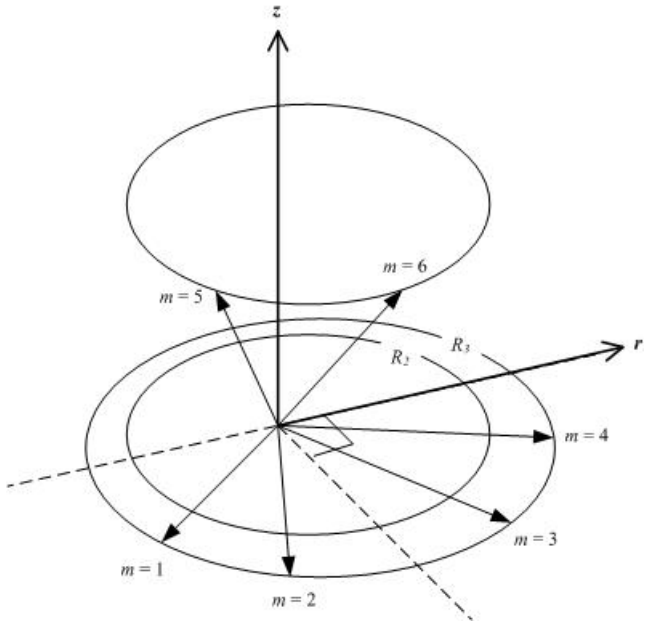

Figure 4-2. Radiative directions for the S_4 approximation.

The simplification of the radiative transport equation (RTE) in cylindrical co-ordinates used in the discrete ordinates method expresses the intensity in one radiative direction as function of radial direction and azimuthal angle (Modest, 2003):

$$\frac{\mu^m}{r}\frac{\partial\left(rI^m\right)}{\partial r}-\frac{1}{r}\frac{\partial\left(\eta^m I^m\right)}{\partial\psi}=\kappa I_B-\kappa I^m \tag{4-61}$$

The six radiative directions are labelled by the superscript m, and μ^m and η^m are directional cosines. κ is the absorption coefficient of the gas and is estimated as described in Section 4.5.2.1, and I_B is the blackbody radiative intensity of the gas, defined by (Siegel and Howell, 2002):

$$I_B=\frac{\sigma}{\pi}T^4 \tag{4-62}$$

Carlson and Lathrop (1968) introduced a simplified expression for the azimuthal variations, using the 7 geometrical coefficients $\alpha^{m\pm½}$, that maintain conservation of the intensities:

$$\frac{\partial\left(\eta^m I^m\right)}{\partial\psi}\simeq\frac{\alpha^{m+1/2}I^{m+1/2}-\alpha^{m-1/2}I^{m-1/2}}{w^m} \tag{4-63}$$

The directions $m \pm ½$ bound the edges of the angular range assigned by the quadrature weight w^m. The half-node intensities are simplified by setting $I^{m\pm½} = ½ (I^{m\pm1} + I^m)$. Values for the directional cosines and the weight factors are given by Modest (2003) and quoted in Table 4-5. The directional cosines μ^m are defined as negative for direction numbers $m = 1, 2, 5$ and positive for $m = 3, 4, 6$.

Table 4-5. Data for directional cosines and quadrature weights at cylindrical coordinates (Modest, 2003).

m	μ^m	w^m
1	–0.9082483	2.0943951
2	–0.2958759	2.0943951
3	0.2958759	2.0943951
4	0.9082483	2.0943951
5	–0.2958759	2.0943951
6	0.2958759	2.0943951

The α-terms as defined in Modest (2003) are for the S_4 method defined by:

$$\alpha^{1/2} = \alpha^{9/2} = \alpha^{13/2} = 0 \tag{4-64}$$

$$\alpha^{m+1/2}\Big|_{m=1,2,3,5} = \alpha^{m-1/2} + w^m \mu^m \tag{4-65}$$

The final form of the RTE to be solved can then be simplified in the following way:

$$\frac{\mu^m}{r} I^m + \mu^m \frac{\partial I^m}{\partial r} - \frac{\alpha^{m+1/2}\left(I^m + I^{m+1}\right) - \alpha^{m-1/2}\left(I^{m-1} + I^m\right)}{2 r w^m} = \kappa I_B - \kappa I^m \tag{4-66}$$

The boundary conditions at the inner wall of the annulus (at $r = R_2$) give the three radiation intensities in the positive direction (i.e. in the direction out from this wall). This condition is thus valid for the intensities in the directions m whose directional cosines are positive (i.e. for $\mu^m > 0$). These intensities are caused by emission from the wall plus reflection of the gas radiation into the wall, which is given by the radiation intensities in negative direction, weighted and multiplied with their respective directional cosines before summation:

$$I^m(R_2)\Big|_{m=3,4,6} = \varepsilon_{w2} \frac{\sigma}{\pi} T_{w2}^4 + \frac{(1-\varepsilon_{w2})}{\pi} \sum_{m'=1,2,5} w^{m'} \left|\mu^{m'}\right| I^{m'}(R_2) \tag{4-67}$$

Correspondingly, the intensities in the three directions from the outer wall (at $r = R_3$) and into the annulus are expressed by the boundary conditions at this wall. These are the intensities in the negative direction (i.e. directions m having $\mu^m < 0$) and are therefore functions of the weighted intensities in the three positive directions:

$$I^m(R_3)\Big|_{m=1,2,5} = \varepsilon_{w3} \frac{\sigma}{\pi} T_{w3}^4 + \frac{(1-\varepsilon_{w3})}{\pi} \sum_{m'=3,4,6} w^{m'} \mu^{m'} I^{m'}(R_3) \tag{4-68}$$

The boundary conditions were simplified by assuming grey walls, so that $\rho_w = 1 - \varepsilon_w$.

The equation system is solved by expressing the derivatives of I^m by central differences in two forms: for iteration in backward and in forward radial direction. The intensities I^3, I^4 and I^6 are solved by iteration in the positive r-direction and I^1, I^2 and I^5

are solved in the negative direction. The two directions are solved successively with direct substitution. The iteration procedure is described by Fiveland (1982).

The radial change in radiation heat, used in the energy equation (Equation (4-51)), is the emitted energy rate minus the absorbed energy rate:

$$\frac{\partial q_{rad}}{\partial r} = -\kappa\left(\sum_{m=1}^{6} I^m w^m - 4\sigma T^4\right) \tag{4-69}$$

The axial profile of the total heat flux through the reactor tube wall (i.e. at $r = R_2$) is the sum of the conductive and the radiative heat fluxes:

$$q_{w2} = h_2\left(T(R_2) - T_{w2}\right) + q_{rad,w2} \tag{4-70}$$

where the radiation heat flux is given by:

$$q_{rad,w2} = \varepsilon_{w2}\left(\sum_{m=1,2,5}\left|\mu^m\right| I^m(R_2)\, w^m - \sigma T_{w2}^4\right) \tag{4-71}$$

The net heat flux through the outer wall of the annulus at $r = R_3$ is defined zero as this is an adiabatic wall:

$$q_{w3} = h_3\left(T_{w3} - T(R_3)\right) - q_{rad,w3} = 0 \tag{4-72}$$

The radiation heat flux is:

$$q_{rad,w3} = \varepsilon_{w3}\left(\sum_{m=3,4,6}\mu^m\, I^m(R_3)\, w^m - \sigma T_{w3}^4\right) \tag{4-73}$$

The wall temperature T_{w3} that maintains zero net heat flux through wall *3* is found by iteration of Equation (4-72).

4.5.2.1 Gas absorption coefficient by the WSGG model

The calculation of the gas emissivity is performed by the weighted-sum-of-grey-gases (WSGG) model as described by Smith et al. (1982). The emissivity of the gas mixture is expressed by a summation of three fictitious grey gases representative for the system:

$$\varepsilon_g = \sum_{q=1}^{3} a_{\varepsilon,q}\left(1 - e^{-k_q \cdot P \cdot L_M}\right) \tag{4-74}$$

$a_{\varepsilon,q}$ and k_q are the weight factor and the absorption coefficient for the q-th grey gas, respectively. The function for $a_{\varepsilon,q}$ depends on temperature and composition and is given by Smith et al. (1982) with data for the constants quoted in Table 4-6:

$$a_{\varepsilon,q} = b_{\varepsilon,q,1} + b_{\varepsilon,q,2}\, T + b_{\varepsilon,q,3}\, T^2 + b_{\varepsilon,q,4}\, T^3 \tag{4-75}$$

The constants k_q are found in Smith et al. (1982) for H_2O/CO_2-mixtures of $p_{H2O}/p_{CO2} = 2$, giving the values $k_1 = 0.4201$, $k_2 = 6.516$, $k_3 = 131.9$.

The mean beam length, L_M, in Equation (4-74) is scaled for pressures above 1 atm according to Edwards and Matavosian (1984):

$$L_M = L_M P^n \tag{4-76}$$

The scaling exponent n is dependent on temperature and on the sum of the partial pressures of absorbing gases and is cited in Table 4-7.

Table 4-6. Data for b_ε of Equation (4-75), valid for a gas mixture of $p_{H2O}/p_{CO2} = 2$ (Smith et al., 1982).

	$b_{\varepsilon,q,1}$	$b_{\varepsilon,q,2}$	$b_{\varepsilon,q,3}$	$b_{\varepsilon,q,4}$
$q = 1$:	$6.508 \cdot 10^{-1}$	$-5.551 \cdot 10^{-4}$	$3.029 \cdot 10^{-7}$	$-5.353 \cdot 10^{-11}$
$q = 2$:	$-0.2504 \cdot 10^{-1}$	$6.112 \cdot 10^{-4}$	$-3.882 \cdot 10^{-7}$	$6.528 \cdot 10^{-11}$
$q = 3$:	$2.718 \cdot 10^{-1}$	$-3.118 \cdot 10^{-4}$	$1.221 \cdot 10^{-7}$	$-1.612 \cdot 10^{-11}$

Table 4-7. Scaling exponent n for pressure scaling of the mean beam length in Equation (4-76) (Edwards and Matavosian (1984). p_A is the partial pressure of absorbing gases, i.e. $p_A = p_{H2O} + p_{CO2}$.

	$p_{H2O} \cdot L_M < 0.05$	$p_A \cdot L_M < 0.5$	$p_A \cdot L_M < 5$	$p_A \cdot L_M > 5$
$T < 1000$ K:	0.46	0.72	0.70	0.60
$T \geq 1000$ K:	0.17	0.51	0.57	0.52

The gas absorption coefficient, κ, is finally estimated from the gas emissivity (Siegel and Howell, 2002):

$$\kappa = -\frac{\ln\left(1-\varepsilon_g\right)}{L_M} \tag{4-77}$$

4.6 Combining the reactor and annulus models

The overall iteration is initiated by specifying the reactor wall temperature profile on the annulus side, T_{w2}. This is input to the annulus model, where the heat flux, $q_{w2,a}$, is calculated from Equation (4-70). This heat flux is then input to the reactor model where the internal tube skin temperature is calculated from $q_{w2,a}$ and the bulk temperature at the discretization point close to the wall:

$$T_{w1} = T_b(R_1) + \frac{R_2}{R_1}\frac{q_{w2,a}}{h_1} \tag{4-78}$$

The heat flux calculated in the reactor model, $q_{w2,b}$, is defined with outer tube wall surface as basis, similar to the definition of $q_{w2,a}$, and calculated from the boundary condition of Equation (4-35):

$$q_{w2,b} = \frac{R_1}{R_2} h_1 \left(T_{w1} - T_b(R_1) \right) \tag{4-79}$$

This heat flux and the wall temperature of Equation (4-78) give the external tube skin temperature to be given as input for the next iteration:

$$T_{w2} = T_{w1} + q_{w2,b} \frac{R_2 \ln(R_2/R_1)}{\lambda_w} \tag{4-80}$$

Convergence is reached when the wall temperature T_{w2} is unchanged. An additional convergence test consists in comparing the heat flux profiles of Equations (4-70) and (4-79) with heat flux profiles resulting from the changes in bulk gas energy in both the reactor tube and in the annular space. These heat flux profiles are found from the enthalpies and mass fluxes of the gas flows, as explained in Section 4.6.1.

4.6.1 Convergence tests

The axial heat flux profiles calculated from Equations (4-70) and (4-79) are compared with heat flux profiles resulting from the changes in enthalpy of the bulk gases in both the reactor tube and in the annular space. The total heat removed from or added to a gas is derived from the outlet and inlet enthalpies and mass flows, which are found from integration over the cross-sectional area of the tube or annulus:

$$\Delta Q = \int_{A_{(1)}}^{A_{(2)}} \left(\rho_g \, v_z \, \Delta H \right)_{out} dA - \int_{A_{(1)}}^{A_{(2)}} \left(\rho_g \, v_z \, \Delta H \right)_{in} dA \tag{4-81}$$

The cross sectional areas are $A_{(1)} = 0$ and $A_{(2)} = \pi R_1^2$ for the reactor tube and $A_{(1)} = \pi R_2^2$ and $A_{(2)} = \pi R_3^2$ for the annular space. The axial profile of the heat flux is found when ΔQ is derived for each axial discretization step.

The enthalpies of Equation (4-81) are functions of temperature and molar fractions:

$$\Delta H(T) = \Delta H^\circ + \int_{T^\circ}^{T} c_P(T) \, dT \tag{4-82}$$

The reference temperature is $T^\circ = 298$ K and the standard enthalpy of formation, ΔH°, is calculated from ΔH°_i, shown in Table 4-8:

$$\Delta H^\circ = \sum_i x_i \Delta H_i^\circ \Big/ \sum_i x_i M_i \tag{4-83}$$

Table 4-8: Values of the standard enthalpies of formation [kJ/ kmole] (Aylward and Findlay, 1974).

	$i = 1$ (CH_4)	$i = 2$ (H_2O)	$i = 3$ (CO)	$i = 4$ (H_2)	$i = 5$ (CO_2)	$i = 6$ (N_2)
ΔH°_i	$-75 \cdot 10^3$	$-242 \cdot 10^3$	$-111 \cdot 10^3$	0	$-394 \cdot 10^3$	0

The integral of the specific heat capacity (the second term of Equation (4-82)) is found from Equation (4-13), with the constants a_i as given in Table 4-3:

$$\int_{T^\circ}^{T} c_{P,g}(T)\,dT = R\frac{\sum_{i=1}^{6} x_i \left[\begin{array}{l} a_{0,i}\left(T - T^\circ\right) + \frac{a_{1,i}}{2}\left(T^2 - \left(T^\circ\right)^2\right) + \\ \frac{a_{2,i}}{3}\left(T^3 - \left(T^\circ\right)^3\right) + \frac{a_{3,i}}{4}\left(T^4 - \left(T^\circ\right)^4\right) + \frac{a_{4,i}}{5}\left(T^5 - \left(T^\circ\right)^5\right) \end{array} \right]}{\sum_{i=1}^{6} x_i M_i} \tag{4-84}$$

Equation (4-81) can be used to find the heat flux profile as function of tube length, by letting the subscripts *out* and *in* represent the boundaries of one axial discretization point. The profiles resulting from reactor bed and annulus calculations can then be compared with the heat flux profiles calculated from the convective and radiative heat fluxes, represented by Equations (4-35) and (4-70), respectively.

Equation (4-81) can also be used to find the total heat added to the reactor bed (*out* at $z = L$ and *in* at $z = 0$). ΔQ can then be compared with the total heat supply calculated from the wall heat flux of Equation (4-35):

$$Q_b = 2\pi R_2 \int_0^L \frac{R_1}{R_2}\left[h_1\left(T_{w1} - T_b(R_1)\right)\right] dz \tag{4-85}$$

Correspondingly, the total heat of Equation (4-81) calculated for the annular section (*out* at $z = 0$ and *in* at $z = L$) can then be compared with the total heat removed from the wall heat flux of Equation (4-70):

$$Q_a = 2\pi R_2 \int_0^L \left[h_2\left(T_a(R_2) - T_{w2}\right) + q_{rad,w2}\right] dz \tag{4-86}$$

4.7 Numerical methods

The radial derivatives in the conservation equations for the bulk flows in the reactor tube and in the annular space are solved by the discretization routines *dss020* and *dss042* given by Schiesser (1991). The axial derivatives are solved by the MATLAB built-in integrator for stiff, ordinary differential equations, *ode15s*. The dss-routines are able to solve boundary value problems, while the ode-solvers from MATLAB are solvers for initial value problems.

The differential equations describing transport into the catalyst pellets in the heterogeneous model are also solved by the dss-routines.

5 FRAMEWORK FOR THE CHOICES OF THE EMPIRICAL PARAMETERS

The MATLAB model of the GHR involves several empirical parameters for the description of mass and heat transport. There is a variety of correlations to be found in the published literature and all have different validity ranges and have been obtained in different experimental systems. A substantial part of the work for this thesis has been to obtain an overview of the literature within these fields and to evaluate which correlations are suitable for the GHR model. The literature study done on heat transfer modelling in pseudo-homogeneous fixed bed models was summarized in the review in Sections 2.2 and 2.3. The description of mass and heat transport modelling in the gas-solid interphase and in the solid phase in a heterogeneous model was described in Section 2.4. The evaluations of the empirical correlations summarized in Table 4-4 and of the annulus effective radial thermal conductivity, described in Section 4.5.1, are summarized here. Most of the empirical correlations in this section are expressed in form of dimensionless groups, whose definitions are found in Table 2-1. All calculations in this section are based on the model case *GHR-1*, described in Section 7.

5.1 The parameters involved in the reactor models

5.1.1 The pellet mass transfer coefficient, k_g

Four different empirical correlations for the mass transfer coefficient, k_g, found in literature have been evaluated here. Simulations of the heterogeneous reactor model with a constant profile of T_{w2} as input was performed to find the overall effects of the different correlations.

The correlation given by Cussler (1997) was stated without literature source and validity range:

$$k_{g,i} = 1.17\, v_s\, Re_p^{-0.42}\, Sc_i^{-0.67} \tag{5-1}$$

Dwivedi and Upadhyay (1977) reanalyzed previous experimental data to develop an expression valid for fixed and fluidized beds at Reynolds numbers ranging from 10 up to $1.5 \cdot 10^4$:

$$k_{g,i} = 0.4548 \frac{v_s}{\varepsilon} Re_p^{-0.4069} Sc_i^{-2/3} \quad (5\text{-}2)$$

Comti et al. (2000) introduced a wall energy criterion to generalize the expression for the Sherwood number. They concluded that their prediction was almost identical to the results using the correlation of Dwivedi and Upadhyay (1977) in the range of Reynolds numbers relevant for steam reformers. This correlation has therefore not been included in the test simulations.

Wakao and Funazkri (1978) corrected previous published mass transfer data for the effective axial dispersion coefficient and obtained higher mass transfer rates for gas phase systems than those where axial dispersion was neglected. Most of these data came from experiments where the gas velocities were low and the axial dispersion consequently should have been allowed for in the component balance. The resulting correlation was proven also for the range of high Reynolds numbers, which means that it is also valid for conditions where the axial dispersion is negligible in proportion to the axial convection, leading to the simplification to a plug flow model of the reactor. The following correlation was deduced for the range of Reynolds number 3 to 10^4:

$$Sh_i = 2 + 1.1 Re_p^{0.6} Sc_i^{1/3} \quad (5\text{-}3)$$

As pointed out in Section 2.5 the mass transfer resistance in the gas film surrounding the catalyst pellet is usually neglected in steam reformer models. In order to be able to discuss the need of including this in the model, without having to discuss the exact correlation used, a correlation giving high mass transfer coefficients was employed here. This is because an unrealisticly high value is equivalent to a model where the mass transfer is disregarded. The correlation of Wakao and Funazkri (1978) gave the highest coefficients of the correlations evaluated and was therefore chosen for the model. Figure 5-1 shows the axial profiles of the mass transfer coefficient of methane resulting from the three test simulations based on Equations (5-1) to (5-3). The profiles for the gas temperature and the compositions are not significantly affected by these small variations in mass transfer coefficient. The maximum variations in outlet temperature and methane conversion are 0.26 ºC and 0.02 percentage points, respectively.

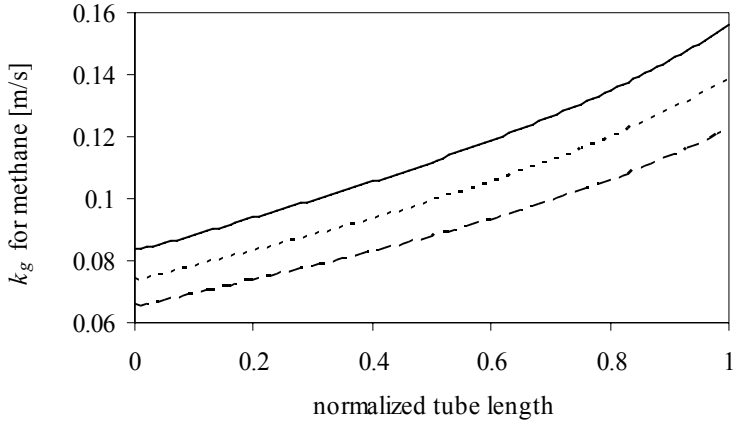

Figure 5-1. Mass transfer coefficients, $k_{g,CH4}$, resulting from the evaluated correlations for k_g. — Wakao and Funazkri (1978), - - - Dwivedi and Upadhyay (1977), – – Cussler (1997).

5.1.2 The pellet heat transfer coefficient, h_p

The heat transfer coefficient in the gas film surrounding the pellet, h_p, is used in the heterogeneous reactor model. The reactor model was tested with a constant profile of T_{w2} as input to evaluate two different empirical correlations for h_p.

The fluid-solid heat transfer coefficient correlated by Handley and Heggs (1968) is given by:

$$Nu_p = \frac{0.255}{\varepsilon} Pr^{1/3} Re_p^{2/3} \tag{5-4}$$

Wakao et al. (1979) collected published heat transfer data and corrected them for the axial thermal dispersion. This was done because the data were obtained from experiments of low gas velocities, i.e. of conditions where the axial thermal dispersion should be included in the energy balance. The developed correlation was verified for high Reynolds numbers, where the axial dispersion of heat may be ignored from the energy equation due to the larger convective contribution. The correlation is analogous to the mass transfer coefficient correlation of Wakao and Funazkri (1978), valid for Reynolds numbers in the range of 15 to 8500:

$$Nu_p = 2 + 1.1 Pr^{1/3} Re_p^{0.6} \tag{5-5}$$

The selected correlation (Wakao et al., 1979) gave the highest heat transfer coefficient, which is shown in Figure 5-2. As discussed for the mass transfer coefficient, the intention is here to investigate the need for modelling the heat transfer resistance in the gas film as this is often disregarded in steam reformer modelling. Choosing a correlation giving a high heat transfer coefficient should therefore give a conservative estimate of its effect with regard to this study. The chosen correlation gives a temperature drop across the gas film of about 1–7 ˚C, as is seen in Figure 5-3. Rostrup-Nielsen et al. (1988) claim that the bulk-catalyst temperature difference in steam reformers usually should be in the range of 5–10 ˚C, which is about the same range as

the simulated ones. The simulation results showed almost equal outlet reactor temperature and methane conversion for the two correlations, varying with only 0.38 ˚C and 0.03 percentage points, respectively.

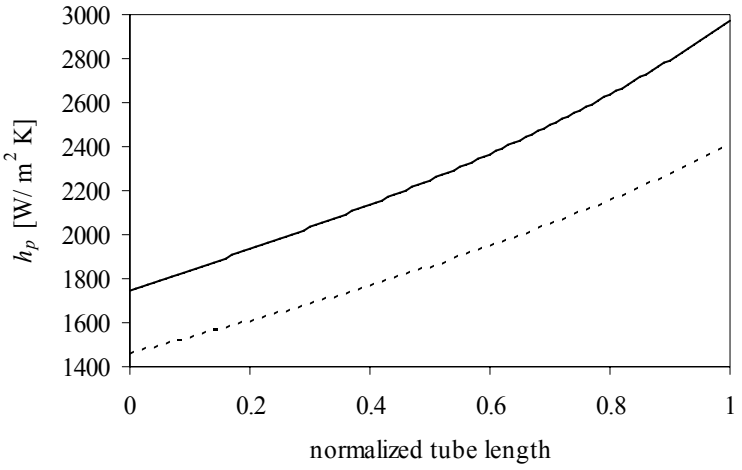

Figure 5-2. Pellet heat transfer coefficients, h_p, appearing from the two tested correlations. — Wakao et al. (1979), - - - Handley and Heggs (1968).

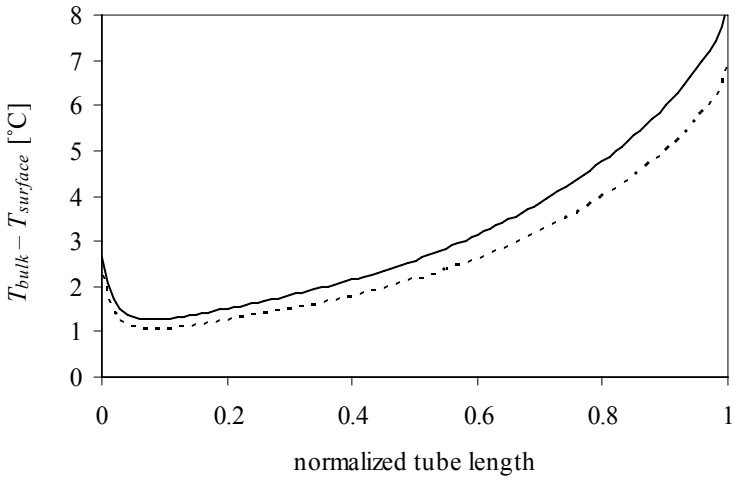

Figure 5-3. Temperature difference over the gas film resulting from both correlations. — Wakao et al. (1979), - - - Handley and Heggs (1968).

5.1.3 The diffusion coefficient, $D_{M,i}$

The component diffusion coefficients in the gas mixture, $D_{M,i}$, were estimated by the correlation of Wilke (1950). The correlation is widely used for multi-component mixtures although it is valid only for a component i diffusing in a stagnant, non-transferring mixture (Krishna and Wesselingh, 1997). The diffusivity of a component i in a gas mixture M is expressed by the binary diffusion coefficients D_{ik} and the mole fractions x_k, when k denotes the second component:

$$\frac{1}{D_{M,i}} = \sum_{k \neq i} \frac{x_k}{D_{ik}} \tag{5-6}$$

The binary diffusion coefficients are calculated from the method of Fuller et al. (1966), with the diffusion volumes $\sum_i V$ as listed by Perry and Green (1997):

$$D_{ik} = \frac{1.013 \cdot 10^{-2} T^{1.75} \left(1/M_i + 1/M_k\right)^{1/2}}{P\left[\left(\sum_i V\right)^{1/3} + \left(\sum_k V\right)^{1/3}\right]^2} \tag{5-7}$$

The *pseudo-binary* method is a simpler approach for estimating the molecular diffusion coefficients, where the diffusion coefficients for binary mixtures in Equation (4-21) are used for the gas mixture, i.e. $D_{M,i} = D_{ik}$. This approach was tested with methane defined as component k. The simulation results showed an increase in outlet reactor temperature of 1.7 ˚C and an increase in methane conversion by 1.4 percentage points compared with the simulation with Wilke's equation. These results show that although the Wilke equation is recommended in many textbooks, the pseudo-binary model may also be used for this purpose.

5.1.4 The thermal conductivity of the pellets, λ_c

The thermal conductivity of the catalyst pellets is set to the value of 0.208 W/ m K, which was measured for activated alumina at 1 atm and 322 K by Touloukian et al. (1970).

5.1.5 The fixed bed effective radial dispersion coefficient, $E_{er,b}$

The two correlations for the effective radial dispersion coefficient, $E_{er,b}$, given in Equation (2-11) (Fahien and Smith, 1955) and Equations (2-12) to (2-15) (Delgado, 2006), were evaluated in the reactor model. Test simulations using the total GHR model with the heterogeneous reactor model were performed, using both correlations. The resulting axial profiles of the effective radial dispersion coefficients are reported in Figure 5-4. The simulation results were remarkably similar; both the outlet temperatures T_b and T_a were equal in the two cases, and the methane conversion was reduced only by 0.2 % (and 0.04 percentage points) from the simulation with the diffusion coefficient of Fahien and Smith (1955) to the simulation with the diffusion coefficient of Delgado (2006). It was therefore decided to use the simplest expression; Equation (2-11) by Fahien and Smith (1955).

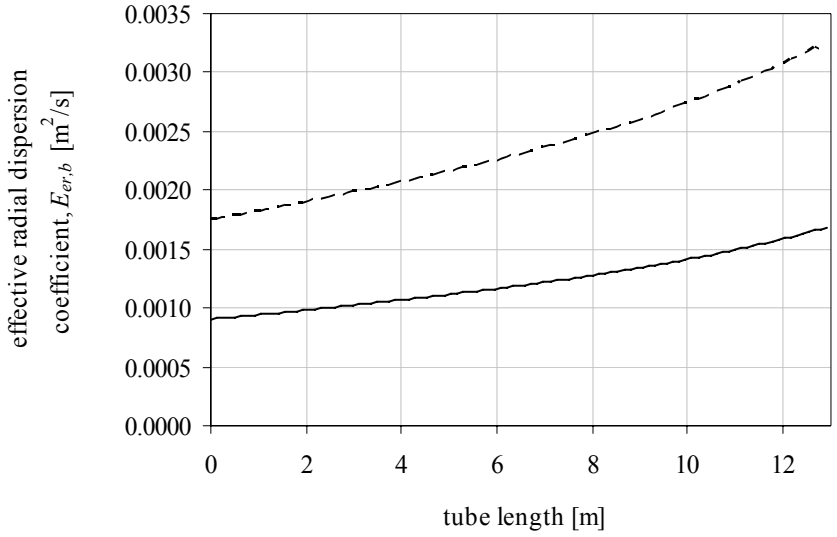

Figure 5-4. Comparison of estimated fixed bed effective radial dispersion coefficients. —— Fahien and Smith (1955) and – – – Delgado (2006).

5.1.6 The fixed bed effective radial thermal conductivity, $\lambda_{er,b}$

The effective radial thermal conductivity in the reactor bed, $\lambda_{er,b}$, is normally a function of radial position. However, the radial variation was found to be small and its effect on the simulation results was found to be negligible. Therefore, the model equations for $\lambda_{er,b}$ were simplified by using radial mean values, which are estimated as given in Appendix E. As a consequence, the conduction term of the energy equation (Equation (4-32)) shortens to:

$$\frac{1}{r}\frac{\partial}{\partial r}\left(r\,\lambda_{er,b}\frac{\partial T}{\partial r}\right)=\lambda_{er,b}\left(\frac{1}{r}\frac{\partial T}{\partial r}+\frac{\partial^2 T}{\partial r^2}\right) \tag{5-8}$$

Borkink and Westerterp (1994) summarized several other arguments for modelling $\lambda_{er,b}$ from average values, where the two most important are: 1) In a real physical system the superficial velocity, $v_{z,s}$, and the bed porosity, ε, increase with increasing tube radius. $\lambda_{er,b}$ increases with $v_{z,s}$ and decreases with ε. The only exception from this opposing effect is seen close to the wall where $\lambda_{er,b}$ rises sharply. This is here modelled by the use of h_w. 2) Local values of $\lambda_{er,b}$ as function of tube radial position is hardly possible to measure experimentally.

Peters et al. (1988) gave an empirical correlation for the effective radial thermal conductivity of a fixed bed together with the empirical heat transfer coefficient described in Section 5.1.7. Since this heat transfer coefficient was chosen for the reactor model the effective radial thermal conductivity given with this was considered to be a natural choice. This correlation is given by the equation:

$$\lambda_{er,b} = \lambda^{0}_{er,b} + \lambda_g \frac{Re_p Pr}{Pe_h} \tag{5-9}$$

The Peclet number for radial heat transfer, Pe_h, can with negligible error be replaced with the Peclet number for mass transfer, Pe_m, for Reynolds numbers greater than 1000. Pe_m was given by the following equation for $100 < Re_p < 880$:

$$Pe_m = 3.2 + 49.4\left(d_p / d_t\right) \tag{5-10}$$

The effective radial thermal conductivity for stagnant gas, $\lambda^{0}_{er,b}$, was correlated as derived by Kunii and Smith (1960), which still stands as the most suitable correlation (Dixon, 1988):

$$\lambda^{0}_{er,b} = \lambda_g \varepsilon + \lambda_g \frac{0.895\left[1-\varepsilon\right]\left(\ln\left[\frac{\lambda_p}{\lambda_g} - 0.5439\left(\frac{\lambda_p}{\lambda_g} - 1\right)\right] - 0.4561\frac{\lambda_p - \lambda_g}{\lambda_p}\right)}{0.5 \cdot 0.7042\left[\frac{\lambda_p - \lambda_g}{\lambda_p}\right]^2} \tag{5-11}$$

5.1.7 The fixed bed wall heat transfer coefficient, h_1

A great number of empirical correlations for the heat transfer coefficients at the wall in a fixed bed have been published, with many of them summarized in Section 2.3.2.1. Only the correlations valid at steam reforming operating conditions have been chosen for evaluation in this work. Five different correlations were evaluated in Wesenberg et al. (2001) against calculations from data based on Statoil in-house empiricism. The simulations were performed in a pseudo-homogeneous reactor model with a constant effective thermal conductivity.

The correlation from Li and Finlayson (1977) is based on experiments with air and is valid for spheres with d_p/d_t between 0.05 and 0.3, for Reynolds numbers between 20 and 7600 and for Biot numbers less than 12:

$$Nu_w = 0.17\, Re_p^{\,0.79} \tag{5-12}$$

Wall temperatures were held constant. Data influenced by length effects were eliminated, so that the desired asymptotic form of the heat transfer coefficient was achieved. An extension by multiplying with $(Pr/0.7)^{1/3}$ was suggested to include the Prandtl number dependence, but this was not confirmed by experiments. This form is denoted the *modified* Li and Finlayson correlation on the result diagrams below.

Dixon et al. (1984) studied mass transfer in packed beds with low tube-to-particle diameter ratio to provide correlations for Nu_w and Pr in terms of Re_p and d_t/d_p. The authors showed good agreement with heat transfer data for Reynolds numbers up to 8000 at $d_t/d_p = 3.3$ the, but only for $Re_p < 500$ at $d_t/d_p > 7.4$:

$$Nu_w = \left(1 - 1.5\left[d_p/d_t\right]^{1.5}\right) Re_p^{0.59} Pr^{0.33} \tag{5-13}$$

De Wasch and Froment (1972) developed an expression where the wall heat transfer coefficient is proportional to the product of the Reynolds number and the tube-to-particle diameter ratio. The use of a static contribution, h^0_w, gives the coefficient at zero flow:

$$h_w = h_w^0 + 0.01152\left(d_t/d_p\right) Re_p \tag{5-14}$$

h_w is here given in kcal/(hr m^2 K). The experiments were done with air at 50°C and Re_p < 450. Data for h_w^0 were given only for catalysts for other applications than syngas production and the mean value of h_w^0 = 70 kcal/(hr m^2 K) was therefore used in this test.

Peters et al. (1988) put the main focus on low tube-to-particle diameter ratios (1.7–10) and high Reynolds numbers (up to 8000). The Nusselt number is dependent on the particle-to-tube diameter ratio and the Prandtl number as well as the Reynolds number. Also here the experiments were performed with dry air. The authors claim that the correlation for spheres is valid for Reynolds numbers less than 8000:

$$Nu_w = 4.9\left(d_p/d_t\right)^{0.26} Re_p^{0.45} Pr^{0.33} \tag{5-15}$$

The main objective of the work of Dixon and Cresswell (1979) is a theoretical rather than an empirical approach. Correlating the wall heat transfer coefficient to the Biot number instead of the Nusselt number gives a unique relationship with the Reynolds number, making the wall heat transfer coefficient independent on particle size and conductivity. The correlation is valid for $Re_p > 40$:

$$Bi_w = 3.0\, Re_p^{-0.25} \tag{5-16}$$

Equations (5-12) to (5-15) were used in the test simulations for different cases with steam reforming. Equation (5-16) was not tested because of the choice of a constant effective thermal conductivity and the direct proportionality between h_w and λ_{er}. The dependency of h_w and λ_{er} require a consistent empirical model for λ_{er}.

As indicated by Tsotsas and Schlünder (1990), and as emphasized in Section 2.3.4, the wall heat transfer coefficient in form of the wall Nusselt number correlate well with the Reynolds number in the range of high Reynolds numbers. Large differences in these test simulation results were therefore not expected. The estimated wall heat transfer coefficients, bulk temperatures and methane conversions from the test simulations are presented in Figure 5-5, Figure 5-6 and Figure 5-7, respectively. These results were compared with empirically derived data from the steam reformer in Statoil's methanol plant at Tjeldbergodden. These data are restricted and all data are thus presented on normalized form.

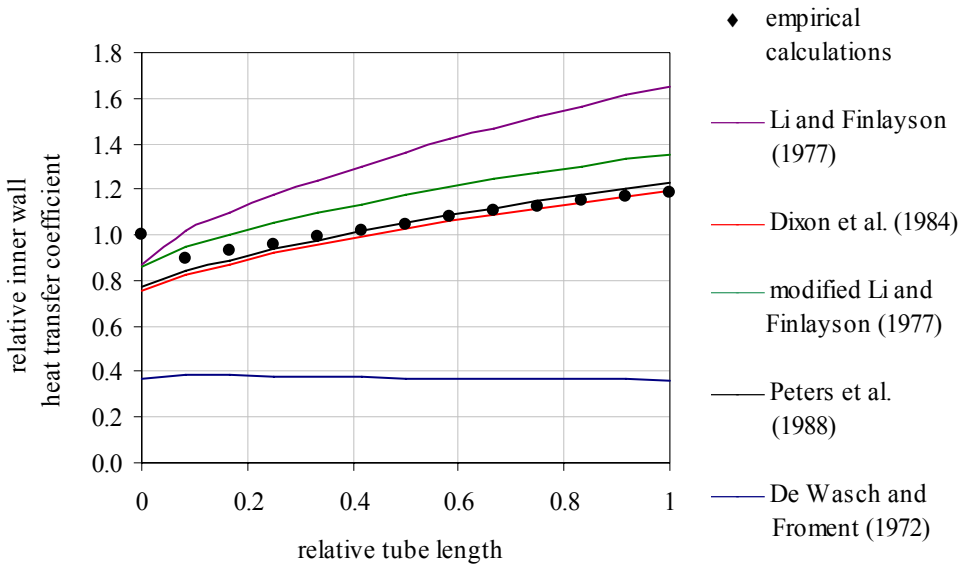

Figure 5-5. Relative heat transfer coefficients at the inner wall of the fixed bed calculated from the five tested correlations compared with calculations from empirical data.

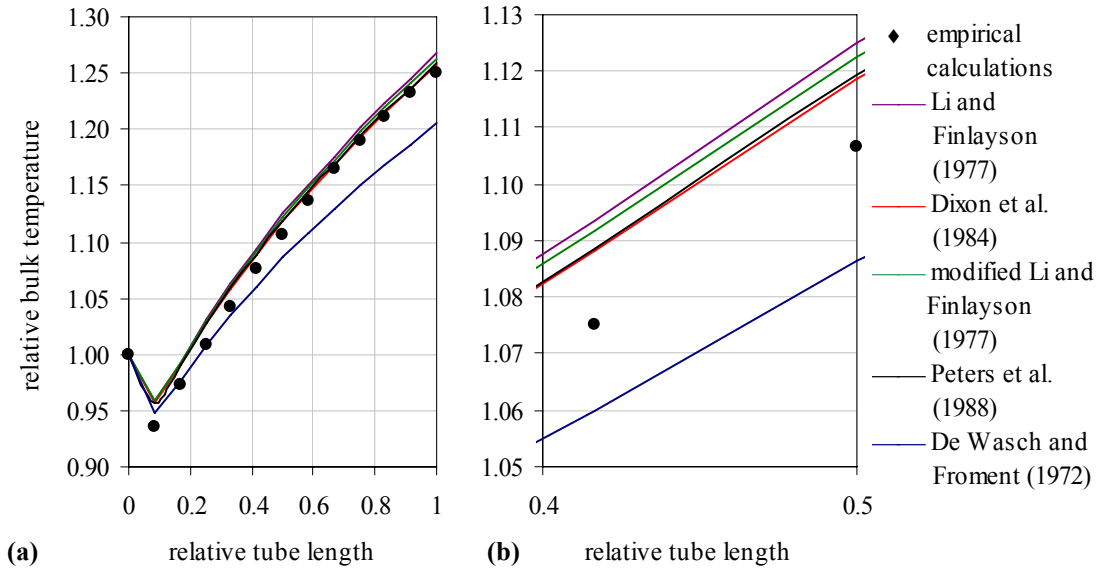

Figure 5-6. Axial profiles of the radial mean bulk temperatures, relative to inlet temperature, calculated with the use of the five evaluated correlations for wall heat transfer coefficient (a). Expanded view of the temperatures at z = 0.5–0.6 L (b). Comparison with empirical data.

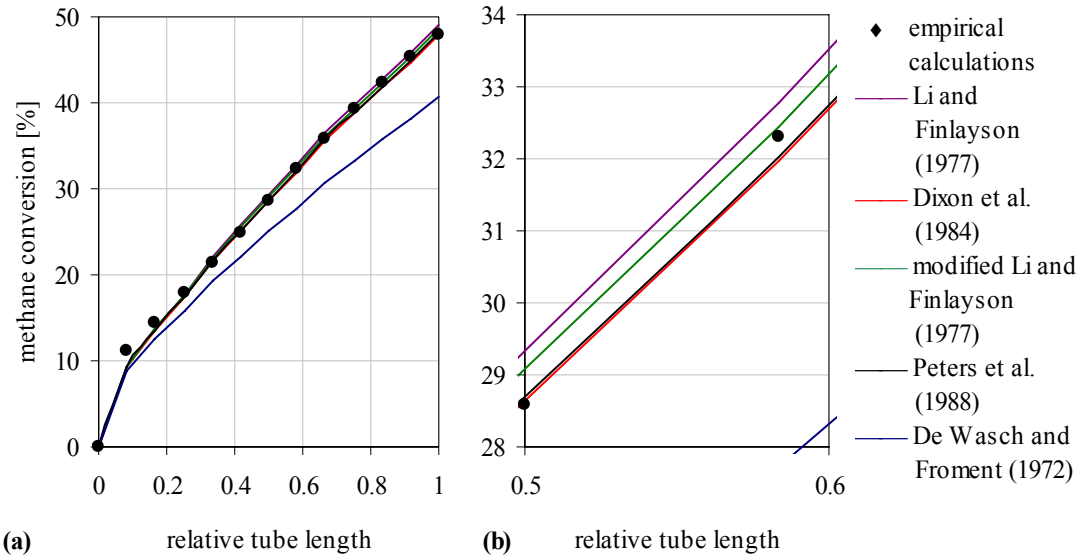

Figure 5-7. Methane conversion computed with the five evaluated heat transfer coefficients for fixed beds (a). Expanded view of the conversion at the range z = 0.5–0.6 L (b). Comparison with empirical data.

The given results show that the correlations of Peters et al. (1988) in Equation (5-15) and Dixon et al. (1984) in Equation (5-13) give predictions closest to the compared data. In steam reformers the typical range for the d_t/d_p ratio is 12–15 and the Reynolds numbers are usually in the range of 10^3–10^4. The correlation of Peters et al. (1988) was proven for d_t/d_p = 1.7–10 and Re_p < 8000, and the correlation of Dixon et al. (1984) was proven by the authors for Re_p < 500 when d_t/d_p > 7.4, and later verified by Tsotsas and Schlünder (1990) for Re_p < 10^4 with d_t/d_p = 10. This concludes that both correlations are out of the steam reformer range, but still very close. They are therefore both recommended here for the use of steam reformers, and the correlation of Peters et al. (1988) was chosen for the GHR model.

5.1.8 The friction factor for the fixed bed pressure drop equation

The equation of Ergun (1952) is very often used to express the friction loss in steam reformer models and also in packed bed models in general. Hicks (1970) evaluated several empirical correlations to deduce an equation which is valid at higher Reynolds numbers ($Re_p/(1-\varepsilon)$ > 300), given by Equation (4-30). Ergun's equation is valid only up to $Re_p/(1-\varepsilon)$ < 500, which is lower than seen in steam reformers. Typical values for steam reformers are $10^3 < Re_p < 10^4$ and $\varepsilon = 0.5$, which gives $2\cdot10^3 < Re_p/(1-\varepsilon) < 2\cdot10^4$. The two equations were compared, and the equation of Hicks resulted in a 2.9 bar pressure drop and the equation of Ergun gave a 5.9 bar pressure drop for the given industrial case. The typical operating pressure drop in a steam reformer is 3 bar. Based on these calculations, on the validity of the correlations, and on the fact that the geometry of the chosen catalyst is favourable as regards pressure drop, the equation of Hicks (1970) was chosen for the reactor model.

5.2 The parameters of the annulus model

5.2.1 The annulus wall heat transfer coefficients, h_2 and h_3

There are not many correlations for the wall heat transfer coefficients for annular ducts published in open literature. Both Gnielinski (2002) and Mills (1992) recommend using the wall Nusselt number relation of Gnielinski (1976) derived for straight tubes and valid for $3 \cdot 10^3 < Re_h < 10^6$, multiplied with the correction factors of Petukhov and Roizen (1964) for annular ducts. They also both recommend the same formula for the friction factor, F, referred by Mills (1992) to as Petukhov's formula (Petukhov, 1970), and with reference to Filonenko (1954) by Gnielinski (2002). This gives the equation system of Equations (4-54) to (4-58).

Dirker and Meyer (2005) compared this correlation with other correlations to derived a new expression for the Nusselt number based on the radial mean fluid temperature, not the fluid temperature at the wall as needed for the annulus model of Section 4.5. This means that this correlation cannot be used for this model. Dirker and Meyer (2005) listed the cited correlations used in their study, and the correlation of Petukhov and Roizen (1964) was the only correlation valid for both the Reynolds numbers and aspect ratios found in the annulus model of this thesis ($10^4 < Re_h < 3 \cdot 10^5$ and $1 < d_3/d_2 < 14.3$, respectively). Based on this, it was decided to use the equation system discussed above.

5.2.2 The annulus effective radial thermal conductivity, $\lambda_{er,a}$

The effective radial thermal conductivity in the annular section is a function of both radial and axial position. This is shown from the simulation results of the FLUENT model in Figure 5-8 and Figure 5-9.

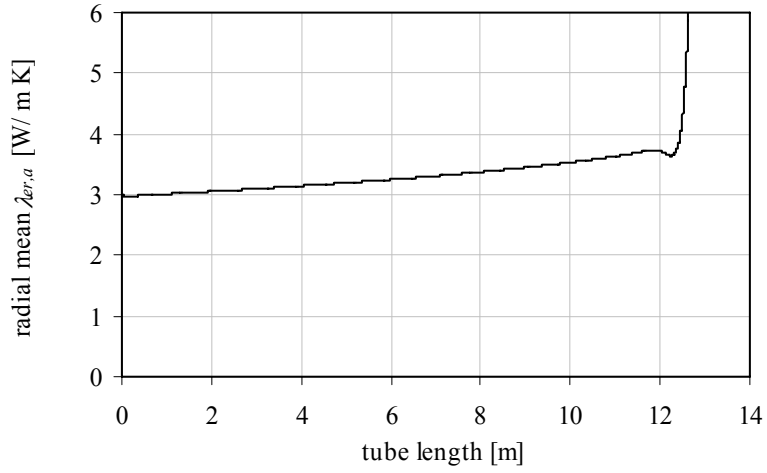

Figure 5-8. Example of the axial dependency of $\lambda_{er,a}$ calculated in the FLUENT annulus model using the k-ε turbulence model.

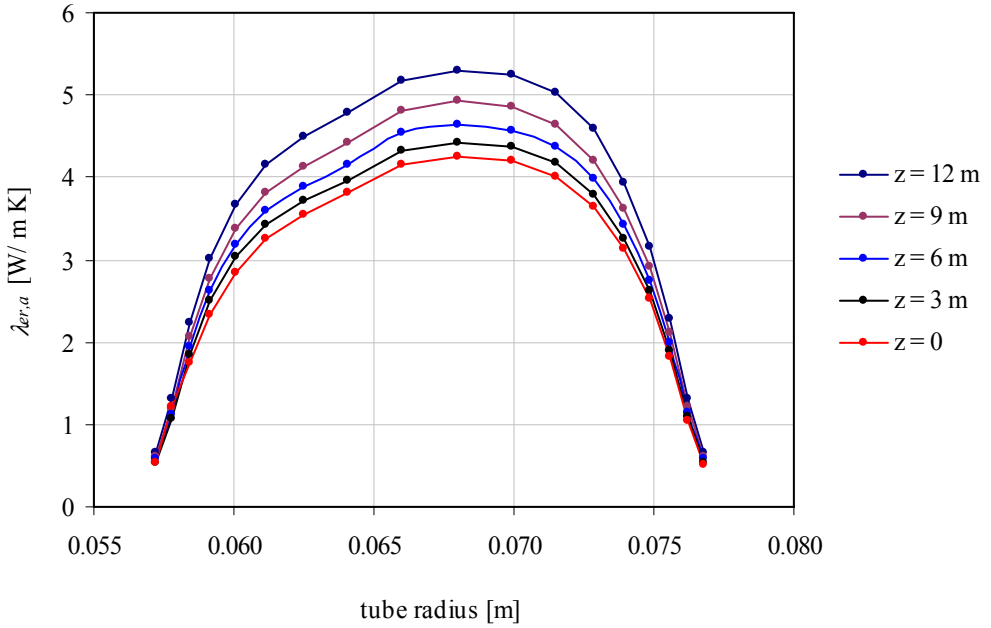

Figure 5-9. Example of the radial dependency of $\lambda_{er,a}$ calculated in the FLUENT annulus model using the *k-ε* turbulence model.

The data of $\lambda_{er,a}$ from the FLUENT simulations were used to develop a function for $\lambda_{er,a}$ which could be used in the MATLAB model. The importance of including the spatial variations was looked into, owing to the request of keeping the function for $\lambda_{er,a}$ as simple as possible. The test simulations involved the following cases:

Case 1: Axially dependent $\lambda_{er,a}$. The radial mean values of $\lambda_{er,a}$ are used for generating the function $\lambda_{er,a}(z)$, which varies from 3 to 3.7. The large values at the entrance region, as indicated in Figure 5-8, are disregarded to ensure numerical stability.

Case 2: Radially dependent $\lambda_{er,a}$, based on the radial profile at $z = 0.46L$. This axial position represents the mean value of the function of case 1. $\lambda_{er,a}$ is parabolic with the value of 0.57 W/ m K at the walls and of 4.64 W/ m K at the maximum (which is centred in the annulus).

Case 3: The radial mean value of the profile of case 2. $\lambda_{er,a} = 3.3$ W/ m K.

Case 4: $\lambda_{er,a}$ is enhanced to $\lambda_{er,a} = 10$ W/ m K.

Case 4 was included to investigate the effects of enhancing turbulence in the annular section.

The comparison of simulation results from these tests is given in Figure 5-10, Figure 5-11 and Figure 5-12. The outlet conditions shown in Figure 5-10 and Figure 5-11 are also summarized in Table 5-1. As seen from the results in this table, the axial variations in $\lambda_{er,a}$ (case 1) gives negligible effect compared to using the mean value of this function (case 3). On the other hand, the results from case 2, where the radial variations are included, stand out from the other results. The effect of the function of

radial position is clear from Figure 5-12 which shows that the radial temperature profiles of case 2 is steeper close to the walls than the other cases. Based on these result it was decided to include the radial dependence of $\lambda_{er,a}$ in the MATLAB model.

The inclusion of the radial profile was also observed to be of considerably greater importance than to find the exact values of this function. This means that changing the values of the profile function by 10 % gives negligible effects on the overall simulation results, while changing the shape of the radial profile may give noticeable effects. Therefore, the profile chosen from the FLUENT simulations could be read about midways in the axial direction without putting effort into finding the exact mean values. The small variance in this profile compared to an averaged profile will not give differences in overall simulation outputs. This importance of including the radial profile is verified in the comparison of two different turbulence models in FLUENT in Section 5.2.3. The differences in the values and similarities in profile shape of the effective radial thermal conductivities are clear from Figure 5-14, and the almost identical comparing simulation results from using two of these radial profiles are seen in Table 5-2.

One drawback with having $\lambda_{er,a}$ as a function of radial position is that this demands a good radial numerical resolution to obtain a satisfactory overall heat balance. The resolution has been tested in Section 6.3. It should be noted that the radial variation in $\lambda_{er,a}$ increases with increasing turbulence, which means that even better radial numerical resolution will be required for such cases.

The effect of increasing turbulence in the annular section can be seen from case 4 compared with case 3. The outlet temperature was reduced by 14 ºC, which represents the enhanced heat transport. This is also seen on the reactor model simulations, where the methane conversion was increased by 2 % (and 0.6 percentage points).

Table 5-1. Outlet temperature of the annular section and methane conversion in the fixed bed resulting from test simulations of various functions for $\lambda_{er,a}$.

	Outlet temperature, annulus [ºC]	Methane conversion in reactor bed [%]
Case 1:	574.1	30.80
Case 2:	583.9	28.85
Case 3:	574.9	29.51
Case 4:	561.2	30.11

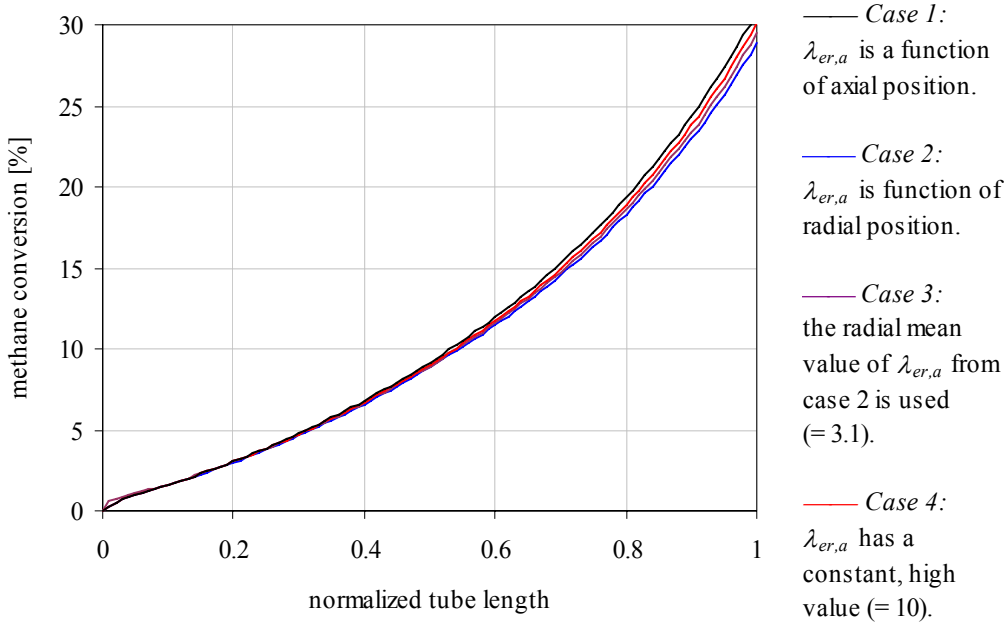

Figure 5-10. Methane conversion resulting from test simulations with varying effective radial thermal conductivity, $\lambda_{er,a}$, in the annulus model.

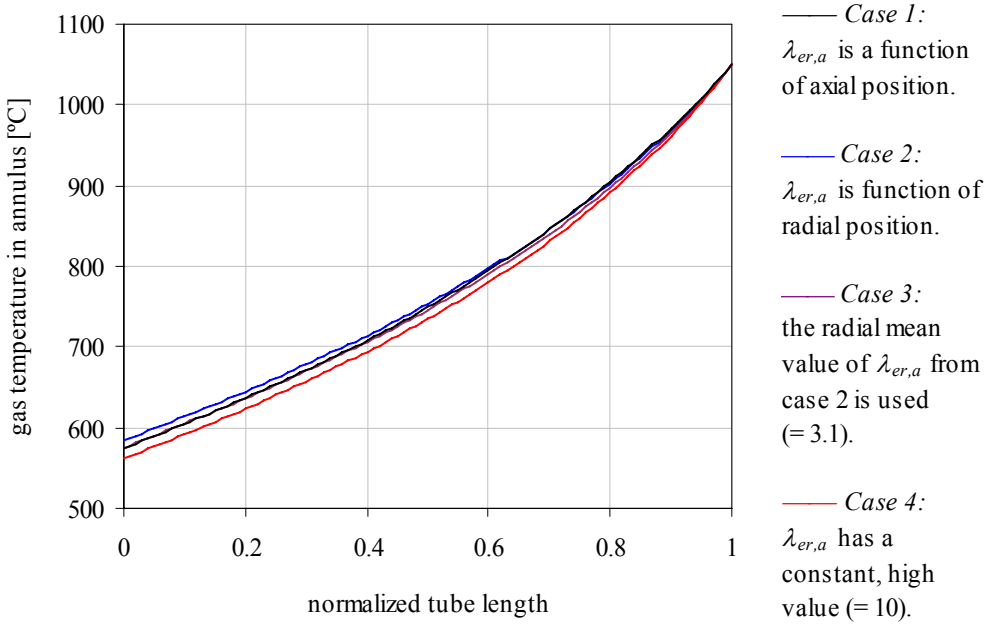

Figure 5-11. Gas temperature in annulus resulting from test simulations with varying effective radial thermal conductivity, $\lambda_{er,a}$, in the annulus model.

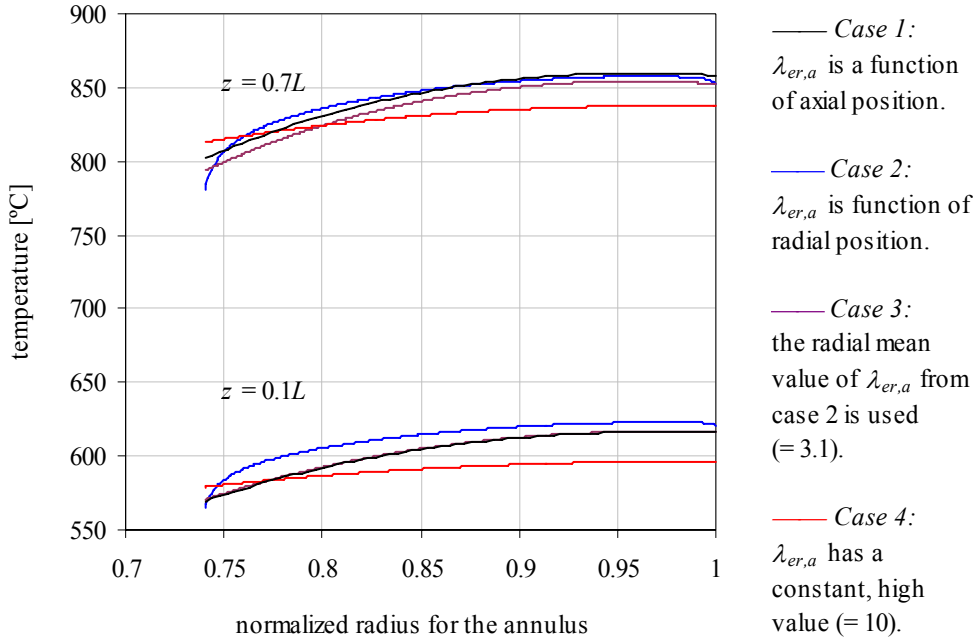

Figure 5-12. Radial temperature profiles estimated in the test runs of varying effective radial thermal conductivity, $\lambda_{er,a}$, in the annulus model. The profiles are given for the two axial positions $z = 0.1L$ and $z = 0.7L$.

In order to verify the effective thermal conductivity model for the annulus, the annulus models in MATLAB and in FLUENT were tested without the radiation model. This was done to eliminate any differences in the radiation models so that only the turbulent heat transport was present. In addition the differences in correlation for the wall heat transfer coefficient were eliminated by using the calculated profile of h_{w2} from FLUENT in the MATLAB model. The previous assumption that the λ_{er} calculated in a corresponding CFD code could be used in the finite difference model could then be tested to see if it gave the same radial heat flux profile as the CFD model. The CFD model was run with the k-ε turbulence model, and the finite difference model implied no calculations of turbulence other than the effect on radial heat transport through the imported λ_{er}.

The resulting axial profile for wall temperature from the finite difference model was used as input to the CFD model, which again produced a radial profile for λ_{er} and wall heat transfer coefficient that was input to the finite difference model. Manual iteration with these two models quickly resulted in a stable output and the two models gave the same temperature profiles. Only two iterations were needed. The outlet temperature from the annulus was 5.4 °C lower in the MATLAB simulation compared with the FLUENT simulation. Even the radial temperature profiles were nearly identical, as can be seen in from the dotted and the solid lines in Figure 5-13. This confirms that an enhanced effective radial thermal conductivity profile calculated from the k-ε turbulence model in a CFD code can be used in a simpler finite difference model with no turbulence model and describe the effect of turbulent flow on radial heat transfer well. The calculation of the heat transfer coefficients are on the other hand different,

which is visualized by the stippled line of Figure 5-13. This line represents a test simulation without the import of the wall heat transfer coefficients, h_2 and h_3, calculated from the FLUENT code. h_2 and h_3 were the calculated as given in Section 4.5. The simulation results can on the other hand not suggest if the correlation for the wall heat transfer coefficient in the finite difference GHR model is more or less physical reliable than the correlation used in the FLUENT code.

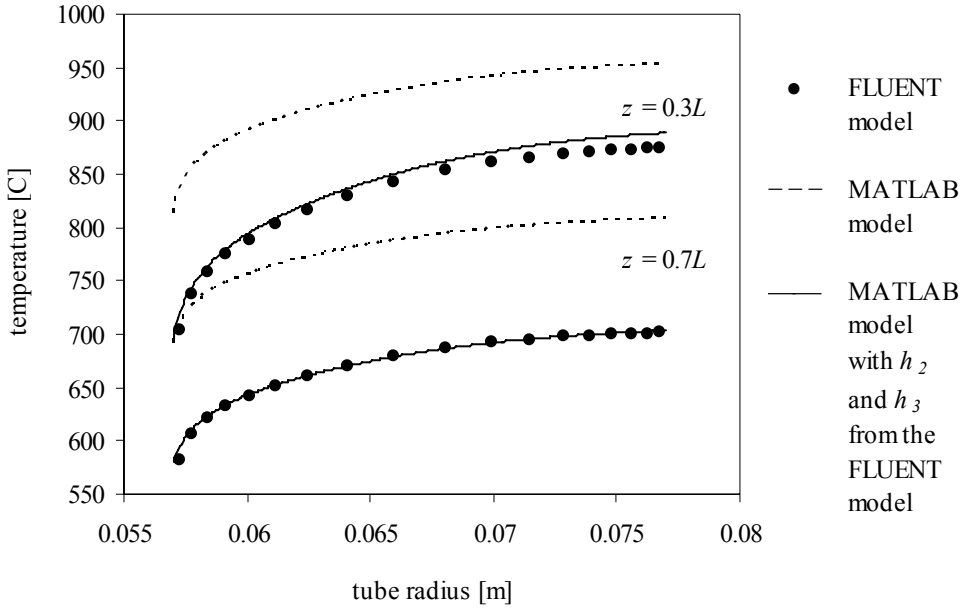

Figure 5-13. Comparison of radial temperature profiles resulting from equivalent test simulations of the annular section in the FLUENT model (dotted line) and in the MATLAB model (solid line). The test simulations are without radiation models. The stippled lines result from MATLAB simulations with wall heat transfer coefficients as specified for the GHR model.

5.2.3 Evaluation of different turbulence models in FLUENT

The sensitivity to the choice of turbulence model was looked into by reproducing the FLUENT simulation with the Reynolds stress turbulence model instead of the k-ε turbulence model. The radial profiles of $\lambda_{er,a}$ from these two FLUENT simulations at different axial positions are plotted in Figure 5-14. The radial profiles at $z = 0.46L$ were exported to perform corresponding simulations of the complete GHR model in MATLAB. The results from these simulations are given in Table 5-2. As can be seen from the figure the estimated $\lambda_{er,a}$ from the two turbulence models are not equal. The maximum difference at $z = 0.46L$ is a 24 % reduction in the Reynolds stress case relative to the k-ε case. This difference is on the other hand too small for giving effects on the GHR model. This is shown by the almost identical results of the table. Therefore the results from the FLUENT model based on the k-ε turbulence model are assumed satisfactorily for this modelling purpose.

The estimated outlet temperatures from the FLUENT simulations shown in Table 5-2 are on the other hand 36 °C and 32 °C lower than from the MATLAB simulations for the k-ε case and the Reynolds stress case, respectively. This is

nevertheless acceptable because these differences are likely to come from the possible differences in calculation method for the radiative heat flux in the FLUENT code and in the GHR model. Also, the use of the exported $\lambda_{er,a}$ in the MATLAB model was verified for cases where radiative heat transport was disregarded in Section 5.2.2.

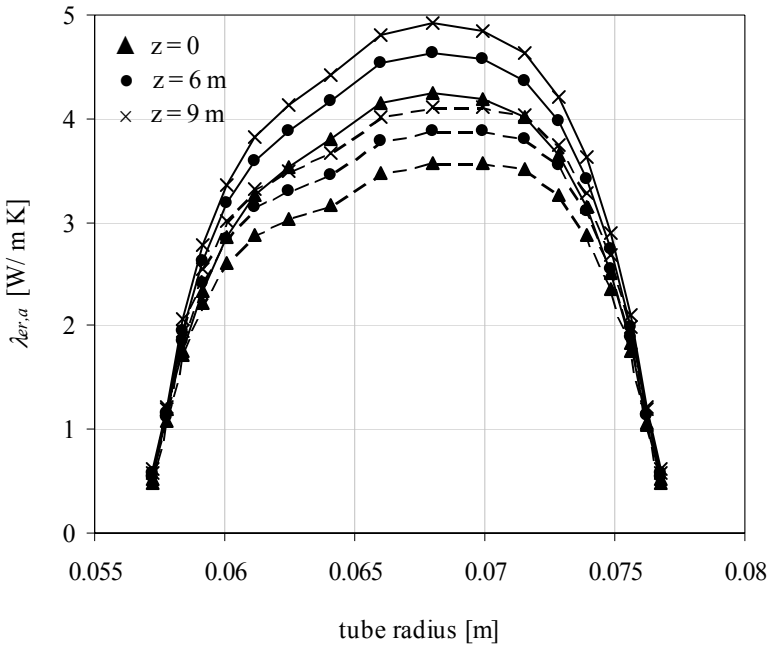

Figure 5-14. Effective radial thermal conductivities in the annular section, calculated in the FLUENT model. — *k-ε* turbulence model, – – Reynolds stress turbulence model.

Table 5-2. Simulation results from comparative GHR models using the radial dependent functions of $\lambda_{er,a}$ calculated in FLUENT models based on the *k-ε* turbulence model and on the Reynolds stress model.

	Outlet temperature, annulus, ºC	Outlet temperature, reactor bed, ºC	Methane conversion, %
A) MATLAB model with $\lambda_{er,a}$ from B)	583.8	704.2	28.85
B) FLUENT model with the *k-ε* model	547.6		
C) MATLAB model with $\lambda_{er,a}$ from D)	583.4	704.0	28.49
D) FLUENT model with the Reynolds stress model	551.1		

6 ANALYSIS OF NUMERICAL RESOLUTION

Deciding the numerical resolution is important to balance the need for satisfactory accuracy against the need for acceptable computation times. The suitable resolutions in the tubular and annular spaces and in the catalyst pellet slab were therefore analyzed as given in this section.

Test simulations were performed to evaluate the needed spatial resolutions in the models. The precisions of the test simulations were determined by comparing the resulting total heat fluxes calculated by varying methods. Also the heat flux *profiles* were checked. The different calculated heat fluxes are defined as:

$Q_{b,F}$: calculated from the heat flux equation in the reactor bed model; Equation (4-85).
$Q_{a,F}$: calculated from the heat flux equation in the annulus model; Equation (4-86).
$Q_{b,E}$: calculated from enthalpy changes in the reactor bed; Equation (4-81).
$Q_{a,E}$: calculated from enthalpy changes in the annulus; Equation (4-81).

The results from the test simulations are presented as the relative error:

$$\text{relative error} = \frac{|Q_F - Q_E|}{Q_F} \tag{6-1}$$

Additionally, the computation time of the test simulations were considered when deciding the suitable numerical resolution.

6.1 Axial numerical resolution

The axial step length used during the solving of the differential equations is decided automatically in the ODE-solvers in MATLAB, depending on the gradients of the differential equations. The step length therefore varies throughout the reactor length, with small step lengths at the inlet and increasing lengths throughout.

The step length of the *output* of the ODE-solvers can on the other hand be specified from the input file. This means that the matrix of temperatures and partial pressures resulting from the reactor or annulus simulation attains a predefined length of rows. This is utilized in the models to assure that the reactor models and the annulus model produce results of the same format in such a way that these results can be

compared and checked for convergence. This predefined step length is defined from the specified number of axial discretization steps, denoted N_z.

Simulations of varying number of axial discretization steps, N_z, were performed to find the adequate number. The results of these test simulations are given in Figure 6-1. These tests were performed for radial numerical resolution optimized for the number of 100 axial steps. This can be seen from the graph showing that $N_z = 100$ gives the minimum relative errors. The choice of this numerical resolution is based on general observations of the overall performance of the model system.

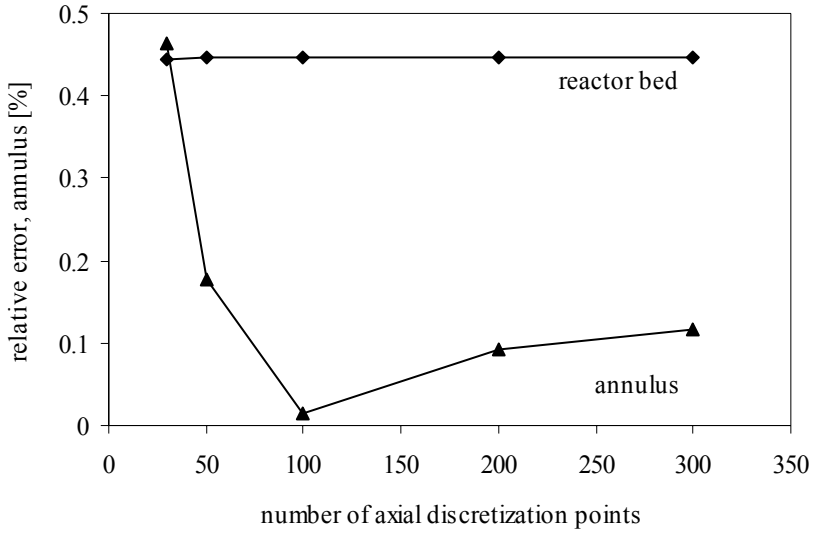

Figure 6-1. Relative error (defined in Equation (6-1)) and relative computation time resulting from the test simulations of varying N_z. Simulation of the total GHR model (heterogeneous reactor model and annulus model).

6.2 Radial numerical resolution in the reactor bed

The needed spatial resolution in the radial direction in the reactor tube was tested by running the heterogeneous reactor model with a varying number of radial discretization points, $N_{r,b}$. The input for the reactor simulations was a constant axial heat flux profile at the outer tube wall. The total heat flux given from this input was finally compared to the added heat calculated from an enthalpy balance of the gas mixture (Equation (4-81)) and these results were presented as relative errors, as defined in Equation (6-1). The results are shown in Figure 6-2. It can be seen that the radial resolution in the reactor model can be kept relatively low, and that an increase from 10 to 15 points hardly improves the accuracy. Another crucial point when deciding the needed resolution is the computation time, which increases strongly with the numerical resolution. A number of 15 radial steps was chosen because this is where the relative error curve flattens out and where computation time still is tolerable. The relative error in total heat supply to the reactor is at this point 0.55 %, which was deemed satisfactory.

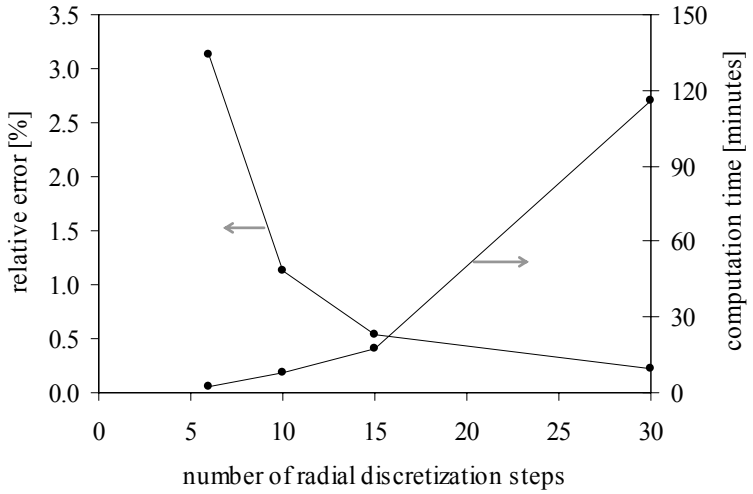

Figure 6-2. Relative error (defined in Equation (6-1)) and computation time resulting from the test simulations of varying $N_{r,b}$. Simulations of the heterogeneous reactor model with a predefined axial heat flux profile as input.

6.3 Radial numerical resolution in the annular volume

The accuracy of the annulus model was tested for a varying number of radial discretization points, $N_{r,a}$. The annulus model was run with a constant profile of the outer tube wall temperature, T_{w2}, as input. The overall heat loss was calculated from the convective and radiative heat fluxes (Equation (4-86)) and from the change in enthalpy (Equation (4-81)) to estimate the relative errors, as defined in Equation (6-1). These results are given in Figure 6-3 together with the respective computation times.

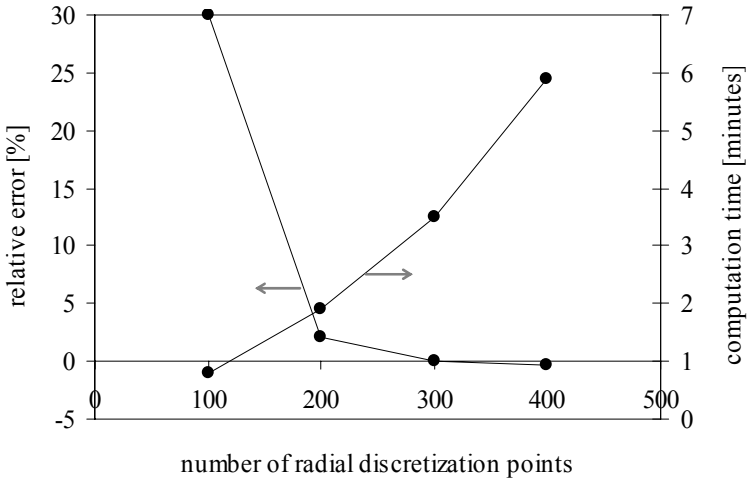

Figure 6-3. Relative error (defined in Equation (6-1)) and computation time resulting from the test simulations of varying $N_{r,a}$. Simulations of the annulus model with a predefined axial wall temperature (T_{w2}) profile as input.

6.4 Depth of active layer and resolution in the catalyst pellets

The pellet equations are solved only for a predefined depth in the pellet; the active layer. This is because the internal diffusion limitations make the inner core of the pellet unavailable for reaction. In the inner core there is assumed no change in composition and temperature. By simulating only the active layer and not through the whole pellet volume, considerable computation time can be saved and still satisfactorily spatial resolution in the pellet can be maintained.

To check the accuracy of the calculations, simulations were performed with different depths of active layer and with different spatial numerical resolution. Both outlet conditions and pellet profiles were compared in the evaluation, shown in Table 6-1 and in Figure 6-4 and Figure 6-5, respectively. As can be seen in Figure 6-4 and Figure 6-5 the depth of the active layer is between 5 and 10 % of the equivalent pellet radius. Both the temperature and the partial pressure profiles are flat inside this point (case 1 to 3). The numerical discretization was investigated in cases 3 and 5 for comparison with cases 2 and 4, respectively, and it is obvious from the outlet data in Table 6-1 that sufficient numerical resolution is an important point for achieving precise simulations. The outlet results show good precision for the cases of good resolution (cases 2 and 4) and also for case 5 where the number of discretization points is reduced to the half compared to case 4. But when the resolution is reduced four times (case 3 compared to case 2) the precision is reduced, as seen by the decreased outlet temperature and increased methane conversion. It can also be concluded from Table 6-1 and Figure 6-4 and Figure 6-5 that it is better to use a somewhat small depth of active layer, as 5 % which is seen from the figure to be shorter than the active layer, combined with a good numerical discretization (case 5), than to use a deep enough active layer combined with long node distances (case 3).

Based on these results it was chosen to use a depth of active layer of 5 % of the equivalent radius, combined with the resolution of 5 discretization points for the simulations. This conclusion is also based on the computation time, which is reported in Table 6-1 for each simulation of the heterogeneous reactor model only. It is important to note that these results are strongly dependent on pellet geometry.

Table 6-1. Tests of necessary depth of active layer and needed numerical resolution in the solution of the pellet equations. The computation time applies for simulation of the reactor model only.

	input variables:		results:		
case	depth of active layer, X	number of discretization steps	outlet temperature, ˚C	conversion CH_4, %	computation time, minutes
1	0.3	20	708.26	29.22	28
2	0.2	20	708.37	29.21	23
3	0.2	5	706.87	29.27	7
4	0.05	10	708.45	29.22	12
5	0.05	5	708.38	29.22	8

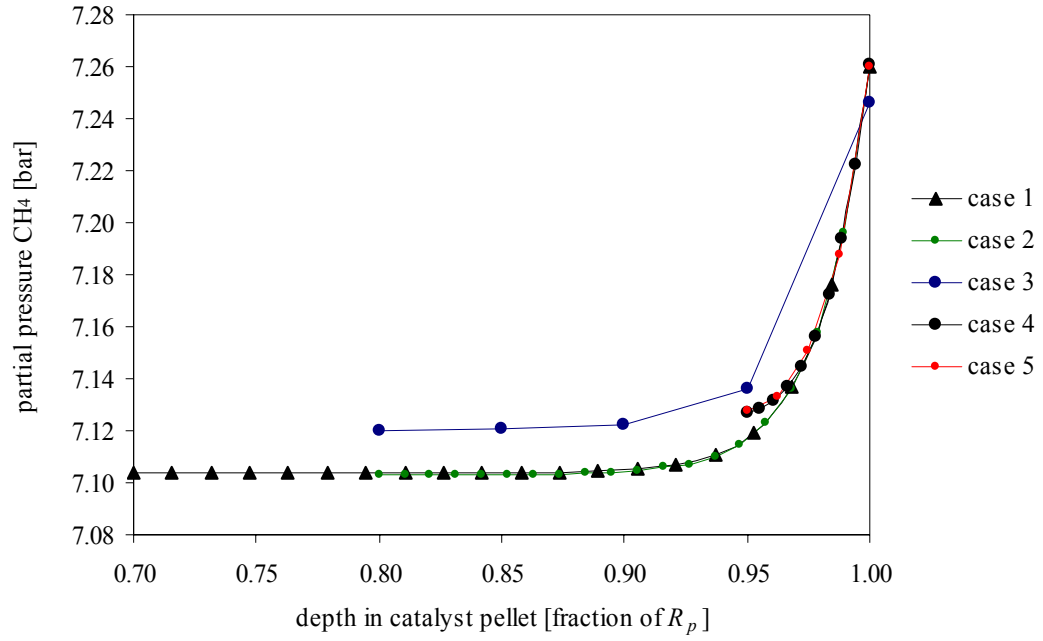

Figure 6-4. Pellet profiles of the partial pressure of methane at a fixed point of the reactor ($z = 0.9L$, $r = 0.8R_1$) for varying depth of active layer and varying numerical resolution.

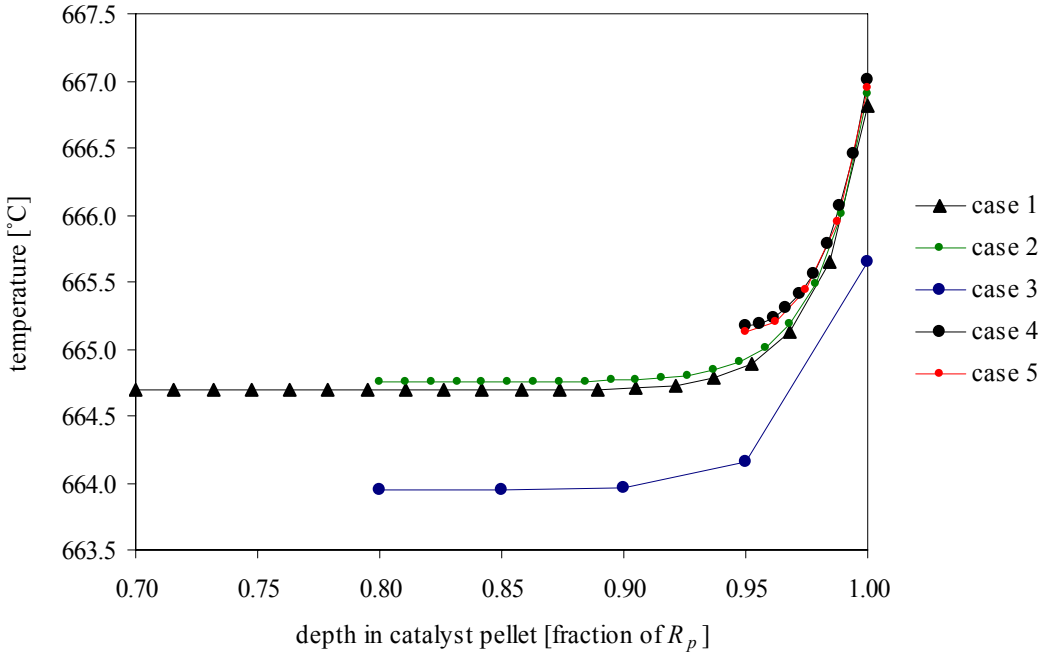

Figure 6-5. Pellet profiles of temperature at a fixed point of the reactor ($z = 0.9L$, $r = 0.8R_1$) for varying depth of active layer and varying numerical resolution.

7 RESULTS AND DISCUSSION

This section summarizes the simulation results of the two chosen simulation cases which differ in geometry for the annular section. All background data for the cases are described in Section 7.1 and the results are presented and compared in illustrations in Section 7.2. Section 7.3 describes the work done within evaluation of the gas–pellet mass and heat transport resistances, and the approaches to equilibrium for the coke formation reactions are calculated with respect to pellet position and axial and radial position in Section 7.4. The performance of the GHR model is tested in Section 7.5 where simulation results are compared with a publication done on modelling of an equivalent reformer.

7.1 Case description

The simulation case chosen is based on a typical North Sea natural gas composition combined with a steam-to-carbon ratio of 2.0 in the tubular reactors of the GHR. The natural gas has been prereformed before entering the GHR, and methane is therefore the only hydrocarbon component in the system. The composition given in mole percents is 85.8 % CH_4, 12.12 % CO_2, 1.98 % N_2 and 0.089 % H_2. The GHR is operating as a primary reformer in series configuration with a secondary autothermal reformer, as illustrated in Figure 1-2. About one third of the methane is converted in the primary reformer.

The total feed rate chosen for the reactor is 23 kmole/h per tube, which is equivalent to a mass flux of 70000 kg/m^2 h. The Reynolds number, Re_p, is decreasing from 5800 to 4100 through the reactor for this case. According to Rostrup-Nielsen et al. (1988), typical operating conditions in steam reformers are 40000–70000 kg/m^2 h per tube, Re_p = 1000–10000, and effectiveness factors for the catalytic reactions, η_j, less than 0.1.

The geometry of the modelled reactor tube and the annular space between the reactor tube and the enclosing sheath tube is illustrated in Figure 4-1. Two cases of different geometry have been chosen and the respective geometrical data are given in Table 7-1. The steam reformer catalyst R-67-7H from Haldor Topsøe AS was chosen as an example and the geometry and density data of this catalyst are given in Appendix F. Other specifications for the GHR model not mentioned previously are: wall emissivity

$\varepsilon_{w2} = \varepsilon_{w3} = 0.6$, wall thermal conductivity $\lambda_w = 100$ W/m K, pellet porosity $\varepsilon_p = 0.5$, and pellet tortuosity factor $\tau_p = 3.54$ (Xu and Froment, 1989b).

Table 7-1. Geometrical data for the simulation cases *GHR-1* and *GHR-2*.

	model case *GHR-1*	model case *GHR-2*
tube length, L	12.93 m	12.93 m
tube inner radius, R_1	0.045 m	0.045 m
tube outer radius, R_2	0.057 m	0.057 m
annulus inner radius, R_3	0.077 m	0.120 m

The mass and heat balances for the GHR were found from simulations of the flowsheet involving both the primary reformer and the secondary reformer. These simulations were performed in the process simulation tool Pro/II, and the methane conversion, outlet temperature and pressure drop in the primary reformer were specified according to the MATLAB GHR simulation results. The properties of the reactor product and the inlet gas to the heating section of the GHR are closely related by the fact that the product of the primary gas heated reformer is reformed further in the secondary autothermal reformer, which product gas is the heating gas for the GHR. The mass balances for the simulation cases *GHR-1* and *GHR-2* are given in Table 7-2 and Table 7-3, respectively.

Table 7-2. Gas compositions, temperatures and pressures used in the simulation of the model case *GHR-1*. Inlet and outlet gases on the reactor side and the annular side of the GHR. All flow rates are per tube.

	catalytic tube		annular section	
	feed gas (given)	product gas (GHR model)	inlet gas (Pro/II model)	outlet gas (GHR model)
temperature [˚C]	400	708	1050	584
pressure [bar]	40.0	37.1	38.7	38.7
mole fraction CH_4	0.290	0.160	0.0008	0.0008
mole fraction CO_2	0.041	0.065	0.072	0.072
mole fraction CO	0	0.048	0.113	0.113
mole fraction H_2O	0.657	0.380	0.451	0.451
mole fraction H_2	0.005	0.340	0.359	0.359
mole fraction N_2	0.007	0.003	0.004	0.004
flow [kmole/h]	23.0	26.8	40.9	40.9

Table 7-3. Gas compositions, temperatures and pressures used in the simulation of the model case *GHR-2*. Inlet and outlet gases on the reactor side and the annular side of the GHR. All flow rates are per one tube.

	catalytic tube		annular section	
	feed gas (given)	product gas (GHR model)	inlet gas (Pro/II model)	outlet gas (GHR model)
temperature [˚C]	400	682	1050	650
pressure [bar]	40.0	37.1	38.7	38.7
mole fraction CH_4	0.290	0.187	0.0008	0.0008
mole fraction CO_2	0.041	0.077	0.072	0.072
mole fraction CO	0	0.023	0.113	0.113
mole fraction H_2O	0.657	0.465	0.451	0.451
mole fraction H_2	0.005	0.242	0.359	0.359
mole fraction N_2	0.007	0.006	0.004	0.004
flow [kmole/h]	23.0	26.5	40.9	40.9

The parameters chosen in Sections 5 and 6, based on test simulations with the case *GHR-1*, were used in the model simulations. The numerical resolution of 300 nodes in the annulus was also used in the *GHR-2* case and this resulted in a relative energy balance error (as defined in Equation (6-1)) of 1 %. Despite the fact that the cross sectional area is increased relative to the *GHR-1* case, the same number of grid points could be used in the *GHR-2* case because the turbulence was decreased, resulting in a less pronounced profile for $\lambda_{er,a}$ and consequently less need for high radial numerical resolution.

7.2 Simulation results

The axial profiles presented are ranging from $z = 0$ to 12.93 m, where $z = 0$ is defined as the top of the reformer, with the reactor inlet and the annulus outlet.

7.2.1 The annular section

The two simulation cases differ in the size of the annular space where the heating gas flows. The case *GHR-2* is characterized by low velocities, $v_{z,a}$, and low Reynolds numbers, Re_h. Consequently the turbulent intensity and effective radial thermal conductivity are lower. The data for $\lambda_{er,a}$ resulting from the two CFD simulations and used in the GHR cases are illustrated in Figure 7-1. The data show nonsymmetric profiles which are resulting from the skew distributed velocity profile of an annular channel. The annulus velocities and Reynolds numbers are given in Figure 7-2 and Figure 7-3, respectively.

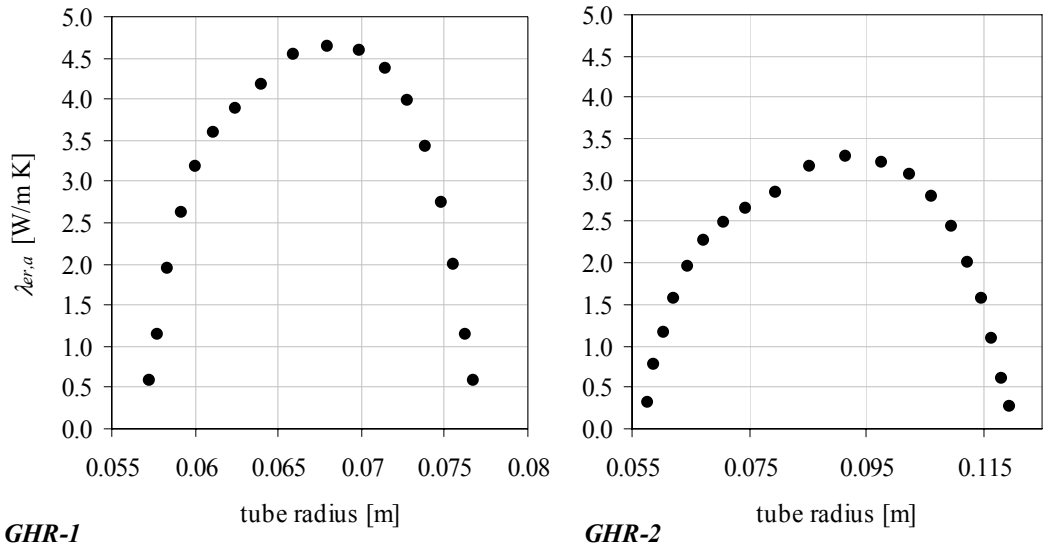

Figure 7-1. The data for the effective radial thermal conductivities, $\lambda_{er,a}$, imported from the FLUENT simulations of the cases *GHR-1* and *GHR-2*, and used in the MATLAB simulations of the complete GHR.

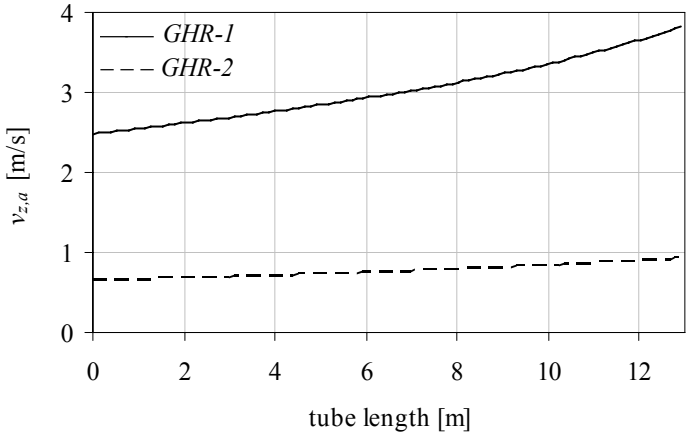

Figure 7-2. The velocities in the annular sections, $v_{z,a}$, for the two simulation cases *GHR-1* and *GHR-2*.

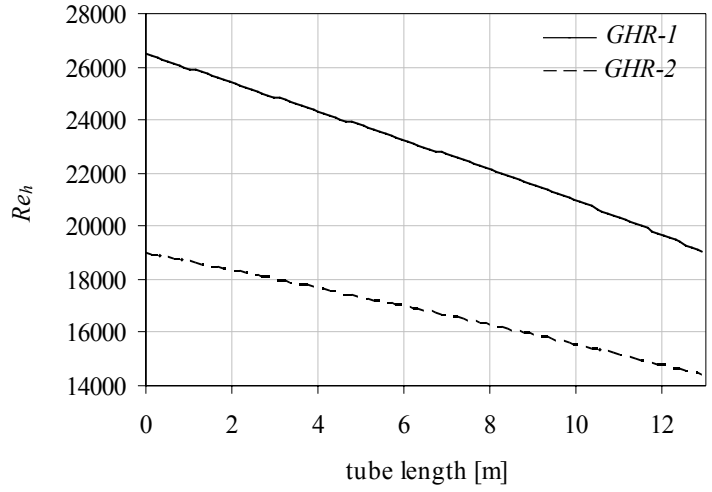

Figure 7-3. The annulus Reynolds numbers, Re_h, resulting from the cases *GHR-1* and *GHR-2*.

The pressure drops in the annular section are low; about 0.3 bar in both cases. The wall heat transfer coefficients h_2 and h_3 are functions of the Reynolds numbers, the Prandtl numbers and the radius ratios R_3/R_2, and are therefore not equal in the two cases, as seen in Figure 7-4.

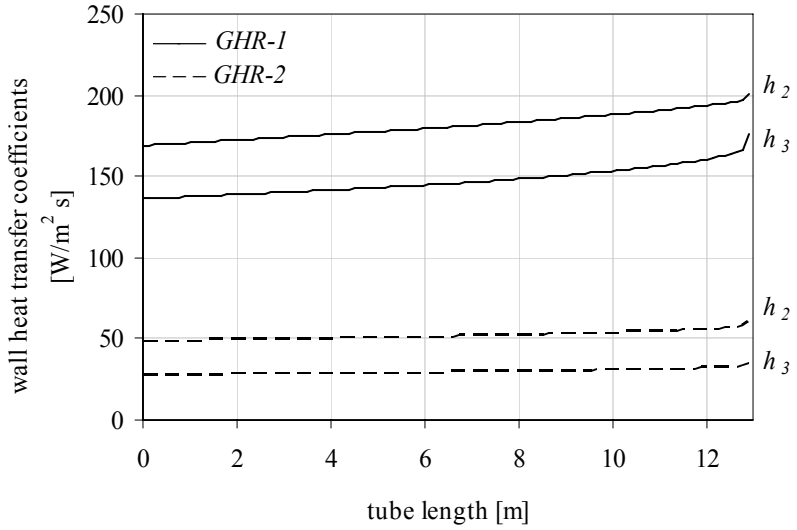

Figure 7-4. The estimated heat transfer coefficients for the inner wall and the outer wall of the annular volume, h_2 and h_3, respectively, for the simulation cases *GHR-1* and *GHR-2*.

The gas temperature profiles of the two simulation cases are shown as function of axial position in Figure 7-20 and as function of both axial and radial position in Figure 7-5 for case *GHR-1* and in Figure 7-6 for case *GHR-2*. Radial variations at three different axial positions are shown in detail in Figure 7-7. As expected, in the case of smaller annular cross sectional area, *GHR-1*, the heat transport to the reactor tube is

enhanced, resulting in a lower heating gas outlet temperature. In this case one consequently operates with higher tube skin temperatures in the hot zone, as seen in Figure 7-20, which naturally give tougher conditions for the tube material. Increasing turbulence with sheath tubes in this zone is not necessarily beneficial, as seen from the higher tube temperatures in case *GHR-1*. This can be solved by using only sheath tubes for the upper part of the reactor tubes, where the hot gas has been cooled down and where the steam reforming reactions need a high heat flux.

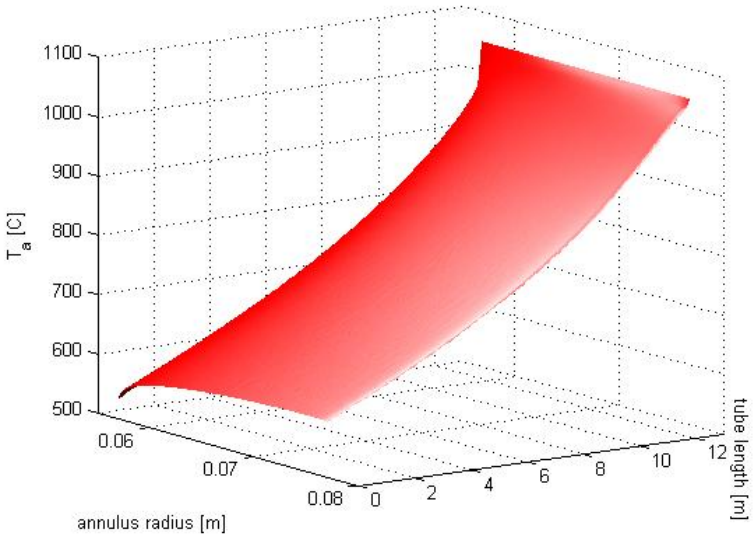

Figure 7-5. The plot of the axial and radial variations in annulus gas temperature in the simulation case *GHR-1*.

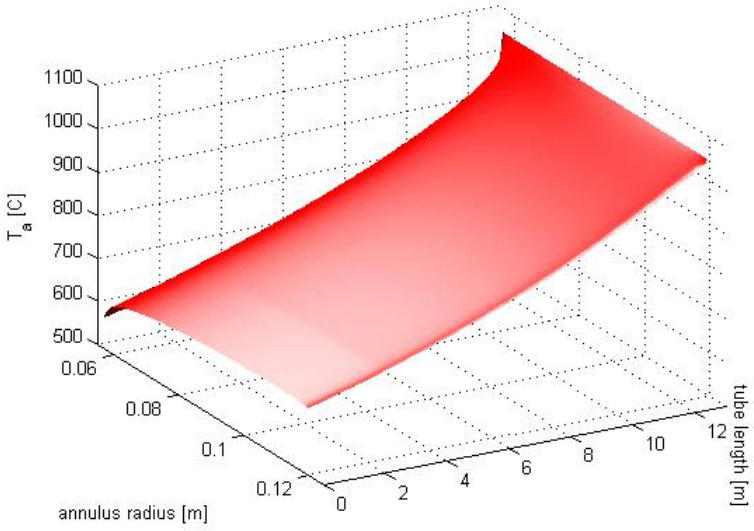

Figure 7-6. The plot of the axial and radial variations in annulus gas temperature in the simulation case *GHR-2*.

The radial changes in the gas temperatures at the inner wall of the annulus are high because of the high gradient of the effective radial thermal conductivity at the wall. This can clearer be seen from Figure 5-12 where the temperature profile in resulting from the test simulations using different $\lambda_{er,a}$ profiles. As is seen, the temperature profile for a constant $\lambda_{er,a}$ is flatter close to the wall than for the case with a profiled $\lambda_{er,a}$.

The gradient of the gas temperature close to the outer wall of the annulus is caused by the adiabatic condition combined with radiative emission from the wall.

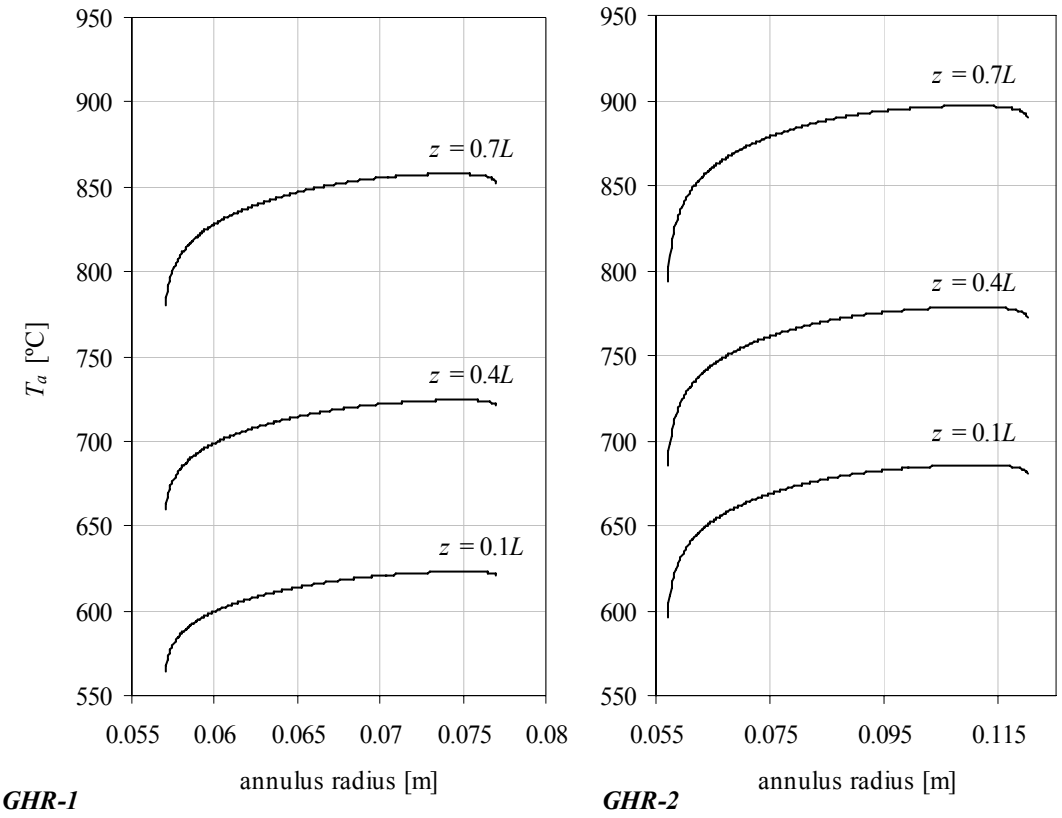

Figure 7-7. Radial temperature profiles at different axial positions as calculated in the simulation cases *GHR-1* and *GHR-2*.

The differences in heat flux calculated for the two simulation cases are shown in Figure 7-8. The convective heat transport in case *GHR-2* is considerably reduced compared with *GHR-1*. This is caused by a combination of the reduced wall heat transfer coefficient h_2 (Figure 7-4) and effective radial thermal conductivity (Figure 7-1), both resulting from reduced gas velocities and thereby turbulent intensity. This reduced heat transport is partly counter acted by the radiative heat transport being higher in case *GHR-2* compared with *GHR-1*. The main reason for this is the lower wall temperature, T_{w2}. Lower wall temperature leads to lower wall emission, as seen from the last term of Equation (4-71), and thereby higher radiative heat flux.

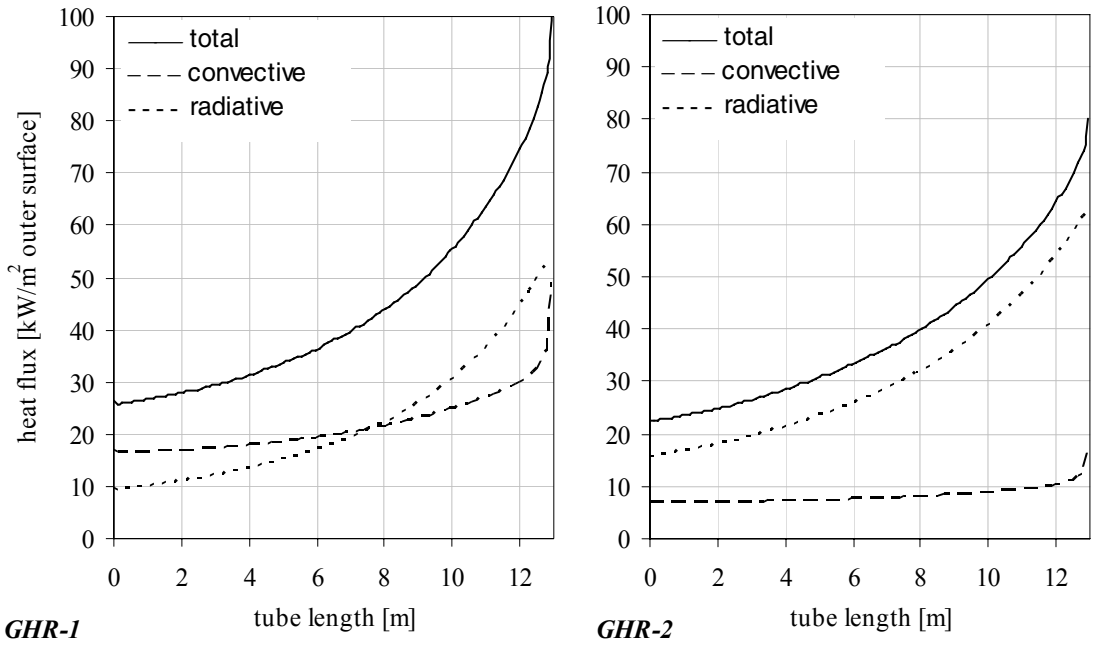

Figure 7-8. The heat flux profiles resulting from the simulation cases *GHR-1* and *GHR-2*, showing the contribution from radiative heat transport and convective heat transport.

7.2.2 The reactor tube

As a consequence of the reduced heat transport in case *GHR-2* compared with *GHR-1*, the reactor outlet temperature and the methane conversion are also reduced in case *GHR-2*. The profiles of the reactor gas temperatures and wall temperatures are seen in Figure 7-20 and the axial and radial variations in gas temperatures are shown in Figure 7-10 for the *GHR-1* case and in Figure 7-11 for the *GHR-2* case. The radial temperatures at three different axial positions are also given in Figure 7-9. The radial temperature profiles are in reasonable agreement with the temperature profile shown by Rostrup-Nielsen et al. (1988) measured in a full-size monotube pilot plant for a wall fired steam reformer. This can be taken as support for the level of effective radial thermal conductivity used in the reactor bed model. As can be seen, the radial profiles are rather flat, indicating effective radial transport of energy regardless of axial position.

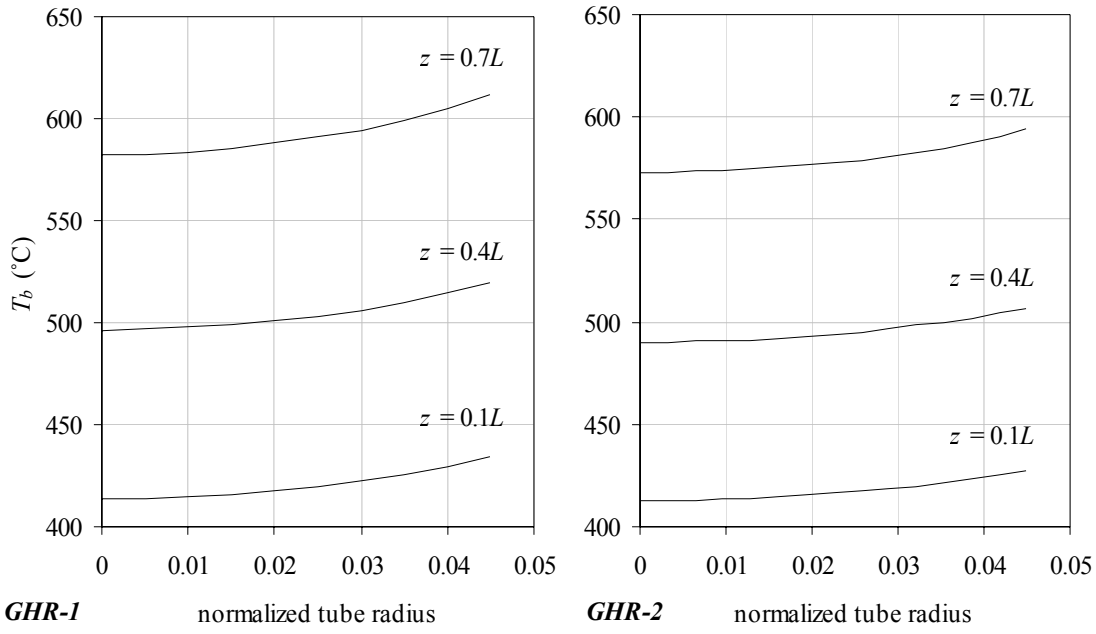

Figure 7-9. The radial variations in gas temperature in the reactor bed, T_b, at different axial positions.

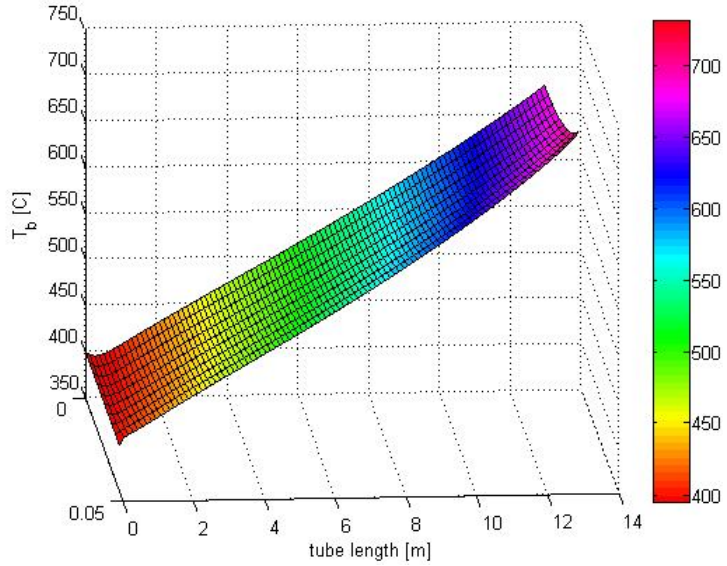

Figure 7-10. The axial and radial variations in gas temperature in the reactor bed, T_b, calculated in the simulation case *GHR-1*.

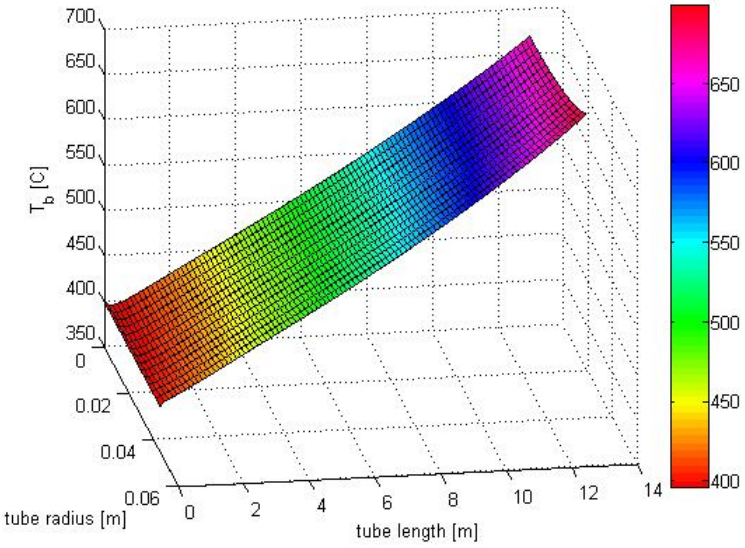

Figure 7-11. The axial and radial variations in gas temperature in the reactor bed, T_b, calculated in the simulation case *GHR-2*.

The methane conversions resulting from the two simulation cases are shown in Figure 7-12. The compositions, given by mole fractions, are given in Figure 7-13 on wet basis and in Figure 7-14 on dry basis. As expected, the methane conversion is lower in case *GHR-2* than in case *GHR-1* due to the lower heat flux. The conversion is reduced by 3.3 percentage points, which is equivalent to 11 %.

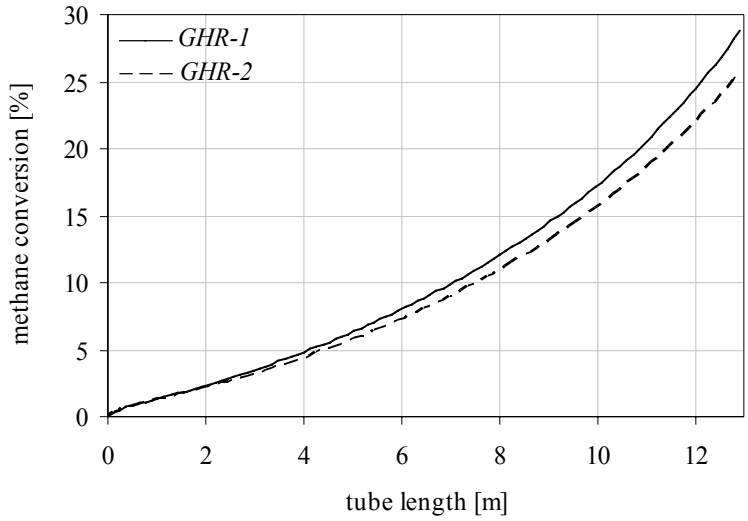

Figure 7-12. The simulated methane conversions from the cases *GHR-1* and *GHR-2*.

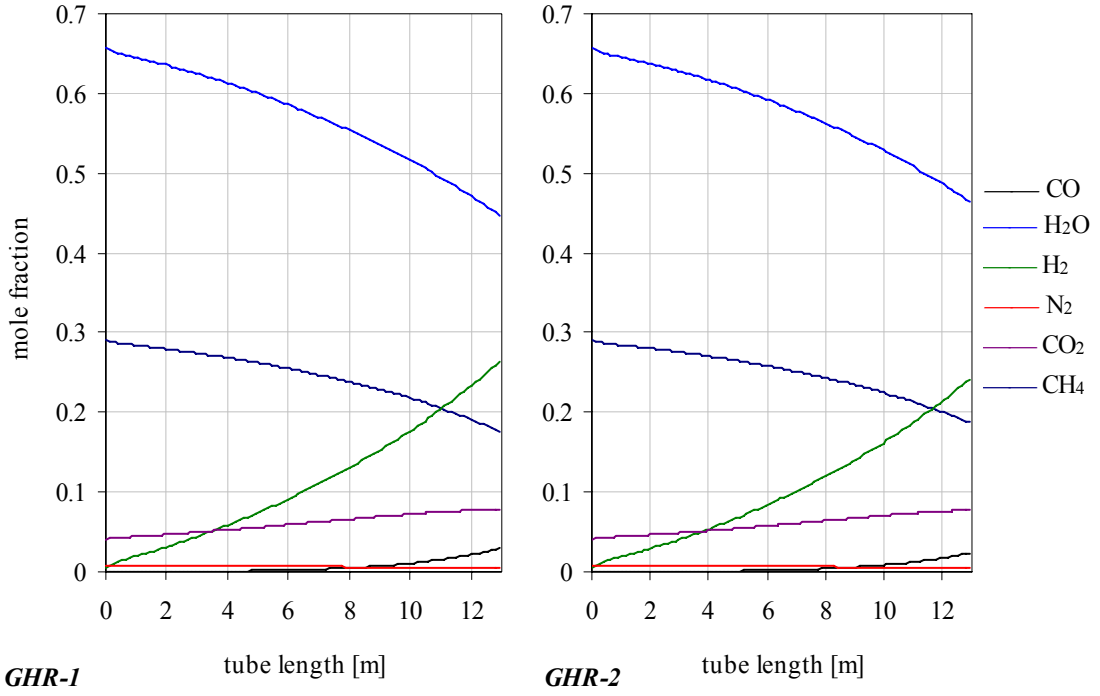

Figure 7-13. The axial changes in mole fractions (wet basis) from the results of the simulation cases *GHR-1* and *GHR-2*.

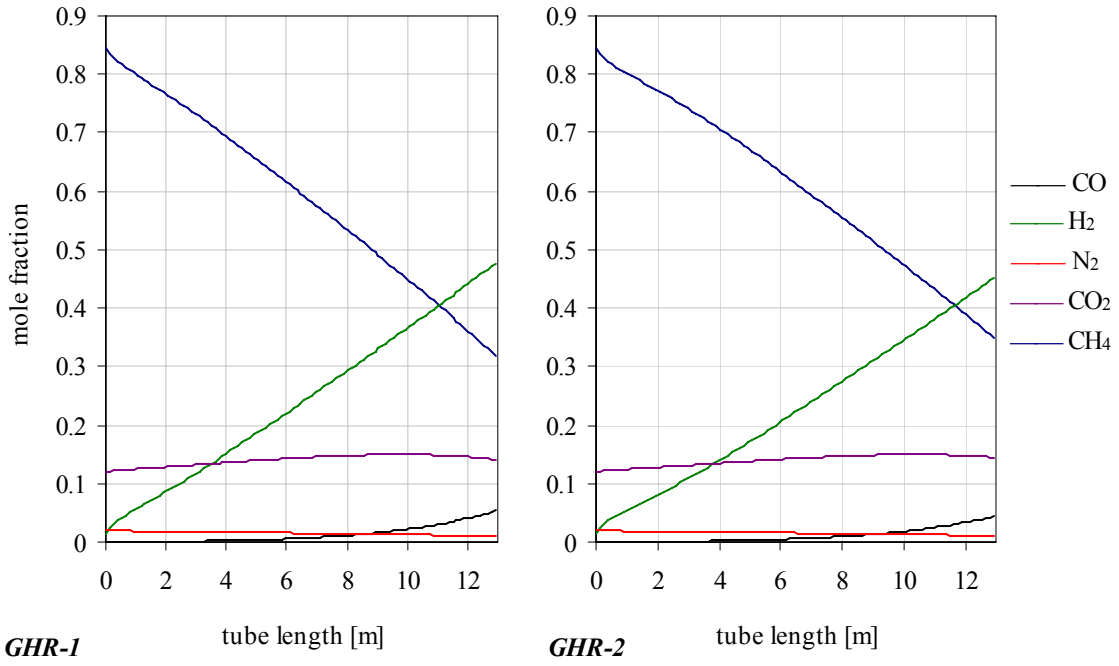

Figure 7-14. The dry basis mole fractions resulting from the simulation cases *GHR-1* and *GHR-2*.

The axial profiles of the effectiveness factors η for the three reactions, as given by Equation (4-46), are shown in Figure 7-15a. The low values of the calculated effectiveness factors indicate that there are large mass transfer limitations within the pellets, which also was seen when investigating the thickness of the active layer in the pellets in Section 6.4. The discontinuity of the shift reaction (reaction 2) seen in Figure 7-15a at $z = 0.38L$ stems from the shift from forward reaction to reverse reaction on the surface of the pellets where equilibrium is reached. The reaction rate involves the equilibrium properties of the reaction so that the rate is positive for forward reaction and negative for reverse reaction. When the reaction rate calculated from surface data shifts, the effectiveness factor becomes negative and a discontinuity appears. When the reactions calculated from pellet data also shift the effectiveness factor again becomes positive (as seen at $z = 0.86L$). η_2 is also negative at the inlet because there is no CO in the feed gas. This gives negative reaction rates calculated from surface conditions. Still the reaction rates calculated from internal pellet conditions are positive because CO is generated immediately at the reactor inlet. This results in the negative ratios. The CO content establishes so rapidly on the surface and in the bulk that the negative η_2 cannot be seen from Figure 7-15.

Figure 7-15b shows the alternative effectiveness factor η' calculated from Equation (4-47). η' is defined as η, apart from being relative to bulk conditions instead of surface conditions. η is about 10 to 40 % greater than η'. This means that there are mass and heat transport limitations in the gas film, which is discussed in Section 7.3.

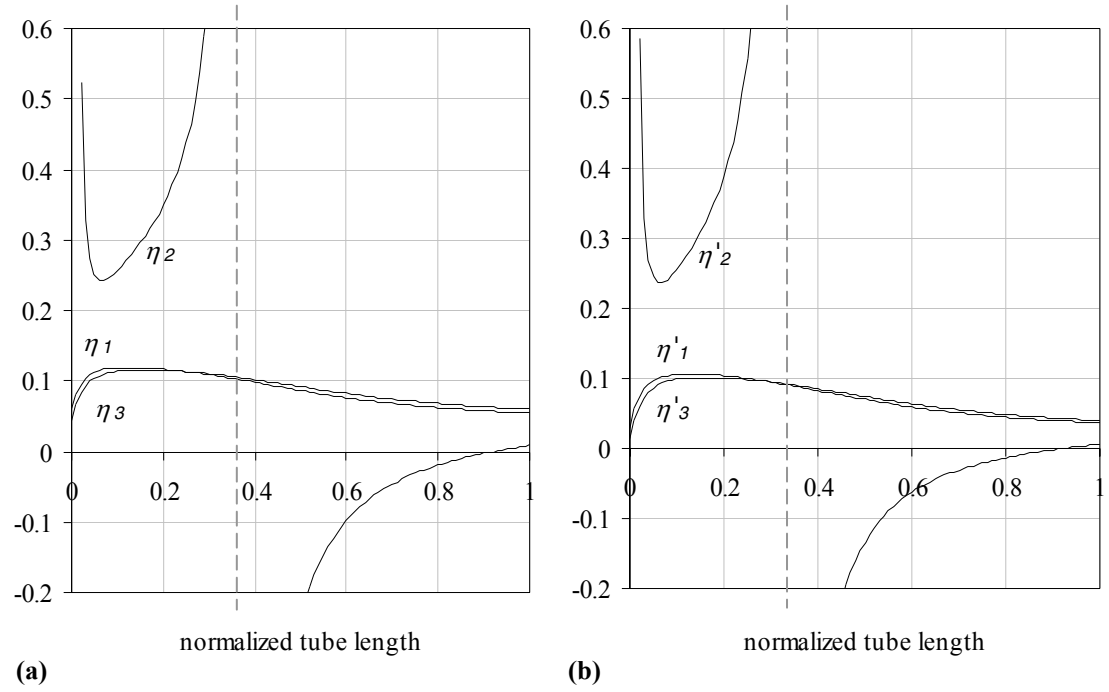

Figure 7-15. The effectiveness factors η_j (a) and η_j' (b) for the steam reforming reactions (index 1 and 3) and the shift reaction (index 2). η_j are relative to the pellet surface conditions and η_j' are relative to the bulk conditions.

The reactor side Reynolds numbers, Re_p, superficial gas velocities, $v_{zs,b}$, pressure drops, heat transfer coefficients, h_1, and effective radial thermal conductivities, $\lambda_{er,b}$, are almost unchanged from case *GHR-1* to case *GHR-2*. These are reported in Figure 7-16, Figure 7-17, Figure 7-18 and Figure 7-19, respectively.

As seen from Figure 7-17 the velocity of case *GHR-2* is lower than of case *GHR-1* which is due to the lower heat flux leading to lower temperature and lower increase in the number of moles. The larger Re_p in case *GHR-2* compared to in *GHR-1*, shown in Figure 7-16, is the result of lower estimated viscosity of the gas mixture in *GHR-2*.

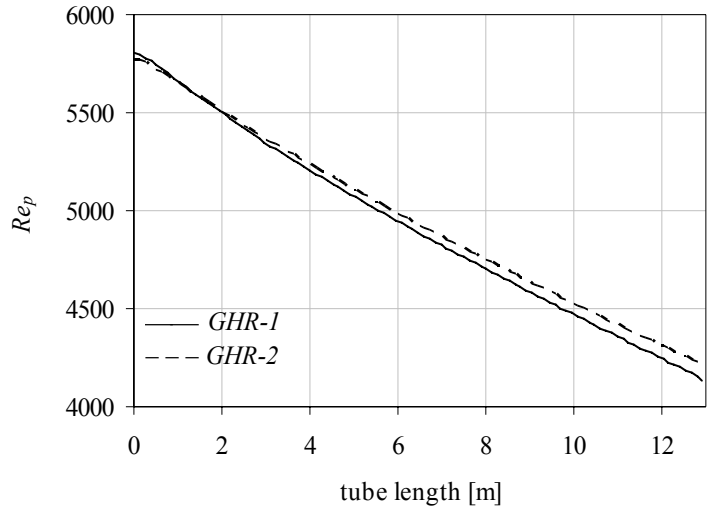

Figure 7-16. The Reynolds numbers, Re_p, calculated in the two simulation cases *GHR-1* and *GHR-2*.

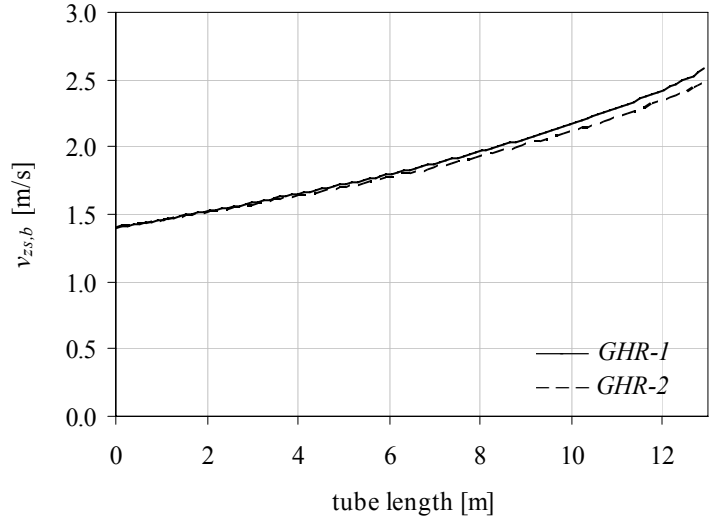

Figure 7-17. The superficial axial velocities in the packed bed, $v_{zs,b}$, from the simulation results of the cases *GHR-1* and *GHR-2*.

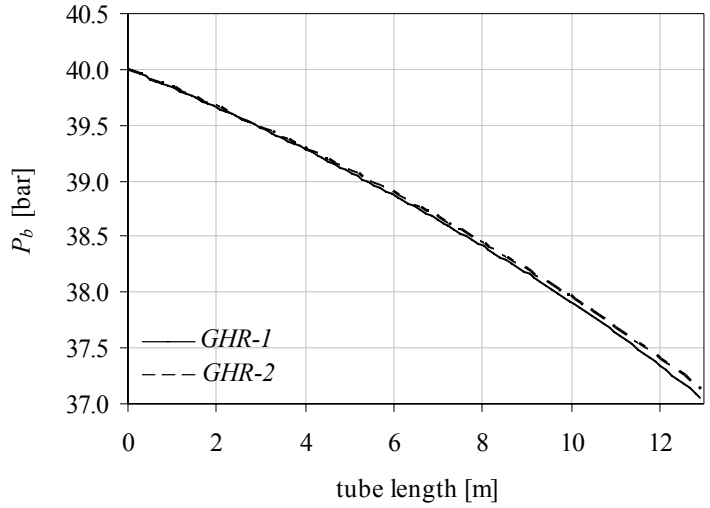

Figure 7-18. The pressure variations in the fixed bed resulting from the simulation cases *GHR-1* and *GHR-2*.

The calculated thermal conductivity of the gas mixture, λ_g, is lower in case *GHR-2* than in *GHR-1*. This leads to lower heat transfer coefficient, h_1, and higher effective radial thermal conductivity of the bed, $\lambda_{er,b}$, as seen in Figure 7-19.

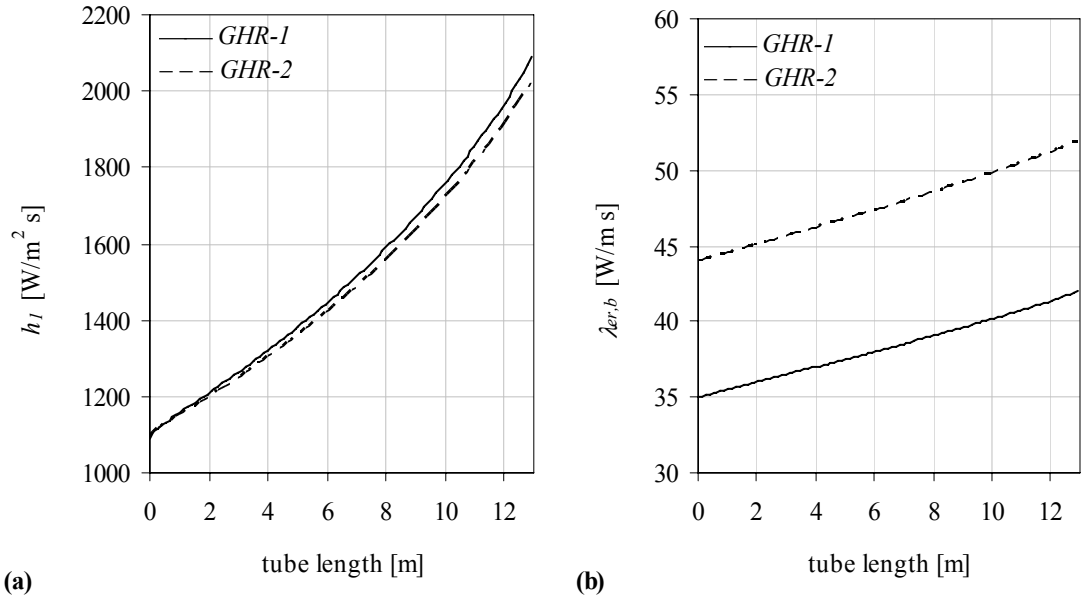

Figure 7-19. The estimated inner wall heat transfer coefficients, h_1, (a) and effective radial thermal conductivities, $\lambda_{er,b}$, (b) of the cases *GHR-1* and *GHR-2*.

7.2.3 The temperature profiles of the complete GHR model

The axial profiles of the tube wall temperatures, T_{w1}, T_{w2} and T_{w3}, and the bulk gas temperatures on the reactor bed side, T_b, and on the annular side, T_a are illustrated in Figure 7-20. The gas temperatures are average values weighted on cross sectional area and local gas flow. From the graphs it can be seen that the temperature driving forces are evenly distributed along the tube length. This is an ideal operation and an advantage as it indicates low entropy production (Sauar et al., 1999) and thereby good energy utilization. Comparisons of the gas temperatures resulting from the two cases have been discussed in Sections 7.2.1 and 7.2.2.

Figure 7-20 shows higher difference between T_a and T_{w3} in case *GHR-2* compared to case *GHR-1*. This is caused by the lower turbulent intensity, resulting in lower h_3, in case *GHR-2*. When the convective heat transport is low and the wall is defined adiabatic, a low wall temperature establishes to provide an equally low radiative heat flux.

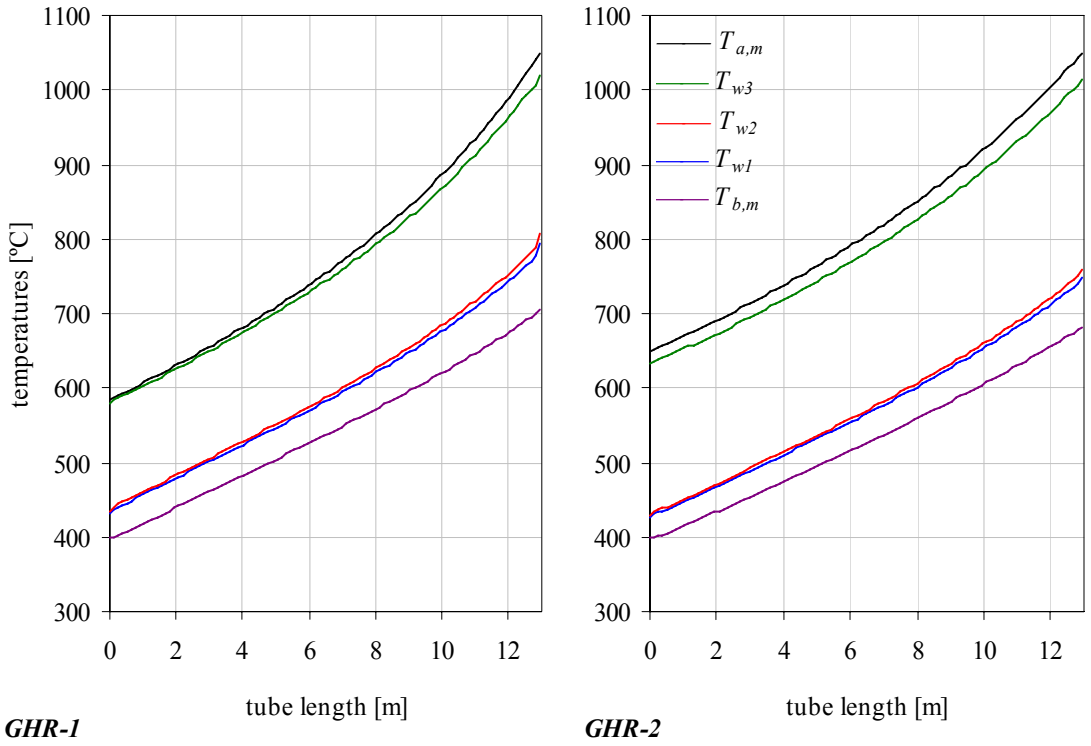

Figure 7-20. The resulting temperature profiles from the simulation cases *GHR-1* and *GHR-2*. The gas temperatures are radial mean values.

7.2.4 Convergence tests

The simulation results were checked for mass and heat continuity, and the overall relative errors in the heat balances were as shown in Table 7-4. The convergences of the axial changes in the heat fluxes, shown in Figure 7-21, are satisfying. These heat fluxes are calculated from the convective and radiative heat fluxes, as given in Equation (4-86)

for the annular section and in Equation (4-85) for the reactor side, and from the enthalpy changes in Equation (4-81).

Table 7-4. Relative errors in overall heat balances, as defined in Equation (6-1), resulting from the simulation cases *GHR-1* and *GHR-2*.

	case *GHR-1*	case *GHR-2*
relative error, reactor side	0.55 %	0.45 %
relative error, annular side	0.03 %	1.08 %

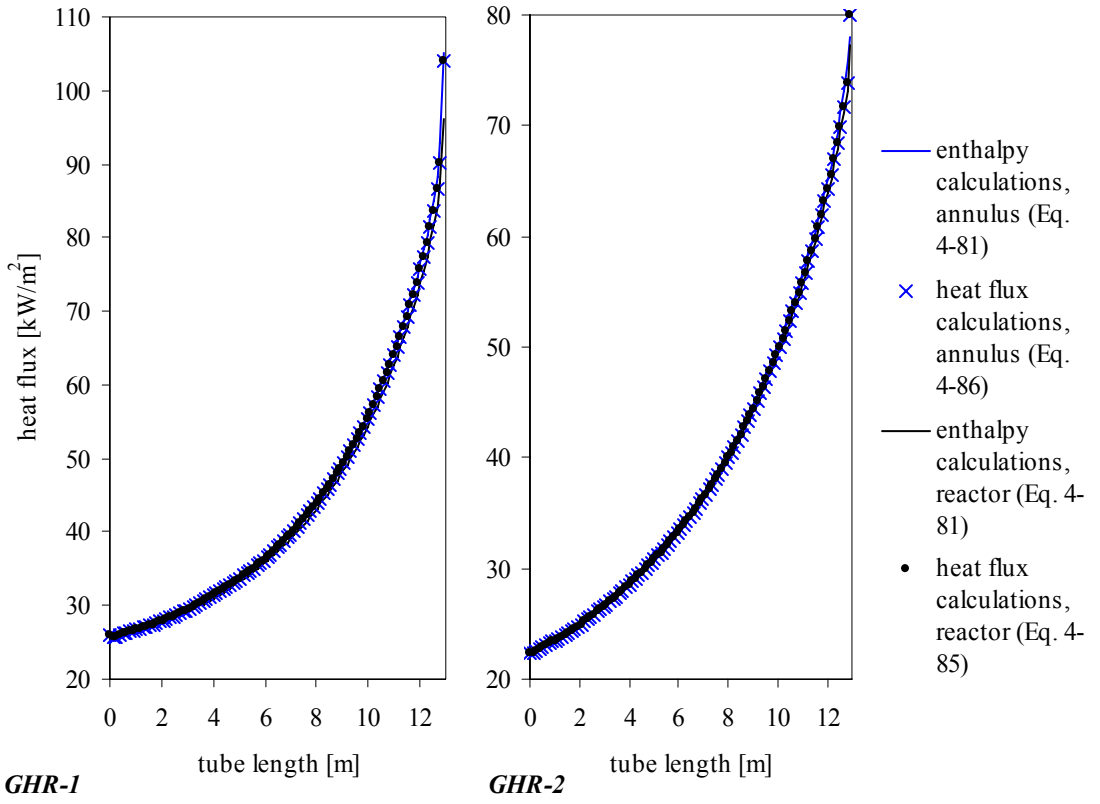

Figure 7-21. Convergence checks by heat flux calculations from the convective and radiative heat fluxes and from the changes in internal enthalpy for the cases *GHR-1* and *GHR-2*.

7.3 Study of gas–solid transport limitations

7.3.1 The criteria of Maers

The bulk/pellet interphase mass and heat transfer resistances are usually ignored and assumed insignificant in steam reformer modelling. The effects of including these resistances are therefore studied here. Quite often the importance of interphase

resistances is evaluated by the use of the criteria of Maers (1971) which are quoted in Equations (7-1) and (7-2).

According to Maers (1971), mass transfer resistance across the gas film can be disregarded relative to surface reaction kinetics if:

$$\left| \frac{r_i \, \rho_c \, R_p \, n_i}{C_i \, k_{g,i}} \right| < 0.15 \tag{7-1}$$

E_i is the activation energy, C_i is the concentration in the bulk and n_i is the reaction order of the reactant i. Calculations for methane in the simulation case *GHR-1* show that the term on the left varies from ca. 0.01 to 0.03 (inlet to outlet), indicating that there should be no mass transfer limitations in the gas film surrounding the pellets.

The Maers criterion for heat transfer is that heat transfer in the gas film can be disregarded if the following expression is fulfilled:

$$\left| \frac{\left(-\Delta H_i\right) \rho_c \, r_i \, R_p}{h_p \, T_b} \right| \frac{E_i}{R T_b} < 0.15 \tag{7-2}$$

The term on the left hand side varies from about 0.006 to about 0.003 (inlet to outlet) for methane for the simulation case *GHR-1*. According to the criterion there should be no heat transfer limitations in this fixed bed reactor.

7.3.2 The reaction effectiveness factors

The effect of interphase transport limitations was also investigated by calculating the efficiency factors η and η' from the simulation case *GHR-1*, where the mass and heat transfer resistances were included. The efficiency η is defined on basis of particle surface conditions (Equation (4-46)) which means that it expresses the reduction factor of the reaction rates caused by pellet internal resistances. These are given by the effective diffusion coefficients and the effective thermal conductivity. The alternative efficiency η' is defined on basis of bulk conditions (Equation (4-47)) so that the interphase resistances, represented by the mass and heat transfer coefficients, are also included in the denominator. These efficiency factors are compared in Figure 7-15 for all three reactions. Both efficiency factors for reaction 1 are also plotted in Figure 7-22 which shows that the alternative efficiency η', represented by the blue line, is lower than η. This means that η' is reduced because of the interphase transport limitations causing concentration and/or temperature gradients across the gas film of the pellets.

To investigate which of the two interphase resistances were of significance, two new simulations were performed: without mass transfer resistance and without heat transfer resistance. These test simulations were performed by increasing the mass transfer coefficients to 1.5 m/s and the heat transfer coefficient to 10^5 W/m^2 K, respectively. The effects from these increased parameters are equal to the effects of a model disregarding the mass and heat transfer resistances. This is shown in Figure 7-23 where the resulting partial pressures and temperatures show zero gradients in the gas

film between the bulk and the catalyst surface for these test cases. This indicates that this approach for the test simulations is satisfactorily. The alternative efficiency factors η' from these results are represented by the red and green lines, respectively, in Figure 7-22. The change in efficiency η from the base case is however negligible. The increases in η' in the two simulations compared to η' from the base simulation (black line) show that both resistances contribute in reducing η' compared with η, and to about the same degree. From this it is clear that mass and heat transfer resistances do have significant effects on the calculations of the catalyst efficiency. This is contrary to the expectations from Maers' criteria, given in Equations (7-1) and (7-2), which both were satisfied. It also shows that it is very important to take interphase transport limitations into account when interpreting reaction rate data into kinetic constants.

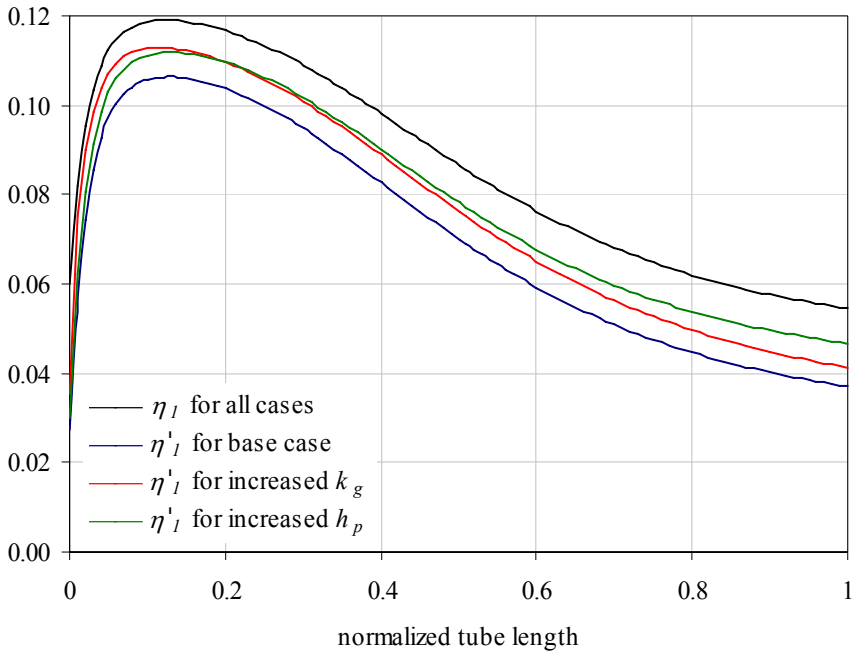

Figure 7-22. The effectiveness factors η and η' for reaction 1. The cases of increasing k_g and h_p correspond to disregarding interphase mass transport limitations and heat transfer limitations, respectively.

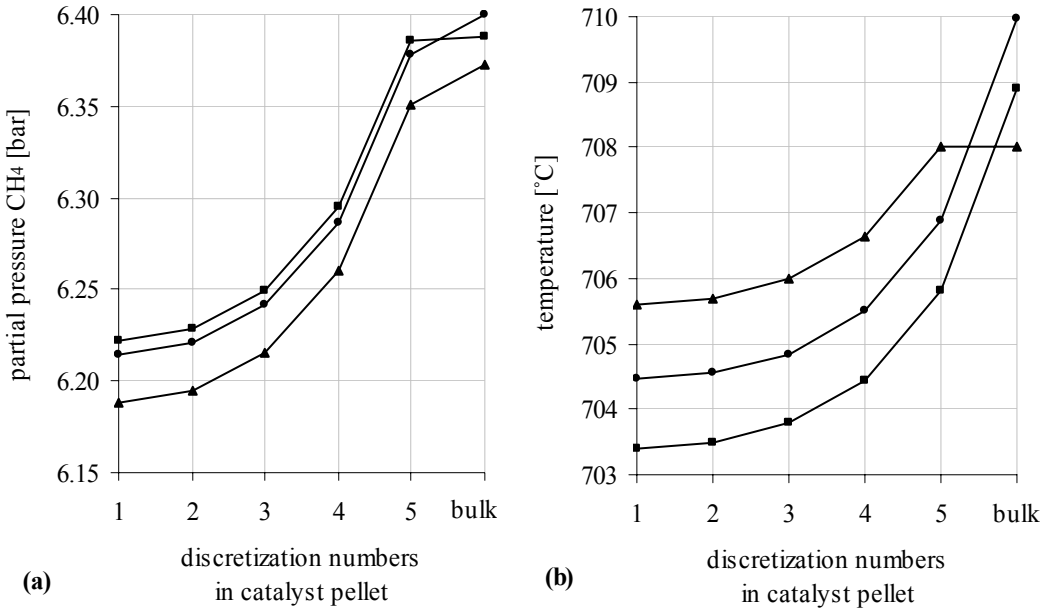

Figure 7-23. Methane partial pressure (a) and temperature (b) profiles in the bulk and in the pellets. The data are for the outlet mixture gas. 5 discretization points in the pellet are used, where the discretization figure 5 represents the pellet surface and the figure 1 represents the depth of the active layer. ● is the base case, ▲ is the case of increased heat transfer coefficient h_p, and ■ is the case of increased mass transfer coefficients $k_{g,i}$.

7.3.3 Implications for the use of pseudo-homogeneous models

The effectiveness factors calculated in the heterogeneous model may be used in a pseudo-homogeneous model to calculate the reaction rates directly from the bulk partial pressures and temperature. When simulating a pseudo-homogeneous model as the one described in Section 4.4.2, the results from using both η from Equation (4-46) and η' from Equation (4-47) can be compared to evaluate the need for including mass and heat transfer resistance in the gas film. Table 7-5 shows the results from these simulations compared with simulation of a heterogeneous model, using the simulation case *GHR-1*. The use of constant effectiveness factors was also evaluated.

Table 7-5. Outlet temperatures and methane conversions resulting from simulations of a pseudo-homogeneous model.

	outlet temperature (˚C)	CH_4 conversion (%)
heterogeneous model	708.1	29.5
pseudo-homogeneous model using η	705.2	29.7
pseudo-homogeneous model using η'	708.1	29.5
pseudo-homogeneous with constant η (= 0.09)	702.5	29.8

The pseudo-homogeneous model using η' and the heterogeneous model give equal results as expected. The pseudo-homogeneous model using η estimates somewhat lower temperature and higher methane conversion (2.9 ˚C and 0.7 %, respectively). This

indicates that the film resistances included in the calculation of η' has some effect on the overall simulation results even if that effect is relatively small. The significant differences between η and η' seen in Figure 7-15 and Figure 7-22 have little influence on the overall results because η and η' are very low. This implies that ignoring the interphase mass and heat transport resistances introduces only small discrepancies in the results of heterogeneous and pseudo-homogeneous steam reformer models. But care must be taken under experimental studies of kinetics as the interphase transport limitations are of the outmost importance for the observed local reaction rates.

The results from using constant effectiveness factors show that this can in many cases be an acceptable simplification. This simplification has great effect on computation time, as it reduces the computation time by a factor of 15.

7.4 Equilibrium calculations for the coking potential

Wagner and Froment (1992) analyzed the three equilibrium reactions for coke formation in steam reformer catalysis and developed expressions for the respective equilibrium constants. The reactions, the CO reduction, the methane cracking and the Boudouard reaction, are given by Equations (1-6), (1-7) and (1-8), respectively. The estimation of the limits for where the properties of the gas mixture are in favour for coke deposit, rather then coke gasification, are quoted in Appendix B.

The coking potentials for the three reactions were calculated as function of both the axial and the radial position, and both from the bulk conditions and from the conditions in the pellet core. Calculations from bulk conditions give the potentials as would have been estimated in a pseudo-homogeneous reactor model and calculations from the pellet core conditions gives the other extremity as only a heterogeneous model is able to estimate. The limit for where the reaction equilibriums are in favour of coke formation is when the estimated coking potential is below 1. The calculated methane cracking potential is far from this limit, ranging from $5 \cdot 10^{8}$ to $5 \cdot 10^{10}$. The calculated potentials for the case *GHR-1* for the Boudouard reaction are given in Figure 7-24 and Figure 7-25 for the bulk and pellet core conditions, respectively, and the potentials for the CO reduction are given in Figure 7-26 and Figure 7-27 for the bulk and pellet core conditions, respectively. All values are greater than 1, indicating that all equilibriums are shifted to the coke gasification reactions rather than to the coke formation reactions.

The minimum potentials for the Boudouard reaction are 3.3 estimated from bulk conditions and 2.9 estimated from the conditions in the pellet core. For the CO reduction the respective minimum values are 3.2 and 2.9. This shows that the precision of a heterogeneous model including the restrictions in interphase and intraparticle mass and heat transport is of great value in cases where the coking potentials are close to 1. Calculations from the bulk conditions will predict higher potentials than found in the pellet cores.

These equilibrium calculations give an indication of the danger for coke formation to occur. They are on the other hand not sufficient at process conditions where the kinetics of these reactions normally is so slow that this prevents coke from

forming. Wagner and Froment (1992) emphasize the need for additional kinetics data for a complete evaluation.

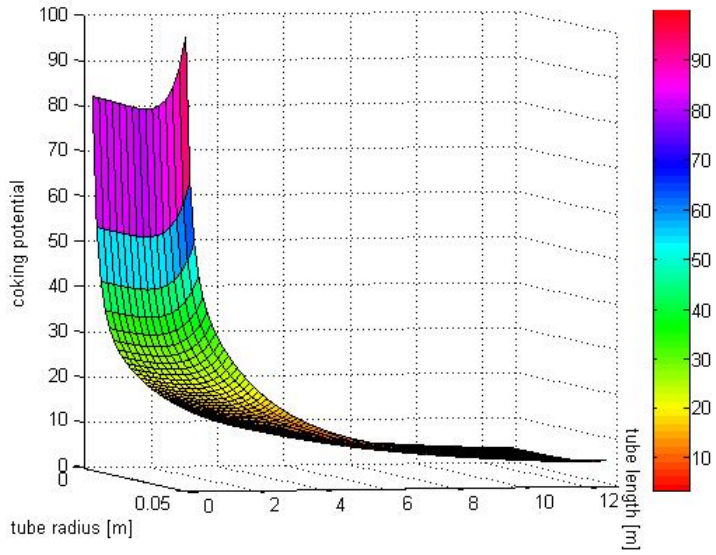

Figure 7-24. The potential for the Boudouard reaction calculated from bulk conditions (case *GHR-1*).

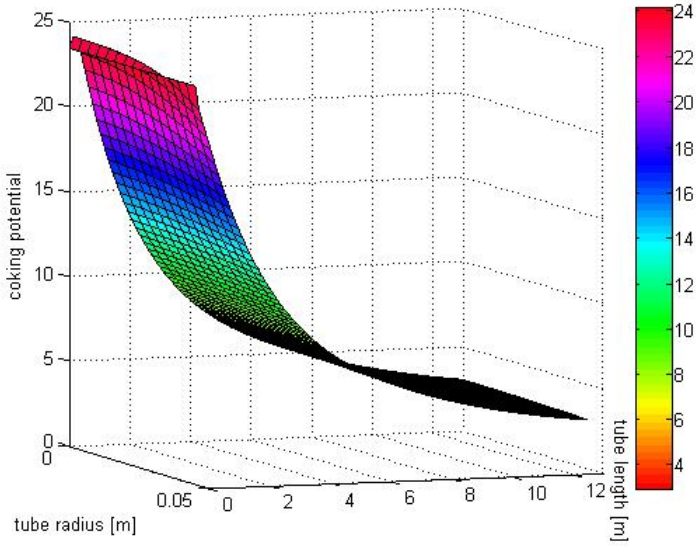

Figure 7-25. The potential for the Boudouard reaction, calculated from the conditions in the core of the pellets (case *GHR-1*).

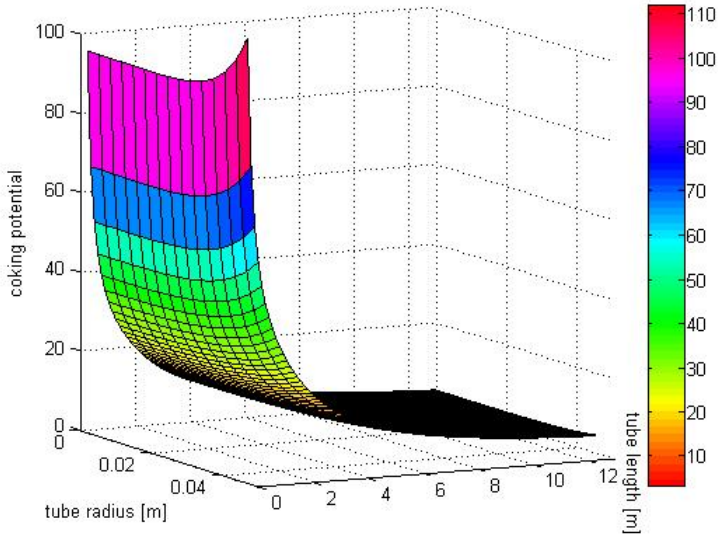

Figure 7-26. The potential for the CO reduction, calculated from the bulk conditions (case *GHR-1*).

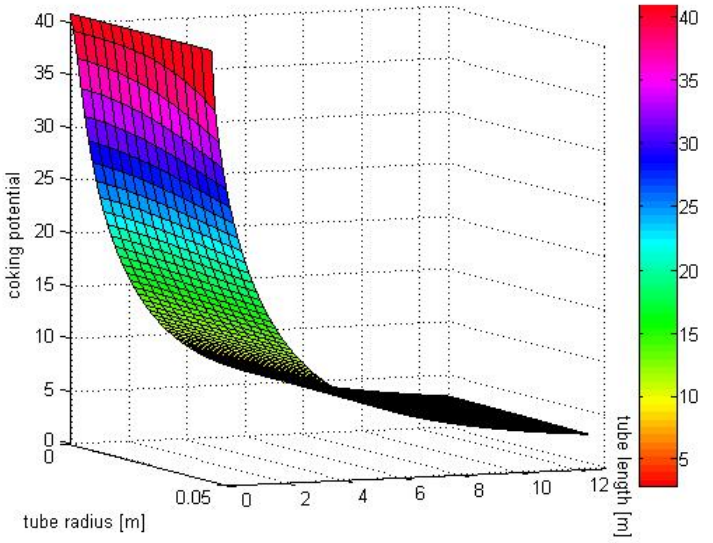

Figure 7-27. The potential for the CO reduction, calculated from the conditions in the core of the pellets (case *GHR-1*).

7.5 Case study: the model of Yu and Sosna (2001)

Yu and Sosna (2001) published a simple model for a GHR of similar geometrical design as given in this thesis. The reactor tubes and the enclosing sheath tubes were of the same length. They compared simulation results with plant data and used a pseudo-homogeneous reactor model with efficiency factors tuned towards the plant data. They obtained overall simulation results almost equal to the plant data. Their model differs from the model of this thesis in mainly three aspects:

1) “Gas-to-gas” mass and heat transfer coefficients were used to model the radial distribution of concentrations and temperatures in the reactor tube.

2) The radiation heat flux was modelled by the use of a radiative heat transfer coefficient.

3) The kinetics models of Khomenko et al. (1971) and Sosna et al. (1989) were employed for the steam reforming reactions and the shift reaction, respectively.

Simulations were performed with the GHR model described in this thesis and with input data from Yu and Sosna (2001), quoted in Table 7-6. The simulation results differ significantly from the plant data and the simulation results of Yu and Sosna (2001). This is mainly due to considerably unbalanced energy flows in their publication. This can be seen from the mass and heat balance summarized in Table 7-6, where also simulation results from this thesis are given. Their annulus heat loss is 13.5 % higher than their reactor heat supply. A second reason why the simulation results differ from the results of Yu and Sosna (2001) is that for this thesis the heterogeneous reactor model was used, while Yu and Sosna (2001) used a pseudo-homogeneous model tuned from the plant data. The resulting temperature profiles, composition profiles and heat flux profiles are given in Figure 7-28, Figure 7-29 and Figure 7-30, respectively. The radiative heat flux in the annular section varies from 30 to 54 % of the total heat flux, while Yu and Sosna (2001) reported 5.5 to 15 %.

Table 7-6. Mass and heat balance from the publication of Yu and Sosna (2001) compared with simulation results from the GHR model with heterogeneous reactor model. All flow rates are per tube. Green figures: given by Yu and Sosna (2001). Blue figures: calculated from the data given by Yu and Sosna (2001). Black figures: data from own simulation results.

	reactor side			annulus side		
	natural gas and steam	product gas	product, simulation	feed gas	outlet gas	outlet gas, simulation
flow [Nm^3/ h]	64.74 *			495.6		
flow [kmole/ h]	9.43	11.2		20.0	20.0	20.0
S/C	2.78					
mole fractions, dry basis:						
CH_4	0.900	0.257	0.200			
CO	0.008	0.0473	0.0631			
H_2	0.030	0.554	0.607			
CO_2	0.0269	0.123	0.116			
N_2	0.0351	0.0185	0.0141			
mole fractions:						
CH_4	0.249	0.132	0.112	0.00290	0.00290	0.00290
H_2O	0.723	0.475	0.440	0.351	0.351	0.351
CO	0.00222	0.0243	0.0353	0.0775	0.0775	0.0775
H_2	0.00746	0.297	0.340	0.357	0.357	0.357
CO_2	0.00832	0.0630	0.0651	0.0669	0.0669	0.0669
	0.00973	0.00821	0.00792	0.144	0.144	0.144
temperature [°C]	439	694	798	955	515	506
pressure [bar]	25	24.0	24.4	22	22	22
energy gain [kW]		79.0	93.6			
energy loss [kW]					89.7	93.6

* *Natural gas only (i.e. without steam)*

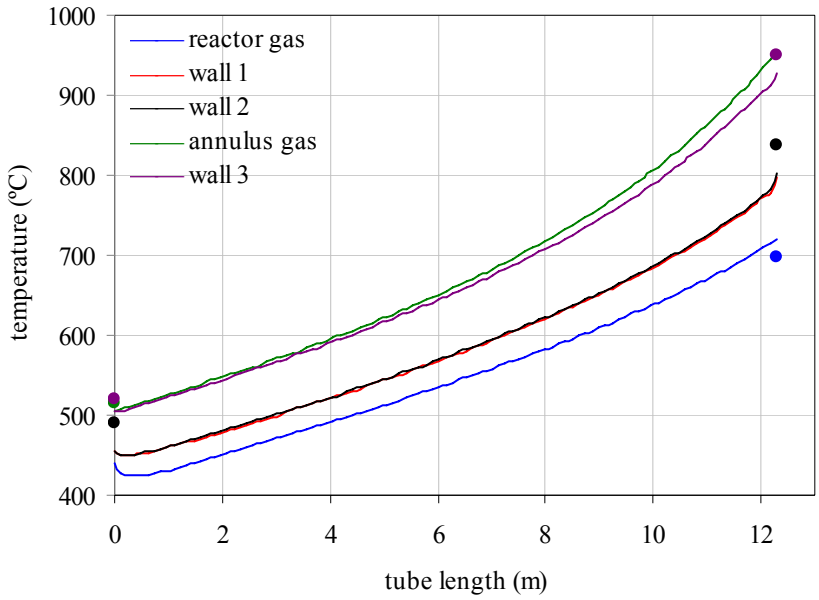

Figure 7-28. Temperature profiles from the simulation reproduction of the publication of Yu and Sosna (2001). —— own simulation results, • simulation data from Yu and Sosna (2001).

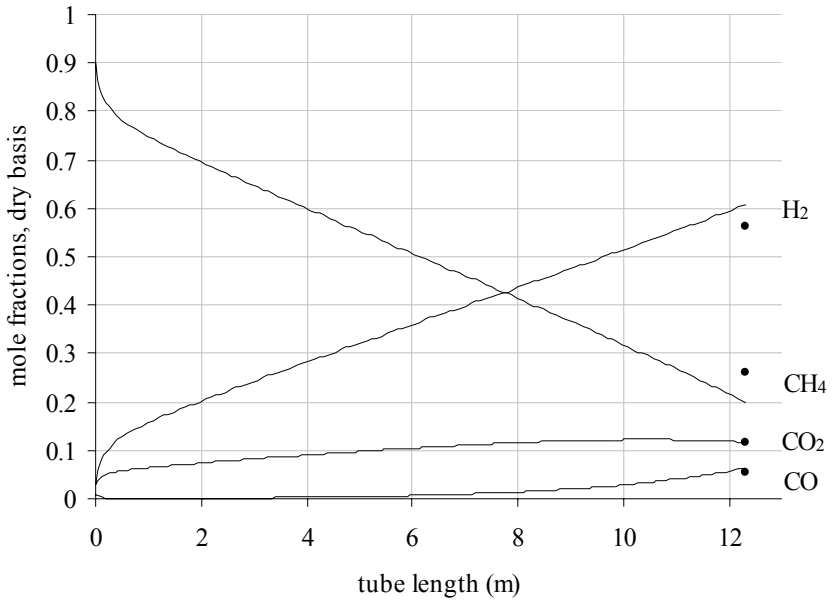

Figure 7-29. Composition profiles on dry gas basis from the simulation reproduction of the publication of Yu and Sosna (2001). —— own simulation results, • simulation data from Yu and Sosna (2001).

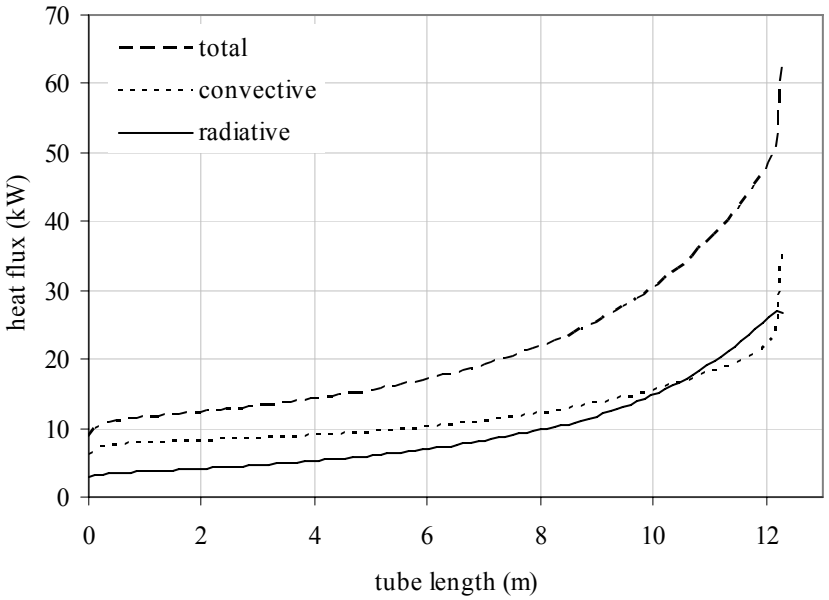

Figure 7-30. Heat flux profiles from the simulation reproduction of the publication of Yu and Sosna (2001).

8 CONCLUSIONS

The conclusions of this section summarize the discussions and conclusions of the previous sections.

A steady state model of a gas heated steam reformer (GHR) has been developed. The heterogeneous and pseudo-homogeneous, two-dimensional, finite difference dispersion models of a steam reformer tube of Svendsen et al. (1996) were modified and extended to interact with the annular heating section of a GHR. The chosen geometry for the modelled reformer was reactor tubes enclosed by sheath tubes, with the heating gas in counter current flow in the annular section. The chosen process layout was the case of a GHR operating as a primary reformer in series configuration with a secondary, autothermal reformer. One third of the natural gas is converted to synthesis gas in the primary reformer and the remaining is converted in the secondary reformer. The hot product gas of the secondary reformer is the heating gas of the GHR and is cooled down in the annular sections, providing heat for the heating and endothermic reactions in the catalyst beds. The process conditions are as for synthesis gas production for methanol or Fischer-Tropsch synthesis, and the steam-to-carbon ratio in the GHR process gas is 2.0.

All empirically derived correlations involved in the reactor models and in the annulus model were evaluated to decide which were the most suitable for the given process conditions of a steam reformer.

8.1 The annulus model

The annulus model involves a detailed gas radiation model by the discrete ordinates method, something which is not found in previous published literature within steam reformer modelling. This model is able to predict the radiation intensities as functions of the annular geometry and of the gas and wall temperatures.

The annulus model was simplified by assuming plug flow, but nevertheless accounting for the effects from turbulent flow on the convective, radial heat transport by the use of the effective radial thermal conductivity. The model was supported by an additional model in computational fluid dynamics (CFD) code, FLUENT, where the turbulent flow was estimated by the k-ε turbulence model. The resulting radial profiles of the effective radial thermal conductivity from the CFD model were imported to the annulus model of the GHR model. This simplified method was checked both for

dependency of the chosen turbulence model and for consistency of the estimated radial and axial temperature profiles from the GHR annulus model and the CFD model. The chosen turbulence model was found to be adequate for this purpose as it gave equal simulation results as the Reynolds stress turbulence model. The method of importing the effective radial thermal conductivity to a plug flow model was accepted because it gave equal temperature profiles to the CFD model when all other differences in the models were excluded (i.e. differences in the correlation for the wall heat transfer coefficients and in the radiation models).

8.2 Gas-pellet transport limitations

The effects from modelling the gas-pellet mass and heat transport limitations in the catalytic bed were investigated. Most of the previous published steam reformer models exclude these interphase resistances and also the intraparticle resistance to heat transport. All these publications assert that these resistances are negligible but none have shown the consequences of this simplification.

The reaction effectiveness factors based on pellet surface conditions and based on bulk conditions were compared to see the extent of the interphase transport limitations on the effectiveness factors. These two methods for calculating the effectiveness factors should give equal values if no interphase transport restrictions are present. The effects from these restrictions were seen in reduced effectiveness factors estimated from the bulk conditions compared to from surface conditions. The reduction varied with axial position, and the maximum reduction was 40 %. This means that the local effects from the interphase resistance to mass and heat transport on the reaction kinetics are noticeable. Both mass and heat transport resistances were found to contribute. On the other hand, the overall rector simulations were hardly affected by the interphase transport limitations. This was investigated by running equivalent simulations using the pseudo-homogeneous reactor model with both types of effectiveness factors: those including and those disregarding the interphase transport resistances. The simulation results were very close, with only 2.9 ˚C difference in the reactor outlet temperature and 0.7 % difference in the methane conversion. The simulation results of the heterogeneous model and the pseudo-homogeneous model based on effectiveness factors relative to the bulk conditions were on the other hand identical, as expected.

The importance of using a heterogeneous reactor model including all interphase and intraparticle transport resistances was seen in the equilibrium calculations for coke formation by the Boudouard reaction and the CO reduction. The comparing calculations by pellet internal conditions and by bulk conditions showed that the former conditions were closest to the conditions where the equilibrium reactions shift towards coke formation. The modeling of the gas-pellet transport limitations is thus important if the reactor model is to be used for estimating the potential for coke formation.

8.3 Suggestions for further work

The clear weakness of the method of simplifying the radial turbulent heat transport in the annulus is the dependence on external CFD calculations. One option to make the model self-contained would be to make test runs in the CFD model to map the dependency of the effective radial thermal conductivity to annulus geometry and flow. This kind of data matrix would be sufficient for this purpose as the simulation results have shown that small deviations in the values of the effective radial thermal conductivity has limited effect on the overall GHR simulation results, while on the other hand the inclusion of its radial variations is of great importance.

Extending the annulus model of the GHR model to include the flow and turbulence equations will increase the complexity of the model and the computational effort needed for the simulations. This should therefore not be considered when simplicity and efficiency is requested, as was the case for this thesis.

The annulus model can also be extended to describe different geometrical layouts of a GHR. The simplest forms would be to model an annular section equivalent to the shell side in a GHR without sheath tubes, and to model partial sheath tubes placed in the coolest section of the GHR only. The heat transfer enhancement by longitudinal fins on the outside of the reactor tubes can also be modelled.

The complete GHR model can easily be extended to include sub-functions estimating the danger for metal dusting occurring on the tubes. Additional input data giving the material type will then be needed. The potential for coke formation on the catalyst pellets would have given more information if kinetic data existed in addition to the equilibrium data used for this thesis.

REFERENCES

Aasberg-Petersen, K., Bak Hansen, J.-H., Christiansen, T.S., Dybkjær, I., Seier Christensen, P., Stub Nielsen, C., Winter Madsen, S.E.L. and Rostrup-Nielsen, J.R., "Technologies for large-scale gas conversion", *Appl. Cat. A: General*, **221**, pp. 379-387 (2001)

Abbott, J. and Crewdson, B., "Gas heated reforming improved Fischer-Tropsch process", *Oil & Gas J.*, **100** (16), pp. 64 (2002)

Achenbach, E., 'Heat and flow characteristics of packed beds', *Exp. Thermal Fluid Sci.*, **10**, pp. 17-27 (1995)

APCI, Presentation at the IBC GTL Commercialization summit, Singapore (2002)

Aylward, G.H: and Findlay, T.J.V., *SI chemical data*, 2nd edition, John Wiley & Sons: Hong Kong (1974)

Borkink, J.G.H and Westerterp, K.R., "Influence of tube and particle diameter on heat transport in packed beds", *AIChE J.*, **38** (5), pp. 703-715 (1992)

Borkink, J.G.H, Westerterp, K.R., "Significance of the radial porosity profile for the description of heat transport in wall-cooled packed beds", *Chem. Eng. Sci.*, **49** (6), pp. 863-876 (1994)

Borman, P.C., Borkink, J.G.H. and Westerterp, K.R., "Heat transfer in a wall heated tubular packed bed reactor at elevated pressures and temperatures", *Chem. Eng. Comm.*, **114**, pp. 17-47 (1992)

Burghardt, A. and Aerts, J., "Pressure changes during diffusion with chemical reaction in a porous pellet", *Chem. Eng. Proc.*, **23**, pp. 77-87 (1988)

Carlson, B.G. and Lathrop, K.D., "Transport Theory – The method of discrete ordinates on computing methods in reactor physics", In: *Computing methods in reactor physics*, Greenspan, H., Kelber, C.N. and Okrent, D. (editors), Gordon & Breach: New York (1968)

Comiti, J., Mauret, E. and Renaud, M., "Mass Transfer in Fixed Beds: Proposition of a generalized Correlation based on and Energetic Criterion", *Chem. Eng. Sci*., **55**, pp. 5545-5554 (2000)

Cussler, E.L., *Diffusion: Mass transfer in fluid systems*, 2nd ed., Cambridge University Press: Cambridge (1997)

De Deken, J.C., Devos, E.F. and Froment, G.F. , "Steam reforming of natural gas: Instrinsic kinetics, diffusional influences, and reactor design", *ACS Symp. Series.*, **196**, pp. 181-197 (1982)

De Groote, A.M. and Froment, G.F., "Reactor modelling and simulations in synthesis gas production", *Rev. Chem. Eng.*, **11** (2), pp. 145-183 (1995)

De Wasch, A.P. and Froment, G.F., "Heat Transfer in Packed Beds"', *Chem. Eng. Sci.*, **27**, pp. 557-576 (1972)

Delgado, J.M.P.Q., "A critical review of dispersion in packed beds", *Heat Mass Transfer*, **42**, pp. 279-310 (2006)

Delmas, H. and Froment G.F., "A simulation model accounting for structural radial nonuniformities in fixed bed reactors", *Chem. Eng. Sci.*, **43** (8), pp. 2281-2287 (1988)

Derkx, O.R. and Dixon, A.G., "Determination of the fixed bed wall heat transfer coefficient using computational fluid dynamics", *Num. Heat Ttransfer, Part A*, **29**, pp. 777-794 (1996)

Derkx, O.R. and Dixon, A.G., "Effect of the wall Nusselt number on the simulation of catalytic fixed bed reactors", *Catal. Today*, **35**, pp. 435-442 (1997)

Dirker, J. and Meyer, J.P., "Convective heat transfer coefficients in concentric annuli", *Heat Transfer Eng.*, **26** (2), pp. 38-44 (2005)

Dixon, A.G. and Cresswell, D.L., "Theoretical Prediction of Effective Heat Transfer Parameters in Packed Beds", *AIChE J.*, **25** (4), pp. 663-676 (1979)

Dixon, A.G., DiCostanzo, M.A. and Soucy, B.A., "Fluid-phase radial transport in packed beds of low tube-to-particle diameter ratio", *Int. J. Heat Mass Transfer*, **27** (10), pp. 1701-1713 (1984)

Dixon, A.G., "Wall and particle-shape effects on heat transfer in packed beds", *Chem. Eng. Comm.*, **71**, pp. 217-237 (1988)

Dixon, A.G. and van Dongeren, J.H., "The influence of the tube and particle diameters at constant ratio on heat transfer in packed beds", *Chem. Eng. Proc.*, **37**, pp. 23-32 (1998)

Dwivedi, P.N. and Upadhyay, S.N., "Particle-fluid mass-transfer in fixed and fluidized-beds", *Ind. Eng. Chem. Proc. Des. Dev.*, **16** (2), pp. 157-165 (1977)

Dybkjær, I., "Tubular reforming and autothermal reforming of natural gas – an overview of available processes", *Fuel Proc. Techn.*, **42**, pp. 85-107 (1995)

Edwards, D.K. and Matavosian, R., "Scaling rules for total absorptivity and emissivity of gases", *J. Heat Transfer*, **106**, pp. 684-689 (1984)

Elnashaie, S.S.E.H., Adris, A.M., Soliman, M.A. and Al-Ubaid, A.S., "Digital Simulation of Industrial Steam Reformers of Natural Gas using Heterogeneous Models", *Can. J. Chem. Eng.*, **70**, pp. 786-793 (1992)

Elnashaie, S.S.E.H. and Abashar, M.E.E., "Steam Reforming and Methanation Effectiveness Factors using Dusty Gas Model under Industrial Conditions", *Chem. Eng. Proc.*, **32**, pp. 177-189 (1993)

Ergun, S., "Fluid flow through packed columns", *Chem. Eng. Prog.*, **48** (2), pp. 89-94 (1952)

Fahien, R.W. and Smith, J.M., "Mass transfer in packed beds", *AIChE J.*, **1** (1), pp. 28-37 (1955)

Ferreira, R.M.Q., Marques, M.M., Babo, M.F. and Rodrigues, A.E., "Modelling of the methane steam reforming reactor with large-pore catalyst", *Chem. Eng. Sci.*, **47** (9-11), pp. 2909-2914 (1992)

Filonenko, G.K., "Hydraulic resistances in pipes", *Teploenergetica (in Russian)*, **1**, pp. 40-44 (1954)

Fiveland, W.A., "A discrete ordinates method for predicting radiative heat transfer in axisymmetric enclosures", *ASME paper no. 82-HT-20* (1982)

Fogler, H. S., *Elements of chemical reaction engineering*, 2nd ed., Prentice-Hall: Englewood Cliffs, N.J. (1992)

Froment, G.F. and Bischoff, K.B., *Chemical reactor analysis and design*, 2nd ed., Wiley: New York (1990)

Froment, G.F. and Hofmann, P.K., "Design of fixed-bed gas-solid catalytic reactor", In: *Chemical Reaction and Reactor Engineering*, Carberry, J.J. and Varma, A. (editors), Marcel Dekker: New York (1987)

Fuller, E.N., Schettler, P.D. and Giddings, J.C., "A new method for prediction of binary gas-phase diffusion coefficients", *Ind. Eng. Chem.*, **58** (5), pp. 19-27 (1966)

Gnielinski, V., "New equations for heat and mass transfer in turbulent pipe and channel flow", *Int. Chem. Eng.*, **16**, pp. 359-368 (1976)

Gnielinski, V., Forced convection in ducts, In: Heat exchanger design handbook 2002, G.F. Hewitt (editor), Begell House: New York (2002)

Grevskott, S., Rusten, T., Hillestad, M., Edwin, E. and Olsvik, O., "Modelling and simulation of a steam reforming tube with furnace", *Chem. Eng. Sci.*, **56** (2), pp. 597-603 (2001)

Gunn, D.J. "Theory of axial and radial dispersion in packed beds", *Trans. IChemE*, **47**, T351-T359 (1969)

Haldor Topsøe AS, http://www.haldortopsoe.dk/site.nsf/vALLWEBDOCID/KVOO-5PGFBN/$file/Hydrogen-UK_HTCR.pdf (2005a)

Haldor Topsøe AS, http://www.topsoe.com/site.nsf/vALLWEBDOCID/KVOO-5PGF7A/$file/Cat%20-%20Topsoe%20R-67%20leaflet.pdf (2005b)

Handley, D. and Heggs, P.J., "Momentum and heat transfer mechanisms in regular shaped packings", *Trans. IChemE*, **46** (9), T251-T264 (1968)

Hicks, R.E., "Pressure drop in packed beds of spheres", *Ind. Eng. Chem. Fundam.*, **9** (3), pp. 500-502 (1970)

Hottel, H.C. and Sarofim, A.F., *Radiative Transfer*, McGraw-Hill: New York (1967)

Johnson Matthey, http://www.jmcatalysts.com (2005)

Kehoe, J.P.G. and Aris, R., "Communications on the theory of diffusion and reaction – IX. Internal pressure and forced flow for reactions with volume change", *Chem. Eng. Sci.*, **28**, pp. 2094-2098 (1973)

Khomenko, A.A., Apelbaum, L.O., Shub, F.S., Snagovskii, S. and Temkin, M.I., "Kinetics of the reaction of methane with water vapour and the reverse reaction of hydrogenation of carbon monoxide on the surface of nickel", *Kinet. Katal.*, **12**, pp. 423 (1971)

Krishna, R. and Wesselingh, J.A., "The Maxwell-Stefan approach to mass transfer", *Chem. Eng. Sci*., **52** (6), pp. 861-911 (1997)

Kulkarni, B.D. and Doraiswamy, L.K., "Estimation of Effective Transport Properties in Packed Bed Reactors", *Catal. Rev. Sci. Eng.*, **22** (3), pp. 431-483 (1980)

Kunii, D. and Smith, J.M., "Heat transfer characteristics of porous rocks", *AIChE J.*, **6** (1), pp. 71-78 (1960)

Kvamsdal, H.M., Svendsen, H.F., Hertzberg, T. and Olsvik, O., "Dynamic simulation and optimization of a catalytic steam reformer", *Chem. Eng. Sci.*, **54**, pp. 2697-2706 (1999)

Lemcoff, N.O., Pereira Duarte, S.I. and Martinez, O.M., "Heat transfer in packed beds", *Rev. Chem. Eng.*, **6** (4), pp. 229-292 (1990)

Li, C.-H. and Finlayson, B.A., "Heat Transfer in Packed Beds – A Reevaluation", *Chem. Eng. Sci.*, **32**, pp. 1055-1066 (1977)

Loock, S., Ernst, W.S., Thomsen, S.G. and Jensen, M.F., "Improving carbon efficiency in an auto-thermal methane reforming plant with Gas Heated Heat Exchange Reforming technology", paper no. O96-001, *7th World Congress of Chemical Engineering*, Glasgow, (2005)

Mahan, J.R., *Radiation heat transfer: a statistical approach*, Wiley: New York (2002)

Martin, H., Nilles, M., "Radiale Wärmeleitung in durchströmten Schüttungsrohren", *Chem. Ing. Tech.*, **65** (12), pp. 1468-1477 (1993)

Mears, D.E., "Tests of transport limitations in experimental catalytic reactors", *Ind. Eng. Chem. Proc. Des. Dev.*, **10** (4), pp. 541-547 (1971)

Mills, A.F., *Heat Transfer*, Irwin: Chicago (1992)

Modest, M.F., *Radiative heat transfer*, 2nd ed., Academic Press: Amsterdam (2003)

Nan, H.S., Dias, M.M. and Rodrigues, A.E., "Effect of forced convection on reaction with mole changes in porous catalyst", *Chem. Eng. J.*, **57**, pp. 101-114 (1995)

Papageorgiou, J.N. and Froment, G.F., "Simulation models accounting for radial voidage profiles in fixed-bed reactors", *Chem. Eng. Sci.*, **50** (19), pp. 3043-3056 (1995)

Pedernera, M.N., Pina, J., Borio, D.O. and Bucala, V., "Use of a heterogeneous two-dimensional model to improve the primary steam reformer performance", *Chem. Eng. J.*, **94**, pp. 29-40 (2003)

Perry, R.H., and Green, D.W., *Perry's Chemical Engineers' Handbook*, 7th ed., McGraw-Hill: New York (1997)

Peters, P.E., Schiffino, R.S. and Harriott, P., "Heat Transfer in Packed-Tube Reactors", *Ind. Eng. Chem. Res.*, **27**, pp. 226-233 (1988)

Petukhov, B.S. and Roizen, L.I., "Generalized relationships for heat transfer in a turbulent flow of a gas in tubes of annular section", *High Temp. (USSR)*, **2**, pp. 65-68 (1964)

Petukhov, B.S., "Heat transfer and friction in turbulent pipe flow with variable physical properties", In: *Advances in heat transfer*, vol. 6, J.P. Hartnett and T.F. Irvine (editors), Academic Press: New York, (1970)

Piña, J., Schbib, N.S., Bucalá, V. and Borio, D.O., "Influence of the Heat-Flux Profiles on the Operation of Primary Steam Reformers", *Ind. Eng. Chem. Res.*, **40**, pp. 5215-5221 (2001)

Poling, B.E., Prausnitz, J.M. and O'Connell, J.P., *The properties of gases and liquids*, 5th ed., McGraw-Hill: New York (2001)

Reid, R.C., Prausnitz, J.M. and Poling, B.E., *The properties of gases and liquids*, 4th ed., McGraw-Hill: New York (1987)

Rostrup-Nielsen, J.R., "Catalytic steam reforming", In: *Catalysis – Science and Technology*, Anderson, J.R. and Boudart, M. (editors), Springer-Verlag: Berlin (1984)

Rostrup-Nielsen, J.R., Christiansen, L.J. and Bak Hansen, J.-H., "Activity of steam reforming catalysts: Role and assessment", *All. Cat.*, **43**, pp. 287-303 (1988)

Sauar, E., Nummedal, L. and Kjelstrup, S., "The principle of equipartition of forces in chemical reactor design: The ammonia synthesis", *Comp. Chem. Eng.*, **23**, pp. 499-502 (1999)

Schiesser, W.E., *The numerical method of lines in integration of partial differential equations*, Academic Press: San Diego (1991)

Siegel, R. and Howell, J.R., *Thermal radiation heat transfer*, 4th ed., Taylor & Francis: New York (2002)

Smith, T.F., Shen, Z.F. and Friedman, J.N., "Evaluation of coefficients for the weighted sum of grey gases model", *J. Heat Transfer*, **104**, pp. 602-608 (1982)

Soliman, M.A., El-Nashaie, S.S.E.H., Al-Ubaid, A.S., Adris, A., "Simulation of steam reformers for methane", *Chem. Eng. Sci.*, **43** (8), pp. 1801-1806 (1988)

Sosna, M.H., Yanatinskii, B.V., Sokolinskii, Y.A., Evenchik, N.S. and Nikitina, L.N., "Channel model", *Theoretical Found. Chem. Eng. (in Russian)*, **23**, pp.785 (1989)

Spalding, D.B., "Mathematical modelling of fluid-mechanics, heat-transfer and chemical-reaction processes", Lecture 9: Idealisations of radiation, *Report no. HTS/80/1*, Imperial College of Science and Technology, London (1980)

Stehlík, P., Šika, J., Bébar, L. and Raus, L., "Contribution to the research and development of radiation chambers in steam reforming", *Coll. Czech Chem. Comm.*, **54**, pp. 2357-2374 (1989)

Stehlík, P., "Radiative component in thermal calculation of tubular heat exchangers", *Heat Transfer Eng.*, **16** (1), pp. 19-28 (1995)

Svendsen, H.F., Grevskott, S., Lysberg, M., "Pseudohomogen og heterogen todimensjonal dispersjonsmodell for gassfase fixed-bed reaktorer", *SINTEF report*, No STF66 F96035 (1996)

Touloukian, Y.S., Powell, R.W., Ho, C.Y., Klemens, P.G., Thermal conductivity: non-metallic solids, IFI/Plenum, New York (1970)

Tsotsas, E. and Schlünder, E.-U., "Heat Transfer in Packed Beds with Fluid Flow: Remarks on the Meaning and the Calculation of a Heat Transfer Coefficient at the Wall", *Chem. Eng. Sci.*, **45** (4), pp. 819-837 (1990)

Veldsink, J.W., van Damme, R.M.J., Versteg, G.F. and van Swaaij, W.P.M., "The use of dusty-gas model for the description of mass transport with chemical reaction in porous media", *Chem. Eng. J.*, **57**, pp. 115-125 (1995)

Viskanta, R. and Mengüç, M.P., "Radiation heat transfer in combustion systems", *Prog. Energy Combust. Sci.*, **13**, pp. 97-160 (1987)

Vortmeyer, D. and Haidegger, E., "Discrimination of three approaches to evaluate heat fluxes for wall-cooled fixed bed chemical reactors", *Chem. Eng. Sci.*, **46** (10), pp. 2651-2660 (1991)

Wagner, E.S. and Froment, G.F., "Steam reforming analyzed", *Hydroc. Proc.*, **71** (7), pp. 69-77 (1992)

Wakao, N. and Funazkri, T., "Effect of fluid dispersion coefficients on particle-to-fluid mass transfer coefficients in packed beds. Correlation of Sherwood numbers", *Chem. Eng. Sci.*, **33**, pp. 1375-1384 (1978)

Wakao, N., Kaguei, S. and Funazkri, T., "Effect of fluid dispersion coefficients on particle-to-fluid heat transfer coefficients in packed beds. Correlation of Nusselt numbers", *Chem. Eng. Sci.*, **34**, pp. 325-336 (1979)

Wesenberg, M.H., Grislingås, A. and Grevskott, S., "Modelling of steam reformer tubes", paper no. 961, *6th World Congress of Chemical Engineering*, Melbourne (2001)

Wesenberg, M.H., Ströhle, J. and Svendsen, H.F., "Gas heated steam reformer; two-dimensional finite difference model with heater side discrete ordinates radiation scheme", paper no. P16-007, *7th World Congress of Chemical Engineering*, Glasgow, (2005)

Wesenberg, M.H. and Svendsen, H.F., "Mass and heat transfer limitations in a heterogeneous model of a gas heated steam reformer", submitted to *Ind. Eng. Chem. Res.* (2006)

Wesenberg, M.H., Ströhle, J. and Svendsen, H.F., "A study of the heating section of a gas heated reformer", submitted to *Int. J. Chem. Reactor Eng.* (2006)

Wijngaarden, R.J., Westerterp, K.R., "Do the effective heat conductivity and the heat transfer coefficient at the wall inside a packed bed depend on chemical reaction? Weaknesses and applicability of current models", *Chem. Eng. Sci.*, **44** (8), pp. 1663-1663 (1989)

Wijngaarden, R.J., Westerterp, K.R., "Radial heat transport in packed beds at elevated pressures", *Chem. Eng. Proc.*, **31**, pp. 157-160 (1992)

Wilke, C.R., "Diffusional properties of multicomponent gases", *Chem. Eng. Prog.*, **46** (2), pp. 95-104 (1950)

Winterberg, M., Tsotsas, E., Krischke, A. and Vortmeyer, D., "A simple and coherent set of coefficients for modelling of heat and mass transport with and without chemical reaction in tubes filled with spheres", *Chem. Eng. Sci.*, **55**, pp. 967-979 (2000)

Winterberg, M. and Tsotsas, E., "Modelling of heat transport in beds packed with spherical particles for various bed geometries and/or thermal boundary conditions", *Int. J. Therm. Sci.*, **39**, pp. 556-570 (2000a)

Winterberg, M. and Tsotsas, E., "Correlations for effective heat transport coefficients in beds packed with cylindrical particles", *Chem. Eng. Sci.*, **55**, pp. 5937-5943 (2000b)

Xiu, G., Li, P., Rodriges, A.E., "Adsorption-enhanced steam-methane reforming with intraparticle-diffusion limitations", *Chem. Eng. J.*, **95**, pp. 83-93 (2003)

Xu, J. and Froment, G.F., "Methane Steam Reforming, Methanation and Water-Gas Shift: I. Intrinsic Kinetics", *AIChE J.*, **35** (1), pp. 88-96 (1989a)

Xu, J. and Froment G.F., "Methane steam reforming: II. Diffusional limitations and reactor simulation", *AIChE J.*, **35** (1), pp. 97-103 (1989b)

Yu, Y.H. and Sosna, M.H., "Modeling for Industrial Heat Exchanger Type Steam Reformer", *Korean J. Chem. Eng.*, **18** (1), pp. 127-132 (2001)

APPENDICES

Appendix A. Reaction kinetics

Xu and Froment (1989a) developed expressions for the reaction kinetics for the three participating reactions, denoted reaction 1, 2 and 3, respectively:

$$CH_4 + H_2O \rightleftharpoons CO + 3\,H_2 \tag{A-1}$$

$$CO + H_2O \rightleftharpoons CO_2 + H_2 \tag{A-2}$$

$$CH_4 + 2\,H_2O \rightleftharpoons CO_2 + 4\,H_2 \tag{A-3}$$

The rate expressions include the fact that these are equilibrium reactions so that the reaction rates are positive for the forward reactions of Equations (A-1) to (A-3) and negative for the respective backward reactions.

The reaction rates r_j for reactions 1 to 3 are expressed by the equations:

$$r_1 = \frac{k_1}{3.6\,p_{H_2}^{2.5}} \frac{\left(p_{CH_4} p_{H_2O} - p_{H_2}^3 p_{CO} / K_1\right)}{\left(\mathrm{DEN}\right)^2} \tag{A-4}$$

$$r_2 = \frac{k_2}{3.6\,p_{H_2}} \frac{\left(p_{CO} p_{H_2O} - p_{H_2} p_{CO_2} / K_2\right)}{\left(\mathrm{DEN}\right)^2} \tag{A-5}$$

$$r_3 = \frac{k_3}{3.6\,p_{H_2}^{3.5}} \frac{\left(p_{CH_4} p_{H_2O}^2 - p_{H_2}^4 p_{CO_2} / K_3\right)}{\left(\mathrm{DEN}\right)^2} \tag{A-6}$$

The rate coefficients k_j are given by:

$$k_1 = A_1 \exp\left[-10^3 \frac{E_1}{RT}\right] \tag{A-7}$$

The Arrhenius constants A_j and the activation energies E_j are quoted from Froment and Bischoff (1990) in Table A-1. The equilibrium constants are:

$$K_1 = 10^{-11650/T+13.076} \tag{A-8}$$

$$K_2 = 10^{1910/T-1.784} \tag{A-9}$$

$$K_3 = K_1 K_2 \tag{A-10}$$

The denominator DEN is defined as:

$$\mathrm{DEN} = 1 + K_{CO} p_{CO} + K_{H_2} p_{H_2} + K_{CH_4} p_{CH_4} + K_{H_2O} p_{H_2O} \big/ p_{H_2} \tag{A-11}$$

The adsorption coefficients for the components i in Equation (A-11) are:

$$K_i = A_{ad,i} \exp\left[10^3 \frac{-\Delta H_{ad,i}}{RT}\right] \tag{A-12}$$

The pre-exponential factors for adsorption, $A_{ad,i}$, and the adsorption enthalpies, $-\Delta H_{ad,i}$, are also quoted from Froment and Bischoff (1990) in Table.

Table A-1: Arrhenius constants and activation energies for the three reaction rates given in Equations (A-1) to (A-3), respectively, and pre-exponential factors for adsorption and adsorption enthalpies for actual components (Froment and Bischoff, 1990).

Reaction parameters:			
	j = rxn. 1	j = rxn. 2	j = rxn. 3
A_j	$4.225 \cdot 10^{15}$	$1.955 \cdot 10^{6}$	$1.02 \cdot 10^{15}$
E_j [kJ/ kmole]	$240.1 \cdot 10^{3}$	$67.13 \cdot 10^{3}$	$243.9 \cdot 10^{3}$

Component parameters:				
	i = CO	i = H_2	i = CH_4	i = H_2O
$A_{ad,i}$	$8.23 \cdot 10^{-5}$	$6.12 \cdot 10^{-9}$	$6.65 \cdot 10^{-4}$	$1.77 \cdot 10^{5}$
$-\Delta H_{ad,i}$ [kJ/ kmole]	$-70.65 \cdot 10^{3}$	$-82.9 \cdot 10^{3}$	$-38.28 \cdot 10^{3}$	$88.68 \cdot 10^{3}$

Appendix B. Equations for the potential for catalyst coking

The potential for coke formation on the surface of the catalyst pellets can be evaluated by equilibrium calculations of the coking reactions. Wagner and Froment (1992) correlated the equilibrium constants based on experiments:

CO-reduction: $$CO + H_2 \rightleftharpoons C + H_2O \quad \text{(B-1)}$$

Methane cracking: $$CH_4 \rightleftharpoons C + 2\,H_2 \quad \text{(B-2)}$$

Boudouard reaction: $$2\,CO \rightleftharpoons C + CO_2 \quad \text{(B-3)}$$

The equilibrium constants are quoted here:

CO-reduction: $$K_R = \exp\left(\frac{13640}{T} - 14.84\right) \quad \text{(B-4)}$$

Methane cracking: $$K_M = \exp\left(-\frac{9573}{T} - 11.62\right) \quad \text{(B-5)}$$

Boudouard reaction: $$K_B = \exp\left(\frac{18150}{T} - 19.08\right) \quad \text{(B-6)}$$

These parameters have the denominations [bar], [bar^{-1}] and [bar^{-1}], respectively, and this must be allowed for when estimating the approaches to equilibrium from the partial pressures. Finally, the combination of partial pressures and gas temperature is within the equilibrated state for coke formation if one or more of the following criteria are met:

CO-reduction: $$\frac{10^5}{K_R}\frac{p_{H_2O}}{p_{CO}\,p_{H_2}} > 1 \quad \text{(B-7)}$$

Methane cracking: $$\frac{10^{-5}}{K_M}\frac{p_{H_2}^2}{p_{CH_4}} > 1 \quad \text{(B-8)}$$

Boudouard reaction: $$\frac{10^5}{K_B}\frac{p_{CO_2}}{p_{CO}^2} > 1 \quad \text{(B-9)}$$

Appendix C. Wall boundary condition for radiative heat transfer

The radiative heat flux through the wall boundaries of the annular section is not part of the energy boundary conditions for the gas/wall interfaces. The cause lies in the chosen solution method, the finite difference method, which is an analytical form. On the other hand both the radiative heat transport and any source terms are allowed for when using a numerical (finite volume) boundary condition. In the following this is explained by an example illustrated in Figure C-1 and quoted from Siegel and Howell (2002).

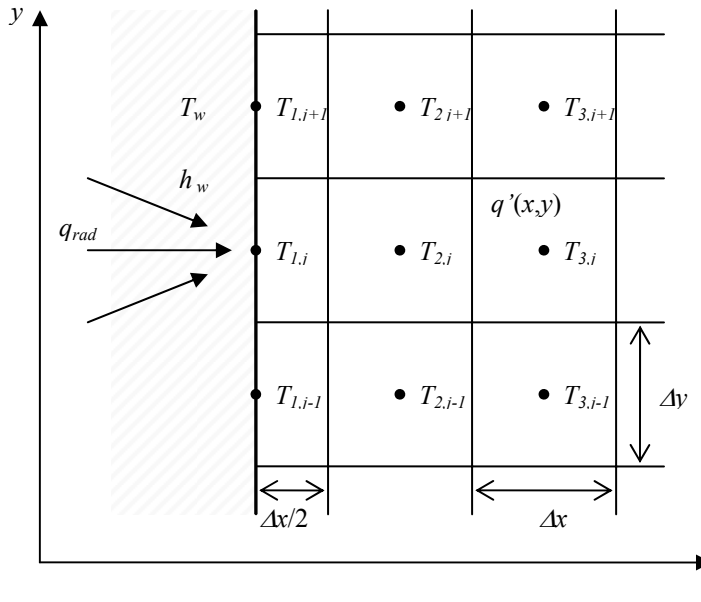

Figure C-1. Numerical boundary comditions. Reproduced from Siegel and Howell (2002).

The medium of the grid elements seen in Figure C-1 is a participating grey gas with transparent boundary at $x = 0$. The element $(1,j)$ at $x = 0$ is exposed to the diffuse radiative energy flux q_{rad} and borders on the wall temperature T_w, where the wall heat transfer coefficient is h_w. The conductivity of the medium, λ, is uniform. A volumetric energy source denoted $q'(x,y)$ is present. The boundary condition of this system can then be written by summarizing the conductive transport, the radiative transport, the convective heat transport at the interface and the heat source term, respectively:

$$\begin{aligned} &-\lambda\,\Delta y\frac{T_{1,j}-T_{2,j}}{\Delta x}-\lambda\frac{\Delta x}{2}\frac{T_{1,j}-T_{1,j+1}}{\Delta y}-\lambda\frac{\Delta x}{2}\frac{T_{1,j}-T_{1,j-1}}{\Delta y} \\ &-\nabla\cdot\mathbf{q}_{rad,i,j}\frac{\Delta x}{2}\Delta y-h_w\Delta y\left(T_{1,j}-T_w\right)+q'\frac{\Delta x}{2}\Delta y=0 \end{aligned} \tag{C-1}$$

It is clear from this boundary condition that when converting to an analytical form, in the limit $\Delta x \to 0$, the terms from conduction in y-direction, radiation and heat source vanish:

$$-\lambda \lim_{x\to 0}\left(\frac{T_{1,j}-T_{2,j}}{\Delta x}\right)-h_w\left(T_{1,j}-T_w\right)=0 \tag{C-2}$$

This is now valid at any position *y*. The analytical form of the boundary condition is at this:

$$-\lambda \left.\frac{\partial T}{\partial x}\right|_{x=0}=h_w\left(T_{x=0}-T_w\right) \tag{C-3}$$

Appendix D. Normalized equations for the reactor models

The differential equations of the reactor models are too stiff for solving their original form and therefore they are normalized for implementation in MATLAB. The annulus model was also attempted normalized but without any resulting computation time savings. The annulus model was therefore solved on the form presented in Section 4.5. The definitions of the normalized parameters are summarized in Table D-1.

Table D-1. Definitions of the normalized parameters.

temperature:	$\theta = \frac{\left(T - T^0\right)}{T^0}$	(D-1)	tube length:	$h = \frac{z}{L}$	(D-2)
total pressure:	$\beta = \frac{P}{P^0}$	(D-3)	tube radius:	$\omega = \frac{r}{R_l}$	(D-4)
partial pressure:	$\beta_i = \frac{p_i}{P^0}$	(D-5)	pellet depth:	$\omega_p = \frac{y}{R_p}$	(D-6)
superficial velocity:	$u = \frac{v_{z,s}}{v^0}$	(D-7)			

Inserting the parameters of Table D-1 into the bulk equations of the heterogeneous model gives:

Equation (4-25), component balances:

$$\frac{\partial \beta_i}{\partial h} = -\frac{\beta_i}{u}\frac{\partial u}{\partial h} + \frac{\beta_i}{(\theta+1)}\frac{\partial \theta}{\partial h} - \frac{k_{g,i} a_v L}{v^0 u}\left(\beta_i - \beta_{i,p}^s\right) + \frac{1}{R_l^2 v^0 u}\left(\frac{\partial E_{er,b}}{\partial \omega}\frac{\partial \beta_i}{\partial \omega} + E_{er,b}\frac{\partial^2 \beta_i}{\partial \omega^2} - \frac{E_{er,b}}{(\theta+1)}\frac{\partial \theta}{\partial \omega}\frac{\partial \beta_i}{\partial \omega} + \frac{E_{er,b}}{\omega}\frac{\partial \beta_i}{\partial \omega}\right) \quad \text{(D-8)}$$

Equation (4-26), boundary conditions for the component balances:

$$\left.\frac{\partial \beta_i}{\partial \omega}\right|_{\omega=0,1} = 0 \quad \text{(D-9)}$$

Equation (4-28), total mass balance giving the superficial velocity:

$$\frac{\partial u}{\partial h} = \frac{u}{(\theta+1)}\frac{\partial \theta}{\partial h} - \frac{u}{\beta}\frac{\partial \beta}{\partial h} - \frac{a_v L}{v^0 \beta}\sum_i k_{g,i}\left(\beta_i - \beta_{i,p}^s\right) \quad \text{(D-10)}$$

Equation (4-30), pressure drop equation:

$$\frac{d\beta}{dh} = -6.8\frac{L}{P^0}\frac{(1-\varepsilon)^{1.2}}{\varepsilon^3} Re^{-0.2}\frac{\rho_m v_{sm}^2}{d_p} \quad \text{(D-11)}$$

Equation (4-32), temperature equation:

$$\frac{\partial \theta}{\partial h} = \frac{L}{\rho_k \, c_{P,g} \, v^0 \, u}\left(\frac{\lambda_{er,b}}{R_l^2}\left(\frac{1}{\omega}\frac{\partial \theta}{\partial \omega} + \frac{\partial^2 \theta}{\partial \omega^2}\right) - h_p \, a_v \left(\theta - \theta_p^s\right)\right) \tag{D-12}$$

Equations (4-34) and (4-35), boundary conditions for the temperature equation:

$$\left.\frac{\partial \theta}{\partial \omega}\right|_{\omega=0} = 0 \tag{D-13}$$

$$-\lambda_{er,b}\left.\frac{\partial T}{\partial \omega}\right|_{\omega=1} = h_l \, R_l \left(\theta(1) - \theta_{wl}\right) \tag{D-14}$$

The normalized pellet equations in the heterogeneous model obtain the following form:

Equation (4-39), component balances:

$$\frac{\partial^2 \beta_{p,i}}{\partial \omega_p^2} - \frac{1}{\left(\theta_p + 1\right)}\frac{\partial \theta_p}{\partial \omega_p}\frac{\partial \beta_{p,i}}{\partial \omega_p} + \frac{R\left(\theta_p + 1\right)T^0 \, R_p^2 \, \rho_c}{P^0 \, \varepsilon_p \, D_{m,i}^e}\sum_{j=1}^{3} \nu_{ij} \, r_j = 0 \tag{D-15}$$

Equations (4-40) and (4-41), the boundary conditions of the component balances:

$$\left.\frac{\partial \beta_{p,i}}{\partial \omega_p}\right|_{\omega_p=0} = 0 \tag{D-16}$$

$$D_{m,i}^e \left.\frac{\partial \beta_{p,i}}{\partial \omega_p}\right|_{\omega_p=X} = k_{g,i}\left(\beta_i - \beta_{p,i}^s\right) \tag{D-17}$$

Equation (4-42), the temperature equation:

$$\lambda_c \frac{\partial^2 T_p}{\partial y^2} + \sum_{j=1}^{3} \rho_c r_j \left(-\Delta H_j\right) = 0 \tag{D-18}$$

Equations (4-43) and (4-44), the boundary conditions of the temperature equation:

$$\left.\frac{\partial \theta_p}{\partial \omega_p}\right|_{\omega_p=0} = 0 \tag{D-19}$$

$$-\lambda_c \left.\frac{\partial \theta_p}{\partial \omega_p}\right|_{\omega_p=X} = h_p\left(\theta_p^s - \theta\right) \tag{D-20}$$

The equations for the pseudo-homogeneous model are normalized analogous to the bulk equations of the heterogeneous model:

Equation (4-48), the component balances:

$$\frac{\partial \beta_i}{\partial h} = -\frac{\beta_i}{u}\frac{\partial u}{\partial h} + \frac{\beta_i}{(\theta+1)}\frac{\partial \theta}{\partial h} + \frac{R\,T\,L}{v^0\,u}\sum_j \eta'_j \nu_{ij} r_j + \frac{1}{R_l^2\,v^0\,u}\left(\frac{\partial E_{er,b}}{\partial \omega}\frac{\partial \beta_i}{\partial \omega} + E_{er,b}\frac{\partial^2 \beta_i}{\partial \omega^2} - \frac{E_{er,b}}{(\theta+1)}\frac{\partial \theta}{\partial \omega}\frac{\partial \beta_i}{\partial \omega} + \frac{E_{er,b}}{\omega}\frac{\partial \beta_i}{\partial \omega}\right) \tag{D-21}$$

Equation (4-49), the total mass balance:

$$\frac{\partial u}{\partial h} = \frac{u}{(\theta+1)}\frac{\partial \theta}{\partial h} - \frac{u}{\beta}\frac{\partial \beta}{\partial h} + \frac{R\,T\,L}{v^0\,\beta}\sum_j\left(\sum_i \nu_{ij}\right)\eta'_j r_j \tag{D-22}$$

Equation (4-50), the temperature equation:

$$\frac{\partial \theta}{\partial h} = \frac{L}{\rho_g\,c_{P,g}\,v^0\,u}\left(\frac{\lambda_{er,b}}{R_l^2}\left(\frac{1}{\omega}\frac{\partial \theta}{\partial \omega} + \frac{\partial^2 \theta}{\partial \omega^2}\right) + \frac{\rho_{cb}}{T^0}\sum_j\left(-\Delta H_j\right)\eta'_j r_j\right) \tag{D-23}$$

Appendix E. The radial mean values of parameters

The notion "radial mean" of a parameter x, x_m, represents average values weighted on the cross sectional area. The radial mean is found by integration over the cross sectional area with weighting on the linear gas velocity, v:

$$x_m = \frac{\int_{A_{(1)}}^{A_{(2)}} v\, x\, dA}{\int_{A_{(1)}}^{A_{(2)}} v\, dA} \tag{E-1}$$

If the parameter x is a function of z and r, then x_m is a function of z only. The integration limits are $A_{(1)} = 0$ and $A_{(2)} = \pi R_1^2$ for the reactor model, and $A_{(1)} = \pi R_2^2$ and $A_{(2)} = \pi R_3^2$ for the annulus model.

Appendix F. Specifications of the catalyst pellets

The physical and geometrical data for the catalyst pellets are real data for the R-67-7H steam reforming catalyst of Haldor Topsøe AS. This is a cylindrical, 7-hole pellet with outer radius R_{ext} = 8 mm, height H_p = 11 mm and hole radius R_{hole} = 1.7 mm (Haldor Topsøe AS, 2005b).

The void fraction of the bed, ε, and the specific surface area, a_v, are calculated from the catalyst density and the catalyst bulk density, which are given by Pedernera et al. (2003) as ρ_c = 1990.6 kg/ m_c^3 and $\rho_{c,b}$ = 1016.4 kg/ m_r^3:

$$\varepsilon = 1 - \frac{1016.4\,\mathrm{m}_c^3}{1990.6\,\mathrm{m}_r^3} = 0.49 \tag{F-1}$$

The specific surface area, a_v, which is the accessible catalyst area per reactor volume, can then be calculated from the void fraction and from the outer surface area and the volume of one pellet, A_p and V_p, respectively:

$$A_p = 2\left[\pi R_{ext}^2 - 7\,\pi R_{hole}^2\right] + 2\,\pi R_{ext}\,H_p = 3.70\cdot 10^{-4}\,\mathrm{m}^2 \tag{F-2}$$

$$V_p = H_p\left[\pi R_{ext}^2 - 7\,\pi R_{hole}^2\right] = 4.48\cdot 10^{-7}\,\mathrm{m}^2 \tag{F-3}$$

$$a_v = (1-\varepsilon)\frac{A_p}{V_p} = (1-0.49)\,\mathrm{m}_c^3/\mathrm{m}_r^3\,\frac{3.70\cdot 10^{-4}\,\mathrm{m}_c^2}{4.48\cdot 10^{-7}\,\mathrm{m}_c^3} = 421.2\,\mathrm{m}_c^2/\mathrm{m}_r^3 \tag{F-4}$$

Finally, the equivalent diameter of the catalyst pellets, d_p, is calculated as given by Froment and Bischoff (1990). This is defined as the diameter of a sphere with the same surface area per unit volume (i.e. m_c^2/m_c^3) as the actual particle:

$$d_p = 6\frac{(1-\varepsilon)}{a_v} \tag{F-5}$$

Paper 1

submitted to *Industrial & Engineering Chemistry Research* (2006)

Mass and heat transfer limitations in a heterogeneous model of a gas heated steam reformer

Margrete H. Wesenberg[†]*, Hallvard F. Svendsen**

Institute of Chemical Engineering, Norwegian University of Science and Technology, N-7491 Trondheim, Norway

* Corresponding author. Tel.: +47 73594100. Fax: +47 73594080. E-mail: hallvard.svendsen@chemeng.ntnu.no.
[†] Statoil Research Centre, N-7005 Trondheim, Norway

Abstract:

A gas heated steam reformer (GHR) which converts natural gas to synthesis gas for methanol or Fischer-Tropsch purposes was modeled for stationary conditions. The model is in two dimensions and comprises a fixed bed reactor model, representing one of the reactor tubes in the GHR, and an annulus model, representing an annular space on the shell side of the GHR. The heterogeneous reactor model is studied in this article, with particular emphasis on the evaluation of mass and heat transfer limitations between the gas and the pellets. Different empirical correlations for mass and heat transfer coefficients were evaluated and it was found that the interphase transport limitations had a negligible effect on the overall reactor simulation results but were of sufficient significance to be needed when studying local observed reaction rates and interpreting these to obtain kinetic rate data.

KEYWORDS: finite difference method, two-dimensional, heterogeneous reactor model, effectiveness factor, particle mass and heat transfer coefficients, convective steam methane reformer.

1. Introduction

The gas heated reformer (GHR), or convective steam reformer, is a compact alternative to the conventional, fired steam reformer (CSR) for production of synthesis gas from natural gas. The high manufacturing costs, the large weight and the large base area of the CSR maintain the interest for a compact and less expensive alternative. The GHR has been commercially proven for large scale ammonia and hydrogen purposes where the steam excess in the reformer is large. There is also interest for the GHR for Fischer-Tropsch and methanol production but this may only be profitable if the steam content in the feed gas is reduced to a steam to carbon ratio below 1.5.

The GHR licensors are in progress with developing the GHR technology which makes lower steam to carbon ratios possible. The high partial pressure of methane and carbon monoxide may take the operation over the equilibrium limit of the coking reactions. Further development of catalyst materials is thus required in order to achieve rapid gasification of coke and thereby avoid catalyst poisoning. Another challenge within GHR technology is related to the life time of the tube material. If syngas is to be used as the heating source on the shell side of the GHR unit,

the tubes are exposed to the risk of metal dusting under the tough operating conditions of warm and pressurized syngas. Research to find suitable materials is therefore in progress with GHR licensors to make such process operation feasible. Because of the danger of coke formation and metal dusting during operation for Fischer-Tropsch and methanol production a numerical model of the GHR is considered useful in the evaluation of safe operational limits. It is also a tool for design and optimization purposes. The simplified two-dimensional model for the reactor tubes and the heating section developed here is considered sufficient for these purposes.

The steam reforming reactions and the water-gas-shift reaction involved are respectively:

$$CH_4 + H_2O \rightleftharpoons CO + 3\,H_2 \tag{1}$$

$$CH_4 + 2\,H_2O \rightleftharpoons CO_2 + 4\,H_2 \tag{2}$$

$$CO + H_2O \rightleftharpoons CO_2 + H_2 \tag{3}$$

The reactions are catalysed by pellets coated with nickel and are as a whole net energy consumers. Effective heat transport to the reactor tubes and further into the centre of the fixed bed is therefore a very important aspect during design and operation of steam reformers. The reactions take place in several tubular fixed bed reactors of low diameter-to-height ratio to ensure efficient heat transport in radial direction. The heat source in GHRs can be flue gas or, as in this study, syngas from a secondary autothermal reformer (ATR). The heat transport from this hot gas is mainly convective, in contrast to CSRs having mainly radiative transport.

A pseudo-homogeneous reactor model may often be sufficient for simulating steam reformers as they are operating in a strongly diffusion controlled regime [1]. Heterogeneous models are on the other hand able to show the details of pellet surface concentrations and temperatures, which are studied here. One-dimensional models can also be sufficient when modelling fixed beds, but in steam reformers the radial temperature changes in the tubes can be as large as 80 ºC. Therefore the two-dimensional model was chosen in this study, which also has the advantage of giving higher accuracy when the limits of coke formation are to be evaluated.

Different types of steam reformer have been studied a number of times. The reactor models are usually two-dimensional heterogeneous [2,3] and pseudo-homogeneous [2,4,5,6] models, and one-dimensional heterogeneous models [2,7,8,9,10,11,12].

The two-dimensional heterogeneous reactor model used in this work sets apart from most of the above referred heterogeneous models by including resistance to mass transfer in the gas film surrounding the catalyst pellets and resistance to heat transfer both in the gas film and internally in the pellets. The most common simplification is to neglect such restrictions and this is studied and discussed in this paper.

The reactor model is coupled to a model for an annular volume [13] where counter current hot gas is cooled down while providing heat to the reactor tube.

2. Mathematical model

The GHR model consists of two main models: the fixed bed reactor tube and the shell side heating section. The model is simplified by modelling one single average tube with its corresponding shell side area, represented by an annular section encircled by a sheath tube. The operating conditions in this study are typical for a primary reformer producing syngas for methanol or Fischer-Tropsch synthesis purposes, with a steam-to-carbon ratio of 2. The computation of the two models together is performed by linking them at the outer reactor tube surface and iterating with the use of the resulting temperature and heat flux profiles at this wall.

The differential equations are solved by a finite difference method using an ODE solver, and the radial derivatives in equations involving both axial and radial variations are discretized by the numerical method of lines [14].

The gases are assumed ideal and their physical properties are given as functions of temperature and composition [15]. The two flows are counter current, with natural gas feed entering the reactor tube at axial position $z = 0$ and product gas exiting at $z = L$ as shown in . The inlet of the hot syngas on the annular side is thus positioned at $z = L$. The radii of the inner and the outer wall of the reactor tube are denoted R_1 and R_2, respectively, and the outer radius inside the annulus is R_3.

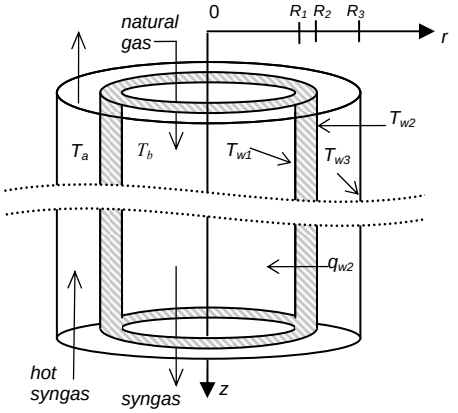

Figure 1. Sketch of the total model consisting of the reactor model and the annulus model. L is typically 12 m and R_2 is about 12 cm.

2.1. The heterogeneous reactor model. The heterogeneous reactor model is composed of two sets of model equations, describing the gas bulk and the solid pellet phase. Catalyst data for the R-67-7H catalyst of Haldor Topsøe A/S was used [3] and the equivalent particle diameter was calculated as shown by Froment and Bischoff [16].

2.1.1. Bulk equations. The conservation equations for five of the six components i (i = CH_4, H_2O, CO, H_2, CO_2 and N_2) in the bulk phase can be expressed in terms of partial pressures when the ideal gas law has been introduced. The partial pressure of the sixth component is found by subtracting the five partial pressures from the total pressure. The axial dispersion is omitted as it is negligible compared to the axial convective transport at the operating velocities of a steam reformer. The local axial mass flux is assumed constant over the radial positions, and this implies zero radial mass flux. The component balance giving the bulk partial pressure p_i is coupled to the component balance for the catalyst pellet through the mass transfer coefficient k_g, the specific outer pellet surface area a_v, and the partial pressure on the pellet surface $p^s_{p,i}$:

$$\begin{aligned}\frac{\partial p_i}{\partial z} = &-\frac{p_i}{v_{z,s}}\frac{\partial v_{z,s}}{\partial z}+\frac{p_i}{T}\frac{\partial T}{\partial z}-\frac{k_{g,i}a_v}{v_{z,s}}\left(p_i-p^s_{p,i}\right)\\ &+\frac{1}{v_{z,s}}\left(\frac{\partial D_{er}}{\partial r}\frac{\partial p_i}{\partial r}+D_{er}\frac{\partial^2 p_i}{\partial r^2}-\frac{D_{er}}{T}\frac{\partial T}{\partial r}\frac{\partial p_i}{\partial r}+\frac{D_{er}}{r}\frac{\partial p_i}{\partial r}\right)\end{aligned} \tag{4}$$

The boundary conditions at the centre of the tube ($r = 0$) and at the tube wall ($r = R_1$) are:

$$\left.\frac{\partial p_i}{\partial r}\right|_{r=0,R_1} = 0 \tag{5}$$

The empirical correlation used for the effective radial dispersion coefficient, D_{er}, is given by [17]:

$$D_{er} = \frac{d_p / v_{z,s}}{10\left[1+19.4\left(d_p/d_t\right)^2\right]} \tag{6}$$

Different types of empirical correlations for the mass transfer coefficients $k_{g,i}$ are evaluated in Section 3.3. Based on this, the following correlation [18] was chosen, valid for $Re_p < 10^4$:

$$Sh = 2 + 1.1 Sc^{1/3} Re_p^{0.6} \tag{7}$$

$D_{m,i}$, as part of the Schmidt number in Equation (7), is the diffusion coefficient of component i in the gas mixture and is calculated according to the Wilke equation [19]:

$$\frac{1}{D_{m,i}} = \sum_{k \neq i} \frac{x_k}{D_{ik}} \tag{8}$$

The binary diffusion coefficients D_{ik} [20] are given as functions of the diffusion volumes [21]:

$$D_{ik} = \frac{1.013 \cdot 10^{-2} T^{1.75} \left(1/M_i + 1/M_k\right)^{1/2}}{P\left[\left(\sum_i V\right)^{1/3} + \left(\sum_k V\right)^{1/3}\right]^2} \tag{9}$$

The differential equation expressing the superficial gas velocity in the reactor bulk results from the sum of the component balances of Equation (4):

$$\frac{\partial v_{z,s}}{\partial z} = \frac{v_{z,s}}{T}\frac{\partial T}{\partial z} - \frac{v_{z,s}}{P}\frac{\partial P}{\partial z} - \frac{k_{g,i} a_v}{P}\sum_i \left(p_i - p_{p,i}^s\right) \tag{10}$$

It is assumed that radial variations in pressure can be neglected, and the radial mean of the velocities, densities and viscosities are therefore used when calculating the change in pressure as a function of axial position. Empirical equations for the friction factor in the pressure drop equation is discussed in Section 3.3, where it was concluded to apply the following equation [22], valid for $Re_p/(1-\varepsilon) > 300$:

$$\frac{dP}{dz} = -6.8 \frac{(1-\varepsilon)^{1.2}}{\varepsilon^3} Re_p^{-0.2} \frac{\rho_m v_{sm}^2}{d_p} \tag{11}$$

The energy transport in axial direction is dominated by the convective term, and axial conduction is therefore neglected. With no radial convection, the only energy transport mechanism in radial direction is the effective conduction. The heat transfer across the gas film enclosing the pellet surface is modelled with the heat transfer coefficient h_p:

$$\frac{\partial T}{\partial z} = \frac{1}{\rho_g C_{P_g} v_{z,s}}\left(\lambda_{er}\left(\frac{1}{r}\frac{\partial T}{\partial r} + \frac{\partial^2 T}{\partial r^2}\right) - h_p a_v \left(T - T_p^s\right)\right) \tag{12}$$

The heat transfer coefficient h_p was calculated according to the empirical correlation of Wakao et al. [23], valid for $Re_p < 10^4$. The choice of correlation is based on the discussion in Section 3.3.

$$Nu_p = 2 + 1.1 Pr^{1/3} Re_p^{0.6} \tag{13}$$

The first boundary condition of the energy equation define symmetry in T at $r = 0$ and the second connects T at $r = R_1$ to the wall temperature, T_{w1}, by the means of the wall heat transfer coefficient h_1. The latter boundary condition is expressed by the equation:

$$-\lambda_{er}\left.\frac{\partial T}{\partial r}\right|_{r=R_1} = h_1 (T(R_1) - T_{w1}) \tag{14}$$

The effective radial thermal conductivity for the bulk phase in Equations (12) and (14), λ_{er}, and the wall heat transfer coefficient of the boundary condition in Equation (14), h_1, are

calculated from empirical correlations valid for the process conditions of steam reformers. The correlation of Peters et al. [24] is used for λ_{er}:

$$\lambda_{er} = \lambda_{er}^{0} + \lambda_g \frac{Re_p\, Pr}{8.0\left(1+19.4\left[d_p/d_t\right]^2\right)} \tag{15}$$

This correlation involves also heat transfer from turbulence, is valid for $Re_p > 100$ and is assumed constant over the radius. The effective radial thermal conductivity for stagnant gas, λ^0_{er} in Equation (15), is correlated as derived by Kunii and Smith [25], which still stands as the most suitable correlation [26]:

$$\lambda_{er}^{0} = \lambda_g \varepsilon + \lambda_g \frac{0.895(1-\varepsilon)\left(\ln\left[\lambda_c/\lambda_g - 0.5439\left(\left[\lambda_c/\lambda_g\right]-1\right)\right] - 0.4561\left(\lambda_c-\lambda_g\right)/\lambda_c\right)}{0.5\cdot 0.7042\left(\left(\lambda_c-\lambda_g\right)/\lambda_c\right)^2} \tag{16}$$

The empirical heat transfer coefficient (h_1) given by Peters et al. [24] has been found to describe the degree of heat transfer well in steam reformers [27] and is valid for cylindrical packings at $0.1 < d_p/d_t < 0.6$ and $100 < Re_p < 8000$:

$$Nu_w = 4.9\left(d_p/d_t\right)^{0.26} Re_p^{0.45} Pr^{0.33} \tag{17}$$

2.1.2. Pellet equations. Two basic assumptions for the pellets are made: negligible change in the internal total pressure and no convective mass transport. The pellet geometry is simplified to a plane surface with the depth specified by the co-ordinate y. The planar geometry is justified by the reactions taking place only in the outer layer of the catalyst pellets [12]. Also, the effectiveness factors for the steam reforming reactions are very low, which implies that such a simplification in geometry has almost no effect on the simulation results.

The transport equation for component i in the pellet is expressed by partial pressures by introducing the ideal gas law. The internal change in total pressure can be disregarded in the diffusion term [28,29,30] but still the increase in the total pressure is allowed for by solving the component balance for each of the participating components. The component balances need to be independent to assure the total mass continuity:

$$D^e_{m,i}\left(\frac{1}{R\,T_p}\frac{\partial^2 p_{p,i}}{\partial y^2} - \frac{1}{R\,T_p^2}\frac{\partial T_p}{\partial y}\frac{\partial p_{p,i}}{\partial y}\right) + \sum_{j=1}^{3} \nu_{ij}\, r_j(p_{p,i}, T_p)\,\rho_c = 0 \tag{18}$$

The radial variations in the effective diffusivities $D^e_{m,i}$ is negligible and are therefore not included in this differential equation. $D^e_{m,i}$ is the effective diffusivity for component i within the pores of the catalyst pellet, and it is calculated from the diffusivity $D_{m,i}$, the Knudsen diffusivity D_K, the tortuosity factor τ and the pellet porosity ε_p [31]:

$$D^e_{m,i} = \frac{\varepsilon_p}{\tau}\left(\frac{1}{D_{m,i}} + \frac{1}{D_K}\right)^{-1} \tag{19}$$

$D^e_{m,i}$ is independent of the Knudsen diffusivity at pressures typical for steam reformers [31].

The rates of the reactions given in Equations (1), (2) and (3), r_j, are modelled as presented by Xu and Froment [32]. The balance equations are solved for a thin layer of the catalyst pellets which is the active part of the pellets, meaning that the inner core is inactive. The thickness of the active layer is equal to a fraction X of the equivalent particle radius R_p and the boundary conditions are therefore defined for $y = 0$ and $y = X{\cdot}R_p$. The component balance boundary conditions define flattening of the partial pressure profiles at $y = 0$ and mass transfer to the pellet surface at $y = X{\cdot}R_p$, with the latter given as:

$$D^{e}_{m,i}\left.\frac{\partial p_{p,i}}{\partial y}\right|_{X R_p} = k_{g,i}\left(p_i - p^{s}_{p,i}\right) \tag{20}$$

The heat balance is composed of conductive heat transport and reaction heat:

$$\lambda_p \frac{\partial^2 T_p}{\partial y^2} + \sum_{j=1}^{3} \rho_c\, r_j(p_{p,i}, T_p)\left(-\Delta H_j\right) = 0 \tag{21}$$

The thermal conductivity of the pellet, λ_p, is constant. The boundary conditions define zero derivative at $y = 0$ and heat transfer at $y = X{\cdot}R_p$ from the bulk gas to the pellet surface, which is:

$$-\lambda_p \left.\frac{\partial T_p}{\partial y}\right|_{X R_p} = h_p\left(T^{s}_{p} - T\right) \tag{22}$$

2.1.3. Effectiveness factors. The effectiveness factor of a catalyst is defined as the actual reaction rate based on the volume of a pellet relative to the reaction rate in a completely active catalyst pellet with temperature and partial pressures equal to those of the pellet surface. The effectiveness factor of the reaction r_j can then be calculated from the expression:

$$\eta_j = \frac{\int_0^{V_p} r_j\, dv}{V_p\, r^{s}_{j}} = \frac{a_v}{\left(1-\varepsilon\right) r^{s}_{j}} \int_0^{X R_p} r_j\, dy \tag{23}$$

As long as there is resistance to mass or heat transfer in the pellet, arising from low effective molecular diffusivity or low thermal conductivity, this effectiveness factor will be less than one. Steam reformers operate with very low effectiveness factors.

An analogous effectiveness factor, η_j', which is relative to the reaction rate calculated from bulk conditions instead of surface conditions, can be defined as:

$$\eta'_j = \frac{a_v}{\left(1-\varepsilon\right) r^{bulk}_{j}} \int_0^{X R_p} r_j\, dy \tag{24}$$

Consequently η'_j will be smaller than η_j if mass or heat transfer limitations in the gas film between the gas bulk and the pellet surface are present.

2.2. The analogous pseudo-homogeneous reactor model. A pseudo-homogeneous model is nearly identical to a heterogeneous model as the one given in Section 2.1. The pellet equations are on the other hand not included and in the bulk equations the terms for mass or heat transport to pellet surface are replaced with reaction terms. The reaction rates are dependent on bulk conditions and are multiplied with effectiveness factors η'_j as given in Equation (24). Equations (4), (10) and (12) are replaced with the following equations, respectively:

$$\begin{aligned}\frac{\partial p_i}{\partial z} = &-\frac{p_i}{v_{z,s}}\frac{\partial v_{z,s}}{\partial z} + \frac{p_i}{T}\frac{\partial T}{\partial z} - \frac{RT}{v_{z,s}}\sum_j \eta_j\, \nu_{ij}\, r_j \\ &+ \frac{1}{v_{z,s}}\left(\frac{\partial D_{er}}{\partial r}\frac{\partial p_i}{\partial r} + D_{er}\frac{\partial^2 p_i}{\partial r^2} - \frac{D_{er}}{T}\frac{\partial T}{\partial r}\frac{\partial p_i}{\partial r} + \frac{D_{er}}{r}\frac{\partial p_i}{\partial r}\right)\end{aligned} \tag{25}$$

$$\frac{\partial v_{z,s}}{\partial z} = \frac{v_{z,s}}{T}\frac{\partial T}{\partial z} - \frac{v_{z,s}}{P}\frac{\partial P}{\partial z} - \frac{RT}{P}\sum_j\left(\sum_i \nu_{ij}\right)\eta_j\, r_j \tag{26}$$

$$\frac{\partial T}{\partial z} = \frac{1}{\rho_g C_{P_g} v_{z,s}} \left(\lambda_{er} \left(\frac{1}{r} \frac{\partial T}{\partial r} + \frac{\partial^2 T}{\partial r^2} \right) + \rho_c \sum_j \left(-\Delta H_j \right) \eta_j \, r_j \right) \tag{27}$$

2.3. The annulus model. The annular section is dominated by turbulent flow but is nevertheless simplified with a plug flow model with an algebraic mass balance equation giving the axial velocity. Radial heat transfer is strongly affected by the turbulent flow and this effect is included in the energy equation by introducing an effective radial thermal conductivity of the gas, $\lambda_{er,a}$. This parameter has been obtained by simulating an equivalent model in a CFD tool (FLUENT) in which the k-ε turbulence model was employed. $\lambda_{er,a}$ reported from these CFD simulations vary both with radial and axial position. When these data were applied in the simplified annulus model involved in the GHR model, the sensitivity for radial variations was found to be significant, while the axial variations in $\lambda_{er,a}$ could be neglected. A function for $\lambda_{er,a}$ dependent on radial position only was therefore read from the results of the CFD simulations at a position midway in the axial direction. Radiation in radial direction was included in the energy balance by using the discrete ordinates method for cylindrical coordinates, also solved with the finite difference method.

2.4. Combining the reactor model with the annulus model. The iteration is initiated by specifying the outer tube skin temperature profile, T_{w2}. This is input to the annulus model, where the heat fluxes are calculated. These heat fluxes are then input to the reactor model where the internal wall temperature profile is calculated. The external tube skin temperature profile is given from the internal tube skin temperature profile and the heat fluxes and is input to the next iteration. Convergence is reached when the wall temperature profile T_{w2} is unchanged. An additional convergence test consists in comparing the heat flux profiles arising from the wall-*2* boundary conditions with heat flux profiles resulting from the changes in bulk gas energy in both the reactor tube and in the annular space.

The annulus model and the linking between the reactor and the annulus model are described in detail in Wesenberg et al. [13].

3. Model testing and validation

3.1. Mass and heat balance. The properties of the gas mixtures at the outlet of the reactor and at the inlet on the annular side are closely related by the fact that the steam reformer product is reformed further in a secondary autothermal reformer which product gas is the inlet gas to the steam reformer annular side. The primary GHR and the secondary ATR were simulated in the process simulation tool ProII to give inputs for the annulus gas. Table 1 shows the properties of the gases used in the simulations, where the reactor feed is given a hypothetical composition close to real operational values. The inlet gas on the annular side is calculated with ProII. The steam-to-carbon ratio is 2.0 and the composition of the natural gas is 85.8 % CH_4, 12.12 % CO_2, 1.98 % N_2 and 0.089 % H_2.

The mass flow for the reactor is balanced, which means that the simplifications made for the component balance in the catalyst phase (Equation (18)) are applicable.

Table 1. Gas compositions, temperatures and pressures used in the model simulations. Inlet and outlet gases on reactor side and on annular side of the GHR. The flow rate is per reactor tube.

	Reactor feed (given)	Resulting product	Annular side (from ProII)
temperature (˚C)	400	708	1050–857
pressure (bara)	40.0	37.1	38.7
mole fraction CH_4	0.290	0.160	0.0008
mole fraction CO_2	0.041	0.065	0.072
mole fraction CO	0	0.048	0.113
mole fraction H_2O	0.657	0.380	0.451
mole fraction H_2	0.005	0.340	0.359
mole fraction N_2	0.007	0.003	0.004
flow (kmole/ hr)	23.0	26.8	40.9

3.2. Resolution and convergence. The axial variations of heat flux calculated in the reactor model and in the annulus model converged satisfactorily within 10 to 15 iterations using the procedure described in Section 2.3. The simulation resulted in a wall temperature profile which gave the same axial distribution of heat fluxes in both the reactor model and in the annulus model. An additional verification of convergence was made by certifying that the heat flux profile was identical to the gas enthalpy profiles in both the reactor and the annulus model. It was found that 100 discretization steps in axial direction were sufficient.

The needed spatial resolution in the radial direction in the reactor tube was investigated. The simulation precision was evaluated by comparing the heat flux profile arising from the boundary condition of Equation (14) with the total enthalpy change. The difference in these two fluxes, relative to the heat flux from the boundary condition, is shown in Figure 2 for varying radial resolution. It can be seen that the resolution in the reactor model can be kept relatively low, and that an increase from 10 to 15 points hardly improves the accuracy. Another crucial point when deciding the needed resolution is the computation time, which increases strongly with the numerical resolution. A number of 15 radial steps was chosen because this is where the relative error curve flattens and where computation time still is tolerable. The relative error in total heat supply to the reactor is at this point 0.55 %, which was deemed satisfactory. The data in Figure 2 are calculated for a depth of active layer of 5 % of the pellet radius and with resolution of 5 discretization points, both of which are evaluated below.

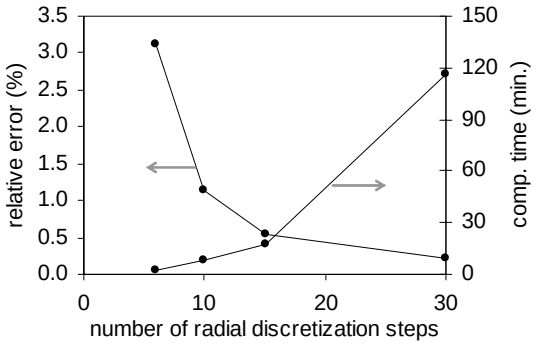

Figure 2. Difference between the integrated heat fluxes calculated from the wall boundary condition and from the total enthalpy change, relative to the boundary condition heat flux. The computation time passes for one simulation of the reactor model only.

The pellet equations are solved only for a predefined depth in the pellet; the active layer. This is because the internal diffusion limitations make the inner core of the pellet unavailable for reaction. Within the active layer there is assumed no change in partial pressures and temperature. By simulating only this depth and not through the whole pellet volume, considerable computation time was saved and still satisfactorily spatial resolution in the pellet was maintained. To check the accuracy of the calculations, simulations were performed with different depths of active layer and with different spatial numerical resolution. Both outlet conditions and pellet profiles were compared in the evaluation, shown in Table 2 and Figure 3, respectively. As can be seen in Figure 3*a* the depth of the active layer is between 5 and 10 % of the equivalent pellet radius. Both the temperature and the partial pressure profiles are almost flat inside this point (case 1 to 3). The numerical resolution was investigated in cases 3 and 5 for comparison with cases 2 and 4, respectively, and it is obvious from the outlet data in Table 2 that this is an important point for achieving precise simulations. The outlet results show good precision for cases 2 and 4 and also for case 5 where the number of discretization points is reduced to the half compared to case 4. But when the resolution is reduced four times (case 3 compared to case 2) the precision is reduced, as seen by the decreased outlet temperature and increased methane conversion. It can also be concluded from Table 2 and Figure 3 that it is better to use a smaller depth of active layer, combined with a good numerical discretization (case 5), than to use a low number of discretization points (case 3). Based on these results it was chosen to use a depth of active layer of 5 % of the equivalent radius, combined with the resolution of 5 discretization points for the simulations. This conclusion is also based on the computation time which is reported in Table 2. It is important to note that these results are strongly dependent on pellet geometry.

Table 2. Tests of necessary depth of active layer and needed resolution in the solution of the pellet equations.

	input variables:		results:		
case	depth of active layer, X	number of discretization steps	outlet temp., ˚C	conversion CH_4, %	computation time, min.
1	0.3	20	708.26	29.22	28
2	0.2	20	708.37	29.21	23
3	0.2	5	706.87	29.27	7
4	0.05	10	708.45	29.22	12
5	0.05	5	708.38	29.22	8

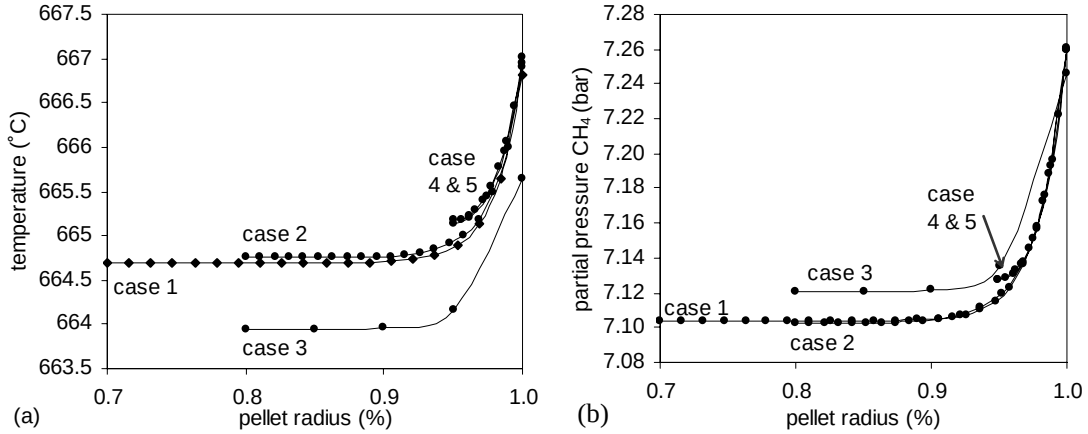

Figure 3. Pellet profiles of temperature (a) and partial pressure of CH_4 (b) at a fixed point in the reactor ($z = 0.9L$, $r = 0.8R_1$) for varying depth of active layer and varying numerical resolution.

3.3. Selection of friction factor for the fixed bed pressure drop equation. The equation of Ergun [33] is commonly used to express the friction loss in steam reformer models. Hicks [22] evaluated several empirical correlations and deduced an equation which is valid at higher Reynolds numbers ($Re_p/(1-\varepsilon) > 300$). Ergun's equation is valid only up to $Re_p/(1-\varepsilon) < 500$, which is lower than seen in steam reformers. The two equations were compared, and the equation of Hicks resulted in a 2.9 bar pressure drop and the equation of Ergun gave a 5.9 bar pressure drop for the given industrial case. Based on these calculations and on the fact that the geometry of the chosen catalyst is favourable as regards pressure drop, the equation of Hicks was chosen for the reactor model.

3.4. Selection of gas/pellet transport parameters. As pointed out in Section 1 the mass transfer resistance in the gas film surrounding the catalyst pellet is usually neglected in steam reformer models. In order to be able to discuss the need for including this in the model, without having to discuss the correlation used, a correlation giving high mass transfer coefficients was employed here. The correlation of Wakao and Funazkri [18] gave the highest coefficients of the correlations evaluated [18,34,35] and was therefore chosen for the model. A comparison of the axial profiles of $k_{g,CH4}$ resulting from the different correlations is shown in Figure 4. The bulk temperatures and compositions are not affected by these small variations in mass transfer coefficient.

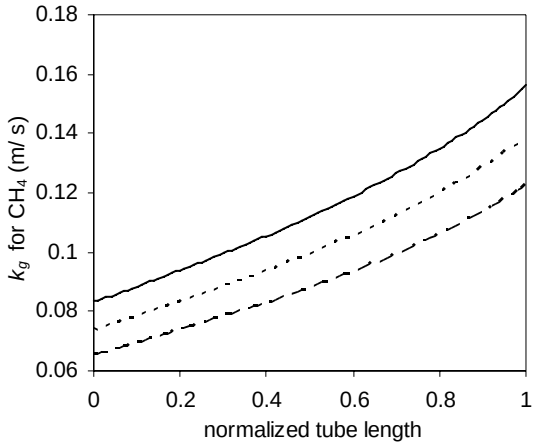

Figure 4. Mass transfer coefficients, $k_{g,CH4}$ resulting from the evaluated correlations for k_g. — Wakao and Funazkri [18], - - - Dwivedi and Upadhyay [34], – – Cussler [35].

Two different correlations for heat transfer coefficient h_p were compared [36,23] and the selected correlation [23] gave the highest heat transfer coefficient, which is shown in Figure 5*a*. As discussed for the mass transfer coefficient k_g, the intention is here to investigate the need for modelling the heat transfer resistance in the gas film when this is often disregarded in steam reformer modelling. Choosing a correlation giving a high heat transfer coefficient should therefore give a conservative estimate of its effect with regard to this study. The chosen correlation gives a temperature drop across the gas film of about 1–7 ˚C, as is seen in Figure 5*b*. Rostrup-Nielsen et al. [1] claim that the bulk-catalyst temperature difference in steam reformers usually should be in the range of 5–10 ˚C, which is in the same range as the simulated ones. The simulation results showed equal outlet temperature and methane conversion for the two correlations.

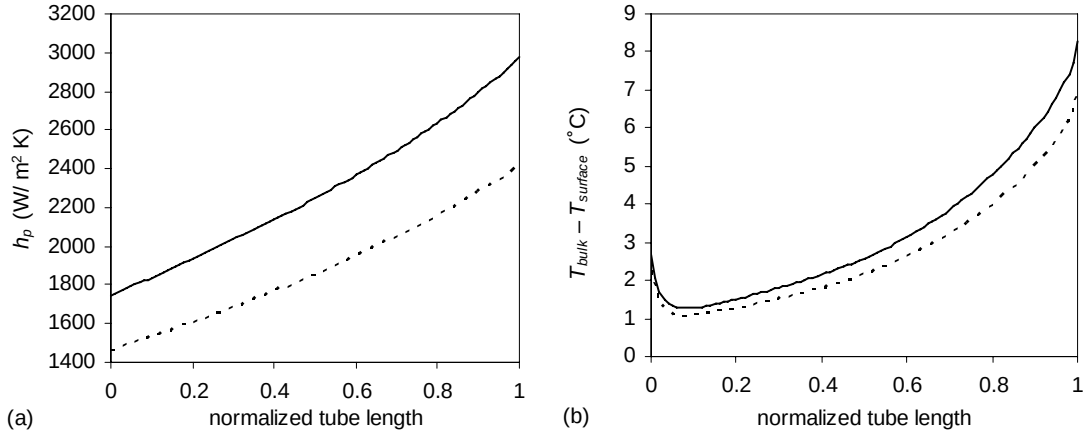

Figure 5. Pellet heat transfer coefficients h_p appearing from the two correlations (a) and temperature difference over the gas film resulting from both correlations (b). — Wakao et al. [23] - - - Handley and Heggs [36]

The component diffusion coefficients in the gas mixture, $D_{m,i}$, shown in Equation (8), were estimated by the correlation of Wilke [19]. The pseudo-binary model is a simpler approach, where

the diffusion coefficients for binary mixtures in Equation (9) are used for the gas mixture, i.e. $D_{m,i} = D_{ik}$. This approach was tested with methane defined as component k. The simulation results showed an increase in outlet temperature of 1.7 ˚C and an increase in methane conversion from 27.3 % to 28.7 % compared with simulation with Wilke's equation. The pseudo-binary model may therefore also be used for this purpose.

3.5. Evaluation of mass and heat transfer resistance between gas and pellet. The interphase mass and heat transfer resistances are usually ignored and assumed insignificant in steam reformer modelling. The effects of including these resistances are therefore studied here. Quite often the importance of interphase resistances is evaluated by the use of the criteria of Maers [37] which are quoted here.

Mass transfer resistance across the gas film can be disregarded relative to surface reaction kinetics if

$$\frac{r_i \rho_c R_p n_i}{k_{g,i} C_i} < 0.15 \tag{28}$$

Calculations for methane show that the term on the left varies from ca. 0.01 to 0.03 (inlet to outlet), indicating that there should be no mass transfer limitations in the gas film surrounding the pellets.

Heat transfer in the gas film can be disregarded if

$$\left| \frac{(-\Delta H_i) r_i \rho_c R_p}{h_p T_b} \right| \frac{E}{R T_b} < 0.15 \tag{29}$$

The term on the left hand side varies from about 0.006 to about 0.003 (inlet to outlet) for methane. According to the criterion there should be no heat transfer limitations in this fixed bed reactor.

The effect of interphase transport limitations was also investigated by calculating the efficiency factors η and η' from the same simulation where the mass and heat transfer resistances were included. The efficiency η is defined on basis of particle surface conditions (Equation (23)) which means that it expresses the reduction factor of the reaction rates caused by pellet internal resistances. These are given by the effective diffusion coefficients and the effective thermal conductivity. The alternative efficiency η' is defined on basis of bulk conditions (Equation (24)) so that the interphase resistances, represented by the mass and heat transfer coefficients, are included in the denominator. Both efficiency factors for reaction 1 are plotted in Figure 6 which shows that the alternative efficiency η', represented by the solid line, is lower than η. This means that η' is reduced because of the interphase transport limitations causing concentration and/or temperature gradients across the gas film of the pellets. To investigate which of the two interphase resistances were of significance, two new simulations were performed: without mass transfer resistance and without heat transfer resistance. The alternative efficiency factors η' from these results are represented by the stippled and dotted lines, respectively, in Figure 6. The change in efficiency η is however negligible. The increases in η' from these two simulations compared to η' from the base simulation (solid line) show that both resistances contribute, and to about the same degree. From this it is clear that mass and heat transfer resistances do have significant effects on the calculations of the efficiency. This is contrary to the expectations from Maers' criteria, given in Equations (28) and (29), which both were satisfied. It also shows that it is very important to take interphase transport limitations into account when interpreting reaction rate data into kinetic constants.

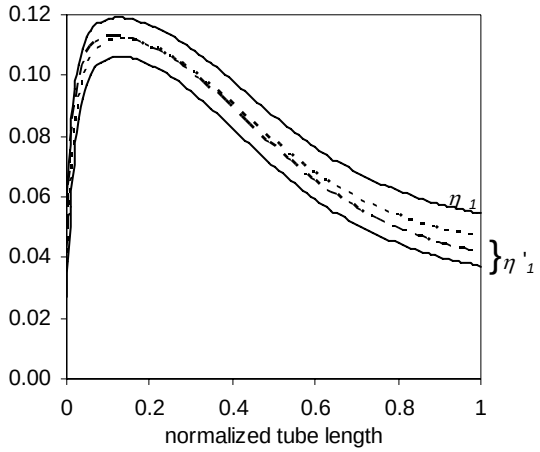

Figure 6. Effectiveness factors η and η' for reaction 1. — Empirical correlations for interphase mass and heat transfer are employed, – – no interphase mass transfer resistance, - - - no interphase heat transfer resistance. η is equal for all three cases.

4. Simulation results

4.1. Temperature profiles. Figure 7 shows the axial profiles of inner and outer reactor tube skin temperatures and of bulk gas temperatures in the reactor bed and in the annular volume. The gas temperatures are average values weighted on cross sectional area gas flow. From the graph it can be seen that the temperature driving forces are evenly distributed along the tube length. This is an ideal operation and an advantage as it indicates a low entropy production [38] and thereby good energy utilisation.

Radial variations in gas temperature at different axial positions in the catalytic bed are shown in Figure 8. The radial temperature profiles are in reasonable agreement with the temperature profile shown by Rostrup-Nielsen et al. [1] measured in a full-size monotube pilot plant for a wall fired steam reformer. This can be taken as support for the level of effective radial thermal conductivity used in the reactor bed model. As can be seen the radial profiles are rather flat indicating effective radial transport of energy regardless of axial position.

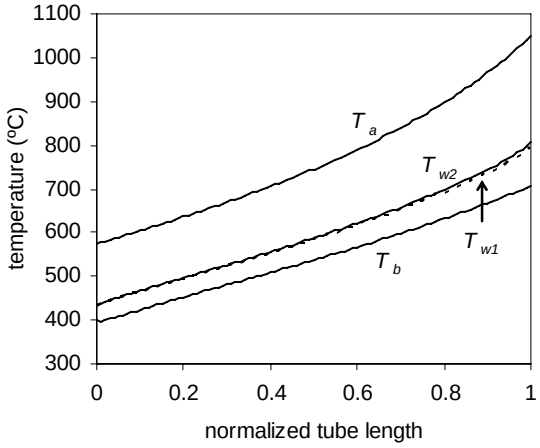

Figure 7. Axial profiles of radial mean bulk temperatures in the annular section (T_a) and in the reactor bed (T_b), and of the outer and the inner wall temperatures of the reactor tube (T_{w2} and T_{w1}, respectively).

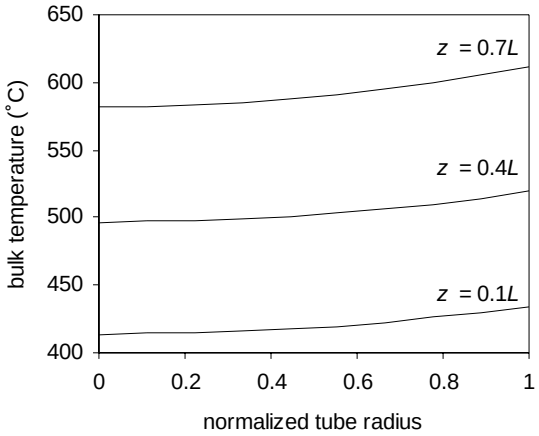

Figure 8. Radial temperature profiles in reactor bed at three axial positions of z.

4.2. Effectiveness factors. The effectiveness factors η for the three reactions were calculated according to Equation (24) shown in the appendix. The results, shown in Figure 9*a*, are as expected when compared with the results of Xu and Froment [12], whose kinetic model is employed here. The low values of the calculated effectiveness factors indicate that there are large mass transfer limitations within the pellets, which also was seen when investigating the thickness of the active layer in the pellets in Section 3.2. The discontinuity of the shift reaction (reaction 2) seen in Figure 9*a* at $z = 0.38L$ stems from the shift from forward reaction to backward reaction on the surface of the pellets where equilibrium is reached. The reaction rate involves the equilibrium properties of the reaction so that the rate is positive for forward reaction and negative for backward reaction. When the reaction rate calculated from surface data shifts, the effectiveness factor becomes negative and a discontinuity appears. When the reactions calculated from pellet data also shift the effectiveness factor again becomes positive (as seen at $z = 0.86L$). η_2 is also negative at the inlet because there is no CO in the feed gas. This gives negative reaction rates calculated from surface conditions. Still the reaction rates calculated from internal pellet conditions are positive because CO is generated immediately at the reactor inlet. This results in the negative ratios. The CO establishes so rapidly on the surface and in the bulk that the negative η_2 cannot be seen from Figure 9.

Figure 9*b* shows the alternative effectiveness factor η' calculated from Equation (24). η' is defined as η, apart from being relative to bulk conditions instead of surface conditions. η is about 10 to 40 % greater than η'. This means that there are mass and heat transport limitations in the gas film, as concluded in Section 3.5.

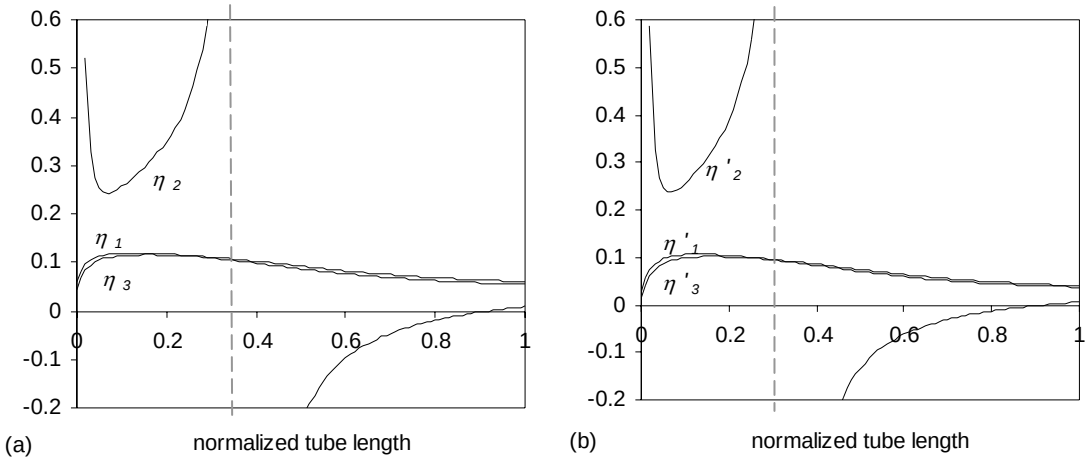

Figure 9. Effectiveness factors for reactions 1, 2 and 3. Comparison of η, which is the observed reaction rates relative to reaction rates of a pellet with no intraparticle transport limitations (a) and η', which is relative to reaction rates with no interphase and intraparticle transport limitations (b).

4.3. Implications for the use of pseudo-homogeneous models. The effectiveness factors calculated in the heterogeneous model may be used in a pseudo-homogeneous model to calculate the reaction rates directly from the bulk partial pressures and temperature. When simulating a pseudo-homogeneous model as the one described in Section 2.2, the results from using both η from Equation (23) and η' from Equation (24) can be compared to evaluate the need of including mass and heat transfer resistance in the gas film. Table 3 shows the results from these simulations compared with simulation of a heterogeneous model. The use of constant effectiveness factors was also evaluated.

Table 3. Outlet temperatures and methane conversions resulting from simulations of a pseudo-homogeneous model.

simulation case	outlet temp. (˚C)	CH_4 conv. (%)
Heterogeneous model	708.1	29.5
Pseudo-homogeneous model using η	705.2	29.7
Pseudo-homogeneous model using η'	708.1	29.5
Pseudo-hom. with constant η (= 0.09)	702.5	29.8

The pseudo-homogeneous model using η' and the heterogeneous model give equal results as expected. The pseudo-homogeneous model using η estimates some lower temperature and higher methane conversion (2.9 ˚C and 0.7 %, respectively). This indicates that the film resistances included in the calculation of η' has some effect on the overall simulation results even if that effect is relatively small. The significant differences between η and η' seen in Section 4.2 have little influence on the overall results because η and η' are very low. This concludes that ignoring the interphase mass and heat transport resistances introduces only small discrepancies in the results of heterogeneous and pseudo-homogeneous steam reformer models. But care must be taken under experimental studies of kinetics as the interphase transport limitations are of the outmost importance for the observed local reaction rates.

The results from using constant effectiveness factors show that this is an acceptable simplification. This simplification has great effect on computation time, as it reduces the computation time by a factor of 15.

5. Conclusions

A gas heated steam reformer (GHR) has been modelled and its fixed bed reactor model has been studied in this article. Operating conditions chosen are typical for a primary reformer for Fischer-Tropsch and methanol synthesis purposes and involves lower steam contents than yet commercially proven.

The model for the packed reactor bed is a two-dimensional heterogeneous dispersion model. Common empirical correlations for mass and heat transfer coefficients in the gas film surrounding the catalyst pellet has been included, as well as intraparticle mass and heat transfer restrictions by using effective molecular diffusivities and thermal conductivity. The effects on the simulation results from including these mass and heat transfer limitations were examined. It was found that the reaction effectiveness factors were strongly affected by this as η for reactions 1 and 3 increased with about 10 to 40 % when the film resistances were excluded. But since the effectiveness factors are already very low (η_1 is maximum 0.12) the difference in the overall simulation results are negligible. This was investigated by running equivalent pseudo-homogeneous reactor simulations resulting in only 2.9 °C lower outlet temperature and 0.7 % increased methane conversion when disregarding compared to including film resistances. The gas film mass and heat transfer resistances can thus be ignored in heterogeneous and pseudo-homogeneous steam reformer reactor models but must still be included under experimental determination of reaction kinetics as the resistances have great influence on observed local reaction rates. The total transport restriction in the gas film was found to be influenced both by the mass transfer and by the heat transfer resistances.

The radial heat transport in the packed bed is rapid and quite flat radial temperature profiles result. The axial temperature profiles show that the driving forces for energy transport between the annulus and reactor sides are nearly constant through the reformer. This indicates low entropy production and good heat utilization.

Nomenclature

a_v = specific outer pellet surface area, m_c^2/m_r^3
C_i = concentration of component *i*, kmole/m^3
C_P = specific heat capacity, J/kg K
d = diameter, m
d_p = equivalent particle diameter, m
D = diffusion coefficient, m^2/s
D_{er} = effective radial dispersion coefficient, m^2/s
d_k = equivalent particle diameter, m
E = Activation energy, kJ/ kmole
h = heat transfer coefficient, W/m^2 K
k = mass transfer coefficient, m/s
L = tube length, m
Nu_p = pellet Nusselt number, $Nu_p = h_p\, d_p / \lambda_g$
Nu_w = wall Nusselt number, $Nu_w = h_w\, d_t / \lambda_g$
p = partial pressure, Pa
P = total pressure, Pa
Pr = Prandtl's number, $Pr = \mu_g\, c_{pg} / \lambda_g$
q = heat flux, W/ m^2
r = radial co-ordinate, m
r_j = reaction rate for reaction *j*, kmole/ kg_c s
R = gas constant, Pa m^3/kmole K

R = radius, m
R_p = equivalent particle radius, m
Re_p = Reynolds number, $Re_p = d_p v_{z,s} \rho_g / \mu_g$
Sc = Schmidt number, $Sc = \mu_g / \rho_g D_m$
Sh = Sherwood's number, $Sh = k_g d_p / \rho_g D_m$
T = temperature, K
v = velocity, m/s
V = Volume, m^3
X = fraction of pellet radius defining the active layer of the pellet
y = depth coordinate for catalyst pellets, m
z = axial co-ordinate, m
Greek Letters
ΔH = heat of reaction, kJ/kmole
ε = void fraction of packed bed
ε_p = catalyst porosity
η = reaction effectiveness factor
λ = thermal conductivity, W/m K
μ = viscosity, Pa s
ν = stoichiometric coefficient of chemical reaction
ρ = density, kg/m^3
ρ_c = density of catalyst bulk, kg cat./m^3 reactor volume
τ = tortuosity factor
Subscripts
1 = position at inner wall of reactor tube
2 = position at outer wall of reactor tube
3 = position at outer wall of annular section
a = annulus
b = reactor bed
c = catalyst bulk
e = effective
g = gas
i = component number
j = reaction number
k = component number
m = mean value with respect to radius
m = gas mixture
p = pellet
r = radial
s = superficial
t = tube
w = wall
z = axial
Superscripts
0 = stagnant
bulk = at bulk conditions
s = surface of pellets

Literature cited

(1) Rostrup-Nielsen, J.R.; Christiansen, L.J.; Bak Hansen, J.-H. Activity of steam reforming catalysts: Role and assessment. *Appl. Catal.* **1988**, *43*, 287.

(2) Ferreira, R.M.Q.; Marques, M.M.; Babo, M.F.; Rodrigues, A.E. Modelling of the methane steam reforming reactor with large-pore catalyst. *Chem. Eng. Sci.* **1992**, *47* (9-11), 2909.

(3) Pedernera, M.N.; Piña, J.; Borio, D.O.; Bucalá, V. Use of a heterogeneous two-dimensional model to improve the primary steam reformer performance. *Chem. Eng. J.* **2003**, *94*, 29.

(4) Kvamsdal, H.M.; Svendsen, H.F.; Hertzberg, T.; Olsvik, O. Dynamic simulation and optimization of a catalytic steam reformer. *Chem. Eng. Sci.* **1999**, *54*, 2697.

(5) Grevskott, S.; Rusten, T.; Hillestad, M.; Edwin, E.; Olsvik, O. Modelling and simulation of a steam reforming tube with furnace. *Chem. Eng. Sci.* **2001**, *56* (2), 597.

(6) Yu, Y.H.; Sosna, M.H. Modeling for industrial heat exchanger type steam reformer. *Kor. J. Chem. Eng.* **2001**, *18* (1), 127.

(7) De Deken, J.C.; Devos, E.F.; Froment, G.F. Steam reforming of natural gas: Instrinsic kinetics, diffusional influences, and reactor design. *ACS Symp. Ser.* **1982**, *196*, 181.

(8) De Groote, A.M.; Froment, G.F. Reactor modelling and simulations in synthesis gas production. *Rev. Chem. Eng.* **1995**, *11* (2), 145.

(9) Elnashaie, S.S.E.H.; Adris, A.M.; Soliman, M.A.; Al-Ubaid, A.S. Digital simulation of industrial steam reformers of natural gas using heterogeneous models. *Can. J. Chem. Eng.* **1992**, *70*, 786.

(10) Piña, J.; Schbib, N.S.; Bucalá, V.; Borio, D.O. Influence of the heat-flux profiles on the operation of primary steam reformers. *Ind. Eng. Chem. Res.* **2001**, *40*, 5215.

(11) Soliman, M.A.; El-Nashaie, S.S.E.H.; Al-Ubaid, A.S.; Adris, A. Simulation of steam reformers for methane. *Chem. Eng. Sci.* **1988**, *43* (8), 1801.

(12) Xu, J.; Froment G.F. Methane steam reforming: II. Diffusional limitations and reactor simulation. *AIChE J.* **1989**, *35* (1), 97.

(13) Wesenberg, M.H.; Ströhle, J.; Svendsen, H.F. A study of the heating section of a gas heated steam reformer. Submitted 2006.

(14) Schiesser, W.E. *The numerical method of lines in integration of partial differential equations*; Academic Press Inc.: San Diego, 1991.

(15) Reid, R.C.; Prausnitz, J.M.; Poling, B.E. *The properties of gases and liquids*; 4th Edition; McGraw-Hill: New York, 1987.

(16) Froment, G.F.; Bischoff, K.B. *Chemical reactor analysis and design*; 2nd Edition; Wiley: Singapore, 1990.

(17) Froment, G.F.; Hofmann, P.K. Design of fixed-bed gas-solid catalytic reactor. In *Chemical Reaction and Reactor Engineering*; J.J. Carberry and A. Varma (Editors); Marcel Dekker, New York, 1987.

(18) Wakao, N.; Funazkri, T. Effect of fluid dispersion coefficients on particle-to-fluid mass transfer coefficients in packed beds. Correlation of Sherwood numbers. *Chem. Eng. Sci.* **1978**, *33*, 1375.

(19) Wilke, C.R. Diffusional properties of multicomponent gases. *Chem. Eng. Prog.* **1950**, *46* (2), 95.

(20) Fuller, E.N.; Schettler, P.D.; Giddings, J.C. A new method for prediction of binary gas-phase diffusion coefficients. *Ind. Eng. Chem.* **1966**, *58* (5), 19.

(21) Perry, R.H.; Green, D.W. *Perry's Chemical engineers' handbook*; 7th Edition; McGraw-Hill: New York, 1997.

(22) Hicks, R.E. Pressure drops in packed beds of spheres. *Ind. Eng. Chem. Fundam.* **1970**, *9* (3), 500.

(23) Wakao, N.; Kaguei, S.; Funazkri, T. Effect of fluid dispersion coefficients on particle-to-fluid heat transfer coefficients in packed beds. Correlation of Nusselt numbers. *Chem. Eng. Sci.* **1979**, *34*, 325.

(24) Peters, P.E.; Schiffino, R.S.; Harriott, P. Heat Transfer in Packed-Tube Reactors. *Ind. Eng. Chem. Res.* **1988**, *27*, 226.

(25) Kunii, D.; Smith, J.M. Heat transfer characteristics of porous rocks. *AIChE J.* **1960**, *6* (1), 71.

(26) Dixon, A.G. Wall and particle-shape effects on heat transfer in packed beds. *Chem. Eng. Comm.* **1988**, *71*, 217.

(27) Wesenberg, M.H.; Grislingås, A.; Grevskott, S. Modelling of steam reformer tubes. 6th World Congress of Chemical Engineering, paper 961, Melbourne (2001).

(28) Burghardt, A.; Aerts, J. Pressure changes during diffusion with chemical reaction in a porous pellet. *Chem. Eng. Proc.* **1988**, *23*, 77.

(29) Kehoe, J.P.G.; Aris, R. Communications on the theory of diffusion and reaction – IX. Internal pressure and forced flow for reactions with volume change. *Chem. Eng. Sci.* **1973**, *28*, 2094.

(30) Veldsink, J.W.; van Damme, R.M.J.; Versteg, G.F.; van Swaaij, W.P.M. The use of dusty-gas model for the description of mass transport with chemical reaction in porous media. *Chem. Eng. J.* **1995**, *57*, 115.

(31) Rostrup-Nielsen, J.R. Catalytic steam reforming. In *Catalysis – Science and Technology;* J.R. Anderson and M. Boudart (Editors); Springer-Verlag: Berlin, 1984.

(32) Xu, J.; Froment, G.F. Methane Steam Reforming, Methanation and Water-Gas Shift: I. Intrinsic Kinetics. *AIChE J.* **1989**, *35* (1), 88.

(33) Ergun, S. Fluid flow through packed columns. *Chem. Eng. Prog.* **1952**, *48* (2), 89.

(34) Dwivedi, P.N.; Upadhyay, S.N., Particle-fluid mass-transfer in fixed and fluidized-beds. *Ind. Eng. Chem. Proc. Des. Dev.* **1977**, *16* (2), 157.

(35) Cussler, E.L. *Diffusion: mass transfer in fluid systems*; Cambridge University Press: Cambridge, 1997.

(36) Handley, D.; Heggs, P.J. Momentum and heat transfer mechanisms in regular shaped packings. *Trans. Inst. Chem. Engrs. Chem. Engr.* **1968**, *46* (9), T251.

(37) Mears, D.E. Tests of transport limitations in experimental catalytic reactors. *Ind. Eng. Chem. Proc. Des. Dev.* **1971**, *10* (4), 541.

(38) Sauar, E.; Nummedal, L.; Kjelstrup, S. The principle of equipartition of forces in chemical reactor design: The ammonia synthesis. *Comp. Chem. Eng.* **1999**, *23*, 499.

Paper 2

submitted to *International Journal of Chemical Reactor Engineering* (2006)

A study of the heating section of a gas heated steam reformer

Margrete H. Wesenberg (1,2), Jochen Ströhle (3), Hallvard F. Svendsen (1)

1 Institute of Chemical Engineering, Norwegian University of Science and Technology, Norway
2 Statoil Research Centre, Norway
3 SINTEF Energy Research, Norway

Corresponding author:
H.F. Svendsen, hallvard.svendsen@chemeng.ntnu.no

Abstract

A gas heated steam reformer (GHR) which converts natural gas to synthesis gas for methanol or Fischer-Tropsch purposes has been modelled for stationary conditions. The model is in two dimensions and is made up of a fixed bed reactor model, representing one of the reactor tubes in the GHR, and an annulus model, representing the annular space on the shell side of the GHR where hot, fully converted syngas emits heat to the reactor tube. The annulus model is evaluated in this article. This model is a plug flow model which involves heat transfer in radial direction caused by radiation and by turbulence. The gas radiation is modelled by the use of the discrete ordinates method and the effect on heat transfer from turbulence is modelled as an effective radial thermal conductivity. Both heat transfer mechanisms vary with the radial position. An additional annulus model, made in the commercial CFD code FLUENT and based on the k-ε turbulence model and the discrete ordinates radiation model, is used to estimate effective radial thermal conductivities. These were implemented in the annulus model of the GHR model. The reactor and the annulus models were combined by simultaneous iterations linked by the wall temperature profile and the heat flux profile on the outer reactor tube wall. The simulation results were used to study the heat flux and temperature profiles along the reactor length and the radial temperature profiles in the annulus.

KEYWORDS: finite difference method, two-dimensional, discrete ordinates method, convective steam methane reformer

1. INTRODUCTION

The gas heated reformer (GHR), or convective steam reformer, is a compact alternative to the conventional, fired steam reformer (CSR) for production of synthesis gas from natural gas. The high manufacturing costs, the heavy weight and the large base area of the CSR maintain the interest for a compact and less expensive alternative. The GHR has been commercially proven for large scale ammonia and hydrogen purposes where the steam excess in the reformer is large. There is also interest for the GHR for Fischer-Tropsch and methanol production but this may

only be profitable if the steam content in the feed gas is reduced to a steam to carbon ratio below 1.5.

The reforming reactions are strongly endothermic and are carried out in several packed beds of catalyst pellets. Effective heat transport to the reactor tubes and further into the centre of the bed is therefore a very important aspect during design and operation of steam reformers. The tubular bed reactors have a low diameter-to-height ratio to ensure efficient heat transport in the radial direction. The heat transport from the shell side of the GHR can be enhanced by increasing turbulence and this has been tested by the different licensors by introducing baffles, sheath tubes on parts of the reactor tubes, perforated sheath tubes, longitudinal (spiral) fins and other more complex tube/annulus configurations. The sheath tube configuration has been chosen in this study, which gives an annular section to be modelled as the shell side of one single reactor tube. As a simplification the modelled sheath tube is enclosing the tube along its whole length. In commercial GHRs with sheath tubes the sheath tubes are limited to the upper part of the reactor tubes to ensure low tube skin temperatures in the lower part of the reactor tubes to avoid reduced tube life time.

The heat source in GHRs can be flue gas or, as in this study, syngas from a secondary autothermal reformer (ATR). The heat transport from this hot gas is mainly convective, in contrast to CSRs having mainly radiative transport. However, heat transport by radiation may also play an important role in the GHRs, as will be seen from the results given here.

Steam reformer models have been studied several times, and often these studies involve only the reactor tube without the shell side or firebox providing the heat to the reactor. The tube skin temperature is then given as a fixed profile in the boundary conditions of the energy equation. De Groote and Froment (1995) modelled the firebox and solved the radiative heat transfer by the zonal method (Hottel and Sarofim, 1967). Xu and Froment (1989) used the one-dimensional, heterogeneous model for the steam reformer tube coupled with a zone model for the firebox where axial variations were accounted for. Grevskott et al. (2000) modelled the heat source both of a side-fired and of a convective steam reformer and used the two-flux method of Spalding (1980) for solving the radiative heat transport. Stehlík et al. (1989) modelled a top-fired steam reformer using a one-dimensional reactor model combined with a firebox model where the thermal radiation fluxes were solved by the zonal method based on the assumption of constant thermal properties in axial direction. Stehlík (1995) also modelled a GHR where an annular space represented the shell side of the GHR, and where the radiative heat flux was modelled by the method of radiative heat transfer coefficients in a one-dimensional annulus model.

This paper is a modelling study of the annular section of a GHR. The total GHR model includes also a two-dimensional heterogeneous reactor model which is described and evaluated by Wesenberg and Svendsen (2006). The basic idea with the annulus model was to develop a model which was just as simple as the reactor model, but still fundamental enough to intercept the effects that turbulence and radiation have on heat transport, as well as being flexible for different types of simulations. The annulus model is therefore held at two dimensions and with plug flow. Radial variations in effective radial thermal conductivity of the gas, which is strongly enhanced due to turbulence, are yet allowed for as this is evaluated as a significant spatial dependency. This requires a very fine radial grid, as discussed below, which brings along a significant increase of computation time compared to a model with constant radial thermal conductivity. The main, and most computation time consuming part of the annulus model though, is the radiation section which is solved by the discrete ordinates method in two dimensions with cylindrical co-ordinates.

2. MATHEMATICAL MODEL

The GHR model consists of two main models: the fixed bed reactor tube and the shell side heating section. The model is simplified by modelling one single average tube with its corresponding shell side area, represented by an annular section encircled by a sheath tube. The operating conditions in this study are typical for a primary steam reformer producing syngas for methanol or Fischer-Tropsch synthesis purposes. The computation of the reactor model and the annulus model together is done by linking the two models at the surface of the outer reactor tube wall and iterating with the use of the calculated temperature and heat flux profiles at this wall (described in Section 2.3).

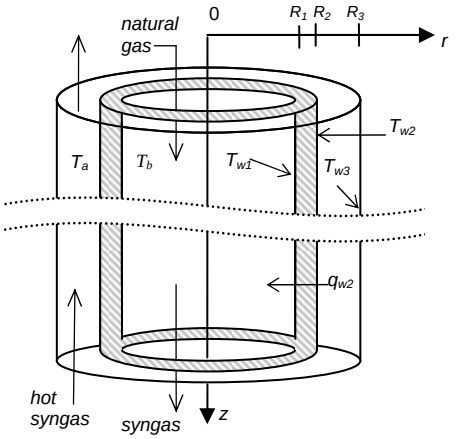

Figure 1. Sketch of the total model consisting of the reactor model and the annulus model.

The gases are assumed ideal and their physical properties are given as function of temperature and composition (Reid et al., 1987). The two flows are counter current, with natural gas feed entering the reactor tube at axial position $z = 0$ and product gas exiting at $z = L$ as shown in Figure 1. The inlet of the hot syngas on the annular side is thus positioned at $z = L$. The radii of the inner and the outer wall of the reactor tube are denoted R_1 and R_2, respectively, and the outer radius inside the annulus is R_3. Axial length L is typically 12 m and radius R_2 is about 12 cm. Heat is transported through the inner wall of the annulus while the outer wall is adiabatic.

The differential equations are solved by a finite difference method using an ODE solver, and the radial derivatives in equations involving both axial and radial variations are discretized by the numerical method of lines (Schiesser, 1991).

2.1 The annulus model

The annular section is described by a plug flow model with an algebraic mass balance equation for calculating the axial velocity. The energy conservation equation involves heat transport caused by axial convection and by radial conduction and radiation. The contribution from conduction to axial heat transport is negligible compared with the convective contribution. Heat transfer by convection is similarly negligible in the radial direction. Turbulent dispersion and radiation are the dominant heat transfer mechanisms in the radial direction, and the effect of turbulence is included in the effective radial thermal conductivity. The radiation from the hot gas is modelled by the method of discrete ordinates in the radial direction only.

The energy equation involving heat transport from axial convection, radial conduction and radial radiation describes the temperature profiles in the annulus:

$$\rho_g \, c_{P_g} \, v_z \frac{\partial T}{\partial z} = \frac{1}{r} \frac{\partial}{\partial r} \left(\lambda_{er} \, r \frac{\partial T}{\partial r} \right) - \frac{\partial q_{rad}}{\partial r} \qquad (1)$$

The procurement of the effective radial thermal conductivity, λ_{er}, is described in detail in Section 2.2.1, and the method for calculating the radiative volumetric heat flux is given in Section 2.2.2. The boundary conditions for $r = R_2$ and at $r = R_3$ conserve the heat across the inner and outer walls of the annulus, respectively:

$$-\lambda_{er}\left.\frac{\partial T}{\partial r}\right|_{R_2} = h_2\left(T_{w2} - T(R_2)\right) \tag{2}$$

$$-\lambda_{er}\left.\frac{\partial T}{\partial r}\right|_{R_3} = h_3\left(T(R_3) - T_{w3}\right) \tag{3}$$

The outer wall of the annulus is adiabatic and this is achieved as described for Equation (17) below. A radiation heat flux term should be included in Equations (2) and (3) when solving by the finite volume method. This term vanishes when converting to the finite difference form, as explained by Siegel and Howell (2002).

The heat transfer coefficients describing the convective heat transfer from the gas in the annulus to the inner and outer wall of the annulus, h_2 and h_3 respectively, are calculated as recommended by Mills (1995). The first step is the calculation of the local Nusselt number for a tube as correlated by Gnielinski (1976) for 3·103 < *Re* < 106:

$$Nu_w = F_C \frac{\left(f/8\right)\left(Re - 1000\right)Pr}{1 + 12.7\sqrt{f/8}\left(Pr^{2/3} - 1\right)} \tag{4}$$

The Nusselt number and the Reynolds number are based on the hydraulic diameter of the annulus. The friction factor in Equation (4) is calculated from the correlation of Petukhov (1970), valid for 104 < *Re* < 5·106:

$$f = \left(0.790 \ln Re - 1.64\right)^{-2} \tag{5}$$

The Nusselt numbers are finally multiplied with the correction factors F_C given by Petukhov and Roizen (1964) for annular ducts. The respective factors for the Nusselt number at the inner wall and at the outer wall are:

$$F_{C,2} = 0.86\left(R_2/R_3\right)^{-0.16} \tag{6}$$

$$F_{C,3} = 1 - 0.14\left(R_2/R_3\right)^{0.6} \tag{7}$$

The ideal gas law is used for the algebraic velocity equation:

$$v_z = \frac{R\,n\,T}{P\,A_a} \tag{8}$$

Here n is the molar flow rate and A_a is the cross sectional area of the annulus.

The pressure drop equation takes the following form when iterating from the inlet of $z = L$:

$$\Delta P = \frac{f\,\rho_g (L-z) v_z^2}{2\,d_h} \tag{9}$$

2.1.1 Turbulence: Although turbulence is not modelled directly, the *effect* of turbulence on the radial heat transfer is accounted for by use of an effective radial thermal conductivity, λ_{er}. This conductivity is the sum of the molecular and the turbulent conductivities, where the latter is the dominating. λ_{er} can be calculated from different types of turbulence models. In this study λ_{er} was found by modelling an identical annulus in a commercial CFD code (FLUENT) where radial flow and turbulence were included. The *k*-ε turbulence model was used and this gave the same results as simulations based on the Reynolds stress model. λ_{er} reported from these CFD simulations vary both with radial and axial position. When these values were applied in the simplified annulus model described above, the sensitivity to radial variations in effective conductivity was found to be significant while the axial variations in $\lambda_{er,a}$ could be neglected. A function for λ_{er} dependent on radial position only was therefore fitted from the results of the CFD simulations at a position midway in the axial direction.

2.1.2 Radiation model: The discrete ordinates method (S_N-method) was applied for calculating the radiation source term in the energy equation and the radiation heat fluxes at the walls. The radiative intensity field can be sufficiently represented by the S_4 approximation (Fiveland, 1982) using 12 different directions in two dimensions, which gives six directions due to symmetry in the axial direction. Therefore, six differential equations must be solved for the six intensities I^m.

The simplification of the radiative transport equation (RTE) in cylindrical co-ordinates used in the discrete ordinates method expresses the intensity in one radiative direction as function of radial direction and azimuthal angle (Modest, 2003):

$$\frac{\mu^m}{r}\frac{\partial\left(r\,I^m\right)}{\partial r} - \frac{1}{r}\frac{\partial\left(\eta^m\,I^m\right)}{\partial \psi} = \kappa I_B - \kappa I^m \tag{10}$$

The six directions are labelled by the superscript *m*, and μ^m and η^m are directional cosines. κ and I_B are the absorption coefficient and the blackbody radiative intensity of the gas, respectively. Carlson and Lathrop (1968) introduced a simplified expression for the azimuthal variations, using the 7 geometrical coefficients $\alpha^m \pm ½$, that maintain conservation of the intensities:

$$\frac{\partial\left(\eta^m\,I^m\right)}{\partial \psi} \simeq \frac{\alpha^{m+1/2}\,I^{m+1/2} - \alpha^{m-1/2}\,I^{m-1/2}}{w^m} \tag{11}$$

The directions $m \pm ½$ bound the edges of the angular range assigned by the quadrature weight w^m. The half-node intensities are simplified by setting $I^{m\pm½} = ½\,(I^{m\pm1} + I^m)$. Expressions for the α-terms and values for the directional cosines and the weight factors can be found in Modest (2003). The directional cosines μ^m are defined as negative for direction numbers m = 1, 2, 5 and positive for m = 3, 4, 6. The final form of the RTE to be solved is then:

$$\frac{\mu^m}{r} I^m + \mu^m \frac{\partial I^m}{\partial r} - \frac{\alpha^{m+1/2}\left(I^m + I^{m+1}\right) - \alpha^{m-1/2}\left(I^{m-1} + I^m\right)}{2\,r\,w^m} = \kappa I_B - \kappa I^m \tag{12}$$

The boundary conditions at the inner wall of the annulus (at $r = R_2$) give the three radiation intensities in the positive direction (i.e. in the direction out from this wall). This

condition is thus valid for the intensities in the directions m whose directional cosines are positive ($\mu^m > 0$). These intensities are caused by emission from the wall plus reflection of the gas radiation into the wall, which is given by the radiation intensities in the negative direction, weighted and multiplied with their respective directional cosines before summation:

$$I^m(R_2) = \varepsilon_{w2}\frac{\sigma}{\pi}T_{w2}^4 + \frac{(1-\varepsilon_{w2})}{\pi}\sum_{\mu^{m'}<0} w^{m'}\left|\mu^{m'}\right| I^{m'} \tag{13}$$

Correspondingly, the intensities in the three directions from the outer wall (at $r = R_3$) into the annulus are expressed by the boundary conditions at this wall. These are the intensities in the negative direction (i.e. directions m having $\mu^m < 0$) and are therefore functions of the weighted intensities in the three positive directions:

$$I^m(R_3) = \varepsilon_{w3}\frac{\sigma}{\pi}T_{w3}^4 + \frac{(1-\varepsilon_{w3})}{\pi}\sum_{\mu^{m'}>0} w^{m'}\mu^{m'} I^{m'} \tag{14}$$

The boundary conditions have been simplified by assuming a grey wall, so that $\rho_w = 1 - \varepsilon_w$.

The equation system is solved by simplifying the derivatives of I^m with central differences and expressing the RTE in two forms: for iteration in backward and in forward radial direction. The intensities I^3, I^4 and I^6 are solved by iteration in the positive r-direction and I^1, I^2 and I^5 are solved in the negative direction. This iteration procedure was described by Fiveland (1982), and direct substitution is used for connecting the two directions.

The radial change in radiation heat flux, used in the energy equation (Equation (1)), is finally given as:

$$\frac{\partial q_{rad}}{\partial r} = -\kappa\left(\sum_{m=1}^{6} I^m w^m - 4\sigma T^4\right) \tag{15}$$

The axial profile of the total heat flux to the reactor tube wall (i.e. at $r = R_2$) is the sum of the conductive and the radiative heat fluxes:

$$q_{w2} = h_2\left(T - T_{w2}\right) + \varepsilon_{w2}\left(\sum_{\mu^m<0}\left|\mu^m\right| I^m w^m - \sigma T_{w2}^4\right) \tag{16}$$

The net heat flux to the outer wall of the annulus (at $r = R_3$) is defined zero as this is an adiabatic wall:

$$q_{w3} = h_3\left(T_{w3} - T\right) - \varepsilon_{w3}\left(\sum_{\mu^m>0}\mu^m I^m w^m - \sigma T_{w3}^4\right) = 0 \tag{17}$$

The wall temperature T_{w3} that maintains zero net heat flux through wall *3* is found by iteration on Equation (17).

The calculation of the gas emissivity is performed by the weighted-sum-of-grey-gases (WSGG) model as described by Smith et al. (1982). The mean beam length used in this expression is scaled for pressures above 1 atm as given by Edwards and Matavosian (1984).

2.2 The reactor model

The fixed bed reactor model is a two-dimensional heterogeneous dispersion model treating the reactions on the catalyst pellet surface and the mass and heat transfer between the bulk and the pellets. Concentration and temperature profiles are solved both for the bulk phase and for the solid catalyst phase. As opposed to most published steam reformer models this model also includes resistances to mass transfer in the gas film surrounding the catalyst pellets and to heat transfer both in the gas film and internally in the particles. The reactor model is described in detail by Wesenberg and Svendsen (2006).

2.3 Combining the annulus model with the reactor model

The iteration is initiated by specifying the reactor wall temperature profile on the annulus side, T_{w2}. This is input to the annulus model, where the heat flux, $q_{w2,a}$, is calculated from Equation (16). This heat flux is then input to the reactor model where the internal tube skin temperature is calculated from $q_{w2,a}$ and the bulk temperature at the discretization point close to the wall:

$$T_{w1} = T_b + \frac{R_2}{R_1}\frac{q_{w2,a}}{h_1} \tag{18}$$

The heat flux calculated in the reactor model, $q_{w2,b}$, is defined with outer tube wall surface as basis similar to the definition of $q_{w2,a}$:

$$q_{w2,b} = \frac{R_1}{R_2} h_1 \left(T_{w1} - T_b(R_1)\right) \tag{19}$$

This heat flux and the wall temperature of Equation (18) give the external tube skin temperature to be given as input for the next iteration:

$$T_{w2} = T_{w1} + q_{w2,b}\frac{R_2 \ln(R_2/R_1)}{\lambda_w} \tag{20}$$

Convergence is reached when the wall temperature T_{w2} is unchanged. An additional convergence test consists in comparing the heat flux profiles of Equations (16) and (19) with heat flux profiles resulting from the changes in bulk gas energy in both the reactor tube and in the annular space. These heat flux profiles are found from the enthalpies and mass fluxes of the gas flows. All axial profiles are calculated for 100 discretization steps, as this was found to be a reasonable axial resolution.

3. MODEL VALIDATION

The properties of the gas mixtures at the outlet of the reactor and at the inlet on the annular side are closely related in the fact that the steam reformer product is reformed further in a secondary autothermal reformer, which product gas is the inlet gas to the steam reformer annular side. The primary GHR and the secondary ATR were simulated in the process simulation tool ProII to give inputs for the annulus gas. Table 1 shows the properties of the gases used in the simulations, where the reactor feed is given a hypothetical composition close to real operational values. The inlet gas on the annular side is calculated with ProII. The steam-to-carbon ratio is 2.0 and the composition of the natural gas is 85.8 % CH_4, 12.12 % CO_2, 1.98 % N_2 and 0.089 % H_2.

Table 1. Gas compositions, temperatures and pressures used in the model simulations. Inlet and outlet gases on reactor side and on annular side of the GHR.

	Reactor feed (given)	Reactor product (from this model)	Inlet gas on annular side (from ProII)	Outlet gas on annular side (from this model)
Temperature (˚C)	400	704	1050	857
Pressure (bara)	40.0	37.1	38.7	38.7
Mole fraction CH_4	0.290	0.160	0.0008	0.0008
Mole fraction CO_2	0.041	0.065	0.072	0.072
Mole fraction CO	0	0.048	0.113	0.113
Mole fraction H_2O	0.657	0.380	0.451	0.451
Mole fraction H_2	0.005	0.340	0.359	0.359
Mole fraction N_2	0.007	0.003	0.004	0.004
Flow (kmole/ hr)	23.0	26.8	40.9	40.9

3.1 Resolution and convergence

The axial variations of heat flux calculated in the reactor model and in the annulus model converged satisfactorily within 10 to 15 iterations using the procedure described in Section 2.3. The simulation resulted in a wall temperature profile which gave the same axial distribution of heat fluxes in both the reactor model and in the annulus model. An additional verification of convergence was made by certifying that the heat flux profile was identical to the gas enthalpy profiles in both the reactor and the annulus model.

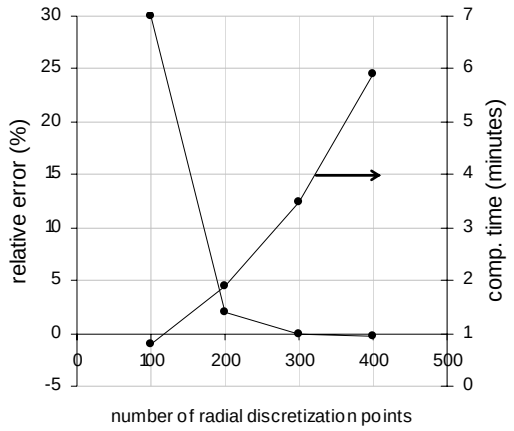

Figure 2. Difference between total enthalpy change and integrated heat flux from the boundary conditions, relative to total enthalpy change.

High spatial resolution in the radial direction in the annulus model was needed due to large variations in the effective radial thermal conductivity. The accuracy of the model was evaluated by comparing the integral of the heat flux (Equation (16)) with the total changes in enthalpy. This difference, relative to the heat flux from the boundary conditions, is shown in Figure 2 for varying radial resolution. A number of 300 radial steps was chosen for the model. The resulting relative difference was found to be about -0.025 %. This was deemed satisfactory.

3.2 Comparison with CFD model

In order to verify the effective thermal conductivity model for the annulus, the annulus model was tested without the radiation model. The previous assumption that the λ_{er} calculated in a corresponding CFD code could be used in the finite difference model to test if it gave the same radial heat flux profile as the CFD model. The CFD model was run with the k-ε turbulence model, and the finite difference model involved no calculations of turbulence other than the effect on radial heat transport through the imported λ_{er}.

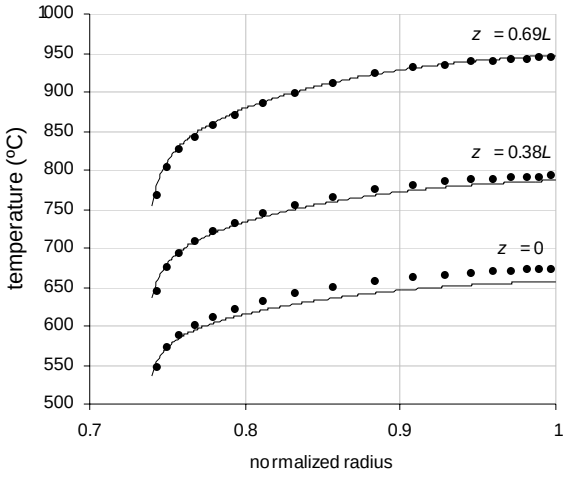

Figure 3. Comparison of temperature profiles from test without radiation in the finite difference model (solid line) and the CFD model (dotted line).

The resulting axial profiles for wall temperature and heat transfer coefficient from the finite difference model were used as input to the CFD model, which again produced a radial profile for λ_{er} that was input to the finite difference model. Manual iteration with these two models quickly resulted in a stable output and the two models gave the same temperature profiles. Even the radial temperature profiles were nearly identical, as can be seen in Figure 3. This confirms that an enhanced effective radial thermal conductivity profile calculated from the k-ε turbulence model in a CFD code can be used in a simpler finite difference model with no turbulence model and describe the effect of turbulent flow on radial heat transfer well.

4. SIMULATION RESULTS

The simulation results of the case given in Table 1 are presented here. Figure 5 shows the axial profiles of wall temperatures and of radial mean gas temperatures. From the graph it can be seen that the temperature driving forces are evenly distributed along the tube length. This is an ideal operation and an advantage as it indicates a low entropy production (Sauar et al., 1999) and thereby good energy utilisation.

The axial variation in heat flux through the reactor tube wall can be seen in Figure 4 together with the convective and radiative contributions. It is clear from the simulations that the radiative heat flux is of the same order of magnitude as the convective heat flux and can absolutely not be disregarded when modelling a GHR. The radiative heat flux varies from 35 % to 52 %. The convective heat flux is quite flat along most of the reactor, but rises sharply at the annulus inlet. This rise is caused by the flat inlet gas temperature profile which rapidly establishes, resulting in a sudden drop in gas temperature at the wall. The radiative heat flux increases with increasing temperature along the reactor, which is as expected.

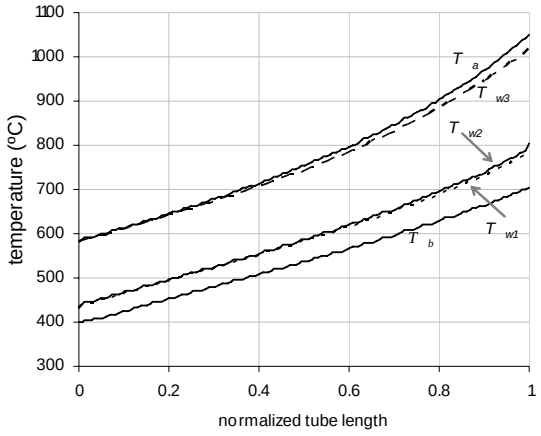

Figure 5. Axial profiles of radial mean bulk temperatures in annular section and in reactor bed, and of outer and inner wall temperatures of reactor tube.

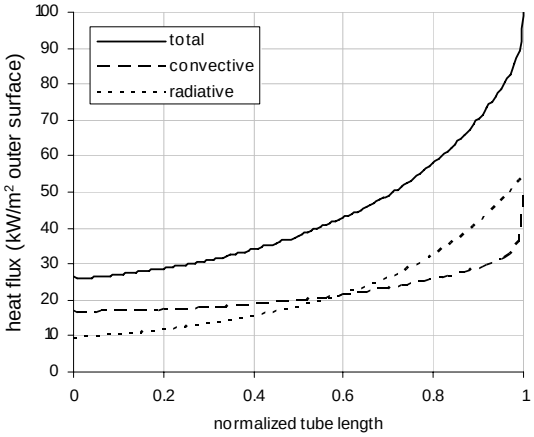

Figure 4. Axial variation of total, convective and radiative heat fluxes in annular section.

4.1 Evaluation of the radial heat transport mechanisms

The heat transport from radiation is considerable less important in a GHR than in a fired steam reformer. Nevertheless, the radiation plays a significant role as indicated on Figure 4. The effect of neglecting radiation from the hot gas in the annulus was investigated by comparing results from simulations with and without radiation. The results are given as radial temperature profiles in Figure 6 and axial temperature profiles and methane conversion profiles in Figure 7. The cases including and disregarding radiation are given in black and red, respectively. From Figure 6 it is readily clear that the annulus temperature predictions will be too high without taking radiation into account. The temperature difference is 50 – 100 °C, which of course cannot accepted in a model. Figure 7 shows that the predicted conversion is reduced by 25 % if radiation is disregarded. The conclusion is that a GHR model must include a radiation model for the annulus.

The role of the effective radial thermal conductivity, λ_{er}, from CFD calculations was also investigated. The radial variations of λ_{er} found from the CFD simulations were of significance for the results of the finite difference simulations, while the axial variations were found to be of less importance. The effect of including the radial variations of λ_{er} was studied by running a comparable simulation where a constant, mean value of λ_{er} was used. The results from this simulation gave an increase in the total heat flux and the methane conversion, both by 2 %. The outlet temperatures from the reactor bed and the annular section increased by 4 ºC and decreased by 9 ºC, respectively. It was thus decided to include the radial variation in λ_{er} in the model. Profiles from the simulations based on the mean λ_{er} are given by the blue lines of Figure 6 and Figure 7.

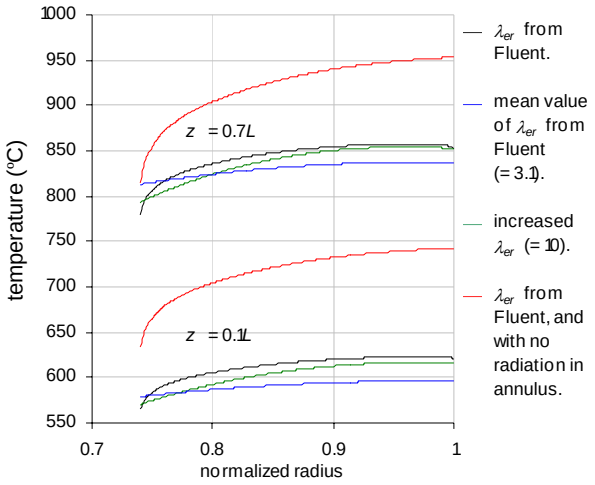

Figure 6. Radial gas temperature profiles of the annular space at two axial positions.

Increasing λ_{er} was also looked into. This gives an indication of the effects of increasing turbulence. A test simulation with a high, constant value of λ_{er} was performed and the results are given by the green lines of Figure 6 and Figure 7. The value of λ_{er} was increased by a factor of 3.25 as compared to the average value resulting from the CFD simulation. The effects were significant; the outlet temperature of the annulus gas and the reactor gas decreased with 26 °C and increased with 9 °C, respectively, and the methane conversion increased with more than 4 %. This test simulation confirms the benefits of increasing the turbulence in a GHR.

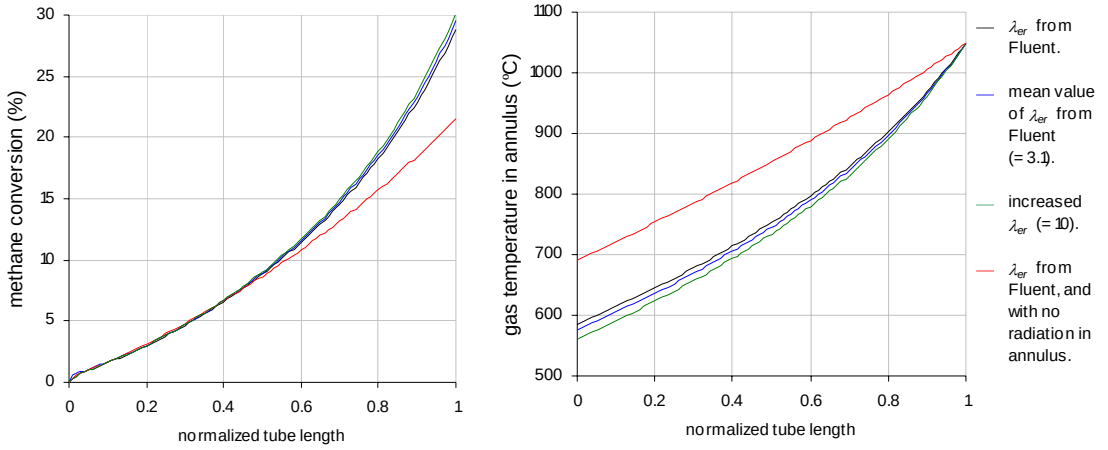

Figure 7. Axial profiles of methane conversion and mean gas temperatures resulting from simulations with varying λ_{er} and simulations with and without radiation.

An apparent weakness of the model is that external evaluation of λ_{er} is needed, in this case by running a simulation in FLUENT. One option to make the model self contained would be to make test runs in the CFD model to map the dependency of the effective radial thermal conductivity to annulus geometry and flow.

A simulation based on the Reynolds stress turbulence model gave almost equal results to the case of using the k-ε turbulence model. This is on the other hand no guarantee for achieving physical correct simulation results because both turbulence models are based on empirical parameters fitted for the case of tubular flow.

5. CONCLUSIONS

The heating section of a gas heated steam reformer (GHR) designed with concentric sheath tubes on the reactor tubes has been modelled. The operating conditions are typical for a primary reformer for Fischer-Tropsch or methanol synthesis purposes and the heating gas is hot synthesis gas from a secondary reformer. The heating section is modelled as an annular volume enclosing a reactor tube. This annular section is modelled with a two-dimensional, finite difference plug flow model using an effective radial thermal conductivity λ_{er} to include the effect that turbulence has on heat transfer in radial direction. λ_{er} is produced from additional CFD simulations where turbulence is modelled by the k-ε model, and is accordingly imported to the annulus model of the GHR model. Heat transfer from radiation is modelled by the discrete ordinates method in the radial direction.

The annulus model was tested for grid resolution and it was found that high radial resolution is needed for satisfactory energy balances to be achieved. The results show that radiation plays a significant role in the annulus side energy transport, varying from 35 % at the low temperature end to 52 % at the high temperature end of the reformer. The radial transport is rapid and quite flat radial temperature profiles result. The axial temperature profiles show that the driving forces for energy transport between the annulus and reactor sides are nearly constant through the reformer. This indicates low entropy production and good heat utilization.

NOTATION

A_a	Cross sectional area of annular space, m2
c_P	Specific heat capacity, J/kg K
d	Diameter, m
f	Friction factor
F_C	Correction factor in Equation (4)
h	Heat transfer coefficient, W/m2 K
I	Radiation intensity, W/m2 sr
L	Tube length, m
n	Molar flow rate, kmole/ s
Nu_w	Wall Nusselt number, $Nu_w = h_w d_t / \lambda_g$
Pr	Prandtl's number, $Pr = \mu_g c_P / \lambda_g$
q	Heat flux, W/ m2
r	Radial co-ordinate, m
R	Gas constant, Pa m3/kmole K
R	Tube radius, m
Re	Reynolds number, $Re = d_h \rho_g v_z / \mu_g$
T	Temperature, K
v	Velocity, m/s
w	Quadrature weight for radiative directions
z	Axial co-ordinate, m

Greek Letters

α	Parameter for cylindrical co-ordinates in the discrete ordinates method
ε	Emissivity
η	Directional cosines for angular directions
κ	Absorption coefficient for gas, m-1
λ	Thermal conductivity, W/m K
μ	Directional cosines for radial direction
ρ	Density, kg/m3
ρ_w	Wall reflectivity
σ	Stefan Boltzmann's constant, W/m2 K4
ψ	Azimuthal angle, rad

Subscripts

1	Position at inner wall of reactor tube
2	Position at outer wall of reactor tube
3	Position at outer wall of annular section
a	Annulus
b	Reactor bed
B	Blackbody
e	Effective
g	Gas
h	Hydraulic
r	Radial
rad	Radiation
t	Tube
w	Wall
z	Axial

Superscripts

m	Angular direction in the discrete ordinates method

REFERENCES

Carlson, B.G. and Lathrop, K.D., "Transport Theory – The method of discrete ordinates on computing methods in reactor physics", in: "Computing methods in reactor physics", H. Greenspan, C.N. Kelber and D. Okrent Eds., Gordon & Breach, New York, 165-266 (1968)

De Deken, J.C., Devos, E.F., Froment, G.F., "Steam reforming of natural gas: Instrinsic kinetics, diffusional influences, and reactor design", ACS Symposium Series, Vol. 196, 181-197 (1982)

De Groote, A.M. and Froment, G.F., "Reactor modelling and simulations in synthesis gas production", Rev Chem Eng, Vol. 11, No. 2, 145-183 (1995)

Edwards, D.K., Matavosian, R., "Scaling rules for total absorptivity and emissivity of gases", J. Heat Transfer, Vol. 106, 684-689 (1984)

Fiveland, W.A., "A discrete ordinates method for predicting radiative heat transfer in axisymmetric enclosures", ASME paper no. 82-HT-20 (1982)

Gnielinski, V., "New equations for heat and mass transfer in turbulent pipe and channel flow", Int. Chem. Eng., Vol. 16, 359-368 (1976)

Grevskott, S., Rusten, T., Hillestad, M., Edwin, E. and Olsvik, O., "Modelling and simulation of a steam reforming tube with furnace", Chem. Eng. Sci., Vol. 56, No. 2, 597-603 (2001)

Hottel, H.C. and Sarofim, A.F., "Radiative Transfer", McGraw-Hill, New York (1967)

Kvamsdal, H.M., Svendsen, H.F., Hertzberg, T. and Olsvik, O., "Dynamic simulation and optimization of a catalytic steam reformer", Chem. Eng. Sci., Vol. 54, 2697-2706 (1999)

Mills, A.F., "Heat and Mass Transfer", Irwin, Chicago (1995)

Modest, M.F., "Radiative heat transfer", 2nd ed., Amsterdam, Academic Press (2003)

Pedernera, M.N., Pina, J., Borio, D.O. and Bucala, V., "Use of a heterogeneous two-dimensional model to improve the primary steam reformer performance", Chem. Eng. J., Vol. 94, 29-40 (2003)

Petukhov, B.S. and Roizen, L.I., "Generalized relationships for heat transfer in a turbulent flow of a gas in tubes of annular section", High Temp. (USSR), Vol. 2, 65-68 (1964)

Petukhov, B.S., "Heat transfer and friction in turbulent pipe flow with variable physical properties", in "The properties of gases and liquids", R.C. Reid, J.M. Prausnitz and B.E. Poling Eds., McGraw-Hill, New York (1970)

Reid, R.C., Prausnitz, J.M. and Poling, B.E., "The properties of gases and liquids", 4th ed., McGraw-Hill, New York, (1987)

Sauar, E., Nummedal, L. and Kjelstrup, S., "The principle of equipartition of forces in chemical reactor design: The ammonia synthesis", Comp. Chem. Eng., Vol. 23, 499-502 (1999)

Schiesser, W.E., "The numerical method of lines in integration of partial differential equations", Academic Press Inc., San Diego (1991)

Siegel, R. and Howell, J.R., "Thermal radiation heat transfer", 4th ed., Taylor & Francis, New York (2002)

Smith, T.F., Shen, Z.F., Friedman, J.N., "Evaluation of coefficients for the weighted sum of grey gases model", J Heat Transfer, Vol. 104, 602-608 (1982)

Spalding, D.B., "Mathematical modelling of fluid-mechanics, heat-transfer and chemical-reaction processes", in "Lecture 9: Idealisations of radiation", report no. HTS/80/1, Imperial College of Science and Technology, London. (1980)

Stehlík, P., Šika, J., Bébar, L. and Raus, L., "Contribution to the research and development of radiation chambers in steam reforming", Coll. Czech. Chem. Comm., Vol. 54, 2357-2374 (1989)

Stehlík, P., "Radiative component in thermal calculation of tubular heat exchangers", Heat Transfer Eng., Vol. 16, No. 1, 19-28 (1995)

Wesenberg, M.H. and Svendsen, H.F., "Mass and heat transfer limitations in a heterogeneous model of a gas heated steam reformer", submitted 2006

Xu, J. and Froment G.F., "Methane steam reforming: II. Diffusional limitations and reactor simulation, AIChE J., Vol. 35, No. 1, 97-103 (1989)

Presentation 1

presented on *the 6th World Congress of Chemical Engineering*, Melbourne (2001)

Heat Transfer in Steam Reformer Tubes

Margrete H. Wesenberg [1], Arne Grislingås [1] and Sverre Grevskott [2]

[1] Statoil Research Centre
Trondheim, Norway
[2] SINTEF Applied Mathematics
Oslo, Norway

Abstract:

The main objective of this study is to evaluate the correlations for wall heat transfer coefficient in steam reformer models. A two-dimensional pseudohomogeneous model has been developed for the catalyst bed in the reformer tubes, and a convection/radiation model is developed for the energy side of the process. Different correlations from literature have been tested in this model, and axial and radial temperature profiles from the simulations are compared with in-house empirically based calculations for real reformer tubes. It was found that the correlations for wall Nusselt number giving the best fit were the two from Dixon et al. [1] and Peters et al. [2]:

$$Nu_w = \left(1 - 1.5\,(d_p/d_t)^{1.5}\right) \cdot Re_p^{0.59} \cdot Pr^{0.33}$$

$$Nu_w = 4.9 \cdot (d_p/d_t)^{0.26} \cdot Re_p^{0.45} \cdot Pr^{0.33}$$

Both correlations were developed by focusing on high particle-to-tube diameter ratios and are also valid at high Reynolds numbers.

INTRODUCTION

Steam reforming is the process that converts hydrocarbons with steam to synthesis gas (H_2, CO and CO_2). The reactions take place in tubular fixed bed reactors over a nickel catalyst, and necessary heat to drive the endothermic reactions is supplied by direct heating of the tube walls. The process conditions are typical 20-40 bar, 700-950°C outlet temperature, and the Reynolds number is in the range of 4000 to 12000. The three reactions for conversion of natural gas used in this study are:

$$CH_4 + H_2O \rightleftharpoons CO + 3H_2$$

$$CH_4 + 2H_2O \rightleftharpoons CO_2 + 4H_2$$

$$CO + H_2O \rightleftharpoons CO_2 + H_2$$

Transfer of energy through the tube walls and into the reaction zone in the catalyst bed is one of the most important mechanisms critical for design and operation of steam reformers. Hot flue gas provides the heat in conventional fired steam reformers, and the heat transfer is governed by radiation and convection. Convective steam reformers are compact units designed as shell and tube heat exchangers, where the heat source is flue gas or synthesis gas from a secondary reformer. The heat transfer is here dominated by convection. In both reformer types the heat flux through the tube wall is driven by conduction, and inside the tube the heat transfer will be influenced by all three mechanisms; conduction and radiation in both phases and convection.

The two-dimensional pseudohomogeneous model is generally used to describe temperature and concentration gradients in radial and axial direction in fixed beds having considerable heat

transfer resistance near the wall. Different correlations are available from literature to describe heat transfer in the radial direction in fixed beds. Most of them are based on cold flow experiments and with Reynolds numbers one order of magnitude lower than for industrial steam reformers. The aim of this study is to evaluate different correlations and compare with empirical data from real reformer tubes.

PROBLEM DESCRIPTION

The reactor model used can be applied both for conventional side fired steam reformers and for convective steam reformers. In this study it is adapted to a convective steam reformer with conditions typical for synthesis gas production for methanol and Fischer-Tropsch processes. The steam reforming reactions are strongly endothermic and require a large mass flow and velocity of the heating medium. The temperature difference between the exiting hot gas and the incoming natural gas is about 300 K.

The radial heat transfer in steam reformer tubes is best described by a two-parameter model, which involves both an effective thermal conductivity in the bed and a resistance to heat transfer near the tube wall, which is the inverse of the wall heat transfer coefficient. The wall heat transfer coefficient, h_{iw}, describes the large temperature drop near the wall and the effective thermal conductivity, k_e, accounts for the smaller temperature difference in the bed.

Many researchers have described these parameters for special systems. Most of these experiments are done in non-reacting systems with air or water as the test fluid and with constant wall temperatures. Experimental tubes often have a small ratio between the tube length and the tube diameter and are therefore different from industrial units. This leads to relations strongly dependent on the tube length, which are not accounted for in the correlations. The Reynolds numbers in laboratory scale tests are often low, and industrial conditions are therefore often out of the validity range of the correlations. Further limitations in the experiments are low heat flux and particle geometries different from industrial catalyst pellets.

The main objective with the simulations is to evaluate different correlations for h_{iw} that best describe the system. The parameter h_{iw} is the most important factor governing the radial heat transfer, and k_e is therefore held constant at 360 W/ (m K) in this study. A change in this value has only small effects on the simulation results. The correlations described in literature usually give h_{iw} expressed by the Nusselt number or the Biot number as function of the Reynolds number and sometimes also the Prandtl number. The simulation results for different correlations for h_{iw} are compared with calculations from in-house empirically based data.

MODEL DESCRIPTION

A two-dimensional pseudohomogeneous reactor model for the reformer tube has been developed. The model consists of two parts; the catalytic tube and the shell side of the convective reformer. The tube side is modeled in cylindrical coordinates as one tube with length L and radius R, and the shell side is modeled in Cartesian coordinates with cross sectional area $\pi \cdot (R_f^2 - R^2)$ and length L. Natural gas is fed at $z = 0$ and hot synthesis gas from a secondary reformer is fed at $z = L$ on the shell side.

The models are connected to each other by the inner and outer wall temperatures, which are the input to the shell side and tube side model, respectively. A more detailed description of this model has been given by Grevskott et al. [3].

Conservation equations for the fixed bed model

A mass balance gives the following equation:

$$\nabla \cdot (c x_i \vec{v}) - \nabla \cdot (c D_i \nabla x_i) = \rho_{cb} \eta_i r_i \tag{1}$$

with boundary conditions:

$$r = 0 \text{ and } r = R: \quad \frac{\partial x_i}{\partial r} = 0 \tag{2}$$

$$z = 0: \quad x_i = x_i^{in} \tag{3}$$

$$z = L: \quad \frac{\partial x_i}{\partial z} = 0 \tag{4}$$

and with total conservation:

$$\nabla \cdot (\rho_g \vec{v}) = 0 \tag{5}$$

The energy balance with axial convection, radial conduction and heat of reaction is:

$$\rho_g C_{Pg} \vec{v} \cdot \nabla T - \nabla \cdot (k_e \nabla T) = \sum_i (-\Delta H_i) \rho_{cb} \eta_i r_i \tag{6}$$

T is the temperature in the pseudophase (gas and catalyst pellets), later referred to as the bulk temperature.

Boundary conditions are:

$$r = 0: \quad \frac{\partial T}{\partial r} = 0 \tag{7}$$

$$r = R: \quad -k_e \frac{\partial T}{\partial r} = \left(\frac{1}{h_{iw}} + \frac{1}{h_s} \right)^{-1} (T - T_{ow}) \tag{8}$$

$$z = 0: \quad T = T^{in} \tag{9}$$

$$z = L: \quad \frac{\partial T}{\partial z} = 0 \tag{10}$$

The reaction rates, r_i, are modeled as described by Xu and Froment [4] and are multiplied by a constant efficiency factor, η_i, estimated by Xu and Froment [5]. The effective thermal conductivity of the bed, k_e, is set to constant value. This effective conductivity involves conduction and radiation in both phases and convection in radial direction.

Darcy's law is used for calculating the pressure drop:

$$-\nabla \cdot (\rho_g \lambda \nabla P) = 0 \tag{11}$$

where λ is the mobility:

$$\lambda = \left(\frac{150 \mu_g (1-\varepsilon)^2}{(\Phi d_p)^2 \varepsilon^3} + 1.75 \frac{\rho_g |\vec{v}| (1-\varepsilon)}{\Phi d_p \varepsilon^3} \right)^{-1} \tag{12}$$

Boundary conditions are:

$$r = 0 \text{ and } r = R: \quad -\rho_g \lambda \frac{\partial P}{\partial r} = 0 \tag{13}$$

$$z = 0: \quad P = P^{out} \tag{14}$$

Conservation equations for the shell side model

Convection, conduction and radiation describe the energy conservation on the shell side. The symbol S is the source term from radiation, described by Grevskott et al. [3]:

$$\rho_g C_{Pg} \vec{v} \cdot \nabla T = \nabla \cdot (k_{gb} \nabla T) + S \tag{15}$$

Boundary conditions:

$$x = R: \quad -k_{gb,r} \frac{\partial T}{\partial x} = \left(\frac{1}{h_s} + \frac{1}{h_{ow}} \right)^{-1} (T - T_{iw}) \tag{16}$$

$$x = R_f: \qquad -k_{gb,r}\frac{\partial T}{\partial x} = 0 \tag{17}$$

$$z = L: \qquad -k_{gb,z}\frac{\partial T}{\partial z} = \rho_g v_z C_{Pg}(T - T^{in}) \tag{18}$$

$$z = 0: \qquad -k_{gb,z}\frac{\partial T}{\partial z} = 0 \tag{19}$$

Wall heat transfer coefficients

The shell side wall heat transfer coefficient (h_{ow}) is given as [6]:

$$Nu_w = 0.163 \cdot Re^{0.632} \cdot Pr^{0.33} \tag{20}$$

The characteristic length of the Reynolds number is the hydraulic diameter on the shell side. Finned tubes may be used to increase the heat transfer, and this is in one case simulated by increasing h_{ow} by a factor estimated in a simple one-dimensional model containing correlations for fins.

The tube side heat transfer is given by a two-parameter model where the parameters are the effective thermal conductivity in the bed and the heat transfer coefficient at the wall. Five different correlations for the inner wall heat transfer coefficient (h_{iw}) have been evaluated against calculations from in-house empirically based data.

The correlation from Li and Finlayson [7] is based on experiments with air and is valid for spheres with d_p/d_t between 0.05 and 0.3, for Reynolds numbers between 20 and 7600 and for Biot numbers less than 12:

$$Nu_w = 0.17 \cdot Re_p^{0.79} \tag{21}$$

Wall temperatures were held constant. Data influenced by length effects were eliminated, so that the desired asymptotic form of the heat transfer coefficient was achieved. An extension by multiplying with $(Pr/0.7)^{1/3}$ was suggested to include the Prandtl number dependence, but this was not confirmed by experiments. This addition will give the correlation:

$$Nu_w = 0.1915 \cdot Re_p^{0.79} Pr^{1/3} \tag{22}$$

Dixon et al. [1] studied mass transfer in packed beds with low tube-to-particle diameter ratio to provide correlations for Nu_w and Pr in terms of Re_p and d_t/d_p. The heat transfer coefficient expressed in terms of the Nusselt number follows the same correlation as for the mass transfer coefficient given by the Sherwood number. Experiments were performed with water. For d_t/d_p = 3.3 the correlation was in good agreement with heat transfer data for Reynolds numbers up to 8000, but for $d_t/d_p > 7.4$ Dixon et al. [1] have only shown good agreement at $Re_p < 500$:

$$Nu_w = \left(1 - 1.5\left(\frac{d_p}{d_t}\right)^{1.5}\right) \cdot Re_p^{0.59} \cdot Pr^{0.33} \tag{23}$$

De Wasch and Froment [8] developed an expression where the wall heat transfer coefficient is proportional to the product of the Reynolds number and the tube-to-particle diameter ratio. The use of a static contribution, h_{iw}^0, gives the coefficient at zero flow:

$$h_{iw} = h_{iw}^0 + 0.01152 \cdot \frac{d_t}{d_p} \cdot Re_p \tag{24}$$

h_{iw} is here given in kcal/(hr m^2 K). The experiments were done with air at 50°C and $Re_p < 450$.

Peters et al. [2] put the main focus on high particle-to-tube diameter ratios (0.1 – 0.6) and high Reynolds numbers (up to 8000). The Nusselt number is dependent on the particle-to-tube diameter ratio and the Prandtl number as well as the Reynolds number. Also here the experiments were performed with dry air. The authors claim that the correlation for spheres is valid for Reynolds numbers less than 8000:

$$Nu_w = 4.9 \cdot \left(\frac{d_p}{d_t} \right)^{0.26} \cdot Re_p^{0.45} \cdot Pr^{0.33} \tag{25}$$

The main objective of the work of Dixon and Cresswell [9] is a theoretical, rather than an empirical, approach. The wall heat transfer coefficient correlated to the Biot number instead of the Nusselt number gives a unique relationship with the Reynolds number, making the wall heat transfer coefficient independent on particle size and conductivity:

$$Bi_w = 3.0 \cdot Re_p^{-0.25} \tag{26}$$

This correlation is valid for $Re_p > 40$.

Equations 21 to 25 are used in the simulation tests for different cases with steam reforming. Equation 26 is not suitable for this simulation model because of the choice of a constant effective thermal conductivity and the direct proportionality between h_{iw} and k_e.

SIMULATION RESULTS

The parameters used for comparing simulation results with the in-house empirical data calculations are methane conversion, radial and axial temperature profiles and inner wall heat transfer coefficients. The simulations were done for different feed compositions, steam-to-methane ratios and reformer sizes. Simple correlations for finned tubes were also tested. All cases gave corresponding results, and only one of the cases is therefore presented here.

The methane conversion is given in Figure 1. The data from the correlations given by Equations 21, 22, 23 and 25 are very close to the empirical data line, and all data are therefore enlarged in Figure 2. The same is done for the relative axial bulk temperature profiles given in Figures 3 and 4. Relative radial temperature profiles are given in Table 1 at three different axial positions, with an example plotted in Figure 5. The calculated relative inner wall heat transfer coefficients are shown in Figure 6. Finally, the relative outlet conditions from the simulations are presented in Table 2.

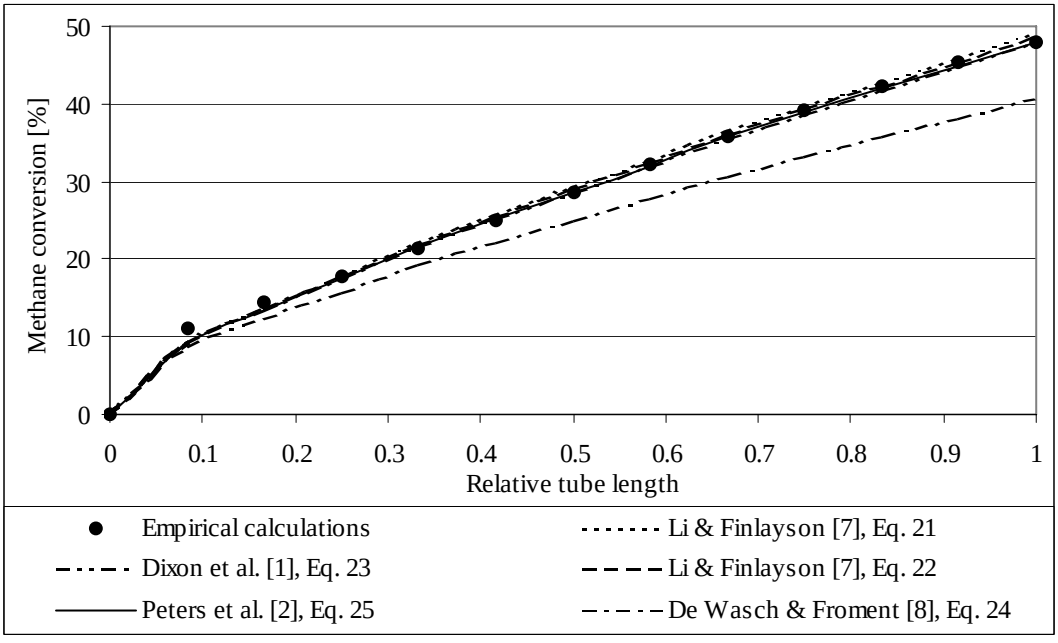

Figure 1: Methane conversion computed with the evaluated inner wall heat transfer coefficients. Comparison with empirical data.

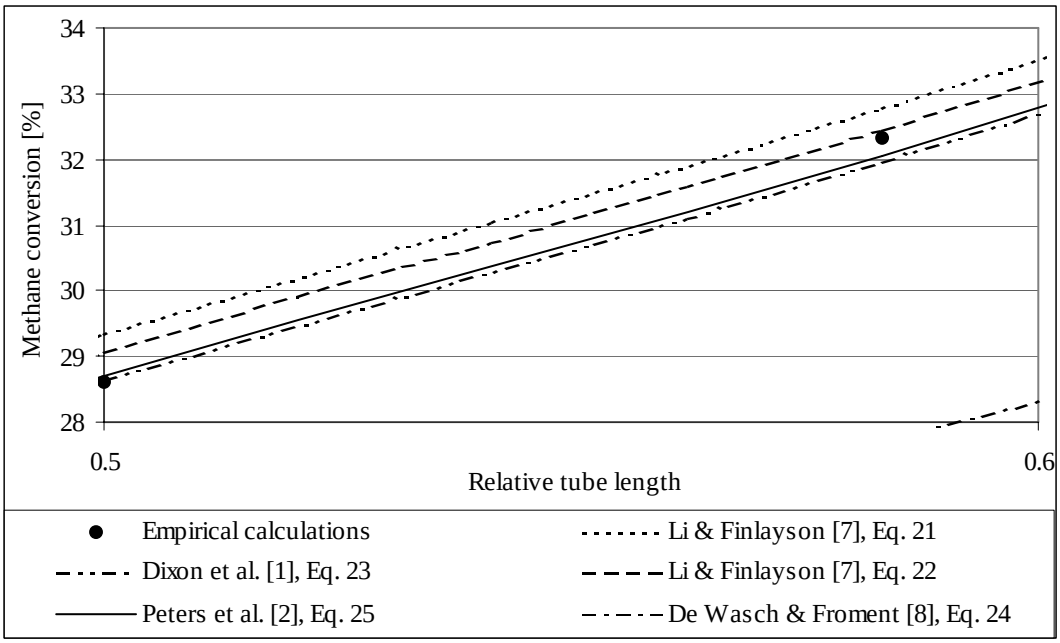

Figure 2: Expanded view of methane conversion at $z = 0.5L - 0.6L$.

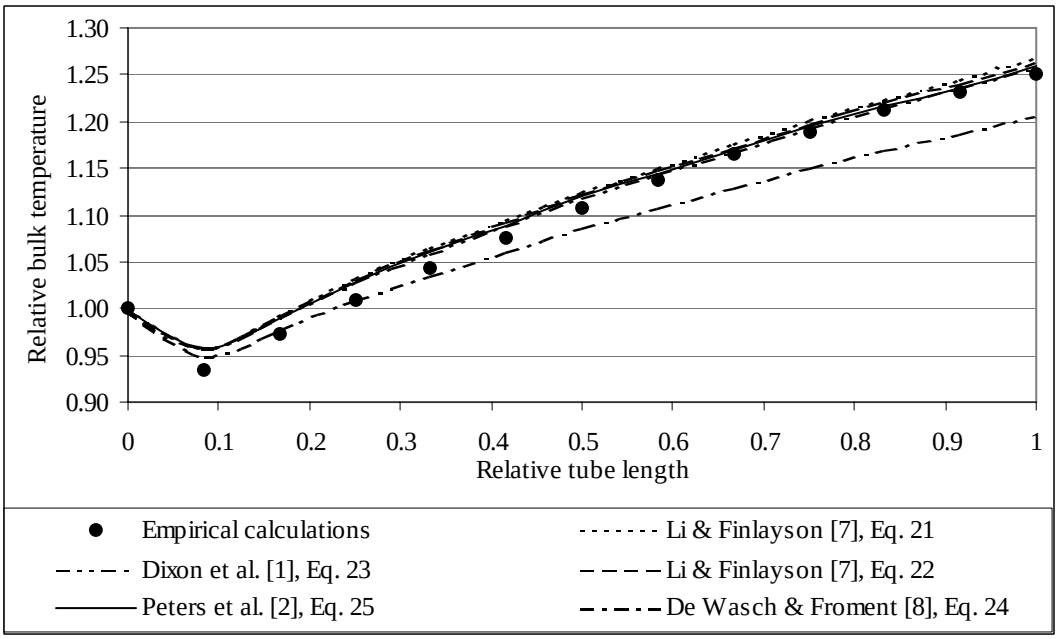

Figure 3: Axial bulk temperature profiles relative to inlet temperature (ºC). Average of radial data. Simulation results from five different correlations for h_{iw} compared with empirical data.

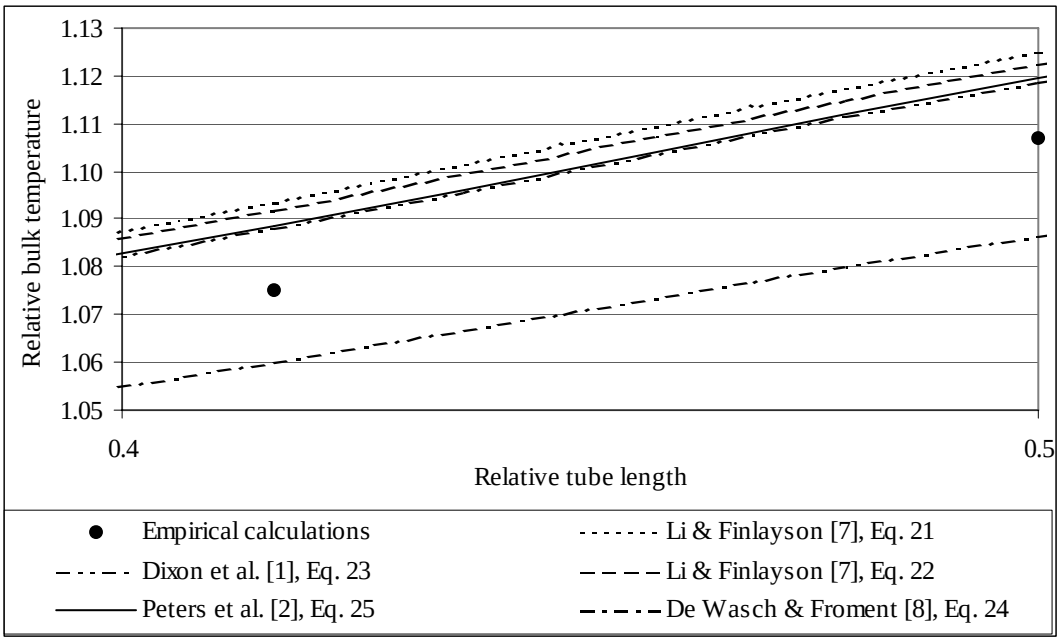

Figure 4: Expanded view of the average axial bulk temperature profiles relative to inlet temperature (ºC) as given in Figure 3 at z = 0.4L - 0.5L.

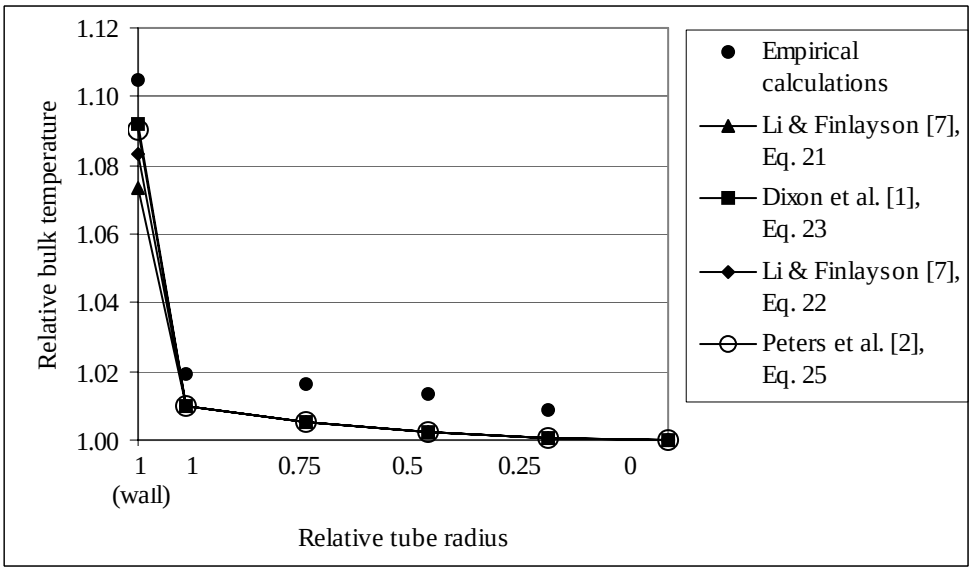

Figure 5: Relative wall temperatures and relative radial bulk temperature profiles as given in Table 1 at axial position z = 0.67 L. The reformer model with the four best correlations for h_{iw} is compared with empirical data. All temperatures are given in ºC and are relative to the tube center temperature for the actual heat transfer model.

Table 1: Relative radial bulk temperature profiles at three different axial positions. All temperatures are relative to the center bulk temperature (ºC) for the actual correlation at the actual position (i.e. relative bulk temperature at $r = 0$ is 1).

	Relative inner tube wall temperature	Relative bulk temperature at $r = R$
Axial position: $z = 0.17\ L$		
Empirical data calculations	1.138	1.026
Li & Finlayson [7], Eq. 21	1.121	1.013
Li & Finlayson [7], Eq. 22	1.129	1.013
Dixon et al. [1], Eq. 23	1.144	1.013
De Wasch & Froment [8], Eq. 24	1.262	1.011
Peters et al. [2], Eq. 25	1.142	1.013
Axial position: $z = 0.67\ L$		
Empirical data calculations	1.105	1.019
Li & Finlayson [7], Eq. 21	1.073	1.010
Li & Finlayson [7], Eq. 22	1.083	1.010
Dixon et al. [1], Eq. 23	1.092	1.010
De Wasch & Froment [8], Eq. 24	1.206	1.008
Peters et al. [2], Eq. 25	1.090	1.010
Axial position: $z = L$ (outlet)		
Empirical data calculations	1.076	1.014
Li & Finlayson [7], Eq. 21	1.059	1.009
Li & Finlayson [7], Eq. 22	1.059	1.009
Dixon et al. [1], Eq. 23	1.077	1.009
De Wasch & Froment [8], Eq. 24	1.186	1.007
Peters et al. [2], Eq. 25	1.075	1.009

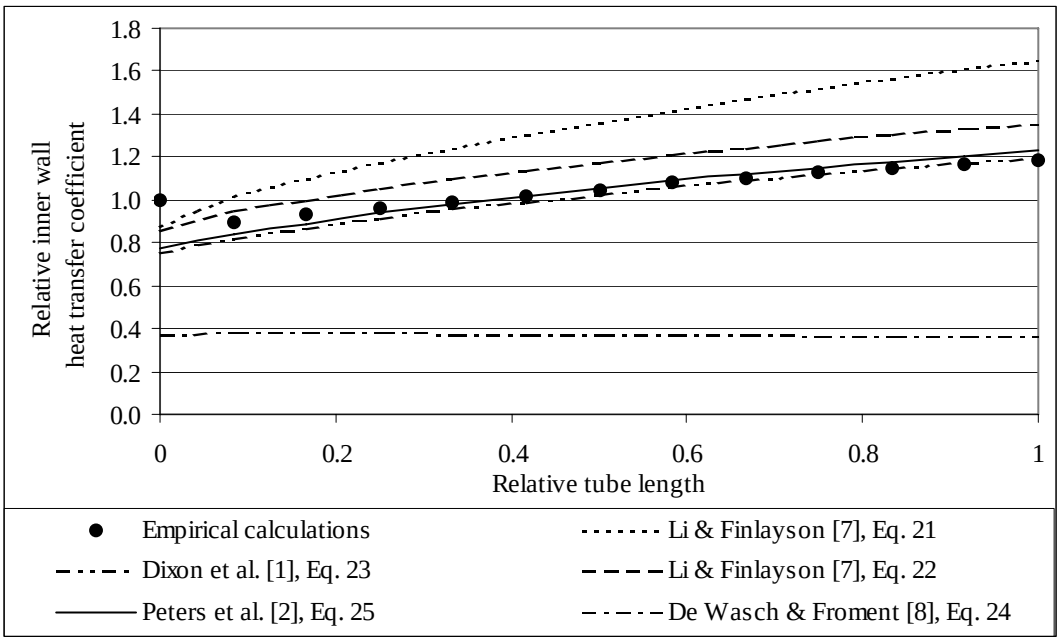

Figure 6: Relative inner wall heat transfer coefficients from the five correlations compared with calculations from empirical data. All h_{iw} are relative to inlet h_{iw} from empirical data.

Table 2: Outlet conditions and mean h_{iw} relative to h_{iw} at the inlet from calculations from empirically based data. Empirical data calculations compared with simulation results based on the five correlations for h_{iw}.

	Outlet / inlet bulk temperature [ºC / ºC]	Methane conversion [%]	Mean relative h_{iw}
Empirical data calculations	1.25	48.0	1.05
Li & Finlayson [7], Eq. 21	1.27	49.2	1.33
Li & Finlayson [7], Eq. 22	1.26	48.6	1.15
Dixon et al. [1], Eq. 23	1.26	47.9	1.01
De Wasch & Froment [8], Eq. 24	1.21	40.7	0.37
Peters et al. [2], Eq. 25	1.26	48.0	1.03

DISCUSSION

The results show that the four correlations for h_{iw} described by Li and Finlayson [7], Dixon et al. [1] and Peters et al. [2] fit well with experimental data. The correlation by De Wasch and Froment [8] in Equation 24 is directly proportional to the Reynolds number and gives too diverging radial temperature profiles and low outlet temperature and conversion to be able to describe this system satisfactorily.

Kulkarni and Doraiswamy [10] recommend the correlation from Li and Finlayson [7] for industrial reactors where the tubes are much longer than the ones used in laboratory experiments. This correlation is developed by reexamining literature data not influenced by length effects, giving an asymptotic heat transfer coefficient as is requested in long tubes.

The later published correlation by Dixon et al. [1] is recommended by Tsotsas and Schlünder [11]. They state that to be able to explain the data scatter, the physical meaning of the wall heat transfer coefficient has to be understood. Focusing on the mathematical methods used, as done by Li and Finlayson [7], is of less importance. The main mechanism for heat transfer at high Peclet numbers is fluid mixing in the voids of the bed, while the heat transfer through the unmixed sublayer in the immediate vicinity of the wall is driven by molecular conduction.

The suggested extension of Equation 21 to include the dependence on the Prandtl number [7] has been evaluated (Equation 22). The results differ some from the results using Equation 21, giving values closer to the empirical data. Equations 21 and 22 give radial temperature profiles deviating slightly more from empirical data than compared to Equations 23 and 25 (Table 1 and Figure 5).

The difference between the correlations in Equations 23 and 25 is mostly linked to the dependence on the particle-to-tube diameter ratio. Both correlations are results from experiments with special attention to high d_p/d_t ratios. The factor containing d_p/d_t in Equation 23 is decreasing with increasing particle-to-tube diameter ratio while it is increasing in Equation 25. The effect of d_p and d_t on the wall heat transfer coefficient is also influenced by the d_p in the Nusselt number and in the Reynolds number, leading to the following expressions for h_{iw} as a function of d_t and d_p for Equation 23 and 25, respectively:

$$h_{iw} = k_g \cdot \left(1 - 1.5\left(\frac{d_p}{d_t}\right)^{1.5}\right) \cdot d_p^{-0.41} \cdot \left(\frac{\rho_g \cdot v \cdot \varepsilon}{\mu_g}\right)^{0.59} \cdot Pr^{0.33} \qquad (27)$$

$$h_{iw} = 4.9 \cdot k_g \cdot d_t^{-0.26} \cdot d_p^{-0.29} \cdot \left(\frac{\rho_g \cdot v \cdot \varepsilon}{\mu_g}\right)^{0.45} \cdot Pr^{0.33} \qquad (28)$$

At constant d_p and velocity and increasing d_t, h_{iw} given by Equation 27 is increasing slightly while h_{iw} by Equation 28 is decreasing. With increasing d_p and constant d_t and velocity

Equations 27 and 28 give decreasing h_{iw}, with the greatest change in the former equation. One of our simulation cases not presented in this paper had a higher d_p/d_t ratio (lower d_t) than the case presented in the previous section, and the results from Equations 23 and 25 were both in good agreement with empirical data. This means that the different d_p and d_t dependencies shown in Equation 27 and 28 have minimal effect for the actual reformer tubes.

Equations 21, 22 and 25 are within the ranges of validity, with Reynolds numbers in the range 4000 to 7000. The particle-to-tube diameter ratio is 0.11 to 0.12, which also is within the requirements. Dixon et al. [1] have only proved Equation 23 for this diameter ratio (i.e. $d_t/d_p >$ 7.4) for Re_p up to 500, but it was later shown by Tsotsas and Schlünder [11] that the correlation was in good agreement with experiments with d_t/d_p at 10 for Re_p up to 10000. Equation 24 is based on experiments with Reynolds numbers less than 450.

CONCLUDING REMARKS

The objective was to evaluate correlations for the inner wall heat transfer coefficient suitable for steam reformers. Steam reformers are characterized by high temperatures, Reynolds numbers and heat fluxes. Five different correlations were tested with constant effective thermal conductivity in the bed. A two-dimensional pseudohomogeneous model was used. The radial bed temperature profiles were compared to empirical data, as well as axial bed temperature and methane conversion profiles.

The correlations that best describe the heat transfer in the reactor are those given by Dixon et al. [1] in Equation 23 and by Peters et al. [2] in Equation 25. The correlations have different dependencies on d_p and d_t, but the effect of this is negligible in the actual region of d_p and d_t for operation of steam reformers. The influence of the Reynolds number is stronger in Equation 23 than in Equation 25 (exponents 0.59 and 0.45, respectively).

For the operation range tested ($Re \sim 5000$, $Pr \sim 0.5$, $d_p/d_t \sim 0.11$) the two wall heat transfer coefficients for the steam reformer tube given by Dixon et al. [1] and Peters et al. [2] are both in good agreement with practical experience, and are recommended for further use.

NOMENCLATURE

Bi_w Wall Biot number, $h_{iw} \cdot R / k_e$
c Total concentration [mole/ m^3]
C_{Pg} Specific heat capacity of gas [J/ kg K]
D_i Dispersion matrix for component i [m^2/ s]
d_h Shell side hydraulic diameter [m]
d_p Equivalent particle diameter [m]
d_t Tube diameter [m]
ΔH_i Heat of reaction for component i [J/ mole]
h_{iw} Wall heat transfer coefficient on bed side of reformer [W/ m^2 K]
h_{iw}^0 Wall heat transfer coefficient on bed side of reformer at stagnant gas [W/ m^2 K]
h_{ow} Wall heat transfer coefficient on shell side of reformer [W/ m^2 K]
h_s Heat transfer coefficient through the tube walls [W/ m^2 K]
k_e Effective thermal conductivity of fixed bed [W/ m K]
k_g Thermal conductivity of gas [W/ m K]
k_{gb} Effective thermal conductivity matrix on shell side [W/ m K]
L Tube length [m]
Nu_w Wall Nusselt number, $h_{iw} \cdot d_p / k_g$ or $h_{ow} \cdot d_p / k_g$
P Pressure [Pa]
P^{out} Outlet pressure [Pa]
Pr Prandtl number, $\mu_g \cdot C_{Pg} / k_g$
r Radial coordinate for tube
R Tube radius [m]

Re Reynolds number, $\rho_g \cdot v \cdot d_h / \mu_g$
Re_p Fixed bed Reynolds number, $\rho_g \cdot v \cdot \varepsilon \cdot d_p / \mu_g$
R_f Diameter for outer limit of shell side for one tube [m]
r_i Reaction rate for component *i* [mole/ kg cat. s]
S Source term from radiation on shell side [W/ m^3]
T Bulk temperature (in pseudophase) [K]
T^{in} Bulk inlet temperature [K]
T_{iw} Inner wall temperature [K]
T_{ow} Outer wall temperature [K]
$\vec{v}$ Gas velocity [m/ s]
x Horizontal coordinate on shell side
x_i Mole fraction of component *i*
x_i^{in} Inlet mole fraction of component *i*
z Axial coordinate on tube and shell side
ε Catalyst bed void fraction
λ Mobility of pressure equation [m^3 s/ kg]
μ_g Gas viscosity [N s/ m^2]
Φ Shape factor for catalyst particles
ρ_{cb} Catalyst bulk density [kg cat./ m^3]
ρ_g Gas density [kg/ m^3]
η_i Efficiency factor for reaction *i*

REFERENCES

1 Dixon, A.G., DiCostanzo, M.A. & Soucy, B.A. (1984), 'Fluid-phase radial transport in packed beds of low tube-to-particle diameter ratio', *International Journal of Heat and Mass Transfer*, **27 (10)**, 1701-1713
2 Peters, P.E., Schiffino, R.S. & Harriott, P. (1988), 'Heat Transfer in Packed-Tube Reactors', *Industrial & Engineering Chemistry Research*, **27**, 226-233
3 Grevskott, S., Rusten, T., Hillestad, M., Edwin, E. & Olsvik, O. (2001), 'Modelling and Simulation of a Steam Reforming Tube with Furnace, *Chemical Engineering Science*, **56 (2)**, 597-603
4 Xu, J. & Froment, G.F. (1989), 'Methane Steam Reforming, Methanation and Water-Gas Shift: I. Intrinsic Kinetics', *AIChE Journal*, **35 (1)**, 88-96
5 Xu, J. & Froment, G.F. (1989), 'Methane Steam Reforming: II. Diffusional Limitations and Reactor Simulation', *AIChE Journal*, **35 (1)**, 97-103
6 Lydersen, A.L. (1979), *Fluid Flow and Heat Transfer*, John Wiley & Sons, Great Britain, 240
7 Li, C.-H. & Finlayson, B.A. (1977), 'Heat Transfer in Packed Beds – A Reevaluation', *Chemical Engineering Science*, **32**, 1055-1066
8 De Wasch, A.P. & Froment, G.F. (1972), 'Heat Transfer in Packed Beds', *Chemical Engineering Science*, **27**, 557-576
9 Dixon, A.G. & Cresswell, D.L. (1979), 'Theoretical Prediction of Effective Heat Transfer Parameters in Packed Beds', *AIChE Journal*, **25 (4)**, 663-676
10 Kulkarni, B.D. & Doraiswamy, L.K. (1980), 'Estimation of Effective Transport Properties in Packed Bed Reactors', *Catalysis Reviews: Science and Engineering*, **22 (3)**, 431-483
11 Tsotsas, E. & Schlünder, E.-U. (1990), 'Heat Transfer in Packed Beds with Fluid Flow: Remarks on the Meaning and the Calculation of a Heat Transfer Coefficient at the Wall', *Chemical Engineering Science*, **45 (4)**, 819-837

Presentation 2

presented on *the 7th World Congress of Chemical Engineering*, Glasgow, (2005)

Gas heated steam reformer; two-dimensional finite difference model with heater side discrete ordinates radiation scheme

MH Wesenberg [1,3], O Olsvik [1], J Ströhle [2] and HF Svendsen [3]

[1] *Statoil Research Centre, N-7005 Trondheim, Norway*
[2] *SINTEF Energy Research, N-7465 Trondheim, Norway*
[3] *Norwegian University of Science and Technology, NTNU, N-7491 Trondheim, Norway*

Abstract:

A gas heated steam reformer designed with concentric sheath tubes on the reactor tubes has been modelled. The counter current flow of heating gas in the annular channel is hot synthesis gas from a secondary reformer. The operating conditions chosen are typical for a primary reformer for Fischer-Tropsch and methanol synthesis purposes. This involves lower steam contents than yet commercially proven and forces new challenges regarding life time of the catalyst pellets and the reactor tubes. A complete reformer model contributes to evaluate the limits for safe operating conditions where coking reactions will not occur. The model can also optimize the geometry to give the most favourable heat flux profile causing the lowest tube skin temperatures possible.

The model for the packed reactor bed is a two-dimensional pseudo-homogeneous dispersion model. The effects of turbulence and radiation on heat transfer are imbedded in the effective radial thermal conductivity and the heat transfer coefficient. The annular section is modelled with a two-dimensional plug flow model using an effective radial thermal conductivity to include the effect of turbulence on heat transfer. Radiative heat transfer is modelled by the method of discrete ordinates in the radial direction only. In both models convection is the only mechanism for heat transport in the axial direction. The two models are solved using the finite difference method, commercial ODE-solvers and the numerical method of lines. The iteration between the outer and inner part models is performed by direct substitution of the wall temperature profile and the axial heat flux distribution. Convergence is reached when the two heat flux profiles are equal and the temperature profiles are unchanged. High radial resolution is needed in both models for these heat fluxes to converge with heat fluxes calculated from enthalpy changes.

Convection is the dominating heat transport mechanism in annular section but the contribution from gas radiation can be 20-40 % of the total heat transfer.

1 Introduction

1.1 Steam reforming in Gas Heated Reformers

The gas heated reformer (GHR), or convective steam reformer, is a compact alternative to the conventional natural gas fired steam reformer (CSR) for production of synthesis gas. The high manufacturing costs, the heavy weight and the large base area of the CSR maintain the interest for a compact and less expensive alternative. The GHR has been commercially proven for large scale ammonia and hydrogen purposes where the steam excess in the reformer is large. There is also interest for the GHR for Fischer-Tropsch and methanol production but this will only be profitable if the steam contents in the feed gas are reduced to steam to carbon ratio below 1.5.

Some licensors of GHRs claim that this low steam to carbon ratio will be feasible in the future. The high partial pressure of methane and carbon monoxide may take the operation over the equilibrium limit of the coking reactions. Further development of catalyst materials is thus required in order to achieve rapid gasification of coke and thereby avoid catalyst poisoning.

There is also one other challenge related to the life time of the tube material. If syngas is to be used as the heating source on the shell side, the tubes are exposed to the risk of metal dusting under the tough operating conditions of warm and pressurized syngas. Research to find suitable materials is therefore in progress with GHR licensors to make such process operation feasible.

Because of this danger of coke formation and metal dusting during operation for Fischer-Tropsch and methanol purposes a numerical model of the GHR is considered useful in the evaluation of safe operational limits. It is also a tool for design and optimization purposes. The simplified two-dimensional model developed here is considered sufficient for these purposes.

The main reforming reaction and the water-gas-shift reaction involved are:

$$CH_4 + H_2O \rightleftharpoons CO + 3H_2 \quad (1)$$

$$CO + H_2O \rightleftharpoons CO_2 + H_2 \quad (2)$$

The reactions are catalysed by pellets coated with nickel and are as a whole net energy consumers. Effective heat transport to the reactor tubes and further into the centre of the fixed bed is therefore a very important aspect during design and operation of steam reformers. The reactions take place in several tubular fixed bed reactors of low diameter-to-height ratio to ensure efficient heat transport in radial direction. The heat transport from the shell side can be enhanced by increasing turbulence. This has been tested by the different licensors by introducing baffles, sheath tubes on parts of the reactor tubes, perforated sheath tubes, longitudinal (spiral) fins and other more complex tube/annulus configurations. The sheath tube configuration has been chosen in this study, which gives an annular section to be modelled as the shell side. The sheath tube is enclosing the tube along its whole length, although the tube skin temperature of the lower parts of the reactor tubes may become too high if heat transfer is enhanced even more by using sheath tubes in this area. The heat source in GHRs can be flue gas or, as in this study, syngas from a secondary autothermal reformer (ATR). The heat transport from this hot gas is mainly convective, in contrast to CSRs having mainly radiative transport. However, heat transport by radiation may also play an important role in the GHRs, as is seen from the results given.

1.2 Models for steam reformers

The reactor model is a two-dimensional pseudo-homogeneous dispersion model treating the reactions and mass and heat transfer in the tube. Concentration and temperature profiles are solved for the pseudo-homogeneous bulk phase. Only one reformer tube is modelled. The model equations are given by Froment and Bischoff (1990).

The shell-side is modelled as a concentric annulus enclosing the reactor tube. Heat is transported through the inner wall of the annulus while the outer wall is adiabatic. The model is simplified to a two-dimensional plug flow model including the dominant heat transport mechanism from turbulence in radial direction by means of an effective thermal conductivity for the gas. Heat is transported by convection in axial direction and by conduction and radiation in radial direction. The radiation term in the energy equation is solved by the discrete ordinates method.

The differential equations are solved by a finite difference method using an ODE solver, and the radial derivatives in equations involving both axial and radial variations are discretized by the numerical method of lines (Schiesser 1991).

According to Rostrup-Nielsen et al. (1988) the pseudo-homogeneous reactor model is sufficient for simulating steam reformers as they are operating in a strongly diffusion controlled regime. The radial temperature increase can be as large as 80 K, and the two-dimensional model has therefore been chosen in this study. This gives higher accuracy if the limits of coke formation are to be evaluated. Two-dimensional steam reformer models have been studied several times, both by the use of pseudo-homogeneous models (Kvamsdal et al. 1999 and Grevskott et al. 2001) and by using heterogeneous models (De Deken et al. 1982, De Groote and Froment 1995 and Pedernera et al. 2003).

Some of these studies involve only the reactor tube and not the shell side or firebox providing the heat to the reactor. The tube skin temperature is then given as a fixed profile in the boundary conditions of the energy equation. Grevskott et al. (2000) modelled the heat source both of a side-fired and of a convective steam reformer and used the two-flux method of Spalding (1980) for solving the radiative heat transport. De Groote and Froment (1995) modelled the firebox and solved the radiative heat transfer by the zonal method (Hottel and Sarofim 1967). Stehlík modelled the firebox of a top-fired steam reformer combined with a one-dimensional reactor model (Stehlík et al. 1989) and the shell side of a GHR connected to a reactor model (Stehlík 1995), and solved the thermal radiation fluxes by the zonal method and by use of radiative heat transfer coefficients, respectively. Xu and Froment (1989a) used the one-dimensional, heterogeneous model for the steam reformer tube coupled with a zone model for the firebox.

2 Mathematical model

The GHR model consists of two main models: the fixed bed reactor tube and the shell side heating section. The model is simplified by modelling one single average tube with its corresponding shell side area, represented by an annular section. The operating conditions in this study are typical for a primary reformer producing syngas for methanol or Fischer-Tropsch synthesis purposes.

The gases are assumed ideal and their physical properties are given as function of temperature and composition (Reid et al. 2001).

The two flows are counter current, with natural gas feed entering the reactor tube at axial position $z = 0$ and product gas exiting at $z = L$. The inlet of the hot syngas on the annular side is thus positioned at $z = L$. The radii of the inner and the outer wall of the reactor tube are denoted R_1 and R_2, respectively, and the outer radius inside the annulus is R_3.

2.1 Reactor model

The conservation equations for the six components i (i = CH_4, H_2O, CO, H_2, CO_2 and N_2) in the bulk phase can be expressed in terms of partial pressures when the ideal gas law has been introduced. The axial dispersion is omitted as it is negligible compared to the axial convective transport at the operating velocities of a steam reformer. The local axial mass flux is assumed constant over the radial positions, and this implies zero radial mass flux. The reaction term is the sum of the stoichiometric coefficient of component i multiplied with the reaction rate over the three reactions j. The axial variations of the partial pressures are calculated from:

$$\frac{\partial p_i}{\partial z} = -\frac{p_i}{v_{z,s}}\frac{\partial v_s}{\partial z} + \frac{p_i}{T}\frac{\partial T}{\partial z} + \frac{D_{er,b}}{v_{z,s}}\left(\frac{\partial^2 p_i}{\partial r^2} - \frac{1}{T}\frac{\partial T}{\partial r}\frac{\partial p_i}{\partial r} + \frac{1}{r}\frac{\partial p_i}{\partial r}\right) + \frac{R_g T}{v_{z,s}}\sum_j \eta_j \nu_{ij} r_j \qquad (3)$$

The empirical correlation for the effective radial diffusion coefficient, including radial dispersion, is as given by Fahien and Smith (1955), valid for $Re_b > 10$. The boundary conditions for the partial pressures define symmetry at the centre of the tube and zero gradient at the tube wall. The reaction rates, r_j, are modelled as given by Xu and Froment (1989b).

Summing up the six component balances gives the total mass balance of the bulk, expressed by the axial change in axial superficial gas velocity:

$$\frac{\partial v_{z,s}}{\partial z} = \frac{v_{z,s}}{T}\frac{\partial T}{\partial z} - \frac{v_{z,s}}{P}\frac{\partial P}{\partial z} + \frac{R_g T}{P}\sum_j \left(\sum_i \nu_{ij}\right)\eta_j r_j \tag{4}$$

The initial superficial velocity is calculated from the molar feed.

It is assumed that the radial variations in pressure can be neglected, and the radial mean of the velocities, densities and viscosities are therefore used when calculating the change in pressure as a function of axial position. The pressure drop in the catalytic bed is calculated from Ergun's equation (Ergun 1952).

The energy transport in axial direction is dominated by the convective term, and axial conduction is therefore neglected. With no radial convection, the only energy transport mechanism in radial direction is the effective conduction:

$$\frac{\partial T}{\partial z} = \frac{1}{\rho_g \cdot Cp_g \cdot v_{z,s}}\left[\lambda_{er,b}\left(\frac{1}{r}\frac{\partial T}{\partial r} + \frac{\partial^2 T}{\partial r^2}\right) + \sum_j \left(-\Delta H_j\right)\eta_j r_j\right] \tag{5}$$

The energy equation has the following two boundary conditions at $r = 0$ and at $r = R_1$, respectively:

$$\frac{\partial T}{\partial r} = 0 \tag{6},$$

$$-\lambda_{er,b}\frac{\partial T}{\partial r} = h_1\left(T - T_{w1}\right) \tag{7}$$

The effective radial thermal conductivity for the pseudo-homogeneous phase in Equation 5, $\lambda_{er,b}$, and the wall heat transfer coefficient of the boundary condition in Equation 7, h_1, are calculated from empirical correlations valid for the process conditions of steam reformers. The empirical correlation used for the conductive and turbulent element of $\lambda_{er,b}$ is described by Peters et al. (1988), valid for $Re_b > 100$, and assumed constant over the radius. The effective radial thermal conductivity for stagnant gas, $\lambda_{er,b}^{s}$, is correlated as derived by Kunii and Smith (1960). The radiative element of $\lambda_{er,b}$ was correlated as given by Singh and Kaviany (1994)

The empirical heat transfer coefficient given by Peters et al. (1988) has been found to describe the degree of heat transfer well in steam reformers (Wesenberg et al. 2001). This correlation is valid for cylindrical packings at $0.1 < d_p/d_t < 0.6$ and $100 < Re_b < 8000$ and was used for h_1 in this work.

2.2 Shell side model

The annular section is described by a plug flow model with an algebraic mass balance equation for calculating the axial velocity. The energy conservation equation involves heat transport caused by axial convection and by radial conduction and radiation. The contribution from conduction to axial heat transport is negligible compared with the convective contribution. Correspondingly is heat transfer by convection negligible in radial direction. Turbulent dispersion is the dominant heat transfer mechanism in radial direction, and this effect is

included in the effective radial thermal conductivity. The radiation from the hot gas is modelled by the method of discrete ordinates in the radial direction only. The condition showing when axial variation of radiation intensity can be neglected is shown by Kim and Baek (1996) from the theory of Sparrow and Cess (1978).

The energy equation involving heat transport from axial convection, radial conduction and radial radiation describes the temperature profiles in the annulus:

$$\rho_g Cp_g v_z \frac{\partial T}{\partial z} = \frac{1}{r}\frac{\partial}{\partial r}\left(\lambda_{er,a} r \frac{\partial T}{\partial r}\right) - \frac{\partial q_{rad}}{\partial r} \tag{8}$$

The effective radial thermal conductivity, $\lambda_{er,a}$, is described in detail in Section 2.2.1, and the method for calculating the radiative volumetric heat flux is given in Section 2.2.2.

The boundary conditions give expression to the inlet temperature (at $z = L$) and to the heat balances across the inner and outer walls of the annulus (at $r = R_2$ and at $r = R_3$), respectively:

$$T = T^0 \quad (9), \qquad -\lambda_{er,a}\frac{\partial T}{\partial r} = h_2\left(T_{w2} - T\right) \quad (10), \qquad -\lambda_{er,a}\frac{\partial T}{\partial r} = h_3\left(T - T_{w3}\right) \quad (11)$$

The outer wall of the annulus is adiabatic and this is achieved as described for Equations 20 and 21. A radiation heat flux term should be included in Equations 10 and 11 when solving by the finite volume method. This term vanishes when converting to the finite difference form, as shown by Siegel and Howell (2002).

The heat transfer coefficients describing the convective heat transport from the gas in the annulus to the inner and outer wall of the annulus, h_2 and h_3 respectively, are calculated as recommended by Mills (1995). The local Nusselt number for a tube is calculated from the empirical correlation of Gnielinski (1976), valid at $3{\cdot}10^3 < Re_a < 10^6$. The Nusselt and the Reynolds numbers are based on the hydraulic diameter of the annulus. The friction factor is calculated from the correlation of Petukhov (1970), valid for $10^4 < Re_a < 5{\cdot}10^6$ with correction factors given by Petukhov and Roizen (1964) for annular ducts. The algebraic velocity equation is deduced from the ideal gas law and the Fanning friction factor was taken from Kakac and Yener (1995) for low Reynolds numbers and from Goudar and Sonnad (2003) for high Reynolds numbers ($Re_a > 10^5$).

2.2.1 Turbulence

Although turbulence is not modelled directly, the effect of turbulence on heat transfer is accounted for by use of an effective radial thermal conductivity, $\lambda_{er,a}$. This conductivity is the sum of the gas conductivity and the turbulent conductivity, where the latter is the dominating. $\lambda_{er,a}$ can be calculated from different types of turbulence models. In this study $\lambda_{er,a}$ was found by modelling an identical annulus in CFD code where radial flow and turbulence were included. The k-ε turbulence model was used. $\lambda_{er,a}$ reported from these CFD simulations vary both with radial and axial position. When these values were applied in the simplified annulus model described above, the sensitivity for radial variations in $\lambda_{er,a}$ was found to be significant while the axial variations could be neglected. A function for $\lambda_{er,a}$ dependent on radial position only was therefore read from the results of the CFD simulations at some position midway in axial direction.

2.2.2 Radiation model

The discrete ordinates method (S_N-method) was applied for calculating the radiation source term in the energy equation and the radiation heat fluxes at the walls. It was assumed that the radiation beams could be sufficiently represented by beams in 12 different quadrature directions, which gives 6 directions by the S_4-method due to symmetry. 6 differential equations for the 6 intensities I must therefore be solved.

The simplification of the radiative transport equation (RTE) used in the discrete ordinates method expresses the intensity in one radiative direction as function of radial direction and azimuthal angle (Modest 2003):

$$\frac{\mu^m}{r}\frac{\partial\left(rI^m\right)}{\partial r}-\frac{1}{r}\frac{\partial\left(\eta^m I^m\right)}{\partial\psi}=\kappa I_B-\kappa I^m \tag{12}$$

The six directions are labelled by the superscript m, and μ^m and η^m are directional cosines. κ and I_B are the absorption coefficient and the blackbody radiative intensity of the gas, respectively.

Carlson and Lathrop (1968) introduced a simplified expression for the azimuthal variations, using the 7 geometrical coefficients $\alpha^{m\pm½}$, that maintain conservation of the intensities:

$$\frac{\partial\left(\eta^m I^m\right)}{\partial\psi}\simeq\frac{\alpha^{m+1/2}I^{m+1/2}-\alpha^{m-1/2}I^{m-1/2}}{w^m} \tag{13}$$

The directions $m \pm ½$ bound the edges of the angular range assigned by the quadrature weight w^m. The half-node intensities are simplified by setting $I^{m\pm½} = ½ (I^{m\pm1} + I^m)$. Expressions for the α-terms and values for the directional cosines and the weight factors can be found in Modest (2003). The directional cosines μ^m are defined as negative for direction numbers m = 1, 2, 5 and positive for m = 3, 4, 6. The final form of the RTE to be solved is then:

$$\frac{\mu^m}{r}I^m+\mu^m\frac{\partial I^m}{\partial r}-\frac{\alpha^{m+1/2}\left(I^m+I^{m+1}\right)-\alpha^{m-1/2}\left(I^{m-1}+I^m\right)}{2rw^m}=\kappa I_B-\kappa I^m \tag{14}$$

The boundary conditions at the inner wall of the annulus give the three intensities in the positive direction (i.e. in the direction out from this wall). These intensities are caused by emission from the wall plus reflection of the gas radiation into the wall, which is given by the radiation intensities in negative direction, weighted and multiplied with their respective directional cosines before summation:

$$I^m=\varepsilon_{w2}\frac{\sigma}{\pi}T_{w2}^4+\frac{(1-\varepsilon_{w2})}{\pi}\sum_{\mu^{m'}<0}w^{m'}\left|\mu^{m'}\right|I^{m'}\quad\text{for }\mu^m>0,\text{ and }r=R_2 \tag{15}$$

Correspondingly, the intensities in the three directions from the outer wall into the annulus are expressed by the boundary conditions at this wall. These are the intensities in the negative direction and are therefore a function of the weighted intensities in the three positive directions:

$$I^m=\varepsilon_{w3}\frac{\sigma}{\pi}T_{w3}^4+\frac{(1-\varepsilon_{w3})}{\pi}\sum_{\mu^{m'}>0}w^{m'}\mu^{m'}I^{m'}\qquad\text{for }\mu^m<0,\text{ and }r=R_3 \tag{16}$$

The boundary conditions have been simplified by assuming grey wall, so that $\rho_w = 1 - \varepsilon_w$.

The equation system is solved by simplifying the derivatives of I^m with central differences and expressing the RTE in two forms: for iteration in backward and in forward radial direction. The intensities I^3, I^4 and I^6 are solved by iteration in the positive r-direction and I^1, I^2 and I^5 are solved in the negative direction. This iteration procedure was described by Fiveland (1982), and direct substitution is used for connecting the two directions.

The radial change in radiation heat, used in the energy equation, is finally given as:

$$\frac{\delta q_{rad}}{\delta r} = -\kappa\left(\sum_{m=1}^{6} I^m w^m - 4\sigma T^4\right) \tag{17}$$

The total heat flux through the reactor tube wall as function of axial position is given at $r = R_2$:

$$q_{w2} = h_2\,(T - T_{w2}) + q_{rad,w2} \tag{18}$$

where the radiation heat flux is given by:

$$q_{rad,w2} = \varepsilon_{w2}\left(\sum_{\mu^m<0} \left|\mu^m\right| I^m w^m - \sigma T_{w2}^4\right) \tag{19}$$

The net heat flux through the outer wall of the annulus at $r = R_3$ is defined zero as this is an adiabatic wall:

$$q_{w3} = h_3\,(T_{w3} - T) - q_{rad,w3} = 0 \tag{20}$$

The radiation heat flux is:

$$q_{rad,w3} = \varepsilon_{w3}\left(\sum_{\mu^m>0} \mu^m I^m w^m - \sigma T_{w3}^4\right) \tag{21}$$

The wall temperature T_{w3} that gives zero net heat transfer is found by iteration.

The calculation of the gas emissivity is performed by the weighted-sum-of-grey-gases (WSGG) model as described by Smith et al. (1982). The mean beam length used in this expression is scaled for pressures above 1 atm as given by Edwards and Matavosian (1984). The scaling exponent involved is dependent on temperature and on the sum of the partial pressures of absorbing gases.

2.3 Iteration connecting the reactor and the annulus models

The iteration is initiated by specifying the reactor wall temperature profile on the annulus side, T_{w2}. This is input to the annulus model, where the heat flux, $q_{w2,a}$, is calculated from Equation 18. This heat flux is then input to the reactor model where the internal tube skin temperature is calculated from $q_{w2,a}$ and the bulk temperature at the discretization point close to the wall:

$$T_{w1} = T_b + \frac{R_2}{R_1}\frac{q_{w2,a}}{h_1} \qquad \text{at } r = R_1 \tag{22}$$

This wall temperature and the heat flux calculated from Equation 7 in the reactor model, $q_{w2,b}$, give the external tube skin temperature to be given as input for the next iteration:

$$T_{w2} = T_{w1} + q_{w2,b} \frac{R_2 \ln(R_2/R_1)}{\lambda_w} \quad (23)$$

The thermal conductivity of the tube material, λ_w, is set to a constant value. Convergence is reached when the two heat flux distributions, $q_{w2,a}$ and $q_{w2,b}$, are equal and the wall temperatures are unchanged.

3 Simulation results and discussion

3.1 Model validation

The properties of the gas mixtures at the outlet of the reactor and at the inlet on the annular side are closely correlated. The steam reformer product is further reformed in a secondary autothermal reformer, which product gas is the inlet gas to the steam reformer annular side. The primary GHR and the secondary ATR were simulated in the process simulation tool ProII to give inputs for the annulus gas. Table 1 shows the properties of the gases used in the simulations, where the reactor feed is given a hypothetical composition close to real operational values. The inlet gas on annular side is calculated with ProII.

Table 1: Gas compositions, temperatures and pressures used in the model simulations.
Inlet and outlet gases on reactor side and on annular side of the GHR.

	Reactor feed (given)	Reactor product (from this model)	Inlet gas on annular side (from ProII)	Outlet gas on annular side (from this model)
Temperature (˚C)	400	751	1050	703
Pressure (bara)	40	32.6	38.7	38.2
Mole fractions:				
CH_4	0.32	0.16	0.0013	0.0013
CO_2	0.021	0.065	0.065	0.065
CO	0	0.048	0.12	0.12
H_2O	0.65	0.38	0.41	0.41
H_2	0.0050	0.34	0.40	0.40
N_2	0.0040	0.0032	0.0022	0.0022
Flow (kmole/ hr)	50.0	62.0	91.8	91.8

3.1.1 Resolution and convergence

The axial variations of heat flux calculated in the reactor model and in the annulus model, converged satisfactorily using the procedure described in Section 2.3. A wall temperature profile was found that gave the same axial distribution of heat fluxes in both the reactor model and in the annulus model, calculated from Equation 7 and Equation 18, respectively. These heat flux distributions were also checked against the total heat flux across the heating surface based on the gas enthalpy changes from inlet to outlet.

High spatial resolution in the radial direction in the annular section was needed due to large variations in the effective radial thermal conductivity. The accuracy of the model was evaluated by comparing the integrated heat fluxes from Equation 7 or Equation 18 with the total enthalpy balance of the reactor. The relative difference as referred in Figure 1 is normalized with respect to the heat flux from the total enthalpy balance. In Figure 1 are shown the results

for varying number of radial discretization points in the annulus and in the reactor part. It can be seen that the number of points in the reactor model can be kept relatively low, and that an increase above 25-30 points does not improve the accuracy. For the annulus model the situation is different. Increasing the number of radial discretization points reduces the difference even up to 800 points. At this stage computation time became significant and a number of 400 radial steps was chosen for the annulus model and 30 steps was chosen for the reactor model. The resulting relative differences were found to be about 0.6 % in the annulus and 1.5 % in the reactor. This was deemed satisfactory. The relative difference in the reactor model was found also strongly dependent on the value of $\lambda_{er,b}$ chosen as it decreases considerably with increasing $\lambda_{er,b}$.

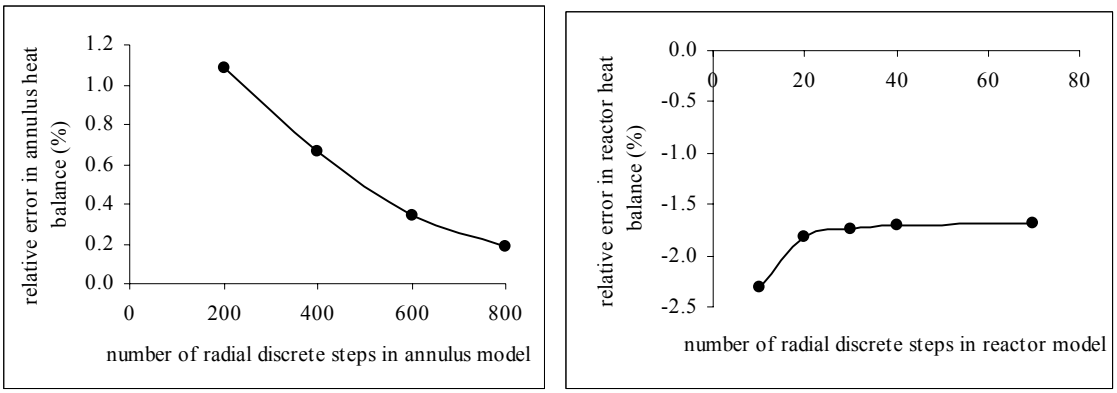

(a) *(b)*

Figure 1: Relative difference between integrated heat flux and the total energy balance as function of the number of discretization steps in radial direction in annular section (*a*) and in reactor tube (*b*). The number of radial discrete steps in *(a)* is fixed to 30 and in *(b)* to 400.

3.1.2 Comparison with CFD model

In order to verify the effective thermal conductivity model for the annulus, the model was simplified by excluding the radiation model. The previous made assumption that the $\lambda_{er,a}$ calculated in a corresponding CFD code (FLUENT) could be used in the finite difference model to give equal radial heat fluxes, was tested. The CFD model was used with the k-ε turbulence model and the finite difference model involved no calculations of turbulence other than the effect on radial heat transport through the imported $\lambda_{er,a}$.

The resulting axial profiles for wall temperature and heat transfer coefficient from the finite difference model were used as input to the CFD model, which again produced a radial profile for $\lambda_{er,a}$ that was input to the finite difference model. Manual iteration with these two models quickly resulted in a stable output and the two models gave the same temperature profiles. Even the radial temperature profiles were nearly identical, as can be seen in Figure 2. This confirms that an enhanced effective radial thermal conductivity profile calculated in a CFD code that uses the k-ε turbulence model can be used in a simpler finite difference model with no turbulence model, to describe the effect of turbulent flow on radial heat transfer.

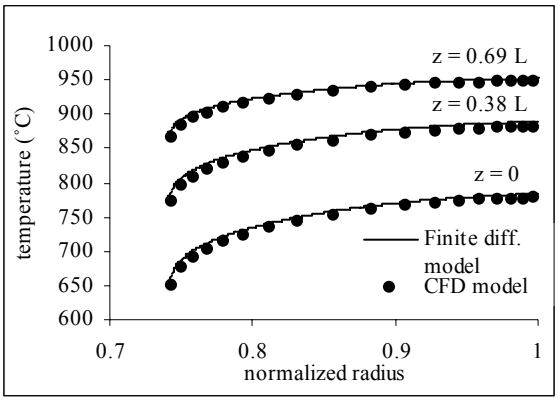

Figure 2: Comparison of temperature profiles from the finite difference model and from the CFD model.

3.2 Simulation results

The axial variation in heat flux through the reactor tube wall can be seen in Figure 3. The convective and the radiative contributions are also shown. The radiative contribution is of the same order as the convective contribution and can absolutely not be disregarded when modelling a GHR. The convective heat flux is flat along most of the reactor, but rises sharply at the reactor inlet. This rise is caused by the flat inlet gas temperature profile and the rapid establishing of the gas temperature profile at the wall. The radiative heat flux increases along the reactor. This is expected as the temperature level increases. The total heat flux profile is also relatively flat in the lower half of the reactor, but, because of the increased radiative flux it rises toward the feedgas entrance.

Figure 4 shows the axial profiles of wall temperatures and of radial mean gas temperatures. From the graph it can be seen that the temperature driving forces are evenly distributed along the tube length. This is an ideal operation and an advantage as it indicates a low entropy production (Sauar et. al 1999) and thereby good energy utilisation.

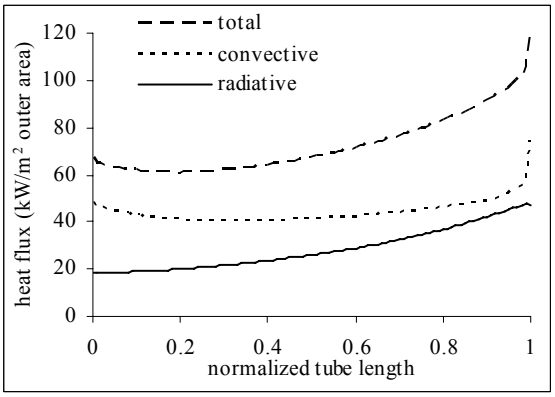

Figure 3: Axial variation of total, convective and radiative heat fluxes in annular section.

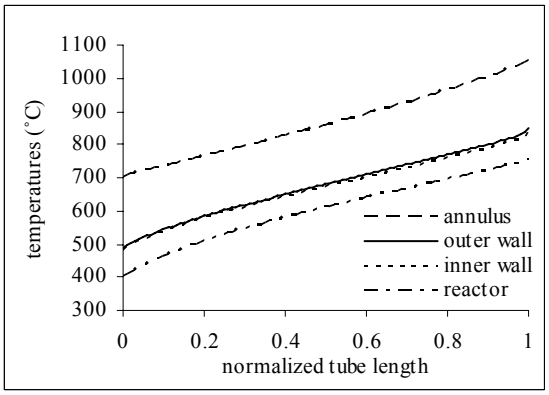

Figure 4: Axial profiles of radial mean bulk temperatures in annular section, in reactor bed, and of outer and inner wall temperatures of reactor tube.

Radial variations in gas temperatures at different axial positions in the catalytic bed and in the annular section are shown in Figure 5. The radial temperature profile of the reactor bed at $z = 0.1L$ (Fig. 5*a*) is comparable to the temperature profile outlined by Rostrup-Nielsen et al.

(1988) that is given for the same temperature level. This can be taken as support for the level of effective radial thermal conductivity in the reactor bed model. The radial profiles are rather flat indicating effective radial transport of energy regardless of axial position. In the reactor a significant rise in temperature can be seen close to the wall. This rise should not be mistaken for the wall heat transfer which gives a much higher temperature rise. Between the graphs lies the wall. As can be seen there is a difference of about 160 ˚C between the annulus and reactor temperatures in the points closest to the wall. This represents the heat transfer resistance in the wall, and to and from the two sides of the wall.

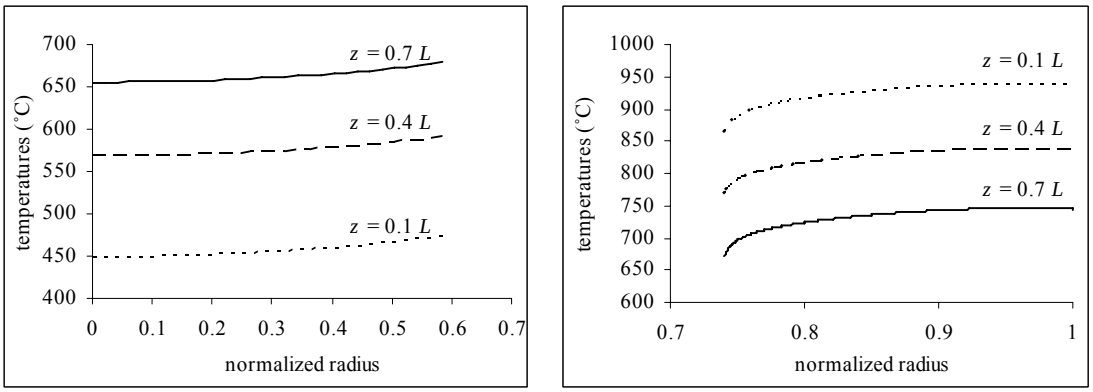

(a) *(b)*

Figure 5: Radial temperature profiles in reactor bed (*a*) and in annulus (*b*) at three axial positions *z*.

Equilibrium constants for the three coking reactions, methane cracking, Boudouard reaction and CO reduction, are given by De Groote and Froment (1995). These were used to calculate the potential for coke formation in the reactor bed, showing that only coking by methane cracking was probable along the first 27 % of the tube length. This is on the other hand not likely to occur, indicated by the kinetics for this reaction.

The radial variations of $\lambda_{er,a}$ found from CFD simulations were of significance for the results of the finite difference simulations, while the axial variations were of less importance. The importance of including the radial variations of $\lambda_{er,a}$ was studied. In comparable simulations where a mean value of $\lambda_{er,a}$ was used the total heat flux increased by 2 %, the methane conversion increased by 3 %, and the outlet temperatures of the reactor bed and of the annular section increased by 6 K and decreased by 7 K, respectively. It is thus important to include this radial variation in $\lambda_{er,a}$.

4 Conclusions

A gas heated steam reformer designed with concentric sheath tubes on the reactor tubes and hot synthesis gas from a secondary reformer in the annular channel has been modelled. Operating conditions chosen are typical for a primary reformer for Fischer-Tropsch and methanol synthesis purposes and involves lower steam contents than yet commercially proven. The model for the packed reactor bed is a two-dimensional pseudo-homogeneous dispersion model. The annular section is modelled with a two-dimensional plug flow model using an effective radial thermal conductivity to include the effect of turbulence on heat transfer. Radiative heat transfer in the annulus is modelled by the discrete ordinates method in the radial direction only.

The model has been tested for grid resolution and high radial resolution is found needed in the annular section for satisfactory energy balances to be achieved. The results show that radiation plays a significant role in the annulus side energy transport, varying from 30 % at the

low temperature end to nearly 50 % at the high temperature end of the reformer. The radial transport is rapid and quite flat radial temperature profiles result. The axial temperature profiles show that the driving forces for energy transport between the annulus and reactor sides are nearly constant through the reformer. This indicates low entropy production and good heat utilization.

Nomenclature

Cp	Specific heat capacity, J/kg K
d	Diameter, m
D	Diffusion coefficient, m^2/s
h	Heat transfer coefficient, W/m^2 K
I	Radiation intensity, W/m^2 sr
L	Tube length, m
p	Partial pressure, Pa
P	Total pressure, Pa
q	Heat flux, W/ m^2
r	Radial coordinate
R	Tube radius, m
Re_a	Reynolds number based on hydraulic diameter in annulus
Re_b	Reynolds number based on equivalent particle diameter in reactor bed
R_g	Gas constant, Pa m^3/kmole K
r_j	Reaction rate for reaction j, kmole/m^3 s
T	Temperature, K
v	Velocity, m/s
w	Quaderature weight for the directions
z	Axial coordinate

Greek symbols:

α	Parameter for cylindrical coordinates in the discrete ordinates method
ΔH	Heat of reaction, kJ/kmole
ε	Emissivity
η	Directional cosines for angular directions
η_j	Effictiveness factor for reaction j
κ	Absorption coefficient for gas, m^{-1}
λ	Thermal conductivity, W/m K
μ^m	Directional cosine of direction m (radial direction)
ν	Stoichiometric coefficient of chemical reaction
ρ	Density, kg/m^3
ρ_w	Wall reflectivity
σ	Stefan Boltzmann's constant, $W/m^2 K^4$
ψ	Azimuthal angle, rad

subscripts:

1	At inner wall of reactor tube
2	At outer wall of reactor tube
3	At outer wall of annular section
a	Annulus
b	Bed
B	Blackbody

e Effective
g Gas
i Component number
j Reaction number
p Pellet
r Radial
rad Radiation
s Superficial
t Tube
w Wall
z Axial

superscripts:
0 Inlet
m Angular direction in the discrete ordinates method
s Stagnant

References

CARLSON, B.G. AND LATHROP, K.D., 1968. Transport Theory – The method of discrete ordinates on computing methods in reactor physics. *In*: H. Greenspan, C.N. Kelber and D. Okrent, eds. *Computing methods in reactor physics*. New York: Gordon & Breach, 165-266.

DE DEKEN, J.C., DEVOS, E.F. AND FROMENT, G.F., 1982. Steam reforming of natural gas: Instrinsic kinetics, diffusional influences, and reactor design. *ACS Symposium Series*, 196, 181-197.

DE GROOTE, A.M. AND FROMENT, G.F., 1995. Reactor modelling and simulations in synthesis gas production. *Reviews of Chemical Engineering*, 11 (2), 145-183.

EDWARDS, D.K. AND MATAVOSIAN, R., 1984. Scaling rules for total absorptivity and emissivity of gases. *Journal of Heat Transfer*, 106, 684-689.

ERGUN, S., 1952. Fluid flow through packed columns. *Chemical Engineering Progress*, 48 (2), 89-94.

FAHIEN, R.W. AND SMITH, J.M., 1955. Mass transfer in packed beds. *AIChE Journal*, 1 (1), 28-37.

FIVELAND, W.A., 1982. A discrete ordinates method for predicting radiative heat transfer in axisymmetric enclosures. *ASME* paper no. 82-HT-20.

FROMENT, G.F. AND BISCHOFF, K.B., 1990. *Chemical reactor analysis and design*, 2nd ed. Wiley: New York.

GNIELINSKI, V., 1976. New equations for heat and mass transfer in turbulent pipe and channel flow. *International Chemical Engineering*, 16, 359-368.

GOUDAR, C.T. AND SONNAD, J.R., 2003. Explicit friction factor correlation for turbulent flow in smooth pipes. *Industrial & Engineering Chemistry Research*, 42, 2878-2880.

GREVSKOTT, S., RUSTEN, T., HILLESTAD, M., EDWIN, E. AND OLSVIK, O., 2001. Modelling and simulation of a steam reforming tube with furnace. *Chemical Engineering Science*, 56 (2), 597-603.

HARTNETT AND T.F. IRVINE, eds. *Advances in Heat Transfer.* Vol. 6. New York: Academic Press.

HOTTEL, H.C. AND SAROFIM, A.F., 1967. *Radiative Transfer.* New York: McGraw-Hill.

KAKAC, S. AND YENER, Y., 1995. Convective Heat Transfer. 2nd ed., Boca Raton: CRC Press, p. 201

KIM, T.Y. AND BAEK, S.W., 1996. Thermal development of radiatively active pipe flow with nonaxisymmetric circumferential convective heat loss. *International Journal of Heat and Mass Transfer*, 39 (14), 2969-2976.

KUNII, D. AND SMITH, J.M., 1960. Heat transfer characteristics of porous rocks. *AIChE Journal*, 6 (1), 71-78.

KVAMSDAL, H.M., SVENDSEN, H.F., HERTZBERG, T. AND OLSVIK, O., 1999. Dynamic simulation and optimization of a catalytic steam reformer. *Chemical Engineering Science*, 54, 2697-2706.

MILLS, A.F., 1995. *Heat and Mass Transfer*. Chicago: Irwin.

MODEST, M.F., 2003. *Radiative heat transfer.* 2nd ed. Amsterdam: Academic Press.

PEDERNERA, M.N., PINA, J., BORIO, D.O. AND BUCALA, V., 2003. Use of a heterogeneous two-dimensional model to improve the primary steam reformer performance. *Chemical Engineering Journal*, 94, 29-40.

PETERS, P.E., SCHIFFINO, R.S. AND HARRIOTT, P., 1988. Heat Transfer in Packed-Tube Reactors. *Industrial & Engineering Chemistry Research*, 27, 226-233.

PETUKHOV, B.S. AND ROIZEN, L.I., 1964. Generalized relationships for heat transfer in a turbulent flow of a gas in tubes of annular section. *High Temperature (USSR)*, 2, 65-68.

PETUKHOV, B.S., 1970. Heat transfer and friction in turbulent pipe flow with variable physical properties. *In:* J.P. REID, R.C., PRAUSNITZ, J.M. AND SHERWOOD, T.K., 2001. *The properties of gases and liquids.* 5th ed. New York: McGraw-Hill.

ROSTRUP-NIELSEN, J.R., CHRISTIANSEN, L.J. AND BAK HANSEN, J.-H., 1988. Activity of steam reforming catalysts: Role and assessment, *Allied Catalysis*, 43, 287-303.

SAUAR, E., NUMMEDAL, L. AND KJELSTRUP, S., 1999. The principle of equipartition of forces in chemical reactor design: The ammonia synthesis, *Computers & Chemical Engineering*, 23, 499-502.

SCHIESSER, W.E., 1991. *The numerical method of lines in integration of partial differential equations.* San Diego: Academic Press Inc.

SIEGEL, R. AND HOWELL, J.R., 2002. *Thermal radiation heat transfer.* 4th ed. New York: Taylor & Francis.

SINGH, B.P. AND KAVIANY, M., 1994. Effect of solid conductivity on radiative heat transfer in packed beds. *International Journal of Heat and Mass Transfer*, 37 (16), 2579-2583.

SMITH, T.F., SHEN, Z.F. AND FRIEDMAN, J.N., 1982. Evaluation of coefficients for the weighted sum of grey gases model. *Journal of Heat Transfer*, 104, 602-608.

SPALDING, D.B., 1980. Mathematical modelling of fluid-mechanics, heat-transfer and chemical-reaction processes. Lecture 9: Idealisations of radiation. *report no. HTS/80/1*, Imperial College of Science and Technology, London.

SPARROW, E.M. AND CESS, R.D., 1978. *Radiation Heat Transfer.* Augmented ed., Washington: Hemisphere, 273-274.

STEHLÍK, P., ŠIKA, J., BÉBAR, L. AND RAUS, L., 1989. Contribution to the research and development of radiation chambers in steam reforming. *Collection of Czechoslovak Chemical Communication*, 54, 2357-2374.

STEHLÍK, P., 1995. Radiative component in thermal calculation of tubular heat exchangers. *Heat Transfer Engineering*, 16 (1), 19-28.

WESENBERG, M.H., GRISLINGÅS, A. AND GREVSKOTT, S., 2001. Modelling of steam reformer tubes. *In: 6th World Congress of Chemical Engineering*, Melbourne.

XU, J. AND FROMENT, G.F., 1989a. Methane steam reforming: II. Diffusional limitations and reactor simulation. *AIChE Journal*, 35 (1), 97-103.

XU, J. AND FROMENT, G.F., 1989b. Methane Steam Reforming, Methanation and Water-Gas Shift: I. Intrinsic Kinetics. *AIChE Journal*, 35 (1), 88-96.